7

CANADIAN THESES ON MICROFICHE

THÈSES CANADIENNES SUR MICROFICHE

National Library of Canada
Collections Development Branch

Canadian Theses on
Microfiche Service

Ottawa, Canada
K1A 0N4

Bibliothèque nationale du Canada
Direction du développement des collections

Service des thèses canadiennes
sur microfiche

NOTICE

The quality of this microfiche is heavily dependent upon the quality of the original thesis submitted for microfilming. Every effort has been made to ensure the highest quality of reproduction possible.

If pages are missing, contact the university which granted the degree.

Some pages may have indistinct print especially if the original pages were typed with a poor typewriter ribbon or if the university sent us an inferior photocopy.

Previously copyrighted materials (journal articles, published tests, etc.) are not filmed.

Reproduction in full or in part of this film is governed by the Canadian Copyright Act, R.S.C. 1970, c. C-30. Please read the authorization forms which accompany this thesis.

AVIS

La qualité de cette microfiche dépend grandement de la qualité de la thèse soumise au microfilmage. Nous avons tout fait pour assurer une qualité supérieure de reproduction.

S'il manque des pages, veuillez communiquer avec l'université qui a conféré le grade.

La qualité d'impression de certaines pages peut laisser à désirer, surtout si les pages originales ont été dactylographiées à l'aide d'un ruban usé ou si l'université nous a fait parvenir une photocopie de qualité inférieure.

Les documents qui font déjà l'objet d'un droit d'auteur (articles de revue, examens publiés, etc.) ne sont pas microfilmés.

La reproduction, même partielle, de ce microfilm est soumise à la Loi canadienne sur le droit d'auteur, SRC 1970, c. C-30. Veuillez prendre connaissance des formules d'autorisation qui accompagnent cette thèse.

THIS DISSERTATION
HAS BEEN MICROFILMED
EXACTLY AS RECEIVED

LA THÈSE A ÉTÉ
MICROFILMÉE TELLE QUE
NOUS L'AVONS REÇUE

Canada

NL 339 (r. 85/09)

THE UNIVERSITY OF ALBERTA

ECONOMIC MINERALOGY OF THE NORTH T-ZONE DEPOSIT, THOR LAKE, NORTHWEST TERRITORIES

by

© Louise de St. Jorre

A THESIS
SUBMITTED TO THE FACULTY OF GRADUATE STUDIES AND RESEARCH
IN PARTIAL FULFILMENT OF THE REQUIREMENTS FOR THE DEGREE
OF Master of Science

Department of Geology

Edmonton, Alberta

Fall, 1986

Permission has been granted to the National Library of Canada to microfilm this thesis and to lend or sell copies of the film.

The author (copyright owner) has reserved other publication rights, and neither the thesis nor extensive extracts from it may be printed or otherwise reproduced without his/her written permission.

L'autorisation a été accordée à la Bibliothèque nationale du Canada de microfilmer cette thèse et de prêter ou de vendre des exemplaires du film.

L'auteur (titulaire du droit d'auteur) se réserve les autres droits de publication; ni la thèse ni de longs extraits de celle-ci ne doivent être imprimés ou autrement reproduits sans son autorisation écrite.

ISBN 0-315-32571-2

THE UNIVERSITY OF ALBERTA

RELEASE FORM

NAME OF AUTHOR Louise de St. Jorre

TITLE OF THESIS ECONOMIC MINERALOGY OF THE NORTH T-ZONE DEPOSIT, THOR LAKE, NORTHWEST TERRITORIES

DEGREE FOR WHICH THESIS WAS PRESENTED Master of Science

YEAR THIS DEGREE GRANTED Fall, 1986

Permission is hereby granted to THE UNIVERSITY OF ALBERTA LIBRARY to reproduce single copies of this thesis and to lend or sell such copies for private, scholarly or scientific research purposes only.

The author reserves other publication rights, and neither the thesis nor extensive extracts from it may be printed or otherwise reproduced without the author's written permission.

(SIGNED) Louise de St. Jorre

PERMANENT ADDRESS:

3615 3RD ST. S.W.
CALGARY, ALBERTA
CANADA T2S 1V6

DATED OCT. 15 1986

THE UNIVERSITY OF ALBERTA

FACULTY OF GRADUATE STUDIES AND RESEARCH

The undersigned certify that they have read, and recommend to the Faculty of Graduate Studies and Research, for acceptance, a thesis entitled ECONOMIC MINERALOGY OF THE NORTH T-ZONE DEPOSIT, THOR LAKE, NORTHWEST TERRITORIES submitted by Louise de St. Jorre in partial fulfilment of the requirements for the degree of Master of Science.

Supervisor

R. St J. Lambert

Date 15th October, 1986

Dedication

To my parents

Abstract

The Thor Lake north T-zone deposit, located 100 km southeast of Yellowknife, NWT, contains economically significant concentrations of Be, Y, REE, Nb, Zr and Ga. The rare-metal mineralization is related to albitization and greisenization of peralkaline granite which forms an integral part of the Blachford Lake alkaline intrusive complex of Aphebian age. Alteration in the T-zone is strongly zoned and is subdivided into four distinct lithologic units designated the Wall, Lower Intermediate, Upper Intermediate and Quartz zones. Textural and mineralogical relationships suggest that the zoned alteration assemblages of the north T-zone probably represent a series of pulsational metasomatic events including an early alkalic stage of K and Na metasomatism and late stage silicification.

The mineralogy of Be, the principal metal of economic interest in the T-zone, is relatively simple with most of the Be occuring in phenakite. Bertrandite, gadolinite and a member of the helvite group are minor contributors to overall Be enrichment. Be mineralization is most abundant in the Upper and Lower Intermediate zones.

The mineralogy of by-product mineralization in the T-zone is considerably more complex than that of Be. Nine Y- and REE-bearing minerals have been identified. Xenotime appears to be the most abundant Y-bearing mineral and is typically intimately associated with Y-rich thorite. Gadolinite is of minor economic significance. Y mineralization occurs predominantly in the Upper Intermediate zone.

The most abundant REE-bearing minerals are the LREE-enriched fluocarbonates. bastnaesite, parisite, roentgenite and synchysite. These phases typically occur as syntaxic intergrowths with two or occasionally three present together in a single polycrystal. The fluocarbonates are ubiquitous in the T-zone but are most economically significant in the Upper Intermediate zone. Monazite, also LREE-enriched, and britholite are not of economic importance. MREEs are present in the Y-bearing minerals xenotime and gadolinite.

Nb mineralization occurs mainly in the Lower Intermediate and Wall zones. Columbite is the most abundant Nb-bearing mineral; ashanite occurs rarely.

Three types of zircon have been identified in the T-zone: bipyramidal, zonally metamictized and as overgrowths on xenotime. Zircon is the only Zr-bearing phase present in the T-zone and appears to be of limited economic significance.

Ga occurs in albite and K-feldspar where it is substituting for Al^{3+} and locally triggers a brilliant blue cathodoluminescence. Economic concentrations of Ga are confined to the Wall zone.

Microbeam techniques including electron microprobe analysis, scanning imagery, ion probe analysis and cathodoluminescence microscopy were of invaluable use in the investigation of the complex mineralogy of the north T-zone rare-metal deposit.

Acknowledgements

First, my sincerest thanks to Dr. D.G.W. Smith, my supervisor, who initiated this project and who provided invaluable assistance and guidance throughout. I also gratefully acknowledge the members of my examining committee, Dr. R.D. Morton, Dr. R.St J. Lambert and Dr. M.L. Wayman, for their help.

Highwood Resources Ltd. of Calgary is gratefully acknowledged for financial support for field and laboratory work, and for allowing the author unlimited access to drill core, assay data, geologic maps and sections from their property. Special thanks are due to Dr. D.L. Trueman, J.C. Pedersen and D.G. Thomas of Highwood for their constant cooperation, encouragement and input.

I thank Steve Launspach and Dave Tomlinson for sharing with me their expertise in the operation of the electron microprobe and data processing; their patience and help were greatly appreciated. Dr. J.V.P. Long of Cambridge University is gratefully acknowledged for making the ion probe laboratory there available for work on this project and Dr. S.J.B. Reed is thanked for his assitance in the collection and interpretation of ion probe data. Dr. J.A.D. Dixon of Cambridge University is thanked for making the cathodoluminescence microscope laboratory avaliable for work on this project. Thanks are also due to Edith Hutcheson for typing the tables of analyses.

Finally, I want to thank all my friends for, among other things, helping me to keep things in perspective; especially my sister Susan, who undoubtedly put up with my worst.

Financial support for this project, provided by D.I.A.N.D. grants YK-83-84-076 and YK-84-85-012 to D.G.W. Smith, is gratefully acknowledged. General laboratory support was financed by NSERC grant A4254 to D.G.W. Smith.

Table of Contents

Chapter Page

I. INTRODUCTION 1

A. REGIONAL GEOLOGY 1

Geology of the Blachford Lake Intrusive Suite 2

Geochemistry of the Blachford Lake Intrusive Suite 5

Geochronology of the Blachford Lake Intrusive Suite 7

Origin of the Blachford Lake Intrusive Suite 8

B. GEOLOGY OF THE THOR LAKE PROPERTY 9

Lake-zone 10

Fluorite-zone 11

R-zone 11

S-zone 12

T-zone 12

C. HISTORY OF PROPERTY DEVELOPMENT 14

D. PURPOSE OF STUDY 16

II. GEOLOGY OF THE T-ZONE 18

A. GENERAL GEOLOGY 18

B. GRANITE 20

Unmineralized granite 21

Mineralized granite 24

Discussion 28

C. WALL ZONE 29

Aplite unit 29

Core unit 33

Breccia unit 35

Discussion 36

D. LOWER INTERMEDIATE ZONE 37

Quartz-magnetite unit 38

Quartz-biotite(±chlorite)-feldspar unit 39

Quartz-biotite(±chlorite)-oxides unit 42

Discussion 46

E. UPPER INTERMEDIATE ZONE 47

Quartz-thorite unit 48

Quartz-bastnaesite group unit 51

Quartz-feldspar-magnetite unit 53

Quartz-feldspar unit 55

Quartz-mica-feldspar unit 58

Quartz-mica unit 60

Discussion 60

F. QUARTZ ZONE 62

G. FELSITE DYKE 63

H. DIABASE DYKE 64

III. ECONOMIC MINERALOGY OF THE T-ZONE 66

A. INTRODUCTION 66

B. PRINCIPAL METAL OF ECONOMIC INTEREST: BERYLLIUM 68

Phenakite 69

Bertrandite 70

Gadolinite 71

Helvite group member 71

C. PROBABLE BY-PRODUCTS: YTTRIUM AND RARE EARTH ELEMENTS 72

Xenotime 73

Gadolinite 75

Thorite 76

LREE-bearing fluocarbonates 78

Monazite 83

Britholite 84

D. POSSIBLE BY-PRODUCTS: NIOBIUM, ZIRCONIUM AND GALLIUM 86

Columbite 86

Ashanite 87

Zircon 88

Ga-bearing feldspar 93

IV. DISCUSSION 98

A. GENERAL REMARKS 98

B. CONSIDERATION OF THE ORIGIN AND GENESIS OF THE NORTH T-ZONE 100

C. PROPOSALS FOR FUTURE RESEARCH RELATED TO THE NORTH T-ZONE 102

V. TABLES 103

VI. FIGURES 109

VII. PLATES 139

REFERENCES CITED 228

APPENDIX I: Quantitative electron microprobe analysis 233

APPENDIX II: Proposed technique for quantitative electron microprobe analysis of REE-bearing minerals 240

List of Tables

Table 2.1-Biotite and chlorite analyses. 104

Table 3.1-Columbite and ashanite analyses from the Lower Intermediate zone (138,91) and Wall zone (129). 105

Table 3.2-Zircon analyses. 106

Table 3.3-Albite analyses from the Wall zone (129), Lower Intermediate zone (164) and felsite dyke (85-2). 107

Table 3.4-K-feldspar analyses from the *aplite* (85-2) and *core* (182Y) units of the Wall zone, and the felsite dyke (85-6). 108

List of Figures

Figure 1.1-Location map for the Thor Lake rare-metal deposits, Northwest Territories, Canada. 110

Figure 1.2-Generalized geological map of the Blachford Lake intrusive suite showing locations of the T- and Lake-zones (after Davidson, 1978, 1982). 111

Figure 1.3-Generalized geological map of the five mineralized zones in the Thor Lake area (after Černý and Trueman, 1985) 112

Figure 2.1-Generalized geological map of the T-zone showing locations of sections A-B and C-D (after Trueman *et al.*, 1985). 113

Figure 2.2-Cross-section A-B through the T-zone. 114

Figure 2.3-Longitudinal section C-D through the T-zone. 115

Figure 2.4-Generalized paragenetic sequence of mineralization for unmineralized granite. .. 116

Figure 2.5-Generalized paragenetic sequence of mineralization for mineralized granite. 117

Figure 2.6-Generalized paragenetic sequence of mineralization for the K-feldspar *aplite* unit of the Wall zone. 118

Figure 2.7-Generalized paragenetic sequence of mineralization for the albite *aplite* unit of the Wall zone. 119

Figure 2.8-Generalized paragenetic sequence of mineralization for the *core* unit of the Wall zone 120

Figure 2.9-Generalized paragenetic sequence of mineralization for the *quartz-magnetite* unit of the Lower Intermediate zone. 121

Figure 2.10-Generalized paragenetic sequence of mineralization for the Lower Intermediate zone, *quartz-biotite(±chlorite)-feldspar* unit. 122

Figure 2.11-Generalized paragenetic sequence of mineralization for the Lower Intermediate zone, *quartz-biotite(±chlorite)-oxides* unit. 123

Figure 2.12-Generalized paragenetic sequence of mineralization for the *quartz-thorite* unit of the Upper Intermediate zone. 124

Figure 2.13-Generalized paragenetic sequence of mineralization for the *quartz-bastnaesite group* unit of the Upper Intermediate zone 125

Figure 2.14-Generalized paragenetic sequence of mineralization for the Upper Intermediate zone, *quartz-feldspar-magnetite* unit 126

Figure 2.15-Generalized paragenetic sequence of mineralization for the *quartz-feldspar* unit of the Upper Intermediate zone. 127

Figure 2.16-Generalized paragenetic sequence of mineralization for the *quartz-mica-feldspar* unit of the Upper Intermediate zone. 128

Figure 3.1-Characteristic energy dispersive spectrum of the helvite group mineral. Be does not appear in spectrum due to absorption by the detector. 129

Figure 3.2-Characteristic energy dispersive spectrum of xenotime. 130

Figure 3.3-Characteristic energy dispersive spectrum of gadolinite. Be does not appear in spectrum due to absorption by the detector. 131

Figure 3.4-Characteristic energy dispersive spectrum of the thorite group mineral. 132

Figure 3.5-Characteristic energy dispersive spectrum of bastnaesite. C and F do not appear in spectrum due to absorption by the detector. 133

Figure 3.6-Characteristic energy dispersive spectrum of parisite. C and F do not appear in spectrum due to absorption by the detector. 134

Figure 3.7-Characteristic energy dispersive spectrum of roentgenite. C and F do not appear in spectrum due to absorption by the detector. 135

Figure 3.8-Characteristic energy dispersive spectrum of synchysite. C and F do not appear in spectrum due to absorption by the detector. 136

Figure 3.9-Characteristic energy dispersive spectrum of monazite. 137

Figure 3.10-Characteristic energy dispersive spectrum of mineral tentatively identified as britholite.. 138

List of Plates

Plate 2.1a-Unmineralized, altered granite of the T-zone. 141

Plate 2.1b-Microcrystalline quartz replacing albite lamellae in perthitic feldspar and along grain boundaries. Associated sericite aggregate mantled by quartz. Unmineralized granite. Crossed polars. Magnification X92. 141

Plate 2.2a-Albite with patchy, irregular twinning partially replaced by quartz at grain boundary. Unidentified mineral of prismatic habit (possibly acmite) partially pseudomorphed by magnetite and enclosed in quartz. Rounded inclusions in albite are K-feldspar-columbite intergrowths. Unmineralized granite. Crossed polars. Magnification X92. 143

Plate 2.2b-Mineralized granite of the T-zone showing "microbrecciated" texture caused by pervasive replacement of feldspar along fractures and parallel to cleavage. 143

Plate 2.3a-Perthitic feldspar overgrown by K-feldspar. Dark lamellae in perthite are K-feldspar, light lamellae are albite. Unidentified acicular mineral is pseudomorphed by magnetite and enclosed in quartz. Mineralized granite. Crossed polars. Magnification X60. 145

Plate 2.3b-K-feldspar partially replacing anhedral LREE-bearing fluocarbonate polycrystals. K-feldspar displays unusual mottled texture. Mineralized granite. Crossed polars. Magnification X240. 145

Plate 2.4a-K-feldspar partially replaced by quartz, biotite and ankerite along fractures and grain boundaries. Mineralized granite. Crossed polars. Magnification X92. 147

Plate 2.4b-Altered acmite in albite. Acmite is partially to entirely replaced by magnetite, ankerite and quartz. Note patchy, irregular twinning in albite. Mineralized granite. Crossed polars. Magnification X92. 147

Plate 2.5a-Semi-opaque inclusions in albite are thorite-bearing intergrowths. White box encloses area shown in Plate 2.5b. Mineralized granite. Crossed polars. Magnification X92. 149

Plate 2.5b-Backscattered electron image showing intergrowth of K-feldspar, biotite, ilmenite and thorite within rounded inclusion in albite. Mineralized granite. Scale bar represents 10 μm. 149

Plate 2.6a-Drill core sample of albite *aplite* unit of the Wall zone (left). Hand samples of K-feldspar *aplite* unit unstained (center) and stained for K-feldspar (right). 151

Plate 2.6b-K-feldspar with interstitial quartz. K-feldspar *aplite* unit, Wall zone. Crossed polars. Magnification X60. 151

Plate 2.7a-K-feldspar with interstitial LREE-bearing fluocarbonate polycrystals. K-feldspar *aplite* unit, Wall zone. Crossed polars. Magnification X92. 153

Plate 2.7b-Randomly oriented albite laths with interstitial chlorite and ankerite. Albite *aplite* unit, Wall zone. Crossed polars. Magnification X92. 153

Plate 2.8a-Albite enclosed in, and partially replaced by, quartz. Opaque mineral is columbite. Albite *aplite* unit, Wall zone. Crossed polars. Magnification X92. 155

Plate 2.8b-Altered K-feldspar partially replaced by quartz and biotite. Albite *aplite* unit, Wall zone. Crossed polars. Magnification X92.......... 155

Plate 2.9a-*Core* unit of the Wall zone, unstained (left) and stained for K-feldspar.......... 157

Plate 2.9b-Early altered alkali feldspar (right) partially replaced by later K-feldspar (left). Columbite present as inclusions in both feldspar types. Note irregular, patchy twinning of later K-feldspar (left). *Core* unit , Wall zone. Crossed polars. Magnification X240. 157

Plate 2.10a-Randomly oriented albite laths with interstitial chlorite and fluorite. *Core* unit, Wall zone. Crossed polars. Magnification X60. 159

Plate 2.10b-Radiating aggregates of albite overgrowing K-feldspar. Note patchy twinning in K-feldspar. *Core* unit, Wall zone. Crossed polars. Magnification X60. 159

Plate 2.11a-*Breccia* unit of the Wall zone. 161

Plate 2.11b-*Quartz-magnetite* unit of the Lower Intermediate zone. 161

Plate 2.12a-K-feldspar overgrown and partially replaced by magnetite aggregates. Interstitial quartz and biotite. *Quartz-magnetite* unit, Lower Intermediate zone. Crossed polars. Magnification X368.......... 163

Plate 2.12b- *Quartz-biotite(±chlorite)-feldspar* unit of the Lower Intermediate zone. Note relict granitic texture. 163

Plate 2.13a-K-feldspar overgrown by aggregates of fine grained biotite. Associated opaque mineral is columbite. *Quartz-biotite(±chlorite)-feldspar* unit, Lower Intermediate zone. Crossed polars. Magnification X60. 165

Plate 2.13b-Albite partially replaced by lath-like and shreddy biotite. *Quartz-biotite(±chlorite)-feldspar* unit, Lower Intermediate zone. Crossed polars. Magnification X60.......... 165

Plate 2.14a- *Quartz-biotite(±chlorite)-oxides* unit of the Lower Intermediate zone.......... 167

Plate 2.14b-Lath-like biotite partially replaced by columbite, fluorite and quartz. *Quartz-biotite(±chlorite)-oxides* unit, Lower Intermediate zone. Plane polarized light. Magnification X60. 167

Plate 2.15a-Fine grained biotite partially replaced by chlorite aggregates. Associated opaque mineral is columbite. *Quartz-biotite(±chlorite)-oxides* unit, Lower Intermediate zone. Plane polarized light. Magnification X240.......... 169

Plate 2.15b-*Quartz-thorite* unit of the Upper Intermediate zone. Drill core (right) displays vermiform features typical of quartz-rich samples. 169

Plate 2.16a-Opaque area is complex intergrowth of thorite, xenotime, synchysite, siderite and fluorite. Host mineral is quartz. Fractures in quartz are filled with ankerite (±siderite) and thorite. *Quartz-thorite* unit, Upper Intermediate zone. Plane polarized light. Magnification X92. 171

Plate 2.16b-*Quartz-bastnaesite group* unit of the Upper Intermediate zone.......... 171

Plate 2.17a-Massive aggregates of acicular LREE-bearing fluocarbonates polycrystals displaying plumose texture. *Quartz-bastnaesite group* unit, Upper Intermediate zone. Plane polarized light. Magnification X92. 173

Plate 2.17b-Radiating aggregates of tabular LREE-bearing fluocarbonate polcrystals enclosed in quartz with interstitial microcrystalline quartz. *Quartz-bastnaesite group* unit, Upper Intermediate zone. Crossed polars. Magnification X60. 173

Plate 2.18a-Subhedral to euhedral LREE-bearing fluocarbonate polycrystals with interstitial quartz and fluorite. Aggregate of acicular polycrystals in top right corner. *Quartz-bastnaesite group* unit, Upper Intermediate zone. Plane polarized light. Magnification X92. 175

Plate 2.18b-*Quartz-feldspar-magnetite* unit of the Upper Intermediate zone. 175

Plate 2.19a-Prismatic acmite grains partially pseudomorphed by hematite. Host mineral is quartz. *Quartz-feldspar-magnetite* unit, Upper Intermediate zone. Crossed polars. Magnification X60. 177

Plate 2.19b-Radial aggregate of acmite needles partially replaced by hematite. Associated mica is polylithionite. Host mineral is quartz. *Quartz-feldspar-magnetite* unit, Upper Intermediate zone. Crossed polars. Magnification X92. 177

Plate 2.20a-Drill core sample of the *quartz-feldspar* unit of the Upper Intermediate zone. 179

Plate 2.20b-Albite partially replacing K-feldspar . Both feldspars are enclosed in, and partially replaced by, quartz. *Quartz-feldspar* unit, Upper Intermediate zone. Crossed polars. Magnification X92.......... 179

Plate 2.21a-Remnant patch of alteration composed of altered albite and K-feldspar with interstitial ankerite and fluorite. All phases partially replaced by host quartz. Note angular boundaries of alteration patch. *Quartz-feldspar* unit, Upper Intermediate zone. Plane polarized light. Magnification X60. 181

Plate 2.21b-*Quartz-mica-feldspar* unit of the Upper Intermediate zone. 181

Plate 2.22a-Polylithionite enclosing anhedral relicts of K-feldspar. Quartz surrounds polylithionite and partially replaces the mica at grain boundaries. *Quartz-mica-feldspar* unit, Upper Intermediate zone. Crossed polars. Magnification X60.......... 183

Plate 2.22b-*Quartz-mica* unit of the Upper Intermediate zone. 183

Plate 2.23a-Quartz zone sample showing blocky REE fluocarbonate grains enclosed in massive quartz. 185

Plate 2.23b-Felsite dyke from the T-zone. 185

Plate 3.1a-Optically continuous phenakite grains interstitial to quartz. Crossed polars. Magnification X60 187

Plate 3.1b-Optically continuous phenakite partially replaced at grain boundaries by microcrystalline quartz aggregates. Crossed polars. Magnification X60. 187

Plate 3.2a-Phenakite (optically discontinuous) grains surrounded by biotite aggregates. Phenakite contains inclusions of quartz and biotite. Crossed polars. Magnification X92 189

Plate 3.2b-Subhedral phenakite and associated monazite in ankerite. Crossed polars. Magnification X92. 189

Plate 3.3a-Bertrandite inclusions in quartz. Crossed polars. Magnification X240. 191

Plate 3.3b-Backscattered electron image showing euhedral bertrandite inclusions in quartz. Scale bar represents 10 μm 191

Plate 3.4a-Backscattered electron image showing member of helvite group as inclusion in phenakite. Scale bar represents 10 μm. 193

Plate 3.4b-Xenotime inclusions in quartz with associated dark purple fluorite and thorite. Crossed polars. Magnification X240. 193

Plate 3.5a-Individual grains and aggregates of opaque xenotime. Host mineral is quartz. White box encloses area shown in Plate 3.5b. Plane polarized light. Magnification X92 195

Plate 3.5b-Backscattered electron image showing minute Fe-oxide inclusions in xenotime. Oxide inclusions may cause xenotime to appear opaque as in Plate 3.5a. Scale bar represents 10 μm 195

Plate 3.6a-Xenotime-thorite intergrowths enclosed in quartz. Fractures in quartz are filled with thorite. White box encloses area shown in Plate 3.6b. Plane polarized light. Magnification X240. 197

Plate 3.6b-Backscattered electron image showing nature of xenotime-thorite intergrowth. White spots are burn marks in thorite caused by the electron microprobe. Fractures in quartz are filled with thorite. Scale bar represents 5 μm 197

Plate 3.7a-Backscattered electron image showing xenotime and associated thorite enclosed in synchysite. All three minerals are partially replaced by surrounding siderite. Scale bar represents 5 μm. 199

Plate 3.7b-Backscattered electron image showing partial replacement of xenotime (and thorite) by gadolinite and associated apatite. Monazite appears to cross cut gadolinite. Fluorite occurs as a late phase interstitial to other minerals. Scale bar represents 10 μm. 199

Plate 3.8a-Xenotime grains with zircon overgrowths and associated monazite. Host mineral is quartz. White box encloses area shown in Plate 3.8b. Crossed polars. Magnification X368. 201

Plate 3.8b-Backscattered electron image showing zircon overgrowths on corroded ovoids of xenotime. Associated monazite appears to cross-cut xenotime and zircon. Scale bar represents 2 μm. 201

Plate 3.9a-Gadolinite with interstitial fluorite. Associated monazite and thorite also shown. Plane polarized light. Magnification X368. 203

Plate 3.9b-Gadolinite and apatite with interstitial fluorite. Crossed polars. Magnification X200. 203

Plate 3.10a-Thorite aggregates in biotite. Biotite occurs interstitial to albite. White box enclosed area shown in Plate 3.10b. Plane polarized light. Magnification X92. 205

Plate 3.10b-Backscattered electron image showing thorite aggregates. White spots are burn marks caused by the electron microprobe. Note compositional inhomogeneity in thorite. Scale bar represents 5 μm. 205

Plate 3.11a-Radiating aggregates of acicular LREE-bearing fluocarbonate polycrystals in quartz. White box encloses area shown in Plate 3.11b. Crossed polars. Magnification X92. 207

Plate 3.11b-Backscattered electron images showing syntaxic intergrowth of bastnaesite and parisite in acicular polycrystals. Scale bar represents 20 μm. 207

Plate 3.12a-Subhedral LREE-bearing fluocarbonate polycrystals in ankerite. Black spots in ankerite are holes. White box encloses are shown in Plate 3.12b. Plane polarized light. Magnification X240. 209

Plate 3.12b-Backscattered electron image showing syntaxic intergrowth of parisite, roentgenite and bastnaesite in a subhedral polycrystal. Scale bar represents 10 μm. 209

Plate 3.13a-LREE-bearing fluocarbonate polycrystal showing lamellae-like intergrowth of different phases. White box encloses area shown in Plate 3.13b. Crossed polars. Magnification X240. 211

Plate 3.13b-Backscattered electron image showing lamellae-like syntaxic intergrowth of roentgenite, bastnaesite and parisite. Scale bar represents 20 μm. 211

Plate 3.14a-LREE-bearing fluocarbonate polycrystal partially replaced by K-feldspar and ankerite. Associated monazite enclosed in ankerite. White box encloses area shown in Plate 3.14b. Crossed polars. Magnification X240. 213

Plate 3.14b-Backscattered electron image showing syntaxic intergrowth of bastnaesite and parisite in partially replaced polycrystal. Scale bar represents 20 μm. 213

Plate 3.15a-Backscattered electron image showing syntaxic intergrowth of bastnaesite and parisite in tabular polycrystals. Note lamellae-like intergrowth appears to run parallel to long axis of tabular grains. Scale bar represents 20 μm. 215

Plate 3.15b-Subhedral monazite grains enclosed in ankerite. Quartz appear to partially replace monazite and ankerite. Opaque inclusions in ankerite are thorite intergrowths with chlorite. Crossed polars. Magnification X92. 215

Plate 3.16a-Britholite intergrown with parisite, monazite and chlorite. Host mineral is quartz with associated purple fluorite. White box encloses area shown in Plate 3.16b. Plane polarized light. Magnification X92. 217

Plate 3.16b-Backscattered electron image of britholite, parisite, monazite and chlorite intergrowth in quartz. Note altered, inhomogeneous appearance of parisite. Scale bar represents 20 μm. 217

Plate 3.17a-Columbite aggregates included in quartz and replacing lath-like biotite. Note difference in relief between associated quartz and phenakite. Plane polarized light. Magnification X92. 219

Plate 3.17b-Backscattered electron image showing columbite with anhedral inclusions of bastnaesite and ashanite. White spots in ashanite are burn marks caused by the electron microprobe. Host mineral is quartz. Scale bar represents 5 μm.. 219

Plate 3.18a-Bipyramidal zircons forming skeletal outline of unidentified preexisting mineral. Host mineral is quartz with associated altered K-feldspar and fluorite. Crossed polars. Magnification X92. 221

Plate 3.18b-Zonally metamictized zircons with interstitial biotite and columbite. Crossed polars. Magnification X240. 221

Plate 3.19a-Backscattered electron image of zonally metamictized zircons. White spots are burn marks caused by the electron microprobe. Scale bar represents 10 μm. 223

Plate 3.19b-Backscattered electron image showing core of zonally metamictized zircon in greater detail. Scale bar represents 5 μm.. 223

Plate 3.20a-Core-type zircons postulated to be comparable to cores of zonally metamictized zircons. Interstitial biotite and columbite. Plane polarized light. Magnification X368. 225

Plate 3.20b-Backscattered electron image showing core-type zircons. Bright areas are columbite. Scale bar represents 20 μm. 225

Plate 3.21-Photomicrograph illustrating red and blue cathodoluminescence of Ga-bearing albite. Interstitial chlorite is nonluminescent. Associated quartz has pale red cathodoluminescence around Fe- and Nb-oxide inclusions. Fluorite has dark blue cathodoluminescence. Magnification X120. 227

List of common gangue minerals and name abbreviations

acmite (ac)

albite (ab)

K-feldspar (kp)

ankerite (ak)

apatite (ap)

biotite (bt)

chalcopyrite (cp)

chlorite (ct)

Fe-oxide (fe)

Fe-sulphide (fs)

fluorite (f)

hematite (hm)

ilmenite (il)

magnetite (mt)

mica (unidentified, colourless) (m)

perthitic feldspar (pf)

polylithionite (pl)

quartz (q)

sericite (st)

siderite (sd)

sphalerite (sp)

Ti-oxide (ti)

List of economic minerals and mineral formulae

Be	phenakite (ph)	Be_2SiO_4
	bertrandite (br)	$Be_4Si_2O_7(OH)_2$
	helvite group (hl)	$(Fe,Mn,Zn)_4(BeSiO_4)_3S$
Y	xenotime (x)	$(Y,Gd,Dy,Er,Fe)PO_4$
	gadolinite (gd)	$(Y,Ce,Nd,Gd,Dy,Ca)_2FeBe_2(SiO_4)_2O_2$
	thorite (th)	$(Th,Fe,Y,P,Ca)SiO_4$
REE	LREE-bearing fluocarbonates (rf)	
	bastnaesite (b)	$(La,Ce,Nd)FCO_3$
	parisite (p)	$(La,Ce,Nd)_2Ca(CO_3)_3F_2$
	roentgenite (r)	$(La,Ce,Nd,Fe)_3Ca_2(CO_3)_5F_3$
	synchysite (s)	$(La,Ce,Nd,Fe)Ca(CO_3)_2F$
	monazite (mz)	$(La,Ce,Nd)PO_4$
	britholite (bh)	$(Ce,Nd,Gd,Dy,Y)_3Ca_2(SiO_4)_3(OH)$
Nb	columbite (cb)	$(Fe,Mn,Ti)Nb_2O_6$
	ashanite (as)	$(Nb,Ta,U,Fe,Mn)_4O_8$
Zr	zircon (zr)	$(Zr,Ca,Ti,Fe,Y,REEs,Th,U)SiO_4$
Ga	albite (ab)	$(Na,K)(Al,Fe,Ga)Si_3O_8$
	K-feldspar (kp)	$(K,Na)(Al,Fe,Ga)Si_3O_8$

Sample numbers

In the interests of conciseness, an abbreviated sample numbering system has been used throughout this thesis. All those samples beginning with 85 were collected during the 1985 field season. All other numberes refer to samples collected in 1984. In the latter case, the second part of the number refers to an area on the thin section, and the lettering to an analytical point. Copies of field notes are deposited in the University of Alberta collections together with samples.

I. INTRODUCTION

The Thor Lake rare-metal deposits contain economically significant concentrations of Be, Y, REEs, Nb, Ta, Zr and Ga. Located approximately 100 km southeast of Yellowknife, Northwest Territories, Canada and about 5 km north of the Hearne Channel of Great Slave Lake (Fig. 1.1) the area may be accessed year round by chartered fixed-winged aircraft from Yellowknife. Seasonally, water access is provided by motor-barge from Yellowknife to a point on the north shore of Hearne Channel south of Thor Lake. The property may also be accessed by winter road driven over ice cover on Great Slave Lake from Yellowknife to Hearne Channel and north to Thor Lake.

The mineral deposits at Thor Lake are located within metasomatically altered and brecciated peralkaline granite and syenite. The host granite and syenite together comprise the youngest unit of a highly differentiated plutonic complex of Aphebian age called the Blachford Lake intrusive suite (Davidson, 1978, 1982). Davidson (1982) suggested that the alteration and mineralization at Thor Lake are the end-products of magmatic differentiation and therefore form an integral part of the intrusive suite.

The five mineralized areas identified at Thor Lake to date are designated the Fluorite-, Lake-, R-, S- and T-zones. The purpose of this study is to examine in detail the unusual mineralogy of the metals of economic interest in the T-zone and the associated alteration assemblages.

A. REGIONAL GEOLOGY

The Thor Lake deposits are an integral part of the Blachford Lake intrusive suite which is located at the southern edge of the Slave Structural Province. The Blachford Lake intrusive suite is a multiphase, subcircular plutonic complex of alkaline character. Some 23 km in diameter, the complex covers an area approximately 235 km^2 and contains a number of gabbroic, syenitic and granitic units which show a range in composition with time from mildly alkaline to peralkaline (Davidson, 1978, 1982). See Figure 1.2 for a generalized geological map of the area.

All the rocks of the complex intrude metasedimentary schists of the Archean Yellowknife Supergroup and Archean calc-alkaline granodiorite and granite plutons of the southern Slave Province. The complex itself is intruded by small diorite and granodiorite plutons and northwest trending diabase dykes of the Mackenzie swarm (Davidson, 1978, 1982). According to Davidson (1978, 1982) the complex is also intruded by east-northeast trending diabase dykes sometimes referred to as the Hearne Dykes (Hoffman, 1980). At Thor Lake, several xenoliths identified as Hearne diabase (S. M. Roscoe, pers. comm.) occur within the Thor Lake syenite which suggests that at least this phase of the complex is younger than the Hearne Dykes. The cross-cutting east-northeast trending dykes in the Thor Lake area are megascopically similar to the northwest trending dykes and may be part of the Mackenzie swarm (D. L. Trueman, pers. comm.).

Although there is no exposed contact between rocks of the Blachford Lake complex and the Aphebian Great Slave Supergroup to the south of Hearne Channel, regional relationships suggest that the alkaline intrusive rocks are older (Davidson, 1978). In addition, Davidson (1978) postulated that the Hearne Channel may be the centre of a major fault which truncates the intrusive complex and brings it into contact with the Great Slave Supergroup. Davidson (1978) noted no evidence of lateral movement in adjacent subsidiary faults.

Geology of the Blachford Lake Intrusive Suite

Mafic rocks of the Blachford Lake intrusive suite were first mapped by Stockwell (1932), although the alkaline nature of the granitoid rocks to the east and their relationship to the mafic rocks was not recognized until later work by Davidson (1972). Davidson (1978) subdivided the complex into six texturally and compositionally distinctive plutonic units as follows: Caribou Lake gabbro, Whiteman Lake quartz syenite, Hearne Channel granite, Mad Lake granite, Grace Lake granite and Thor Lake syenite. Based on exposed cross-cutting relationships of dykes and main contacts, Davidson (1978) recognized a sequence of five intrusive events. The rocks of the last main intrusive event, being compositionally and spatially distinct, are subdivided (Grace Lake granite and Thor Lake syenite) although there is no obvious intrusive relationship to indicate a significant difference in time of emplacement (Davidson, 1978).

A brief description of the rocks successively emplaced during the five main intrusive events of the Blachford Lake alkaline complex follows. These descriptions are based on work by Davidson (1972, 1978, 1982). They are included here to provide a better understanding of the relationship between the differentiated alkaline complex and the subsequent alteration and mineralization present at Thor Lake.

The Caribou Lake gabbro, exposed only on the western side of the complex, is the oldest intrusive unit. The rocks are compositionally and texturally variable ranging from olivine gabbro at the chilled margin, grading eastward through noritic gabbro, pegmatitic hornblende gabbro and leucogabbro to leucoferrodiorite. All phases of the Caribou Lake gabbro contain xenoliths of anorthosite and anorthositic gabbro which may be relicts of an earlier intrusive event.

The Whiteman Lake quartz syenite intrudes the Caribou Lake gabbro and crops out in the northwestern part of the complex. This unit contains two phases, an earlier quartz-poor syenite with clinopyroxene and fayalite as its mafic silicates, and a later quartz-bearing syenite which is the predominant rock type. The Whiteman Lake quartz syenite includes large blocks of the Caribou Lake gabbro and country rock xenoliths.

Exposed in the southwestern part of the complex, the Hearne Channel granite intrudes the Caribou Lake gabbro and is intruded by the Mad Lake granite. The Hearne Channel granite, which contains hornblende and biotite as its mafic minerals, is compositionally uniform and has few host rock xenoliths.

The Mad Lake granite, exposed in two areas of the complex, intrudes the Whiteman Lake quartz syenite and the Hearne Channel granite. Although compositionally similar to the Hearne Channel granite, containing identical mafic silicates, the Mad Lake granite is distinguished from the latter texturally and by differences in matrix mineralogy. The Hearne Channel and Mad Lake granites are probably two phases of the same granitic magma and both are intruded by the Grace Lake granite.

The Grace Lake granite and Thor Lake syenite, emplaced during the last main intrusive event, are the youngest rocks of the Blachford Lake complex. The Grace Lake granite intrudes all earlier rock types along its western border and is the largest unit of the complex covering approximately 55 km². This unit is a coarse grained hypersolvus riebeckite granite and is compositionally and texturally quite uniform. Quartz content, averaging 25% by volume, decreases towards the syenite core with a concomitant increase in amphibole content. Locally the Grace Lake granite contains thin flat-lying lenses of syenite, granite pegmatite and sugary textured quartz-albite-acmite rock.

The Thor Lake syenite occupies the core of the Grace Lake granite covering an area approximately 30 km². This unit is very similar to the Grace Lake granite although it displays more compositional and textural variation than the latter. Davidson (1978) subdivided the Thor Lake syenite into these five sub-units:

> "a) coarse to medium grained, dark green, rusty-weathering fayalite-pyroxene syenite, locally containing enigmatite and hornblende
>
> b) coarse grained hornblende syenite
>
> c) inequigranular hornblende syenite characterized by very coarse, highly poikilitic hornblende
>
> d) subporphyritic hornblende syenite characterized by feldspar euhedra with purple cores and pink margins, and
>
> e) medium grained hornblende syenite with aligned hornblende crystals."

Boundaries between these rock types are gradational over a few tens of metres. The most distinctive type is the mafic sub-unit (a) informally called the "rim syenite" which forms an annular ridge, visible in aerial photographs, along the north and east margins of the Thor Lake syenite. In addition to the five lithologic subunits, sub-horizontal lenses and dykes of syenite pegmatite occur within the Thor Lake syenite. These rocks contain pegmatitic euhedra of amphibole and/or pyroxene and perthitic alkali feldspar in a matrix of aplitic to coarse grained albite with little or no associated quartz. It is not known whether these late-stage phases, which are essentially barren of economic minerals, are related to subsequent alteration and mineralization.

The temporal relationship between the two youngest phases of the Blachford Lake intrusive suite is unclear. In the west the rocks are in sharp contact marked by the disappearance of quartz from the granite with no concomitant change in grain size. In the north and east the granite appears to dip under the "rim syenite". There is no evidence of syenite dykes in the granite or vice versa to indicate an intrusive relationship between the two. Despite obscure contact relationships, the Grace Lake granite and Thor Lake syenite are obviously closely related and are both transected by the unusual mineralization on the Thor Lake property.

Both the Grace Lake granite and Thor Lake syenite contain host metasediment xenoliths and are cut by fine grained, brick-red felsite dykes which latter are generally less than 5 m wide, near vertical and northeast trending. The felsite dykes, of unknown age, also cross-cut the alteration assemblages in the Grace Lake granite and Thor Lake syenite.

For a more detailed description of the rock types which comprise the Blachford Lake intrusive suite and their relationships refer to Davidson (1978).

Geochemistry of the Blachford Lake Intrusive Suite

Geochemical data in addition to the features and relationships described above suggest that magmatic differentiation by fractionation was the dominant process responsible for the development of the Blachford Lake intrusive suite (Davidson, 1982). Chemically it is convenient to consider the intrusive complex in two parts. The older western portion of the complex, which includes the Caribou Lake gabbro, Whiteman Lake quartz syenite, Hearne Channel granite and Mad Lake granite, is relatively aluminous with anorthite present in the normative mineralogy. The younger and much larger part of the complex, consisting of the Grace Lake granite and Thor Lake syenite, is peralkaline with acmite appearing in the normative mineralogy.

Major and minor element chemistry show that continuous trends characterize the units in the western part of the complex but that there are discontinuities in trends between the aluminous and peralkaline rocks of the suite (Davidson, 1981, 1982). This break between the two parts of the complex suggests that the aluminous and peralkaline rocks may not be directly related. In general, trends in the major elements show an increase in silica and alkalis and a decrease in Fe, Mg and Ca towards younger rocks. F, Nb and REEs peak in the peralkaline rocks whereas U, Th and Rb are slightly more enriched in the aluminous granites. All these elements are concentrated in an albitic dyke which cuts the Thor Lake syenite and may be related to proximal alteration and mineralization (Davidson, 1981, 1982).

In terms of major oxides the Grace Lake granite and Thor Lake syenite compare closely with Nockolds' (1954) average peralkaline granite and average peralkaline syenite, respectively. Davidson's (1981, 1982) minor and trace element data reflect enrichment in both the granite and syenite of those elements of economic interest. The rare-metal enrichment, apparent in both phases, suggests the equal possibility of either granite or syenite as progenitor of the mineral deposits. The limited Rb, Sr and Ba data (Davidson, 1981, 1982) indicate a higher degree of differentiation in the granite than the syenite which supports interpretation of the granite as the younger phase. However, because the temporal relationship between the granite and syenite is unclear, the interpretation of the petrochemical data cannot be substantiated by other geological information. The information currently available precludes definition of either the Grace Lake granite or the Thor Lake syenite as progenitor to the ore deposits at Thor Lake although chemical data and field relationships suggest that the two phases are consanguineous.

Chondrite normalized REE patterns for the six main units of the Blachford Lake intrusive suite show a definite enrichment in the light REEs. Davidson (1982) interpreted these patterns as being indicative of a relatively evolved parent magma even for the earliest phases of the complex. Rocks derived from a more primitive magma would produce a comparatively flat profile. Successively intruded members of the complex show increased enrichment in light REEs from oldest to youngest, and there is a progressive development of negative Eu anomalies in the granitic rocks.

For a more complete discussion of the geochemistry of the Blachford Lake complex refer to Davidson (1981, 1982).

Geochronology of the Blachford Lake Intrusive Suite

Stockwell (1932) first described the Blachford Lake complex and thought it to be Archean in age. Later work (Davidson, 1972, 1978) indicated that the rocks were post-Archean in age, and subsequent geochronologic studies (Wanless *et al.*, 1979; Davidson, 1982; Bowring *et al.*, 1984) have confirmed Aphebian ages within the complex.

K-Ar mineral ages from the older, aluminous western portion of the complex and the younger peralkaline part of the suite range from approximately 2170 to 2130 Ma (Wanless *et al.*, 1979). These dates confirm a mid-Aphebian age for the Blachford Lake complex but meaningful age distinctions between the different intrusive phases are not apparent. The K-Ar mineral ages are indistinguishable from whole-rock Rb-Sr isochron ages for the Whiteman Lake quartz syenite, Mad Lake granite and Hearne Channel granite (Davidson, 1982). Although reliable Rb-Sr isochrons cannot be constructed with the available data for the younger peralkaline Grace Lake granite and Thor Lake syenite, the scatter in data allows for ages up to 200 Ma younger (Davidson, 1982).

U-Pb geochronology conducted by Bowring *et al.* (1984) yielded zircon ages of 2175±5 Ma for the Hearne Channel granite and 2094±10 Ma for the Thor Lake syenite. These ages suggest that the peralkaline phase of the Blachford Lake intrusive suite may be as much as 100 Ma younger than the older aluminous portion to the west. However, it is worth noting that the sample of Thor Lake syenite from which the zircons were separated was altered syenite consisting of "radiating albite crystals with cross-cutting veins of carbonate and zircon" (Bowring *et al.*, 1984). The zircons in the sample which comprised 10-20% of the rock "are unusual in habit and isotopic compostion" and "are dominated by two varieties, a xenomorphic type and a bipyramidal type" (Bowring *et al.*, 1984). It seems probable to the author that these zircons represent part of the late-stage mineralization at Thor Lake and if so the zircon ages apply to the mineralizing event and not the Thor Lake syenite itself. Although the mineralization and host syenite may be similar in age, the possibility remains that the peralkaline units could actually be older than 2094±10 Ma.

Origin of the Blachford Lake Intrusive Suite

The origin of the Blachford Lake intrusive suite is somewhat unclear. Hoffman (1980) suggested that the Blachford Lake complex and other alkaline intrusions in the western Slave Province (Big Spruce Lake and Easter Island Dyke) are related to rifting. Hoffman (1980) postulated that at approximately 2100 Ma a thick plate of continental lithosphere came to rest over a pair of deep mantle hot spots located under the present Great Slave Lake and Coronation Gulf. After the intrusion of the alkaline-peralkaline complexes and associated mafic dyke swarms it is suggested that a triple rift junction evolved from each hot spot. One north-south trending rift developed which connected the two hot spots and evolved to become the Wopmay Orogen. Two other rifts extended eastward from the hot spot into what are now referred to as the Athapuscow Aulacogen, which underlies the East Arm of Great Slave Lake, and the Kilohigok Basin. Although rifts may have extended westward from the hot spots their existence is purely hypothetical (Hoffman, 1980).

Recent U-Pb geochronology (Bowring *et al.*, 1984) show ages of around 1900 Ma for the rift sequence of the Wopmay Orogen. The zircon data indicates a significant period of time between the first datable event of the Wopmay Orogen and the alkaline-peralkaline magmatism of the western Slave Province. Based on their results Bowring *et al.* (1984) suggest that the alkaline-peralkaline magmatism of the Blachford Lake complex predates the Wopmay Orogen and therefore is either related to an earlier rifting event or, alternatively, represents a period of anorogenic magmatism. It is interesting to note that geochronologic studies conducted on the Big Spruce Lake alkaline complex (western Slave Province, N.W.T.) by Cavell and Baadsgaard (1986) indicate an average age of 2174±20 Ma for the complex. This age, which is essentially identical to that of the older phase of the Blachford Lake suite, also suggests that alkaline intrusions in the western Slave Province may not be directly related to the Wopmay rifting.

Despite being temporally widely separated (Bowring *et al.*, 1984), the Blachford Lake complex and the Athapuscow Aulacogen are spatially closely associated, suggesting that the two may be related. The alkaline-peralkaline granitic rocks of the intrusive suite are similar in many respects to those of the Nigerian alkaline ring complexes (Bowden and Turner, 1974) and the Arabian shield (Drysdall *et al.*, 1984; Jackson *et al.*, 1985). The alkali granites of both Nigeria and the northwestern Arabian shield are described as anorogenic A-type granites associated with rifting environments. It is also interesting to note that the Nigerian and Arabian granites show similarities to the Blachford Lake complex in terms of late-stage rare-metal (Nb, Zr, REE, Th, U) mineralization. Alkaline intrusions of the Kola Pennisula, USSR such as the Khibina and Lovozero massifs (Vlasov, 1966; Smirnov, 1977) and the Igaliko alkaline intrusive complex in southern Greenland (Northern Miner, 1986) also contain rare-metal mineralization, in altered syenites, similar to that of the Blachford Lake complex.

It is worth noting here that despite being closely related to the Blachford Lake intrusive suite both temporally and spatially, the alkaline syenites and associated carbonatites of the Big Spruce Lake complex do not appear to contain economically significant mineralization (P.A. Cavell, pers. comm). It is possible that the lack of mineralization at Big Spruce Lake is related to the absence of younger peralkaline rocks such as those that are present in the Blachford Lake complex.

B. GEOLOGY OF THE THOR LAKE PROPERTY

The five mineralized areas identified on the Thor Lake property to date are designated the Lake-, Fluorite-, R-, S-, and T-zones. All the mineralized zones occur within the western part of the Thor Lake syenite except the T-zone which transects the syenite-granite boundary (Fig. 1.3). The complex nature of the alteration and mineralization at Thor Lake does not allow for a simple classification as one particular type of ore deposit. Rather, the Thor Lake rare-metal deposits show characteristics of several ore deposit types. Specifically, the deposits at Thor Lake, as noted by Černý and Trueman (1985), display similarities to the albitite, metasomatite and greisen types of Be, Y, REE, Nb, Zr, Th and U mineralization of Smirnov (1977). Based on the alteration assemblages present in the T-zone, these deposits in particular could be described as phenakite-mica-albite type greisens of Shcherba's (1970) Albite-Greisen Formation. Brief descriptions of the five mineralized zones at Thor Lake follow. These descriptions are based on several unpublished internal reports (McGinn, 1976; Thomas, 1977; Hylands and Campbell, 1980) made available by Highwood Resources Ltd., papers by Trueman *et al.* (1985) and Černý and Trueman (1985), and most importantly long discussions with J. C. Pedersen and D. L. Trueman during the author's two field seasons at Thor Lake.

Lake-zone

The Lake-zone, so named because approximately half the deposit underlies Thor Lake (Fig. 1.3), is the largest of the mineralized areas. Although the zone is poorly exposed with less than 5% outcrop, its contacts with the host syenite (Fig. 1.3) are fairly well constrained by diamond drill data and locally by the limited outcrop. The Lake-zone approximates a triangle in plan and, based on the results of a gravity survey conducted in 1983, is interpreted as being an easterly plunging cone which is slightly modified by east-northeast trending vertical faults.

In Figure 1.3 the Lake-zone is divided into two principal lithologies the outer feldspathic Wall zone and inner Core zone (altered breccia). The outer Wall zone contact with the syenite is sharp whereas the inner contact with the Core zone is gradational or intercalated. The Wall zone rocks are characterized by two generations of feldspar, an earlier coarse grained K-feldspar which is overgrown or replaced by later fine grained albite. Accessory minerals include quartz, fluorite, columbite and Fe-oxides. Rocks of the Core zone are texturally and mineralogically diverse ranging from apparently unaltered syenite, locally olivine(or serpentine)-bearing, to areas of coarse grained, perthitic K-feldspar set in a matrix of finer grained amphibole, pyroxene, biotite, albite and Fe-oxides. Accessory minerals include fluorite, carbonate, columbo-tantalite, zircon, bastnaesite, monazite and allanite. The origin of the Core zone is postulated to involve the brecciation of the Thor Lake Syenite, possibly including pegmatitic phases, followed by repeated and chemically diverse events of metasomatism and replacement. The mineralogy and petrology of the Lake-zone is not well documented at present. A detailed petrographic study would be useful in deciphering the types and stages of alteration and mineralization in the Lake-zone deposit.

The last published diamond drill-indicated reserves for the Lake-zone are 64 million tonnes grading 0.4% Nb, 0.03% Ta, 3.5%Zr and 1.7% combined REEs. Results from drilling completed in 1986 indicate that the Lake-zone mineralization is open to a depth of 335 m. The new information on depth extent suggests the existence of a significantly larger tonnage than has been outlined previously in the Lake-zone.

Fluorite-zone

The Fluorite-zone, the smallest and least investigated of the mineralized areas at Thor Lake, occurs as a narrow appendage south of the Lake-zone on the southeastern shore of Long Lake (Fig. 1.3). The zone contains irregular lenses of fluorite-rich alteration in syenite. The fluorite is fine grained, purple in colour and comprises up to 55% of the rock. Accessory minerals include albite, mica and Cu-Fe sulfides. Assays from samples of the altered rock indicate anomalous Nb, REE and U values in the Fluorite-zone. Interestingly, the Fluorite-zone occurs along the southeastern projection of the T-zone. However, whether the two mineralized zones are joined at depth or even directly related is not known at the time of writing. In any case, the Fluorite-zone may represent the southernmost extent of the Thor Lake mineralization.

R-zone

The R-zone is located north of the Lake-zone and is a linear body which follows an east-northeast trending scarp (Fig. 1.3). This feature appears to be an extension of the vertical fault which truncates the southern end of the T-zone. The R-zone extends for approximately 1 km along strike and varies in width from a few metres to a maximum of about 30 m. Albitization is the principal type of alteration and this occurs irregularly throughout the zone as lenses, dykes and stringers. Host rocks of the R-zone are massive to strongly foliated syenite, syenite pegmatite and aplite. The Y and REE mineralization in the R-zone usually occurs in patches of altered syenite associated with Th and minor U. Radioactivity proved to be a useful exploration guide for Y and REEs in this zone. Be and Nb mineralization also occurs locally. Accessory minerals in the altered and mineralized rocks include fluorite, magnetite and quartz. The R-zone may eventually be exploited for supplementary Be, Y and REEs.

S-zone

The S-zone is located just northwest of the R-zone and trends northeast (Fig. 1.3). It is a small linear body which branches locally and extends for approximately 300 m with an average width of 10 m. The northern tip of the zone is offset by one of the east-northeast trending vertical faults which cut the T-zone. Albitization and mica-albite assemblages are the predominant alteration types in the S-zone. Although the alteration is generally irregular in extent and distribution, zoning is locally apparent progressing from an outer unit of albitite, through a transitional mica-albite unit to a mica(polylithionite)-core. The alteration occurs within massive to foliated syenite and pegmatitic syenite. Accessory minerals include fluorite, magnetite, columbite, hematite, Fe-sulfides and quartz.

Like the R-zone, the S-zone contains Be, Y, REE, Nb, Th and U mineralization. Radioactivity anomalies produced by Th and minor U have again been useful in delineating areas of Y and REE enrichment. Trench samples from the S-zone indicate fairly minor concentrations of Be but significant Nb values. The S-zone, like the R-zone, may eventually be exploited for supplementary Be, Y and REEs.

T-zone

The T-zone trends north-northwest away from the northern margin of the Lake-zone (Fig. 1.3). It is an irregular feature which extends for 1 km and varies in width up to approximately 250 m. The vertical extent of the deposit has been verified to a depth of 150 m and in parts remains open. The T-zone is divided into two separate ore bodies, the subcircular body at the north end and an irregular body which crops out at the south end. Both bodies appear to be joined by a near vertical north-northwest trending dyke.

Alteration in the T-zone is strongly zoned and is subdivided into four distinct lithologies designated the Wall, Lower Intermediate, Upper Intermediate and Quartz zones. The Wall zone is a feldspathic unit similar to that in the Lake-zone and marks the outer limit of alteration. The Lower Intermediate zone occurs above the hanging wall of the Wall zone and is comprised of altered granite and quartz-mica-chlorite-feldspar-(Fe,Ti)-oxide assemblages. The Upper Intermediate zone is in gradational contact with and above the Lower Intermediate zone and consists of quartz-mica-fluorite-feldspar assemblages. The Quartz zone, which consists largely of massive, barren, coarse grained quartz, overlies and is, in part, intercalated with the Upper Intermediate zone. Common accessory minerals in the T-zone include fluorite, ankerite, siderite, magnetite, Ti-oxides, pyrite, chalcopyrite, sphalerite, various micas and acmite. Minerals of economic interest include phenakite, bertrandite, gadolinite, helvite-danalite, xenotime, bastnaesite, parisite, synchisite, monazite, columbite and zircon. The T-zone alteration occurs in both the Grace Lake Granite (north end) and the Thor Lake Syenite (south end).

Be is the prinicpal ore metal of the T-zone with Y, REEs, Nb and Ga as potential co-products or by-products. Extensive diamond drilling of the T-zone has outlined reserves of 435,000 tons grading 1.4% BeO and 0.26% Y_2O_3 in the north deposit and 1,300,000 tons grading 0.66% BeO in the south deposit. Although reserves for REEs, Nb and Ga are not presently available, assay data from underground samples and diamond drill core demonstrate significant enrichment of these metals in the T-zone deposits.

The T-zone deposits are currently the subject of a feasibility study for production purposes. This thesis study is confined to the north T-zone which is the area of major economic significance at this time on the Thor Lake property. The alteration zones and economic mineralogy of the T-zone, briefly outlined above, are discussed in much greater detail in the following chapters.

It is interesting to note that there is a distinct metal zoning between the different mineral deposits on the Thor Lake property. Be and Y mineralization are essentially restricted to the R-, S-, and T-zones whereas Ta mineralization is confined to the Lake-zone. REE enrichment is apparent in all five alteration zones and Nb mineralization is also ubiquitous although associated Ta is present only in the Lake-zone. To date, Zr and Ga mineralization have been documented only in the T-zone and Lake-zone.

In addition to a certain distribution pattern between deposits, the economic metals also show preferences for particular lithologic units within a deposit. Be and Y mineralization occur predominantly within the Upper Intermediate and Lower Intermediate zones in the T-zone and comparable alteration assemblages in the R- and S-zones. Nb shows a propensity for the Lower Intermediate zone assemblages (R-, S- and T-zones) and in conjunction with Ta occurs mainly in the Core zone rocks of the Lake-zone. REE and Zr mineralization show no strong lithologic preferences in the deposits although the light REEs are more concentrated in the Upper Intermediate zone of the T-zone. Ga is confined largely to rocks of the Wall zone and occurs less frequently in the Core zone and Lower Intermediate zone assemblages. The distribution of the metals of economic interest in the T-zone will be discussed in detail later.

C. HISTORY OF PROPERTY DEVELOPMENT

Reports of radioactivity in the area first stimulated exploration interest in the Thor Lake property. The ground was initially staked by prospectors in 1970 and obtained by Bluemount Mines Ltd. A shallow trench was opened over the main showing in the R-zone but the claims were eventually allowed to lapse. In 1972 a significant radioactivity anomaly was discovered in the area during an airborne γ-ray spectrometer survey conducted by the Geological Survey of Canada (O.F.R. 124). In 1976 the property was restaked by Highwood Resources Ltd. of Calgary for its U potential. From 1976 to 1979 exploration programs including geological mapping, sampling, trenching and limited diamond drilling were conducted on the Lake-, Fluorite-, R-, S- and T-zones. A total of 13 trenches and 22 diamond drill holes were sampled and assayed from 1976 to 1979. This work resulted in the discovery of significant concentrations of Nb, Ta, Y and REEs. Results also indicated a general paucity of U mineralization on the Thor Lake property. Assay data showed that the anomalous radioactivity was mainly due to Th enrichment. In 1979 lake-bottom radiometric (Lake-zone) and radon gas in soil surveys (Lake- and T-zones) were conducted; results were inconclusive.

In 1980 Placer Development Ltd. acquired the Thor Lake property from Highwood Resources Ltd. through an option agreement. Placer, interested in the Nb and Ta potential of the Lake-zone, conducted magnetometer, scintillometer and VLF surveys over the zone. From subsequent diamond drilling (13 holes) Placer outlined a large Nb, Ta, Zr and REE deposit.

Highwood Resources Ltd. resumed work on the property in 1982 and a bulk sample from the Lake-zone was collected for metallurgical testing. In 1983 a metallurgical research program directed at fine-particle recovery methods for the fine grained columbo-tantalite in the Lake-zone was started.

In 1983 the R-, S- and T-zones were resampled and assayed for Be, the Be-bearing mineral phenakite having been identified earlier by Davidson (1978). Results from the initial exploratory work indicated the presence of significant Be in the R- and T-zones. This work was then followed by surface prospecting of the two zones using a berylometer which is a portable geophysical tool used in the exploration and examination of Be deposits (Brownell, 1959). The berylometer survey indicated that Be mineralization was widespread in the T-zone in particular. Results from diamond drilling of over 70 holes during the fall and winter of 1983/84 established Be reserves in the north and south T-zone deposits. Assay data also stimulated interest in Y, REEs, Nb, Zr and Ga as potential by-products.

During the summer of 1984 geological mapping of the the mineralized zones, started in 1983, was completed. Removal of overburden, surface drilling and blasting were also conducted for assay control and delineation of mineralized areas. A 25 ton bulk sample was collected from the high-grade Be section of the north T-zone deposit for initial metallurgical testing. A mineralogical study of material from the bulk sample was completed by CANMET in March 1985 (Jambor, 1985).

In 1985 Strathcona Mineral Services Ltd. contracted, for Highwood Resources Ltd., Canadian Mine Development Ltd. to drive a 500 m decline into the north T-zone deposit. The decline extends to a vertical depth of 70 m and intersects all the areas of Be and Y mineralization and the different lithologic units. The underground program, in addition to providing a large stockpile of Be-, Y- and REE-bearing material for pilot-plant purposes, provided resolution of drill-indicated reserves, information on rock stability and structure (rock mechanics) and new geological data. Bulk samples from the various areas of Be, Y and REE enrichment within the deposit were sent to Lakefield Research for bench and pilot-plant scale metallurgical work. Additional exploration of the R- and S-zones during the summer, aimed at locating and delineating new Be and Y deposits, included scintillometer surveys, trenching and sampling.

During the fall and winter of 1985/86 a diamond drilling program was conducted to tighten up control and extend reserves in the T-zone and to explore the Lake-zone further. Bench-scale and locked-cycle metallurgical work on material from the T-zone continued through 1985/86. Pilot-plant testwork is on-going at the time of writing.

In September 1986, Highwood Resources Ltd. signed a joint venture agreement with Hecla Mining Company of Canada Ltd., the objective of which is the commercial production of the Thor Lake specialty metals deposit.

D. PURPOSE OF STUDY

This study was started in September 1983 during the initial Be discoveries in the R- and T-zones. Preliminary mineralogical work on high-grade rocks, conducted by prospective consumers of Be, suggested that the mineralogy of Be was relatively simple with most of the Be occuring in phenakite. In 1984 re-assaying of diamond drill core splits from the T-zone drilling indicated significant concentrations of Y, REEs, Nb, Zr and Ga in addition to Be. When this study was initiated the mineralogy of the potential by-product metals in the T-zone was essentially unknown.

The main objective of this study was to examine in detail the mineralogy of the potential by-product metals (Y, REEs, Nb, Zr and Ga) in the north T-zone deposit. Specifically, this study was concerned with the identification and nature of the minerals which contain the elements of economic interest and their distribution within the deposit. Particular emphasis has been placed on Y and REEs which have the greatest potential as by-products and whose mineralogy is the most complex. Certain interesting aspects of the Nb-, Zr- and Ga-bearing minerals were also examined and the mineralogy of Be was studied briefly.

The second objective of the study was to describe the unusual alteration assemblages in which the Be and by-product mineralization occurs. Of particular interest were the mineralogical and textural variations both within a single lithologic unit and from unit to unit in the north T-zone. Relative age relationships between minerals (economic and gangue) were also of interest. The host rock granite and unmineralized dyke rocks were examined.

This study was conducted to provide an understanding of the north T-zone economic mineralogy and associated alteration assemblages. Ultimately, it is hoped that the results will be used to help simplify and optimize mineral beneficiation processes being developed to deal with the complex metallurgical problems encountered in the deposit.

Most of the work presented here has been based on standard optical petrography and qualitative, semi-quantitative and limited quantitative electron microprobe analyses.

II. GEOLOGY OF THE T-ZONE

The following chapter presents an overview of the geology of the T-zone. Included are descriptions at megascopic and microscopic scales of all rock types which comprise the northern portion of the deposit. The geologic history is documented by successive descriptions of the unmineralized and mineralized granite, the transecting zoned alteration assemblages and later cross-cutting unmineralized dykes.

The purpose of this chapter is to provide a basic understanding of the rocks which host the minerals of economic potential described in Chapter 3. The nature and occurrence of these economic minerals becomes meaningful only when put into context with their complex and diverse host alteration assemblages. In addition, a general familiarity with the gangue mineralogy is essential to the development of successful mineral beneficiation processes.

A. GENERAL GEOLOGY

As shown in Figure 2.1, the T-zone is an irregular north-northwest trending feature which extends for approximately 1 km along strike and varies in width to a maximum of about 250 m in the southern portion. The extent of mineralization down-dip is verified to a minimum depth of 150 m by diamond drilling and in part remains open.

In plan (Fig.2.1) the T-zone is easily divided into two parts: the subcircular body at the north end and the irregular shaped body which pinches and swells to the south. The north and south portions of the T-zone are joined at depth by a near vertically dipping, north-northwest trending dyke. The dyke is feldspathic in nature and appears to be joined to, and continuous with, the Wall zone alteration of the T-zone. The dyke extends the entire length of the T-zone and may eventually join with the Lake-zone deposit to the south although this has not yet been substantiated by diamond drilling. In the T-zone the feldspathic dyke ranges in thickness from 3 to 20 m, has been intersected at a depth of 150 m and remains open down-dip.

The dyke crops out at the southernmost tip of the T-zone as a result of uplifting along the prominent east-northeast, vertically dipping faults which truncate the T-zone at its southern end (Fig.2.1). As can be seen in Figure 2.1, at the southern terminus of the T-zone the dyke is centered at the western border of the alteration whereas at the north end of the T-zone the dyke is more centrally located relative to the alteration (Fig.2.2). This suggests that the locus of the dyke shifts from near the western border in the south towards the center of the alteration in the north. At present it is not known whether the feldspathic dyke extends north beyond the T-zone or simply pinches out at the north end of the deposit.

In cross-section (Fig.2.2) the T-zone reaches its maximum width at surface and narrows with depth, exhibiting a keel-like form. The alteration assemblages in general are well zoned and show a concentric layer-like orientation with some intercalation of units. The feldspathic dyke which is below, and continuous with, the outer Wall zone alteration, appears as the narrow neck at the base of the zoned alteration assemblages. Cross-section A-B (Fig.2.2), although specific to the north body, of the T-zone, is representative of geological cross-sections throughout the deposit.

The T-zone appears in longitudinal section as shown in Figure 2.3. Section C-D, which covers that part of the T-zone hosted by granite, crosses the subcircular north body and the northernmost extensions of the irregular south body. In longitudinal section, the alteration assemblages are seen to be sub-horizontally disposed and, as in cross-section, appear well zoned with some intercalation of units. Although the feldspathic dyke appears, in Figure 2.3, to plunge under the hemispherical north body, the view in this section is apparent. In longitudinal sections to the east and west of section C-D the dyke joins and is continuous with the Wall-zone alteration in the north body.

During the summer of 1984 over 800 m of diamond drill core, from the 10 holes available at that time (Fig.2.3), were sampled along longitudinal section C-D. This section was selected for sampling because it provided the quantity and variety of rock types needed to collect a complete and representative suite of samples suitable for use in this study. Supplementary samples from adjacent outcrops, trenches and underground workings were also collected in cases where textural and mineralogical variations of certain rock types were not apparent or available in drill core from holes along section C-D. All the information presented in this study is restricted to the granite-hosted part of the T-zone which includes the hemispherical north body and adjacent alteration to the immediate south as shown in longitudinal section C-D (Fig.2.3).

Having introduced the general geologic setting of the north T-zone, the remainder of this chapter is devoted to detailed descriptions of the seven basic rock types which comprise the deposit. These lithologic types are discussed in the order in which they appear on the legends in Figures 2.2 and 2.3. The descriptions start with the granite country rock, including unmineralized and mineralized varieties. Descriptions of the four alteration assemblages and their various units follow beginning with the Wall zone and proceeding on through the Lower and Upper Intermediate zones to the Quartz zone. Finally, the late cross-cutting, unmineralized felsite and diabase dykes are described to complete the detailed geology of the north T-zone.

Figures 2.1, 2.2 and 2.3 are referred to extensively in the following pages to illustrate the positioning and nature of contact relations between the various rock types. Field photographs and photomicrographs are included to supplement written descriptions and also to illustrate certain interesting textural and mineralogical features.

A tentative paragenetic sequence of mineralization is provided for each unit of the T-zone rock types based on the samples used in this study. It should be noted that although some minerals may appear in several different rock types, they are not necessarily comparable paragenetically. In particular, where several stages (designated 1, 2 and 3) of a mineral such as quartz are identified in one rock they may not necessarily be comparable to several stages of the same mineral (also designated 1, 2 etc.) observed in an alternate rock type.

B. GRANITE

The fresh and essentially unaltered Grace Lake granite proper is well described by Davidson (1978). The following description is based on work by Davidson (1978, 1982). The Grace Lake granite is a massive, coarse grained, equigranular riebeckite-perthite feldspar granite ranging in colour from reddish pink to pale greenish grey. Thin sections show that the fresh granite samples are composed of randomly oriented, euhedral mesoperthite feldspar with interstitial riebeckite and quartz. Fluorite (up to 1%), zircon and monazite are common accessories whereas apatite, sphene and magnetite are absent. Acmite occurs as overgrowths on riebeckite and is associated locally with astrophyllite. Biotite, which occurs exclusively as a secondary mineral, is rarely present and usually occurs with albite and hematite in place of reibeckite. The Grace Lake granite as described by Davidson (1978) contains the typical mineral suite of SiO_2-saturated agpaitic igneous rocks (Currie, 1976).

The granite samples examined in this study are either from areas in close proximity to the alteration assemblages of the north T-zone or from xenoliths within the alteration itself. All the samples studied are in various stages of alteration and replacement. Although these rocks retain their original granitic textures, in most cases little if any of the original mineralogy, as described by Davidson (1978), still exists. Granite of the T-zone is divided here into two types, unmineralized and mineralized. Unmineralized granite is defined here as granite which does not contain mineralization of economic interest whereas mineralized granite contains economically significant concentrations of Be-, Y- and REE-bearing minerals.

Unmineralized granite

Most unmineralized granite of the T-zone is found outside the zoned alteration. The large granite xenoliths within the zoned alteration show some evidence of REE mineralization but are to be considered here as essentially unmineralized. The samples of unmineralized granite described here are from immediately above and below the feldspathic dyke as it appears in Figure 2.3 and also from the large xenolith set within the hemispherical north body. All contacts, between granite and adjacent rock types, are sharp.

Megascopically, samples of unmineralized granite are much as described by Davidson (1978) and typically appear as in Plate 2.1a. The rock is medium to coarse grained, equigranular and ranges from greenish grey to pink in colour. It consists of euhedral to subhedral pink feldspar with interstitial grey-green mafic minerals and quartz. Interstitial fine grained fluorite, and late cross-cutting stringers and irregular patches of yellow carbonate (siderite ±ankerite) are common. Small patches of brick-red LREE-bearing fluocarbonates and late stage microcrystalline quartz are locally present as accessories.

In thin section the major components of the rock are feldspar, chlorite and biotite, quartz and Fe- and Ti-oxides. In some sections relict mesoperthite is preserved and locally is partially replaced by microcrystalline quartz along grain boundaries, fractures and albite lamellae as seen in Plate 2.1b. In most of the granite xenolith samples, all the feldspar is albite with K-feldspar present only as tiny anhedral blebs within the albite laths. It is possible that the original perthitic feldspar has been almost completely replaced in these areas through albitization. This replacement process might also explain the unusual, patchy and irregular twinning observed in the albite shown in Plate 2.2a. It should be noted that potassium feldspar is referred to simply as K-feldspar throughout the text because the structural state of the mineral was not determined as part of this study.

Chlorite and biotite are ubiquitous. Chlorite, the more abundant of the two, occurs as fine grained aggregates interstitial to, and along fractures in, feldspar (perthitic and albitic). Biotite also occupies feldspar interstices and is locally associated with the microcrystalline quartz replacement of feldspar.

At least three stages of quartz mineralization are evident in the samples studied. Anhedral, fine to medium grained quartz (1) aggregates occur interstitial to feldspar and contain abundant fluid and fine grained oxide inclusions. Chlorite and carbonate fill the interstices of this early quartz. Another phase of quartz (2) is anhedral, medium to coarse grained and contains fewer fluid and mineral inclusions than the earlier medium grained quartz (1) aggregates. Quartz (2) occurs interstitial to, and appears to replace, preexisting minerals including the earlier quartz (1) and, as seen in Plate 2.2a, feldspar. A later microcrystalline variety of quartz (3), present in some sections, mantles earlier mineral phases including the coarser grained quartz and sericite aggregates mentioned below. Microcrystalline quartz is also seen partially replacing earlier chlorite and perthitic feldspar as shown in Plate 2.1b. In one thin section, late microcrystalline quartz (3) has caused *in situ* brecciation of the granite.

Magnetite most commonly occurs in aggregates of fine grained euhedra associated with chlorite in feldspar interstices. Minor amounts of Ti-oxides are also present. Fe- and Ti-oxides also occur frequently as fine grained, euhedral inclusions in quartz (1 and 2). An unidentified mineral of prismatic habit (possibly acmite) is partially pseudomorphed by magnetite which is in turn replaced by quartz (2) as seen in Plate 2.2a. Columbite, intergrown with K-feldspar, occurs as the rounded opaque inclusions in albite shown in Plate 2.2a. Magnetite also occurs as similar rounded opaque inclusions in albite, though more rarely.

Minor ankerite and siderite are commonly associated with interstitial chlorite and also occur as patches and along fractures in feldspar. If the patchy carbonate present in thin section is related to the cross-cutting carbonate stringers seen in hand sample, it probably represents the latest mineral phase present. Although fluorite was not present in any of the thin sections, based on its mode of occurrence in hand sample, it is believed to be a late stage phase.

Other accessory minerals identified in thin section are sericite, zircon and LREE-bearing fluocarbonates. Sericite, present in one thin section, occurs as fine grained feathery aggregates (Fig.2.1b) which comprise rounded blebs up to 1.0 X 0.5 cm in size and are mantled by microcrystalline quartz (3). The sericite is unusual in that is is green in colour which, according to Beus and Zalashkova (1964), is typical of greisenized quartz-albite-rich rocks.

A euhedral zircon, observed in one thin section as an inclusion in perthitic feldspar, probably represents primary zircon as noted by Davidson (1978) and is not related to subsequent Zr mineralization present in the T-zone. Conversely, several small bipyramidal zircons, included in quartz (2) in a granite xenolith sample, are similar to zircons seen within the alteration zones and are probably related to the Zr mineralizing event. The REE-fluocarbonates occur as polycrystals formed by the syntaxic intergrowth of two or more minerals of the bastnaesite group. The anhedral polycrystals are typically enclosed in quartz or albite and, like zircon, are present in minor amounts only. Aside from the local presence of zircon and REE-fluocarbonates, the granite is essentially unmineralized and may be considered uneconomic.

A generalized paragenetic sequence of mineralization for the unmineralized granite is presented in Figure 2.4. Owing to the inhomogeneous nature of the rocks, not all the minerals listed will necessarily be present in a particular sample.

It is interesting to note that the only relict minerals from the original Grace Lake granite are perthitic feldspar and possibly some of the early quartz. Although unmineralized in terms of economic potential, the granite has been extensively altered and replaced.

Mineralized granite

All the samples of mineralized granite examined in this study are from the wedge of granite which lies between the southern footwall of the hemispherical north body and the northern hanging wall of the south body (Fig.2.3). Contacts between granite and adjacent alteration assemblages are sharp.

Megascopically, mineralized granite of the T-zone is similar in texture and mineralogy to unmineralized granite shown in Plate 2.1a. The mineralized granite samples studied contain medium to coarse grained, euhedral to subhedral feldspar which are greyish green to pink in colour. Fine grained greenish black mafics, locally mica- or magnetite-rich, and anhedral quartz occupy feldspar interstices. Fine grained, purple fluorite, which is more abundant in mineralized granite than in the unmineralized type, usually occurs in feldspar interstices associated with the mafic minerals. Less commonly, fluorite is present as euhedral inclusions in quartz or intergrown with the LREE (light rare earth element)-bearing fluocarbonates which latter occur in small irregular patches (a few mm in diameter) associated with the fine grained mafics or fluorite.

Occasionally the mineralized granite, and more rarely the unmineralized granite, display a "microbrecciated" texture as shown in Plate 2.2b. Pervasive replacement of feldspar by later mineral phases along grain boundaries, fractures and parallel to cleavage create this texture and not a dynamic process.

Although megascopically similar, mineralized granite in the T-zone may be distinguished from unmineralized granite in thin section by the presence, locally, of phenakite, bertrandite, LREE-bearing fluocarbonates, gadolinite and a Th-bearing silicate. In addition, the samples of mineralized granite examined in this study are generally more altered and mineralogically diverse than the unmineralized granite described above. The principal mineral constituents of mineralized granite apparent in thin section are feldspar, biotite, chlorite, quartz and Fe- and Ti-oxides. Fluorite and ankerite are common accessories and base-metal sulphides are sometimes present.

Three types of feldspar have been identified in different mineralized granite samples. The variation in feldspar mineralogy alone suggests that this particular rock type is very inhomogeneous. Perthitic feldspar, present in one section, is the least common of the three types. The perthitic feldspar is anhedral, medium to coarse grained and contains fine grained inclusions of euhedral magnetite and anhedral grains of fluorite. Biotite replacement of perthitic feldspar is common along fractures and grain boundaries and locally the perthite is overgrown by K-feldspar. Plate 2.3a suggests that the K-feldspar overgrowths and opaque pseudomorphs probably grew in an open space which was subsequently filled by quartz. The K-feldspar overgrowths, which are relatively unaltered and euhedral, are restricted to the open space areas. This relationship, between earlier perthitic feldspar and subsequent potassic-rich overgrowth, was only observed in one thin section but may be a paragenetic link with other samples.

In other thin sections, K-feldspar is the dominant type with no perthite and only minor albite present. Most of the K-feldspar is anhedral, medium grained and displays the unusual texture shown in Plate 2.3b. Fine grained biotite (±chlorite) and associated Fe- and Ti-oxides commonly occur replacing K-feldspar along fractures and grain boundaries. In addition to biotite, quartz and carbonate also replace K-feldspar locally as seen in Plate 2.4a. The K-feldspar itself contains inclusions of, and appears to have replaced, LREE-bearing fluocarbonate polycrystals as shown in Plate 2.3b.

In some of the mineralized granite samples, albite is the predominant feldspar type. Albite occurs as medium to coarse grained subhedral laths which show the patchy and irregular twinning seen in Plate 2.4b. K-feldspar, present in minor amounts in these samples, usually occurs as small, anhedral, turbid grains associated with LREE-bearing fluocarbonate polycrystals similar to the one shown in Plate 2.3b. K-feldspar is also present in the semi-opaque, rounded inclusions in albite shown in Plate 2.5a. The bleb-like inclusions are actually intergrowths of K-feldspar, biotite, ilmenite and a Th-bearing silicate as seen in the backscattered electron image shown in Plate 2.5b. The Th-silicate has been tentatively identified as a member of the thorite group and is referred to herein as thorite. These inclusions and the altered nature of the K-feldspar-REE-fluocarbonate association in the albite-rich granite, suggest that albite is probably the latest feldspar type.

Biotite and chlorite are ubiquitous throughout mineralized granite of the T-zone. Both are usually present in the rock but biotite is more abundant. Biotite shows two different habits, occurring either as stubby lath-like grains or as shreds of mica. The small lath-like grains are randomly oriented and generally occur in aggregates interstitial to, and replacing, all three feldspar types. The shreddy biotite also replaces feldspar but tends to grow in a particular orientation which is determined by the fractures in, and structure of, the feldspar that is being replaced. Both types of biotite are present in Plate 2.4a. More rarely, biotite is intergrown with K-feldspar, ilmenite and thorite in the bleb-like inclusions shown in Plates 2.5a and 2.5b. Chlorite occurs in fine grained aggregates interstitial to, and partially to entirely replacing, biotite as described above.

Most quartz in mineralized granite is fine to medium grained, anhedral and occurs as single grains and aggregates partially replacing all three feldspar types. Quartz also fills open space interstices as seen in Plate 2.3a. Quartz replacement of feldspar usually emanates from grain boundaries inwards but locally occurs along fractures as seen in Plate 2.4a. The quartz contains abundant inclusions of other mineral phases including shreddy biotite, fluorite, Fe- and Ti-oxides, carbonate and bertrandite. Very fine grained quartz is locally associated with magnetite and carbonate replacement of acmite as seen in Plate 2.4b. Rarely, fine grained quartz euhedra occur as inclusions in phenakite.

Magnetite is the most common oxide mineral in mineralized granite which is locally strongly magnetic. Magnetite frequently occurs as individual grains and aggregates in feldspar interstices enclosed by later quartz, biotite, chlorite or ankerite. Less commonly, magnetite and ilmenite are present as inclusions in feldspar. In Plate 2.3a an unidentified mineral is pseudomorphed by magnetite and in Plate 2.4b magnetite mantles and appears to be replacing acmite in albite. Minor amounts of ilmenite and Ti-oxides are occasionally associated with magnetite as described above. Columbite was observed in one thin section as minute inclusions in a LREE-bearing fluocarbonate polycrystal.

Fluorite and ankeritic carbonate are ubiquitous in mineralized granite. Fluorite, in particular, appears to have been present throughout the sequence of mineralization. Fine grained fluorite is present as an early phase, included in the three feldspar types and also occurs as inclusions in later quartz. Late stage fluorite, which is more abundant than the early inclusions, occurs interstitial to, and cross-cuts, earlier mineral assemblages. Most of the carbonate is ankeritic in composition and is probably the latest mineral phase. Ankerite typically occurs interstitial to earlier minerals such as quartz, feldspar and biotite and locally partially replaces feldspar (Plate 2.4a), acmite (Plate 2.4b) and REE-fluocarbonates. Rarely, ankerite is present as anhedral inclusions in quartz.

Acmite is the rarest of the gangue minerals. It typically occurs as altered prismatic grains in coarse grained albite. As can be seen in Plate 2.4b, most of the acmite has been replaced by magnetite, ankerite and microcrystalline quartz; only small patches of acmite remain towards the center of the grains. It is interesting to note that magnetite mantles the acmite and replaces it towards the center of the grain thereby preserving its prismatic outline. It is possible that the opaque pseudomorphs such as those in Plates 2.2a and 2.3a may represent acmite that has been completely replaced by magnetite. It should also be noted that the euhedral acmite observed in mineralized granite samples is probably not the same acmite as that described by Davidson (1978) as overgrowths on anhedral riebeckite in the Grace Lake granite. In contrast, acmite in mineralized granite of the T-zone is euhedral in outline and enclosed by albite. The secondary acmite may be related to an event of Na metasomatism.

Minerals of economic significance identified in the samples of mineralized granite studied here are phenakite, bertrandite, LREE-bearing fluocarbonates, gadolinite and thorite. Phenakite appears to be the latest phase of economic mineralization and usually occurs as anhedral, optically continuous grains, interstitial to quartz. Locally phenakite contains inclusions of quartz, K-feldspar and biotite. Bertrandite occurs as minute tabular inclusions in quartz and, in general, is quite rare. The LREE-bearing fluocarbonates are usually present as anhedral polycrystals enclosed in and being replaced by K-feldspar, ankerite and biotite. Gadolinite was identified in one thin section as a euhedral blocky inclusion in a K-feldspar-REE-fluocarbonate intergrowth. Thorite, intergrown with K-feldspar, biotite and ilmenite, occurs in the semi-opaque bleb-like inclusions in albite shown in Plate 2.5a.

Figure 2.5 presents a generalized paragenetic sequence of mineralization for mineralized granite of the T-zone. Owing to the inhomogeneity of the rocks, not all the minerals listed will neccessarily be present in a single sample.

Discussion

The similarity between Figures 2.4 and 2.5 suggests that unmineralized and mineralized granite of the T-zone are paragenetically comparable. The only relict mineral from the original Grace Lake granite in either granite type of the T-zone appears to be perthitic feldspar and possibly some early quartz. The principal differences between mineralized and unmineralized granite of the T-zone are:

a) their different locations within the T-zone

b) more alteration in mineralized granite

c) more fluorite, carbonate and biotite; and less chlorite in mineralized granite

d) the presence of Be and Y mineralization, in addition to REEs, in mineralized granite.

In terms of economic potential, granite of the T-zone contains significant concentrations of Be and REEs. Based on the samples studied, Y, Nb and Zr mineralization is rare and is probably not of economic interest.

C. WALL ZONE

The Wall zone mantles the other alteration assemblages of the T-zone as shown in Figures 2.1, 2.2 and 2.3. The feldspathic dyke which joins the north and south ends of the deposit at depth is essentially a continuation of the Wall zone and is considered here as part of the latter.

Feldspathic rocks of the Wall zone are subdivided into three lithologies based on mineralogical and textural differences. The three lithologic units within the Wall zone are: *breccia* (3A), *core* (3B) and *aplite* (3C). Each rock type forms a distinct mappable unit and occupies a particular position within the Wall zone. *Aplite*, in sharp contact with granite, is the outermost unit of the Wall zone. The *core* unit lies inside, and in sharp contact with, the *aplite* rock. Wall zone *breccia* is the innermost unit and lies in contact with rocks of the Quartz zone. Based on the samples used in this study, the feldspathic dyke appears to comprise only one of the three lithologic units of the Wall zone. All samples from the dyke are light pink, feldspathic and very fine grained which suggests that the dyke is continuous with the outer *aplite* unit of the Wall zone.

Descriptions of each Wall zone rock type follow, starting with the outer *aplite* unit and progressing inwards to the *core* and *breccia* units.

Aplite unit

Samples of the *aplite* unit used in this study are from Wall zone of the hemispherical north body (Fig.2.3) and the feldspathic dyke below (Fig.2.2). Megascopically, the rocks are fine grained or saccharoidal in texture and range from light pink to pinkish brown in colour. Initial mineralogical information on the feldspathic *aplite* rocks was obtained using a sodium cobaltinitrite solution to stain the *aplite* drill core samples for K-feldspar. Results of the staining indicated that there are actually two types of *aplite*. The first type, light pink in colour in hand sample, is composed mainly of K-feldspar and quartz. The second type, which is darker pinkish brown in colour, is albite-rich and contains minor amounts of K-feldspar and quartz. The quartz content is variable in both *aplite* types and usually occurs as irregular blebs interstitial to feldspar and as fine grained stringers. Fluorite is a common accessory and occurs interstitial to feldspar and in cross-cutting stringers. Minor fine grained mafics and brick-red REE-fluocarbonates are also present. The two varieties of the *aplite* unit are shown in hand sample in Plate 2.6a. The K-feldspar *aplite* is shown stained (yellow) and unstained (pink) to illustrate the abundance of potassic feldspar present in the rock.

Some of the Wall zone *aplite* observed in the underground workings displays primary banding towards the contact between the *aplite* and *core* units. The presence of banded *aplite* suggests that the Wall zone rocks, like the feldspathic dyke, are primary and do not represent alteration or replacement products of some preexisting rock type. The bulk of the Wall zone *aplite* seen underground is light pink in colour and is probably the K-feldspar type. At present, the mineralogy of the banded portions is unknown because samples of the banded rock were not collected for this study. However, it is possible that the presence of two varieties of *aplite*, in the drill core samples used here, is related to the banding.

K-feldspar aplite

The main mineral constituents of this unit are K-feldspar, quartz and fluorite. In thin section the feldspar is present as both anhedral grains and subhedral to euhedral blocky or lath-like grains. As seen in Plate 2.6b, the feldspar is typically fine grained, randomly oriented and may be untwinned or display an unusual mottled texture. It may comprise up to about 80% of the rock.

Aggregates of fine grained purple fluorite occur interstitial to, and locally contain inclusions of, K-feldspar. LREE-bearing fluocarbonates and an Fe-sulphide (pyrite or marcasite) are occasionally present as inclusions in fluorite. Fluorite occurs as fine grained rounded inclusions in later quartz.

Quartz (1) typically has two modes of occurrence. In some areas, anhedral grains of optically continuous quartz occupy feldspar interstices (Plate 2.6b) and locally form cross-cutting stringers. In other areas, aggregates of euhedral to anhedral quartz grains form large blebs which contain inclusions of, and partially replace, feldspar. Both types appear to be contemporaneous. In one thin section, a late stage microcrystalline quartz (2) is also present. The microcrystalline variety mantles the earlier quartz and partially replaces other preexisting mineral phases.

Columbite is the most common accessory in the K-feldspar *aplite* and appears to be the only oxide mineral present. It usually occurs as fine grained inclusions and small aggregates in quartz and in K-feldspar at grain boundaries.

Ankerite, chlorite, LREE-bearing fluocarbonates, bertrandite and phenakite are present as rare accessory minerals. Ankerite is a late stage phase which occurs in patches interstitial to earlier feldspar and quartz and locally replaces anhedral REE-fluocarbonate polycrystals. Fine grained aggregates of chlorite occur interstitial to earlier feldspar, fluorite, quartz and REE-fluocarbonates. Fine to medium grained anhedral LREE-bearing fluocarbonate polycrystals usually occur interstitial to K-feldspar (Plate 2.7a) and are included in, and being replaced by, later quartz, ankerite, fluorite and chlorite. This suggests that REE mineralization in this unit is a relatively early event. Bertrandite and phenakite were only noted in one thin section which, in conjunction with assay data, suggests that Be mineralization is probably of very limited extent in Wall zone *aplite*. Bertrandite, the earlier of the two Be-bearing minerals, occurs as minute tabular inclusions in euhedral to subhedral quartz. Phenakite occurs as fine, anhedral grains which are in optical continuity and appear interstitial to all preexisting mineral phases. It is replaced by microcrystalline quartz (2) at grain boundaries.

Figure 2.6 presents a generalized paragenetic sequence of mineralization for the K-feldspar *aplite* unit of the Wall zone. Not all the minerals listed are necessarily present in a particular rock.

Assay results indicate that the entire Wall zone has economically significant concentrations of Nb and Ga averaging 1.0% Nb_2O_5 and 500 ppm Ga. The K-feldspar *aplite* unit is probably a major contributor to Ga enrichment. Quantitative electron microprobe analyses (Table 3.4) indicate that K-feldspar in this unit contains up to 0.06 (±.01) weight % Ga, where Ga is substituting for Al^{3+}. The other minerals of economic interest present in the

K-feldspar *aplite* unit occur in minor amounts and even columbite, the most common accessory, is more abundant in other units of the Wall zone.

Albite aplite

This *aplite* unit is mainly comprised of albite, quartz, chlorite (±biotite) and columbite. As seen in Plate 2.7b, the albite is fine grained and typically occurs as randomly oriented, subhedral laths. Most feldspar laths display albite twinning and often contain fine grained inclusions of columbite. Albite interstices are most commonly occupied by quartz or chlorite (±biotite). Less frequently, fluorite is present in feldspar interstices and patches of ankerite occur interstitial to, and locally replace, albite laths.

Quartz usually occurs as anhedral grains interstitial to, and locally replacing, feldspar as seen in Plate 2.8a. Aggregates of fine grained quartz are also present and contain abundant inclusions of columbite euhedra as seen in Plate 2.8b. Fluorite and chlorite (±biotite) occur interstitial to quartz.

Chlorite and biotite are ubiquitous in the albite *aplite* rock, filling feldspar and quartz interstices. They usually occur together in fine grained aggregates where chlorite, the more abundant of the two, replaces biotite. Rarely, euhedral lath-like grains of biotite are present interstitial to fine grained quartz, usually associated with fluorite. Chlorite (±biotite) aggregates commonly enclose columbite and are locally associated with fluorite. Plate 2.7b shows a typical chlorite aggregate interstitial to albite.

Columbite appears to be the only oxide mineral present and generally occurs as fine grained, euhedral inclusions in quartz, albite and K-feldspar (Plate 2.8b). In one thin section, a stringer of columbite cross-cuts albite and quartz.

Ankerite, fluorite, K-feldspar and LREE-bearing fluocarbonates are present as accessory phases in albite *aplite* rocks. Ankerite occurs as irregular patches interstitial to, and replacing, albite (Plate 2.7b). Fluorite, associated with chlorite and biotite, occupies quartz interstices and locally replaces REE-fluocarbonate polycrystals. Patches of altered K-feldspar usually appear as in Plate 2.8b partially replaced by quartz and biotite. Small blebs of

LREE-bearing fluocarbonate polycrystals appear to be included in albite aggregates and more rarely are replaced by fluorite in quartz interstices.

A generalized paragenetic sequence of mineralization for the albite *aplite* unit of the Wall zone is given in Figure 2.7.

The albite *aplite* unit of the Wall zone is probably a major contributor to the Nb and Ga enrichment of the Wall zone. High Nb values can be attributed to the abundance of columbite in the rocks. Ga, which substitutes for the Al^{3+} in albite, is particularly enriched in this albite-rich unit of the Wall zone. Quantitative electron microprobe analyses indicate that albite in this unit may contain up to 0.5 weight % Ga.

Core unit

The *core* unit of the Wall zone lies inside, and in sharp contact with, the *aplite* unit. Samples of the *core* unit used in this study are from Wall zone of the hemispherical north body and the northern extension of the south body (Fig.2.3).

Megascopically, the rocks are medium to coarse grained, inequigranular and range from light pink to reddish-pink in colour. The sodium cobaltinitrite staining solution indicates that the *core* unit is comprised of coarse, blocky grains of white or light pink K-feldspar (stained yellow) which are overgrown and replaced by individual grains and aggregates of darker pink platy albite (cleavelandite) as seen in Plate 2.9a. The albite commonly forms in radiating aggregates and may constitute 20-60% of the rock. The K-feldspar content is variable, depending on the amount of albite replacement, and ranges from approximately 35-75%. Fine grained mafics occur as inclusions in both feldspar types; and minor quartz, fluorite and carbonate occur in irregular patches and as fine grained cross-cutting stringers. A typical hand sample of the *core* unit and a stained slab are shown in Plate 2.9a.

Rocks of the *core* unit are mineralogically simple. In thin section the main mineral constituents are K-feldspar and albite with minor quartz, chlorite, columbite, carbonate and fluorite. The K-feldspar is coarse grained and displays the patchy twinning seen in Plate 2.9b. In one thin section, irregular patches of an earlier K-feldspar are present. As can be seen in

Plate 2.9b, the earlier feldspar is strongly altered and is being replaced at grain boundaries by the later, dominant K-feldspar. The early, altered potassic feldspar appears similar to the K-feldspar in the albite *aplite* unit shown in Plate 2.8a and may be related to that Wall zone unit. The later K-feldspar contains minor inclusions of columbite and is cross-cut by fine grained stringers of quartz, fluorite or carbonate. Minor quartz and fluorite occur interstitial to K-feldspar.

In thin section, albite typically appears as fine to medium grained, subhedral laths overgrowing K-feldspar. The laths usually display albite twinning and are randomly oriented as in Plate 2.10a. Locally the laths form radiating aggregates growing into K-feldspar as shown in Plate 2.10b. Albite interstices are commonly occupied by quartz, chlorite or fluorite (Plate 2.10a) and fine grained columbite inclusions are present locally.

Quartz occurs as fine, anhedral grains interstitial to, and locally replacing, albite and K-feldspar. Quartz commonly contains abundant fine grained inclusions of columbite and fluorite. Rarely, it contains fine grained tabular inclusions of bertrandite and occasionally occurs as stringers cross-cutting the feldspars, in association with late fluorite and carbonate.

Chlorite is present as fine grained aggregates which occur interstitial to albite laths and locally enclose columbite to form bleb-like inclusions in albite. Columbite occurs as fine grained, euhedral to subhedral inclusions and aggregates in quartz, albite and K-feldspar. Columbite is most abundant in, and adjacent to, the patches of early, altered K-feldspar (Plate 2.9b) which suggests that Nb mineralization was predominant at an earlier time in this unit.

Purple fluorite appears to be present at several stages of the mineralization sequence in the *core* unit rocks. Early fluorite occurs as fine grained inclusions in quartz. Later stage fluorite occurs interstitial to the two feldspar types and associated with carbonate in late cross-cutting stringers. Carbonate is present as a late stage phase interstitial to, and locally replacing, the feldspars. It also occurs as cross-cutting stringers associated with fluorite. Bertrandite was observed in one thin section as minute tabular inclusions in quartz.

Figure 2.8 presents a generalized paragenetic sequence of mineralization for the *core* unit of the Wall zone.

The presence of columbite and Ga-bearing albite and K-feldspar in the *core* unit contribute to the overall Nb and Ga enrichment of the Wall zone.

Breccia unit

Wall zone *breccia*, the innermost unit, is typically present where Wall zone rocks lie in contact with the Quartz zone (Fig.2.3). All samples used in this study are from trenches in the subcircular north body (Fig.2.1) where the *breccia* unit is present in outcrop.

Megascopically, the *breccia* unit appears as in Plate 2.11a. The rock contains large blocky fragments of the *core* unit imbedded in a matrix of medium to coarse grained quartz. The feldspathic fragments are very angular and generally in parallel alignment which suggests passive *in situ* brecciation by the quartz. The fragments of *core* unit are slightly darker pink in colour due to weathering and they have narrow reaction rims as seen in Plate 2.11b. The reaction rims are dark grey to black in colour and appear to be composed of fine grained mafics. Patches of fine grained mafics and pale green sericitic alteration occur interstitial to feldspar within the fragments. Small mafic aggregates and patches of fine grained purple fluorite are present in the matrix quartz.

In thin section, rocks of the *breccia* unit are similar to those of the *core* unit. The principal differences are an increase in quartz and columbite content and the introduction of sericite in the *breccia* unit. In addition, albite is more abundant than K-feldspar in the fragments of *core* unit. Both feldspar types are more altered in the *breccia* unit. Patches of K-feldspar in particular are partially to entirely replaced by fine grained aggregates of sericite. The sericite also occurs interstitial to albite and replaces the feldspar along fractures and grain boundaries. The micaceous alteration is often associated with bleb-like inclusions of columbite and is locally replaced by later fluorite and carbonate.

Quartz, in thin section, is anhedral, medium grained and occurs in aggregates replacing both feldspars. Individual grains and aggregates of columbite are commonly present at the feldspar-quartz boundary and the feldspar is typically altered in appearance. The increased abundance of columbite in the *breccia* unit, its association with the late sericitic alteration and its presence at quartz-feldspar boundaries suggests that at least some of the columbite is a late stage phase, possibly introduced during brecciation.

Subhedral monazite and anhedral LREE-bearing fluocarbonate polycrystals were identifed in one thin section of the *breccia* unit as inclusions in quartz and a fluorite-carbonate intergrowth. These minerals are also probably late stage phases.

A paragenetic sequence of mineralization for the *breccia* unit has not been included because it is essentially the same as that for the *core* unit (Fig.2.8). The only changes would be the extension of the quartz and columbite lines and addition of sericite and the REE-bearing minerals as late stage phases.

In terms of economic significance, the *breccia* unit is probably the least important of the Wall zone units. Although is has more columbite and albite than K-feldspar within the actual fragments of *core* unit, the Nb and Ga enrichment of the *breccia* unit as a whole is diluted by the abundance of quartz. REE mineralization in the *breccia* unit appears quite limited and is probably not of economic interest.

Discussion

A comparison of Figures 2.6, 2.7 and 2.8 suggests that each unit of the Wall zone is paragenetically unique. However, in general the earliest phase in each unit is always feldspar with quartz and biotite-chlorite as the dominant later phases. Fluorite and carbonate are usually the latest minerals. Columbite is present throughout the mineralization sequence of the Wall zone as a whole which suggests a lengthy period of Nb mineralization. Several different ages of quartz may also be represented between the various units.

In addition, several metasomatic events are evidenced by the Wall zone rocks. The outer K-feldspar *aplite* unit is probably the result of initial potassic metasomatism. Subsequent albitization or sodium metasomatism is evident in the *core* unit rocks where earlier K-feldspar is overgrown and replaced by albite. Abundant matrix quartz in the *breccia* unit suggests a later silicification event.

Overall, columbite and Ga-bearing feldspar are the principal minerals of economic interest in the Wall zone. Based on the samples used in this study, Ga mineralization is predominant in the feldspar-rich *aplite* and *core* units and to a lesser extent in the *breccia* unit. Ga content is higher in albite than K-feldspar which suggests that the albite-rich rocks are the largest contributors to Ga enrichment in the Wall zone. Columbite is predominant in the albite *aplite* unit and to a lesser extent in the *core* and *breccia* units. The columbite content of the K-feldspar *aplite* unit is probably of minor importance. Bertrandite, monazite and LREE-bearing fluocarbonates are not present in economically significant quantities.

D. LOWER INTERMEDIATE ZONE

The Lower Intermediate zone lies inside, and in sharp contact with, the enclosing Wall zone. The rocks are in gradational contact and intercalated with overlying rocks of the Upper Intermediate zone. Contacts with the granite xenoliths within the hemispherical north body are sharp. As seen in Figure 2.3, the Lower Intermediate zone is present in both the north body and northern extension of the south body of the T-zone.

Rocks of the Lower Intermediate zone have been divided into three lithologic units based on textural and mineralogical differences. For mapping convenience each unit is referred to by the megascopic mineral assemblage which characterises the rock. The units are: *quartz-biotite(±chlorite)-oxides* (4A), *quartz-biotite(±chlorite)-feldspar* (4C) and *quartz-magnetite* (4E). The *quartz-magnetite* unit is the outermost unit of the Lower Intermediate zone and lies in contact with the Wall zone. This unit appears to be restricted to the hemispherical north body. Rocks of the *quartz-biotite(±chlorite)-feldspar* unit are present in the north and south bodies. Rocks of this unit locally contain relict granitic textures and are postulated to be altered granite. The *quartz-biotite(±chlorite)-oxides* unit is similar to the *quartz-biotite(± chlorite)-feldspar* unit but contains only minor amounts of feldspar and lacks relict granitic textures. Contacts between these two units, which comprise the majority of the Lower Intermediate zone, are irregular and gradational.

Quartz-magnetite unit

The *quartz-magnetite* unit is the wedge of Lower Intermediate zone which lies between the Wall zone and Upper Intermediate zone in the hemispherical north body as seen in Figure 2.3. The rocks are fine grained, black in colour and strongly magnetic. They are composed of patches of dark brown magnetite enclosed in a black, fine grained matrix. Small blebs of a later, medium grained quartz occur interstitial to and partially replacing, magnetite. Purple fluorite and yellow carbonate are present as late stage cross-cutting stringers. A typical sample of the *quartz-magnetite* unit is shown in Plate 2.11b.

In thin section the main mineral constituents of this unit are magnetite, quartz, biotite and K-feldspar. Accessory phases include columbite, ilmenite, a Ti-oxide, fluorite, zircon and bastnaesite.

Most magnetite is present as very fine grained, euhedral to subhedral individual grains and larger grain aggregates which appear to be overgrowing and replacing altered K-feldspar as seen in Plate 2.12a. Fine grained biotite, quartz and fluorite occupy interstices within the magnetite aggregates. Magnetite also occurs as tabular to acicular pseudomorphs after an unidentified mineral (possibly acmite) similar to those seen in other rock types of the T-zone (see Plate 2.3a). These magnetite pseudomorphs are included in, and partially replaced by, fine to medium grained quartz.

Fine grained quartz is usually intergrown with biotite in the matrix material which encloses magnetite and replaces K-feldspar. A later medium grained quartz occurs as irregular blebs replacing earlier phases. Zircon and the magnetite pseudomorphs are present as inclusions in medium grained quartz.

Biotite is present as anhedral fine grains and grain aggregates interstitial to magnetite and intergrown with quartz in the matrix where it replaces K-feldspar and locally mantles magnetite.

K-feldspar occurs as anhedral, altered grains within the fine grained matrix of the rock. The feldspar is probably the earliest phase present and is overgrown by magnetite (Plate 2.12a) and replaced by fine grained biotite and quartz in the matrix.

Columbite is the most abundant of the accessory oxide minerals and occurs as fine grained inclusions in magnetite and quartz. Ilmenite is present as needle-like inclusions in bastnaesite and adjacent quartz. A Ti-oxide is present rarely intergrown with magnetite. Fine grained fluorite is present locally interstitial to magnetite and intergrown with matrix biotite and quartz.

Aside from columbite, zircon and bastnaesite are the only minerals of economic interest present. Zircon occurs as bipyramidal inclusions in late medium grained quartz. Qualitative electron microprobe analyses indicate that all the LREE-bearing fluocarbonate grains present in the rocks studied here are of the bastnaesite composition and are not polycrystals as seen in other rocks. Bastnaesite usually occurs as anhedral grains partially replaced by magnetite, quartz and fluorite. Locally bastnaesite is mantled by K-feldspar and occurs rarely as minute inclusions in columbite. Thorite is occasionally present as fine grained inclusions in bastnaesite. The economic potential of this unit is probably limited to the minor Nb mineralization indicated by the local presence of columbite.

Figure 2.9 presents a generalized paragenetic sequence of mineralization for the *quartz-magnetite* unit of the Lower Intermediate zone.

Quartz-biotite(±chlorite)-feldspar unit

In the hemispherical north body, rocks of this unit lie between the large central granite xenolith and underlying layer of Upper Intermediate zone (Fig.2.3). In the south body, rocks of this unit are present throughout the Lower Intermediate zone in gradational and irregular contact with rocks of the *quartz-biotite(±chlorite)-oxides* unit. Rocks of the *quartz-biotite(±chlorite)-feldspar* unit are texturally and mineralogically variable. Due to its characteristic inhomogeneity, every variation of this rock type cannot be described. However, the rocks are all similar to a certain extent and the following description is an attempt to present a general overview.

Megascopically, rocks of this unit are typically fine to medium grained and light to dark grey in colour. They usually consist of fine grained mafics (locally micaceous) with isolated patches of pink feldspar and blebs and veinlets of quartz. Small patches of brick-red REE-fluocarbonates are commonly locally disseminated throughout the mafic rock and base metal sulphides are sometimes present. Purple fluorite and yellow carbonate occur as late stage cross-cutting stringers and patchy intergrowths. Locally, relict granitic textures are preserved within the dark altered rock of this unit as seen in Plate 2.12b.

In thin section the main mineral constituents of the unit are albite, K-feldspar, biotite, chlorite, quartz and phenakite. Accessory phases include: fluorite, ankerite and siderite, LREE-bearing fluocarbonates, columbite, magnetite, ilmenite, rutile, sphalerite, an Fe-sulphide, thorite, zircon, monazite and a member of the helvite group.

K-feldspar appears to be the earliest major phase present in this unit. It typically occurs as turbid anhedral, fine grains and grain aggregates overgrown and partially to entirely replaced by biotite as seen in Plate 2.13a. In most samples, where it is preferentially replaced by biotite aggregates, K-feldspar is present in minor amounts. Conversely, K-feldspar-rich samples are noticeably biotite-poor. Anhedral, LREE-bearing fluocarbonate polycrystals are commonly enclosed in, and partially replaced by, K-feldspar.

Albite is the predominant feldspar type in this unit and is usually present as fine to medium grained, subhedral laths. The laths are randomly oriented and display the patchy, irregular twinning typical of albite in the granite described earlier (see Plate 2.4b). Albite is typically overgrown and partially replaced by shreddy or lath-like biotite as shown in Plate 2.13b or by aggregates of fine grained biotite. Locally the biotite aggregates develop within the individual albite laths where inclusions of relict K-feldspar are present. Albite occasionally contains fine grained inclusions of columbite.

Biotite occurs as above, replacing both feldspar types but K-feldspar preferentially. It appears as fine to medium grained, subhedral lath-like or shreddy grains overgrowing and replacing albite as in Plate 2.13b. Fine grained biotite is also present as aggregates overgrowing K-feldspar as in Plate 2.13a and replacing albite along grain boundaries. The two types of biotite are locally intergrown and appear to be contemporaneous. Biotite aggregates commonly enclose fine grained columbite. Rarely, very fine grained aggregates of biotite enclose thorite and occur as greenish brown bleb-like inclusions in quartz and feldspar similar to those shown in Plate 2.5a.

Chlorite occurs as fine grains and aggregates interstitial to, and replacing, earlier biotite. It is less abundant than biotite and is not present in all samples.

Quartz is usually present as irregular patches composed of anhedral, fine to medium sized grains which replace both feldspar types. Subhedral lath-like and shreddy grains of biotite are commonly enclosed in, and partially replaced by, quartz. Aggregates of fine grained biotite(±chlorite) are often present at grain boundaries within quartz blebs. Columbite, magnetite, rutile, fluorite and zircon occur locally as very fine grained inclusions in quartz. Rarely, a late stage microcrystalline variety of quartz is present mantling and partially replacing earlier phases.

Phenakite appears to be the latest major phase present in this unit. It typically occurs as fine grained, anhedral optically continuous grains interstitial to quartz, fluorite or biotite. Individual grains of phenakite commonly contain euhedral inclusions of quartz and fluorite, and less frequently biotite and oxides. Rarely, subhedral phenakite grains are enclosed in ankerite.

Fluorite and carbonate are the most common accessory phases. Both appear to have been present throughout the latter part of the mineralization sequence in this unit. As early phases, fluorite and carbonate occur as minute anhedral inclusions in quartz. As later phases, both minerals are present interstitial to, and locally include or replace, all earlier phases. Carbonate in this unit varies in composition from ankerite to siderite but ankerite is predominant.

Subhedral to anhedral LREE-bearing fluocarbonate polycrystals are common accessories in this unit and are invariably associated with K-feldspar. The REE minerals appear to be included in, and partially replaced by, feldspar. Locally the polycrystals (±feldspar) are partially replaced by fluorite or ankerite, or enclosed in biotite aggregates. Rarely, the polycrystals form radiating acicular aggregates in quartz.

Columbite, magnetite, ilmenite and rutile are present in minor amounts throughout rocks of this unit. Columbite occurs as inclusions in feldspar, quartz and enclosed in biotite aggregates. The Fe- and Ti-oxides are locally present as fine grained euhedral to subhedral inclusions and aggregates in quartz, biotite, carbonate and phenakite. Rarely, sphalerite and an Fe-sulphide occur as inclusions in quartz.

Thorite, sometimes associated with magnetite, occurs as above enclosed in biotite to form semi-opaque bleb-like inclusions in quartz and feldspar. Zircon is a rare accessory phase and is present as euhedral inclusions in quartz. Euhedral to subhedral monazite grains were observed in one sample in ankerite associated with subhedral phenakite. In one thin section, a minute grain of a member of the helvite group was identified as an inclusion in phenakite.

The *quartz-biotite(±chlorite)-feldspar* unit is economically significant in terms of Be and to a lesser extent REE mineralization. High Be assays within the unit are attributed to the abundance of phenakite identified in thin section. LREE enrichment in these rocks is primarily due to the local presence of REE-fluocarbonates and monazite to a lesser extent. Quantitative electron microprobe analyses of some albite in this unit (Table 3.3) indicates that there is Ga mineralization present although it is probably of limited economic importance relative to the feldspar-rich Wall zone rocks. Based on the minor amount of columbite seen in the samples studied here, the Nb potential of the unit is probably not significant.

Figure 2.10 presents a generalized paragenetic sequence of mineralization for the *quartz-biotite(±chlorite)-feldspar* unit of the Lower Intermediate zone. Due to the inhomogeneity of the rocks, not all the minerals listed will neccessarily be present in a particular sample.

Quartz-biotite(±chlorite)-oxides unit

Rocks of this unit are present in the north and south bodies of the T-zone and are in irregular and gradational contact with the *quartz-biotite(±chlorite)-feldspar* unit described above. These rocks are inhomogeneous but in general are fine to medium grained and dark grey to black in colour. They are typically composed of micaceous aggregates and patches of fine grained mafics. Quartz occurs as irregular blebs interstitial to, and locally replaces, the mafic phases. Patches of yellow to light pink coloured carbonate also occur between mafic areas associated with quartz and, locally, with fluorite. Small patches of brick-red REE-fluocarbonates occur within the mafic material and quartz blebs. Yellow to buff coloured carbonate also commonly appear as late cross-cutting stringers. Megascopically rocks of this unit are distinguished from those of the *quartz-biotite(±chlorite)-feldspar* unit by a general lack of feldspar and relict granitic textures. A typical mica-rich sample of the *quartz-biotite(±chlorite)-oxides* unit is shown in Plate 2.14a.

In thin section, the main mineral constituents of this unit are quartz, biotite (±chlorite), Fe-, Ti- and Nb-oxides and phenakite. Common accessories include ankerite and siderite, fluorite, K-feldspar and REE-fluocarbonates. Zircon, xenotime, thorite, a REE-bearing silicate, a Nb,U-bearing oxide, monazite, bertrandite, an Fe-sulphide, sphalerite, bertrandite and rhodocrosite are present less commonly.

At least three stages of quartz are represented in rocks of this unit. The earliest quartz (1) occurs as aggregates of fine grained, anhedral quartz with interstitial carbonate or biotite. The aggregates of quartz (1) are typically enclosed in, and replaced by, a coarser grained quartz (2). The second type of quartz (2) is medium grained, subhedral to anhedral and appears less altered than the earlier quartz (1) . It replaces earlier quartz (1) and associated carbonate and biotite. It also replaces medium grained, lath-like biotite and commonly contains inclusions of columbite, Fe- and Ti-oxides and REE-fluocarbonates. The third type of quartz (3) is a microcrystalline variety which is a late phase. It appears interstitial to, and partially replaces, all preexisting minerals including the earlier types of quartz. Locally microcrystalline quartz forms cross-cutting stringers.

Most biotite in this unit is medium to coarse grained and occurs as lath-like grains which are partially replaced by quartz (2 and 3), fluorite and columbite aggregates (see Plate 2.14b). Locally, an unidentified shreddy, colourless mica also replaces biotite. Jambor (1985) described a similar mica in Be-rich rocks from the north T-zone deposit which he tentatively identified as lepidolite. The shreddy mica seen in rocks of this study may also be lepidolite.

Aggregates of fine grained biotite are also present commonly associated with carbonate and columbite in quartz (1) interstices. Locally the fine grained biotite aggregates overgrow and partially replace K-feldspar and associated REE-fluocarbonates. Plate 2.15a shows biotite aggregates and later chlorite. Fine grained biotite is present as inclusions in quartz (2) and phenakite and the aggregates are partially replaced by quartz (3), fluorite and later carbonate. Quantitative electron microprobe analyses (Table 2.1) indicate that the two types of biotite (medium grained and fine grained) are compositionally similar and may contain up to 2.57 weight % F. Most biotite is compositionally homogeneous within a single grain but varies from one grain to another within a single sample. One medium grained lath-like biotite (sample 15-5 in Table 2.1) shows compositional variation mainly in terms of Fe and Mg within a single grain. Rarely, biotite is present as semi-opaque bleb-like inclusions in quartz (2) intergrown with ilmenite, thorite and REE-fluocarbonates. This type of biotite was not analysed.

Chlorite is present in minor amounts in this unit as fine grained, feathery aggregates interstitial to and replacing both biotite types (see Plate 2.15a). Based on compositional data presented in Table 2.1 the chlorite in this unit may be classified either as brunsvigite according to Hey's (1954) system of nomenclature, or as magnesian chamosite according to a more recent classification scheme suggested by Bayliss (1975).

Columbite is the predominant oxide mineral and usually occurs as fine grained, euhedral to subhedral, individual grains and grain aggregates included in quartz (2) or replacing biotite. It is most abundant in the biotite-rich samples such as that shown in Plate 2.14a. Occasionally columbite contains minute inclusions of a Nb,U-bearing oxide and bastnaesite. Ilmenite occurs as euhedral inclusions in lath-like biotite (Plate 2.14b) and later quartz and phenakite. Ti-oxides are common as fine grained, euhedral inclusions in quartz (2) and phenakite.

Phenakite is present in most of the samples studied. It typically occurs as anhedral, optically continuous grains interstitial to quartz (1 and 2) and biotite. Phenakite locally contains inclusions of quartz, fluorite, ankerite, siderite, a Ti-oxide, ilmenite, biotite, chlorite and REE-fluocarbonates. It is probably the latest mineral present except for late stage cross-cutting stringers of carbonate and fluorite.

Ankerite, siderite and fluorite appear to have been present throughout much of the mineralization sequence of the *quartz-biotite(±chlorite)-oxides* unit. Both carbonates are present as early phases interstitial to quartz (1) and as anhedral inclusions in quartz (2) and phenakite. This early carbonate usually partially replaces biotite, K-feldspar and REE carbonates and locally encloses columbite aggregates. Fluorite is present as euhedral to anhedral inclusions in quartz (2) and phenakite and like the carbonate replaces earlier biotite. As late stage minerals, ankerite(±siderite) and fluorite form stringers which cut all previous assemblages.

K-feldspar is an accessory phase and occurs exclusively as small anhedral relict grains within biotite aggregates. Subhedral to anhedral LREE-bearing fluocarbonate polycrystals are typically enclosed in, and partially replaced by, biotite(±chlorite) aggregates and carbonate. Locally the REE-fluocarbonates are in relict K-feldspar grains. Less commonly, they are included in quartz.

Two types of zircon were identified in two unusual samples of the *quartz-biotite(±chlorite)-oxides* unit. In one sample, fine grained, euhedral, strongly zoned zircons comprise up to 20% of the thin section. This type of zircon is locally included in quartz with interstitial biotite (±chlorite) and columbite. In another thin section, thin rims of zircon are present as overgrowths on corroded ovoids of xenotime. The xenotime-zircon grains are enclosed in quartz (2). Thorite occurs locally with ilmenite and biotite as bleb-like inclusions in quartz (2). A REE-bearing silicate was identified in one thin section as a fine grained intergrowth with monazite and REE-fluocarbonates in quartz (2). The REE-bearing silicate has been tentatively identified as britholite. A Nb,U-bearing oxide is present rarely as minute inclusions in columbite and has been tentatively identified as ashanite. Monazite is present locally associated with the britholite and xenotime. Rarely, bertrandite is present as minute inclusions in fine to medium grained, subhedral quartz (2). An Fe-sulphide, sphalerite and rhodocrosite are rare accessory phases and are most commonly associated with quartz.

Be and Nb enrichment in this unit are directly attributable to the presence of phenakite and columbite which are the most abundant economic minerals in the *quartz-biotite(±chlorite)-oxides* unit. REE enrichment in this unit is of lesser importance and is mainly due to local concentrations of REE-fluocarbonate polycrystals. Zr mineralization appears to be very limited spatially although it may be quite concentrated in a small area. Based on the samples studied here, Y mineralization in this unit is not economically significant.

Figure 2.11 presents a generalized paragenetic sequence of mineralization for the *quartz-biotite(±chlorite)-oxides* unit of the Lower Intermediate zone. In general, the mineralogy of this unit is similar to that of the *quartz-biotite(±chlorite)-feldspar* unit (Fig.2.10) but more diverse. Due to the characteristic inhomogeneity of the rocks, not all the minerals listed in Figure 2.11 will be present in a particular sample.

Discussion

A comparison of Figures 2.9, 2.10 and 2.11 suggests that the *quartz-biotite(±chlorite)-feldspar* and *quartz-biotite(±chlorite)-oxides* units are paragenetically similar whereas the *quartz-magnetite* unit is unique. However , certain generalizations may be applied to all units of the Lower Intermediate zone. Feldspar, where present, is always the earliest phase and is overgrown or replaced by Fe-rich minerals such as magnetite or biotite. Quartz, carbonate and fluorite are ubiquitous in these rocks and are present throughout much of the sequence of mineralization. Nb and REE mineralization also appear to have occurred over lengthy time periods. Be mineralization in contrast is restricted to the later stages of the paragenetic sequence.

The most striking feature of the Lower Intermediate zone is the mafic nature of the rocks due to the predominance of Fe-rich minerals. The abundance of magnetite and biotite(±chlorite) in these rocks may be the result of Fe metasomatism and distinguishes the Lower Intermediate zone from other alterations assemblages within the T-zone.

Overall, phenakite and columbite are the principal minerals of economic interest in the Lower Intermediate zone. LREE-bearing fluocarbonates, Ga-bearing albite and zircon are of lesser importance being restricted to local concentrations within a single unit. Y mineralization within this zone appears to be sparse. The *quartz-biotite(±chlorite)-feldspar* and *quartz-biotite(±chlorite)-oxides* units show the greatest economic potential of the Lower Intermediate zone rocks.

E. UPPER INTERMEDIATE ZONE

Most of the Upper Intermediate zone rocks have gradational boundaries and are intercalated with adajcent rocks of the Lower Intermediate zone and the overlying Quartz zone. As can be seen in longitudinal section (Fig.2.3), the Upper Intermediate zone also appears as small lenses isolated in the Quartz zone. In the northern portion of the T-zone, rocks of the Upper Intermediate zone are confined to the hemispherical body as seen in Figure 2.3. These rocks appear in the larger, irregular body in its southern extension as seen in Figure 2.1. All samples used in this study are from the hemispherical north body.

Rocks of the Upper Intermediate zone are subdivided into six separate lithologies because they are the most mineralogically and texturally diverse rocks in the T-zone. Each lithology forms a distinct mappable unit and is defined by a characteristic mineral assemblage. For mapping convenience each unit is referred to by the megascopic mineral assemblage which characterises the rock. The units are: *quartz-mica* (5A), *quartz-mica-feldspar* (5B), *quartz-feldspar* (5C), *quartz-feldspar-magnetite* (5D), *quartz-bastnaesite group* (5E) and *quartz-thorite* (5F). The order in which the units occur are listed is the result of successive additions as geological mapping progressed and does not neccessarily indicate spatial or temporal relationships between the different rock types.

The *quartz-thorite* unit lies in the central part of the Upper Intermediate zone between the Lower Intermediate and Quartz zones. It also occurs below the large granite xenolith in gradational contact with the biotite-rich units of the Lower Intermediate zone. The *quartz-bastnaesite group* unit lies at the upper boundary of the Upper Intermediate zone intercalated with the Quartz-zone (Fig.2.3). The *quartz-feldspar-magnetite* unit is present locally where Upper Intermediate zone rocks are in direct contact with the Wall zone. The *quartz-feldspar* unit is the wedge of Upper Intermediate zone which separates the magnetite-rich Lower Intermediate zone from the biotite-rich units. The *quartz-feldspar* unit also occurs in the central part of the Upper Intermediate zone above the Lower Intermediate zone and large granite xenolith. The remaining two units are in gradational contact with each other and the *quartz-feldspar* unit. The *quartz-mica* and *quartz-mica-feldspar* units are located in the upper part of the zone at the footwall of the Quartz zone and *quartz-bastnaesite* unit. The central Upper Intermediate zone commonly contains lenses of Quartz zone (Fig.2.3). A description of each Upper Intermediate zone lithologic unit follows.

Quartz-thorite unit

The *quartz-thorite* unit is in gradational contact with the *quartz-feldspar* unit above and below with the Lower Intermediate zone biotite-rich units. All the samples used in this study are from the hemispherical body (Fig.2.3) except one which is from a lens of alteration in granite below the north body.

Rocks of this unit are easily identified in the field and drill core by their characteristic radioactivity. Megascopically, the rocks are typically fine grained and reddish brown in colour. They are principally composed of quartz and irregular patches of fine grained reddish brown material intergrown with dark purple fluorite and dark green mica and chlorite. Locally the rocks contain small patches of brick-red REE-fluocarbonates and late cross-cutting stringers of buff coloured carbonate. In quartz-rich samples, the reddish brown material forms unusual vermiform features in quartz. Rocks of this unit are weakly to strongly sheared. Plate 2.15b shows a typical hand sample of the *quartz-thorite* unit and a quartz-rich drill core sample to illustrate the vermiform features described above.

In thin section, rocks of this unit are composed mainly of quartz, fluorite and complex, fine grained intergrowths which may contain some or all of the following minerals: thorite, siderite, xenotime, gadolinite, apatite, monazite, a REE-fluocarbonate, Fe- and

Ti-oxides, chalcopyrite and an Fe-sulphide. In quartz-rich samples the intergrowths typically appear as irregular blebs, 1 to 3 mm in diameter, in quartz. In quartz-poor samples the intergrowths are present as irregular patches several centimeters in width. Micas, chlorite, phenakite and ankerite are common accessories.

In quartz-rich samples the complex intergrowths are usually composed of fine grained thorite, xenotime, a Ca,Fe-bearing REE-fluocarbonate tentatively identified as synchysite and siderite. Thorite and xenotime appear to be contemporaneous phases as they are commonly intergrown with one another. Synchysite usually encloses xenotime and thorite and in turn is replaced by siderite. Euhedral Fe- and Ti-oxides, monazite and Cu- or Fe-sulphides are commonly present in the intergrowths. These complex intergrowths are usually dark brown in colour and almost opaque, as seen in Plate 2.16a. Locally they are mantled by dark purple fluorite.

In quartz-poor samples the intergrowths are larger and contain gadolinite and apatite in addition to the minerals listed above. Gadolinite replaces xenotime in these samples and the replacement is accompanied by the development of apatite. Due to the semi-opaque appearance, fine grained nature and mineralogical complexity of these intergrowths, standard optical petrographic techniques are inadequate for mineral identification. Qualitative electron microprobe analyses and backscattered electron imagery were used to decipher the mineralogy of these complex intergrowths which are discussed in further detail in the Y and REE mineral sections of Chapter 3.

There are two ages of quartz present in the *quartz-thorite* unit. The earlier type of quartz (1) is anhedral, fine grained and occurs as small aggregates locally associated with micas and phenakite. The second type of quartz (2) is medium grained, anhedral and appears to have developed over a lengthy period of time contemporaneously with the minerals in the reddish brown intergrowths. Quartz (2) typically encloses the intergrowths and locally contains discrete inclusions of euhedral xenotime and fluorite. However, it is also seen enclosed in within the thorite-bearing intergrowths or cut by them. It is commonly full of subparallel fractures (see Plate 2.16a) due to local shearing, which are filled with carbonate or thorite.

Fluorite in these rocks is darker purple in colour than in other rock types of the T-zone. The colour change is possibly due to radiation damage caused by emanations from proximal thorite (Deer *et al.*, 1962). Fluorite is fine to medium grained and is present throughout much of the paragenetic sequence of mineralization. It occurs as aggregates with carbonate interstitial to quartz (1 and 2) and as euhedral inclusions in quartz (2). Fluorite is also present either interstitial to, or enclosed by, the rusty brown intergrowths and locally contains inclusions of the Y- and REE-bearing minerals. Fluorite euhedra are dodecahedral in habit which is typical for rocks of the Upper Intermediate zone.

Quartz-rich samples locally contain subhedral, lath-like grains of the Li-bearing mica polylithionite, as identified by Černý and Trueman (1985), or biotite in quartz (2). The micas are typically strongly altered and partially replaced by quartz, fluorite, carbonate and chlorite. Chlorite occurs as fine grained aggregates replacing micas and locally occurs with fluorite in the reddish brown coloured intergrowths. Phenakite appears as optically continuous grains interstitial to quartz (1) and the thorite-bearing intergrowths. Phenakite grains, in optical continuity, are enclosed in quartz (2). Ankerite (±siderite) is present in quartz interstices associated with fluorite.

The *quartz-thorite* unit is economically significant in terms of its Y, REE and Be content. Y enrichment in these rocks exceeds that of all other rock types of the T-zone due to the abundance of xenotime, gadolinite and thorite. LREE enrichment in this unit is attributed to the presence of at least one REE-fluocarbonate (synchysite?) and monazite to a lesser extent. High Gd and Dy assay values are attributed to the presence of xenotime and gadolinite which are enriched in these middle REEs. The *quartz-thorite* unit also contains economically significant amounts of Be due mainly to the presence of phenakite and to a lesser extent gadolinite.

Figure 2.12 presents a generalized paragenetic sequence of mineralization for the *quartz-thorite* unit of the Lower Intermediate zone based on the samples used in this study. Due to the inhomogeneity and mineralogical complexity of the rocks in this unit, not all minerals listed are necessarily present in a particular sample. In addition, the position of certain minerals within the sequence will vary from sample to sample.

Quartz-bastnaesite group unit

Rocks of the ***quartz-bastnaesite group*** unit are located at the upper boundary of the Upper Intermediate zone and are intercalated with the Quartz zone. The rocks are easily identified in hand sample by their brick-red colour and high density. Typically rocks of this unit are composed of massive, fine grained aggregates of brick-red REE-fluocarbonates of the bastnaesite group. In quartz-rich samples, the REE-fluocarbonates appear as euhedral to subhedral hexagonal or blocky grains enclosed in quartz. Plate 2.23a shows these blocky fluocarbonate grains in a Quartz zone sample. In thin section, these blocky grains are composed of fine grained aggregates of REE-fluocarbonates which suggests that the brick-red minerals in these samples may be pseudomorphs after an earlier, unidentified phase. Quartz occurs in varying amounts as cross-cutting veinlets and blebs, and locally encloses the blocky fluocarbonate aggregates. Fine grained purple fluorite and pale yellow carbonate occur interstitial to the bastnaesite group minerals within the aggregates. Cu- and Fe-sulphides occur locally as inclusions in quartz. A typical hand sample of the ***quartz-bastnaesite group*** unit is shown in Plate 2.16b.

In thin section this unit is composed mainly of REE-fluocarbonate polycrystals, quartz, fluorite and sericite. Accessory minerals include ankerite, sericite, zircon, Fe- and Ti-oxides and chalcopyrite.

The LREE-bearing fluocarbonate polycrystals are composed mainly of syntaxic intergrowths of bastnaesite and parisite. The polycrystals display three distinct habits within this unit and may be acicular, tabular or subhedral to anhedral blocky grains. All three varieties occur together within a single sample and appear to be contemporaneous.

The acicular polycrystals usually occur as massive aggregates which form radiating or plumose textures as seen in Plate 2.17a. These polycrystals are composed of bastnaesite and parisite in varying proportions. The tabular polycrystals are medium grained and typically form radiating bundles as seen in Plate 2.17b. These polycrystals are composed predominantly of bastnaesite with minor parisite. The subhedral polycrystals occur as blocky or rounded six sided grains and are usually enclosed in fluorite, ankerite or quartz. Plate 2.18a shows the subhedral polycrystals with interstitial fluorite and quartz. These polycrystals are composed predominantly of parisite with minor bastnaesite. Locally a third REE-fluocarbonate is intergrown with parisite and bastnaesite in the subhedral polycrystals. It is compositionally similar to parisite but contains more Ca, less REEs and trace amounts of Fe. This mineral is tentatively identified as roentgenite. Locally the LREE-bearing fluocarbonate polycrystals contain minute inclusions of an Fe-oxide.

Two stages of quartz are present in rocks of this unit. Anhedral grains of fine to medium grained quartz (1) are most common and form irregular blebs and veinlets which cross-cut the massive aggregates of REE-fluocarbonate polycrystals and locally occur interstitial to them (Plate 2.17b). It commonly contains inclusions of, and appears to replace, anhedral REE-fluocarbonate polycrystals. It also contains inclusions of fine grained zircon, Ti-oxide aggregates and chalcopyrite. Locally, the oxides and sulphides form along grain boundaries in quartz. A later microcrystalline variety of quartz (2) occurs interstitial to, and locally replaces, all other minerals. Microcrystalline quartz is shown interstitial to tabular polycrystals in Plate 2.17b.

Purple fluorite is present exclusively interstitial to REE-fluocarbonate polycrystals and locally contains inclusions of the subhedral type (see Plate 2.18a) occasionally associated with microcrystalline quartz. Fine grained aggregates of sericite are commonly present in these rocks, interstitial to, and partially replacing, the polycrystals. It is locally associated with quartz (1) and is replaced by microcrystalline quartz.

Ankerite occurs as anhedral grains interstitial to quartz (1) and the REE-fluocarbonate aggregates. It is partially replaced by later microcrystalline quartz. Zircon, Fe- and Ti-oxides and chalcopyrite occur as above. Zircon is not present in economically significant quantities.

A generalized paragenetic sequence of mineralization for the *quartz-bastnaesite group* unit of the Upper Intermediate zone is presented in Figure 2.13.

The *quartz-bastnaesite group* unit is economically significant in terms of La, Ce, Nd and Sm content. LREE enrichment in these rocks exceeds that of all other rock types of the T-zone due to the abundance of minerals of the bastnaesite group.

Quartz-feldspar-magnetite unit

The *quartz-feldspar-magnetite* unit is present where the Upper Intermediate zone lies in contact with the Wall zone (see Fig.2.3). Megascopically, the rocks display an irregular banded texture as seen in Plate 2.18b. The mafic bands are greenish black in colour and are composed mainly of biotite, chlorite and magnetite. The light pink to white coloured bands are composed of fine grained feldspar and quartz. These light coloured bands locally enclose flakes of biotite and irregular patches of fine grained mafics. Irregular blebs of medium grained quartz are common throughout. Locally, where the rocks are more quartz-rich, the mafic bands contain flakes of a greenish grey mica (polylithionite), olive green acmite and fine grained mafics which mantle mantle and partially replace acmite. Purple fluorite and buff to yellow coloured carbonate are present as accessory phases throughout rocks of this unit.

In thin section the mafic-rich areas may be divided into two types: biotite-rich and biotite-free. The first type is composed mainly of biotite, magnetite and chlorite. The second type is composed of acmite, hematite and polylithionite. Quartz, K-feldspar and phenakite are the predominant mineral phases in the non-mafic areas. Accessory minerals include ankerite, fluorite, ilmenite, a Ti-oxide and columbite.

Biotite is typically medium grained and appears as subhedral lath-like grains as described in rocks of the Lower Intermediate zone. It occurs as individual grains isolated in quartz and commonly as grain aggregates which are partially to entirely replaced by magnetite and chlorite. Locally quartz, phenakite, carbonate and fluorite replace biotite at grain boundaries and parallel to cleavage.

Fe-oxides are the most abundant oxide minerals in these weakly to strongly magnetic rocks. Magnetite typically occurs as euhedral grains and grain aggregates which appear to overgrow and replace biotite. Locally magnetite is included in quartz and fluorite. In biotite-free samples, fine grained aggregates of hematite form partial pseudomorphs after acmite (see Plate 2.19). The replacement of acmite by Fe-oxides is locally associated with ilmenite and a Ti-oxide. Hematite commonly occurs parallel to cleavage in polylithionite.

Acmite typically occurs as medium grained, subhedral to euhedral prismatic grains (Plate 2.19a) and grain aggregates which are mantled, and partially to entirely psuedomorphed, by hematite (±ilmenite and a Ti-oxide). Aggregates of acicular acmite locally appear as rounded blebs (1 to 8 mm in diameter) which are again mantled by oxide minerals. In hand sample, acmite appears olive green in colour but is pale yellow in plane polarized light and weakly pleochroic. Acmite is defined by Deer *et al.* (1978) as the weakly pleochroic variety of aegirine. Both types of acmite are usually associated with polylithionite and are enclosed, and partially replaced, by quartz. Plate 2.19b shows a radial aggregate of acmite needles partially pseudomorphed by hematite. Some prismatic grains psuedomorphed by oxides are locally present in the biotite-rich areas although there is no relict acmite or polylithionite present.

Polylithionite appears as medium grained, lath-like grains in quartz associated with acmite and oxide phases. It occasionally contains relict patches of K-feldspar and appears to be replacing the feldspar. Locally it encloses subhedral grains of acmite and more rarely contains inclusions of euhedral columbite. Hematite commonly forms parallel to cleavage in the mica grains (see Plate 2.19b). Polylithionite is present exclusively in biotite-free areas of this rock type.

Quartz, K-feldspar and phenakite comprise the light coloured bands observed in rocks of this unit. Quartz is fine to medium grained and occurs as euhedral to anhedral grains intergrown with phenakite and replacing K-feldspar. Phenakite occurs as anhedral grains which are intergrown with, and locally interstitial to, quartz. The irregular shaped grains of phenakite locally comprise optically continuous plates which cover areas up to approximately

1.5 X 2.0 mm. Phenakite is most abundant in biotite-rich samples and is rarely present in those containing polylithionite. Quartz and phenakite (where present) appear to be the latest minerals and enclose, or partially replace, all earlier major phases.

In biotite-rich samples, K-feldspar is usually present as irregular patches enclosed in, and partially replaced by, quartz and phenakite. In polylithionite-bearing samples, the feldspar occurs as anhedral relicts within mica and as blocky grains in quartz.

Carbonate and fluorite are the most common accessory minerals in rocks of this unit. The carbonate is ankeritic in composition and usually occurs in irregular patches partially replacing micas and acmite. Locally acmite is completely replaced leaving an oxide-outlined prismatic grain with a carbonate core. Fluorite is most common in biotite-rich samples and is typically associated with the carbonate replacement of mica. Both carbonate and fluorite occur as anhedral inclusions in quartz and as later stage phases interstitial to quartz. Ilmenite and a Ti-oxide are locally associated with the hematite replacement of acmite. Columbite is present rarely as inclusions in polylithionite and locally contains minute inclusions of bastnaesite.

A generalized paragenetic sequence of mineralization for the *quartz-feldspar-magnetite* unit is presented in Figure 2.14. As indicated above, not all the minerals listed will neccessarily be present in a particular sample.

Some of the highest Be assay values in the T-zone are from rocks of this unit. Based on the samples studied here, Be enrichment in these rocks can be attributed to the presence of phenakite which appears to be the only mineral of economic interest in the unit. Phenakite is most abundant in biotite-rich samples and is present in the fine grained, light pink coloured bands more often than in the white coloured areas which are more quartz-rich.

Quartz-feldspar unit

The *quartz-feldspar* unit lies in the central part of the Upper Intermediate zone above the large granite xenolith and Lower Intermediate zone. It is in gradational contact with the *quartz-mica-feldspar*, *quartz-mica* and *quartz-thorite* units. The *quartz-feldspar* unit also occurs as the wedge of Upper Intermediate zone which separates the magnetite-rich Lower

Intermediate zone unit from the biotite-rich units. Rocks of the ***quartz-feldspar*** unit which lie between Lower Intermediate zone units appear brecciated in underground workings.

Megascopically, rocks of this unit are typically composed of individual laths and aggregates of salmon pink or red coloured feldspar enclosed in medium to coarse grained milky white quartz. Fine grained purple fluorite and carbonate are commonly present interstitial to feldspar within the aggregates. Fe-sulphides, brick-red fluocarbonates and biotite are present locally within the feldspar aggregates or as inclusions in quartz. Plate 2.20a shows a typical sample of drill core from the ***quartz-feldspar*** unit.

Vugs, ranging from centimeters to meters in size, are commonly present in quartz-rich sections of this unit. The cavities are filled with large quartz crystals up to approximately 20 cm in diameter, medium to coarse grained cubic purple fluorite, carbonate rhombs and framboidal aggregates of an Fe-sulphide. Quartz, fluorite and carbonate are often dusted with fine grained Fe-sulphides.

In thin section, rocks of this unit are comprised mainly of K-feldspar, albite and quartz. Fluorite, carbonate and phenakite are the most common accessory minerals. Biotite, chlorite, sericite, Fe- and Ti-oxides, an Fe-sulphide, REE-fluocarbonates and monazite occur more rarely. The feldspar and accessory minerals usually occur together in irregular patches which are partially replaced by quartz. Locally these patches have angular boundaries (see Plate 2.21a) and may represent remnants of an earlier alteration assemblage which has undergone *in situ* brecciation and partial replacement by quartz.

K-feldspar occurs as individual subhedral, medium grained laths or blocky grains which are enclosed in, and partially replaced by, quartz. It also occurs as aggregates of subhedral to anhedral grains associated with albite, fluorite, carbonate and phenakite in the alteration remnants. K-feldspar in these rocks is typically partially replaced by albite as shown in Plate 2.20b. Replacement by biotite or sericite occurs less commonly. Fluorite, ankerite and siderite usually occur interstitial to, and replace, the feldspars (see Plate 2.21a). Phenakite is present locally.

Albite typically occurs as anhedral grains replacing earlier K-feldspar as shown in Plate 2.20b. Both albite and K-feldspar commonly contain minute inclusions of Fe-oxides and are generally altered in appearance (Plate 2.21a). The oxide inclusions probably give the feldspar of this unit its characteristic red colour.

Quartz is usually medium to coarse grained and occurs as anhedral grains and grain aggregates which enclose the patches of alteration and locally replace them at grain boundaries. Quartz also contains individual laths of altered feldspar and subhedral to anhedral biotite grains. It locally contains fine grained inclusions of fluorite, Fe- and Ti-oxides and an Fe-sulphide. Quartz appears to be the latest major phase present. An even later microcrystalline variety of quartz is present locally.

Fluorite and carbonate most commonly occur interstitial to feldspar within the alteration patches. In this association, they are early phases included in, and replaced by, quartz. Fluorite and carbonate also appear as late stage phases locally filling quartz interstices. Most of the carbonate is ankeritic in composition with lesser amounts of siderite. Both often enclose subhedral REE-fluocarbonate polycrystals and Fe-sulphide aggregates.

Phenakite is typically present within the alteration patches as anhedral, optically continuous grains interstitial to, and replacing, feldspar. It does not appear within the quartz-rich areas and is probably an earlier phase in these particular rocks, unlike most of the rock types described previously where phenakite is contemporaneous with, or slightly later than, quartz.

Biotite (±chlorite) is present locally as subhedral lath-like grains in quartz and irregular patches replacing K-feldspar. Fine grained aggregates of sericite were observed in one sample replacing K-feldspar. REE-fluocarbonate polycrystals are commonly present enclosed in carbonate, K-feldspar or quartz. Monazite is a rare accessory and occurs as subhedral inclusions in altered K-feldspar. Oxide and sulphide minerals occur as described above.

A generalized paragenetic sequence of mineralization for the *quartz-feldspar* unit of the Upper Intermediate zone is presented in Figure 2.15.

The *quartz-feldspar* unit is of economic interest in terms of Be due to the presence of phenakite. LREE enrichment in these rocks is due to the local presence of REE-fluocarbonates and is probably of limited economic significance.

Quartz-mica-feldspar unit

The *quartz-mica-feldspar* unit lies in the central portion of the Upper Intermediate zone in gradational contact with the *quartz-feldspar* unit and overlying rocks of the *quartz-mica* unit. Megascopically, the rocks appear fresh as seen in Plate 2.21b and are composed mainly of milky white quartz with pods of massive, greenish grey polylithionite and salmon pink to red coloured feldspar. Fine grained purple fluorite and buff coloured carbonate commonly occur interstitial to feldspar and mica aggregates. Quartz locally contains individual flakes of mica, feldspar laths or fluorite and is typically strongly fractured. Plate 2.21b shows the *quartz-mica-feldspar* unit in hand sample.

In thin section the main mineral constituents of this unit are K-feldspar, polylithionite and quartz. Fluorite and ankeritic carbonate are the most common accessory minerals. Biotite, chlorite, Fe- and Ti-oxides, phenakite and REE-fluocarbonates are present less frequently.

K-feldspar typically occurs as subhedral, medium grained laths or blocky grains which are overgrown and replaced by polylithionite. Plate 2.22a shows anhedral relicts of K-feldspar enclosed in mica. K-feldspar from this unit is similar in appearance to that from the *quartz-feldspar* unit but is not associated with albite in any of the samples used in this study. Locally, it encloses fine grained REE-fluocarbonate polycrystals and an Fe-oxide.

Polylithionite is present as aggregates of randomly oriented, medium to coarse grained, euhedral to subhedral six-sided crystals which appear lath-like in thin section (see Plate 2.22a). The mica overgrows and replaces K-feldspar and locally encloses anhedral relicts of feldspar. It is replaced by fluorite, ankerite and quartz at grain boundaries and parallel to cleavage. It is more rarely seen replaced by biotite, chlorite or fine grained aggregates of Fe- and Ti-oxides.

Three different types of quartz are present in rocks of this unit. The earliest type of quartz (1) is present as subhedral to anhedral grains interstitial to mica grains within polylithionite aggregates. This type of quartz is always strained and locally displays growth zones. The second type of quartz (2) is typically anhedral, medium to coarse grained and encloses the mica and feldspar aggregates. It is the most common type of quartz and is shown in Plate 2.22a. This type of quartz (2) is not strained and usually replaces polylithionite and feldspar at grain boundaries. The third variety of quartz (3) occurs as microcrystalline aggregates which mantle and replace earlier quartz. Microcrystalline quartz also replaces mica and feldspar but appears to be contemporaneous with phenakite.

Purple fluorite and ankerite occur as irregular patches interstitial to, and partially replace, K-feldspar. They also occur intersitial to polylithionite and typically replace the mica parallel to cleavage. Both fluorite and ankerite locally contain Fe- and Ti-oxide inclusions.

Biotite and chlorite are occasionally present as anhedral or shreddy grains which appear to replace polylithionite. Their presence is rare in these rocks. Aggregates of fine grained Fe- and Ti-oxides locally replace polylithionite and are common as inclusions in quartz (2), fluorite and ankerite. Phenakite appears to be a rare accessory in rocks of this unit. It is present as optically continuous grains which occur interstitial to, and locally contain inclusions of, quartz (2). It is often associated with the microcrystalline variety of quartz and may be contemporaneous with it. Fine grained, anhedral LREE-bearing fluocarbonate polycrystals are present locally in K-feldspar and quartz (2).

A generalized paragenetic sequence of mineralization for the *quartz-mica-feldspar* unit is presented in Figure 2.16. Not all the minerals listed will necessarily be present in a particular sample.

Based on the samples used in this study, the *quartz-mica-feldspar* unit is probably of limited economic significance. Minor Be and LREE enrichment is attributed to the local presence of phenakite and REE-fluocarbonate polycrystals.

Quartz-mica unit

Rocks of this unit occur towards the upper part of the Upper Intermediate zone. The rocks are intercalated with, and locally occur as lenses within, the overlying Quartz zone. Contacts with underlying rocks of the *quartz-mica-feldspar* and *quartz-feldspar* units are gradational.

Megascopically the rocks appear fresh, medium to coarse grained and are composed mainly of massive, greenish grey polylithionite aggregates with interstitial milky white quartz. Locally large pods of polylithionite, up to several tens of meters long and one meter thick, occur with minor accompanying quartz. Fluorite is the most common accessory and may comprise up to 10% of this unit. It is dodecahedral in habit, medium to coarse grained and is often zoned ranging in colour from dark purple to aqua or pale green or grey. The cause of the zoning and unusual habit of fluorite is presently unknown. Plate 2.22b shows a typical fluorite-bearing sample of the *quartz-mica* unit.

In thin section, the mineralogy is essentially the same as that of the *quartz-mica-feldspar* unit. The *quartz-mica* unit is distinguished from the *quartz-mica-feldspar* unit by its greater abundance of polylithionite, its general paucity of feldspar and the presence of zoned fluorite. A paragenetic sequence of mineralization is not given for the *quartz-mica* unit as it is essentially the same as that for the *quartz-mica-feldspar* unit presented in Figure 2.16.

Assay results and petrographic observations suggest that the *quartz-mica* unit is of limited economic interest due to the local presence of phenakite. It may have potential as a source of Li owing to the abundance of polylithionite.

Discussion

The Upper Intermediate zone is composed of the most mineralogically diverse rocks in the T-zone. A comparison of Figures 2.12 through 2.16 suggests that the *quartz-thorite*, *quartz-bastnaesite group* and *quartz-feldspar-magnetite* units are each paragenetically unique. Each unit is mineralogically distinct and does not appear to be directly related to adjacent alteration assemblages. Conversely, the remaining three units of the Upper Intermediate zone are paragenetically similar. The three are differentiated mainly by relative proportions of feldspar and polylithionite and in general mica content appears to increase towards surface with a concommitant decrease in feldspar content.

Despite the mineralogical diversity of this zone, the rocks share certain broad similarities. Quartz, fluorite and carbonate are ubiquitous in this zone and occur throughout much of the sequence of mineralization. In general, feldspar is always present as an early phase and is typically replaced by micas. Fe-bearing minerals are generally present in minor amounts compared to the Lower Intermediate zone with the exception of the *quartz-feldspar-magnetite* unit. In addition, all the units are quartz-rich which is probably the result of extensive silicification in this zone.

Unlike the Lower Intermediate zone, where the rocks are uniformly Fe-rich, the Upper Intermediate zone units are chemically diverse. The *quartz-thorite* unit is characterized by Th and Y (xenotime) enrichment whereas the *quartz-bastnaesite group* unit is strongly enriched in LREEs. The *quartz-feldspar-magnetite* unit does not show strong enrichment in a single element but is moderately enriched in Fe (magnetite), Na (acmite) and Li (polylithionite). The remaining three units are enriched in K and Li due to the abundance of feldspar and polylithionite. Temporal relationships between the different alteration units of the Upper Intermediate zone are unknown.

In terms of economic significance, the Upper Intermediate zone contains the most strongly Be-, Y- and REE-enriched rocks of the T-zone. Phenakite is the predominant Be-bearing mineral in these rocks and is most abundant in the *quartz-feldspar-magnetite* unit. It is present in lesser amounts in the other units except the *quartz-bastnaesite group* unit where it is typically absent. Xenotime is the principal Y-bearing mineral of economic interest with gadolinite and thorite as minor contributors to Y enrichment. Y mineralization of economic proportions in this zone is restricted to the *quartz-thorite* unit. REE-fluocarbonates of the bastnaesite group are the principal LREE-bearing minerals of economic interest in this zone. They occur as accessories in all units of the Upper Intermediate zone but are most abundant in the *quartz-bastnaesite group* unit. Gd and Dy enrichment are confined to the xenotime-bearing *quartz-thorite* unit.

F. QUARTZ ZONE

The Quartz zone occupies the center of the subcircular north body of the T-zone and occurs as smaller, irregular areas in the south body (Fig.2.1). It is typically intercalated and in gradational contact with Upper Intermediate zone assemblages (Fig.2.3). The Quartz zone appears to have caused brecciation in the Wall zone (*breccia* unit) where the two are in direct contact. It also occurs locally as barren, unmineralized lenses within the Upper Intermediate zone.

The Quartz zone is essentially monomineralic and is composed of greater than 95% massive, milky white to translucent grey quartz. The quartz is medium to very coarse grained, with individual crystals ranging from a few centimetres to several tens of centimetres in diameter, and is commonly fractured. It is essentially unmineralized but locally contains small, irregular patches of alteration which typically include: purple fluorite, blocky REE-fluocarbonate polycrystals, buff to yellow coloured carbonate, yellowish green to black coloured sphalerite, chalcopyrite and an Fe-sulphide. A typical sample of the Quartz zone is shown in Plate 2.23a. Rarely, in close proximity to the Upper Intermediate zone, the Quartz zone may also contain patches of micaceous or feldspathic alteration with minor associated zircon, xenotime, thorite, columbite and Fe- and Ti-oxides.

Vugs are commonly present in this zone and range in size from millimetres to metres in scale. They are typically lined with late stage minerals such as: aggregates of euhedral ankerite, dolomite and calcite; cubic purple fluorite; Cu- and Fe-sulphides; and coarse quartz crystals or drusy quartz. Cross-cutting stringers of carbonate are common.

Despite the local presence of LREE-bearing fluocarbonate polycrystals and the more rare occurrence of xenotime and zircon, the Quartz zone is essentially barren and may be considered uneconomic in terms of Be, Y, REE, Nb, Zr and Ga mineralization.

The Quartz zone, which lies in the central portion of the north T-zone and appears to have brecciated pre-existing Wall zone rocks, is postulated to be the latest alteration in the T-zone. It is presumably the result of late stage silicification which may or may not be related to quartz-rich assemblages elsewhere in the T-zone.

G. FELSITE DYKE

In the north T-zone, a narrow felsite dyke is in sharp intrusive contact with all the zoned alteration assemblages as seen in Figure 2.3. The dyke is northeast trending, near vertical and approximately 2 m wide. Megascopically the felsite is fine grained, brick-red in colour and displays a conchoidal fracture. It is easily distinguished from brick-red rocks of the *quartz-bastnaesite group* unit by the higher density and darker colour of the latter. The dyke rock is composed of fine grained, randomly oriented, grey feldspar phenocrysts set in an aphanitic groundmass. Buff to yellow coloured carbonate occurs as fine grained blebs and cross-cutting stringers throughout the dyke. A typical sample of the felsite dyke is shown in Plate 2.23b.

In thin section, the feldspar phenocrysts observed in hand sample are actually composed of several feldspar grains. These groups of phenocrysts, which may be up to 1.0 X 2.0 mm in size, are composed of fine grained, subhedral albite laths. Albite is typically altered in appearance due to fine grained Fe-oxide inclusions and locally contains minute irregular blebs of K-feldspar. Fine grained needle-like inclusions of muscovite are commonly present and inclusions of cubic fluorite are more rare. Albite phenocrysts comprise approximately 2-5% of the rock.

The felsite groundmass is composed mainly of massive, fine grained K-feldspar with interstitial quartz and carbonate. K-feldspar comprises approximately 80-85% of the rock and occurs as very fine grained, anhedral to subhedral laths and blocky grains. Like albite, K-feldspar is altered in appearance due to the abundance of Fe-oxide inclusions which probably give the rock its characteristic brick-red colour. The groundmass feldspar locally contains irregular blebs of albite.

Quartz comprises approximately 5% of the rock and occurs as anhedral grains interstitial to, and locally containing inclusions of, the K-feldspar groundmass. Carbonate ranges from ankerite to dolomite in composition and comprises approximately 10% of the rock. It appears in the groundmass as fine grained, irregular patches interstitial to K-feldspar. Fine grained, euhedral apatite and a Ti-oxide are locally present as inclusions in carbonate.

Quantitative electron microprobe analyses of albite and K-feldspar from the felsite dyke (see Tables 3.3 and 3.4) indicate that they do not contain detectable amounts of Ga. The dyke is essentially unmineralized and may be considered uneconomic in terms of Be, Y, REE, Nb, Zr and Ga.

The age of the felsite dyke is uncertain as intrusive contacts with Neo-Helikian Mackenzie diabase dykes were not observed. It cross-cuts all alteration assemblages of the T-zone and obviously post-dates economic mineralization.

H. DIABASE DYKE

Diabase dykes of the Mackenzie swarm are present locally throughout the T-zone in sharp intrusive contact with the alteration. They are northwest or northeast trending, near vertical and range from less than 1 meter to approximately 20 m in width. The larger diabase dykes in the T-zone are shown in Figure 2.1.

Megascopically, diabase dykes in the T-zone are typically aphanitic, weakly magnetic and range in colour from dark brown to dark grey. Locally the dykes contain randomly oriented, fine grained laths of pink feldspar set in a dark, aphanitic groundmass.

The Mackenzie dykes are well described by Leech (1966) and are composed mainly of plagioclase and pyroxene with interstitial quartz. Plagioclase feldspar is commonly altered to sericite or epidote and locally appears completely altered (Leech, 1966). Olivine, apatite, rutile, magnetite, ilmenite and hematite are common accessory minerals (Leech, 1966). Locally, the dykes are carbonate-rich and may contain both primary and secondary carbonate (Leech, 1966). Cross-cutting carbonate stringers are common, as in all rock types of the T-zone, and are often associated with fine grained Fe-sulphides. Due to the stongly altered nature of feldspar in the T-zone diabase dykes, it was not possible to use quantitative electron microprobe analysis to obtain compositional information including Ga content. Like the felsite, the diabase appears to be unmineralized and is considered uneconomic.

The predominantly northwest trending diabase dykes of the T-zone are assumed to be part of the northwest trending Mackenzie swarm which has been dated, by the K-Ar whole-rock method, between 1000 and 1200 m.y. (Leech, 1966). The dykes cross-cut all alteration assemblages of the T-zone and post-date economic mineralization.

III. ECONOMIC MINERALOGY OF THE T-ZONE

The following chapter presents the detailed mineralogy of Be, Y, REEs, Nb, Zr and Ga in the north T-zone deposits. It is divided into four sections.

The first section (A) provides an introduction to the general complexity of the economic mineralogy and outlines the various methods used to study and identify the minerals. The remaining three sections describe the mineralogy of Be and its various by-products metals.

The mineralogy of Be, the principal metal of economic interest in the T-zone, is detailed in the second section (B). The third section (C) describes the mineralogy of Y and REEs which are currently considered as probable by-products of Be mining. Particular emphasis has been placed on this section as Y and REEs have the greatest economic potential of all the by-product metals and are most complex mineralogically. The last section (D) examines the mineralogy of Nb, Zr and Ga which are considered as possible by-products of Be.

A. INTRODUCTION

Megascopically, few of the minerals of economic interest in the T-zone are readily identifiable. The REE-fluocarbonate polycrystals are easily identified by their characteristic brick-red colour but the different phases within a polycrystal are indistinguishable megascopically. Thorite is also readily identifiable megascopically due to its characteristic rusty brown colour and radioactivity. However, thorite is typically intergrown with several other fine grained minerals such as xenotime which are not recognizable at the megascopic scale. The presence of the Be-bearing minerals phenakite and bertrandite may be indicated in the field with a berylometer. However, phenakite is megascopically indistinguishable from quartz and bertrandite is too fine grained to be visible. Although some of the minerals of economic interest may be identified in hand sample, most phases, including those described above, occur in complex fine grained intergrowths with other minerals which are megascopically indistinguishable from one another.

At the microscopic scale, standard optical petrographic techniques were useful in the identification of certain minerals of economic interest such as phenakite, bertrandite and zircon. However, optical petrography was of limited use in studying very fine grained mineral intergrowths, particularly where the latter are altered and locally metamict.

The grain size and complexity of intergrowths in which many of the minerals of economic interest occur render the proper separation of the minerals difficult or, in most cases, impossible. The electron microprobe which allows non-destructive analysis of minerals *in situ* was used extensively in this study.

Backscattered electron imaging techniques were instrumental in deciphering the nature of the complex and fine grained mineral intergrowths. Several backscattered electron images are included in this chapter to illustrate certain textural relationships between minerals. The black and white images reflect differences in average atomic number between the various phases present. The brightest mineral in the image has the highest average atomic number whereas the darkest mineral (typically the host mineral) has the lowest average atomic number.

In addition to providing textural information, the electron microprobe provided compositional information for the minerals of economic interest. All quantitative electron microprobe analyses were obtained using combined wavelength and energy dispersive techniques. Operating conditions and standards used for each run are reported in Appendix I. Quantitative electron microprobe analyses are restricted to minerals which do not contain REEs. An attempt was made in this study to develop a new technique for quantitative electron microprobe analysis of REE-bearing minerals. Owing to unstable environmental conditions which affected the performance of the instrument being used, the development of this technique was not possible. However, the proposed technique is discussed in Appendix II.

Much of the compositional information presented in this chapter is qualitative. All qualitative data are reported as major, minor or trace concentrations of an element. The ranges have been arbitrarily set at 100-3% for major, 5-0.1% for minor and less than 1% for trace amounts. Several energy dispersive spectra, with labelled peaks, are included in this chapter to illustrate qualitative compositional information for certain minerals. All spectra were obtained on an ORTEC EEDS II energy dispersive spectrometer attached to an a ARL SEMQ electron microprobe operated at 15 kV. The spectra were processed through an in-house computer program called QKNDRTY. Some semi-quantitative electron microprobe analyses are also included in this chapter. Element concentrations in these analyses have been arbitrarily rounded to the nearest weight percent.

Limited use of an ion probe and a cathodoluminescence microscope provided additional information for selected minerals discussed in this chapter.

In cases where positive mineral identifications were not possible due to lack of quantitative compositional information or limited amount of sample, tentative identifications have been made. These particular minerals have been tentatively identified on the basis of all available information including physical and optical properties and qualitative or semi-quantitative electron microprobe analyses. MinIdent (Smith and Leibovitz, 1986), a computer program for mineral identification with a data base of over 3700 mineral species, was of aid in the tentative identification of these minerals.

B. PRINCIPAL METAL OF ECONOMIC INTEREST: BERYLLIUM

A total of four Be-bearing minerals were identified in this study. The minerals, all Be-bearing silicates, are listed below:

a) phenakite
b) bertrandite
c) gadolinite
d) a member of the helvite group.

Based on the samples used in this study, phenakite appears to be the most abundant Be-bearing mineral in the north T-zone and contains the highest concentration of Be. Approximately 90% of the Be enrichment in the T-zone is probably attributable to the presence of phenakite. Bertrandite, gadolinite and the helvite group mineral together probably comprise less than 10% of the overall Be enrichment. Ion probe analyses indicate that trace amounts of Be are also present in zonally metamictized zircons. The ion probe used was the AEI IM20 instrument in the Department of Earth Science at Cambridge University (Banner and Stimpson, 1974) which has been modified by the addition of computer control of mass selection and intensity recording.

Phenakite

Megascopically, phenakite (Be_2SiO_4) displays all the properties of quartz. In thin section, the two minerals are easily distinguished by their marked differences in relief and birefringence as shown in Plates 3.1a, 3.1b and 3.2a.

Phenakite typically occurs as anhedral, optically continuous grains which vary in size from approximately 10 μm to 1.5 mm but are generally between 100 μm and 1 mm in diameter. Several individual grains, in optical continuity, together may cover areas up to 2 X 4 mm in size. Optically continuous phenakite is most commonly associated with quartz and typically occurs intergrown with, or interstitial to, quartz as shown in Plate 3.1a. Locally, it is partially replaced by late stage microcrystalline quartz aggregates which gives phenakite grain boundaries a ragged appearance as shown in Plate 3.1b. Most phenakite in the T-zone occurs as described above and contains few mineral inclusions except quartz. Fluorite, biotite, Fe- and Ti-oxides, a helvite group mineral and REE-fluocarbonate polycrystals are locally present as inclusions in, or partially replaced by, phenakite.

Rarely, phenakite occurs as optically discontinuous grains. Unlike the common optically continuous phenakite described above, this type has sharp grain boundaries and is not directly associated with quartz. Such phenakite occurs as subhedral to anhedral grains which are isolated from quartz by some other mineral. Plate 3.2a shows sharply bounded anhedral phenakite grains surrounded by biotite. In Plate 3.2b subhedral, rhombohedral phenakite and associated monazite are enclosed in ankerite. It is postulated here that the subhedral type of phenakite, with its sharp grain boundaries, may have developed due to its isolation from quartz.

Both types of phenakite appear to be contemporaneous and differ only in terms of host material. In general, phenakite appears to have formed as a relatively late stage mineral associated with fine to medium grained quartz which is usually one of the later phases in most rock types, as described in Chapter 2. Locally, phenakite is partially replaced by later microcrystalline quartz or chlorite and is sometimes cross-cut by carbonate or fluorite stringers.

Compositionally, phenakite appears homogeneous in thin section and backscattered electron images. Although the soft radiation of Be is heavily absorbed by the detector used in electron microprobe analysis, phenakite may be differentiated from quartz and bertrandite by relative proportions of Si.

Based on the samples used in this study, phenakite is the most common Be-bearing mineral in the T-zone. It is most abundant in the biotite-bearing units of the Lower Intermediate zone, the ***quartz-feldspar-magnetite*** unit of the Upper Intermediate zone and mineralized granite. It occurs in lesser amounts in the ***quartz-thorite***, ***quartz-feldspar*** and ***quartz-mica-feldspar*** units of the Upper Intermediate zone. It is rarely present in the Wall zone and is probably not present in economically significant amounts.

Phenakite is a desirable ore mineral because is contains a substantially higher concentration of Be than beryl which has traditionally been the world's major source of the metal. Most phenakite in the north T-zone is greater than 100 μm in size and is relatively free of inclusions except for quartz. Its average grain size and simple association with quartz make phenakite of the T-zone equally desireable in terms of its amenability to beneficiation.

Bertrandite

Bertrandite ($Be_4Si_2O_7(OH)_2$) is the second most common Be-bearing mineral in the north T-zone. Typically it occurs as aggregates of randomly oriented or radiating tabular grains in quartz. As shown in Plate 3.3a, bertrandite aggregates may occur towards the center of the host quartz or across grain boundaries and are easily distinguished from quartz by differences in relief and birefringence. Individual crystals vary in length from 5-10 μm and are usually less than 5 μm in diameter as shown in Plate 3.3b.

Compositionally, bertrandite appears homogeneous in backscattered electron images and may be distinguished from phenakite by relative proportions of Si in the two minerals. In addition, bertrandite displays moderate damage during electron microprobe analysis which is presumably due to dehydration. Bertrandite and phenakite are probably similar in terms of relative positioning in the paragenetic sequence. Bertrandite may be slightly earlier because it occurs as inclusions within medium grained quartz whereas phenakite is typically intergrown with, or interstitial to, quartz.

Bertrandite was first identified in rocks of the T-zone by Jambor (1985). In his study, Jambor noted a local predominance of bertrandite over phenakite which suggests that bertrandite might be an appreciable contributor to Be enrichment in that zone.

Based on the samples studied here, bertandite appears to be a rare accessory in all rock types and is probably of limited economic significance. The disparity in results between this study and that of Jambor (1985) supports the suppostion that rocks of the T-zone in general are extremely inhomogeneous in nature.

Gadolinite

A third Be-bearing mineral in the north T-zone is one which has been tentatively identified as gadolinite ($(Y,Ce,Nd,Gd,Dy,Ca)_2FeBe_2(SiO_4)_2O_2$). It is of minor importance as a Be-bearing phase but is one of the principal Y-bearing minerals and is described in detail in the Y and REE section of this chapter.

Helvite group member

The least common Be-bearing mineral in the north T-zone is a sulfosilicate tentatively identified as a member of the helvite group ($(Fe,Mn,Zn)_4(BeSiO_4)_3S$). It was identified in one, apparently unusual, sample where it occurs as subhedral inclusions in phenakite associated with sphalerite and an Fe-sulphide. As shown in Plate 3.4a, the mineral is extremely fine grained (typically less than 10 μm in diameter) and is altered in appearance.

Qualitative electron microprobe analyses indicate that this mineral contains major Si, S, Fe and Mn with minor amounts of Zn. Compositionally, this member of the helvite group appears to lie somewhere between danalite and helvite which are the Fe and Mn end members respectively. Figure 3.1 shows a characteristic energy dispersive spectrum of the sulfosilicate. Although Be does not appear in the spectrum due to the absorption of its soft radiation by the detector used in energy dispersive analysis, the relative proportions of the detectable elements and the accompanying low element totals suggest that the mineral is a Be-bearing sulfosilicate of the helvite group.

Based on the samples studied here, the sulfosilicate of the helvite group is present exclusively in the *quartz-biotite(±chlorite)-feldspar* unit of the Lower Intermediate zone. It should be noted that the particular sample in which the helvite group member was identified was enriched in Zn- and Fe-sulphides. Other sulphide-rich Be-bearing rock types in the T-zone may also contain the helvite group mineral.

The Be-bearing sulfosilicate appears to be rare in rocks of the T-zone and is not of economic importance but is included here for completeness.

C. PROBABLE BY-PRODUCTS: YTTRIUM AND RARE EARTH ELEMENTS

The three Y-bearing minerals identified in this study are:

a) xenotime

b) gadolinite

c) thorite.

Xenotime, a phosphate, is the most important Y-bearing mineral in the north T-zone because it contains the highest concentrations of Y. Gadolinite and thorite, both silicates, are of lesser importance in terms of Y content although they are intimately associated with xenotime and do contribute to the overall Y enrichment of the rocks. Y also occurs, in minor to trace amounts, in purple fluorite, zonally metamictized zircons and a REE-silicate tentatively identified as britholite.

Six REE-bearing minerals were identified in this study including four fluocarbonates, one phosphate and one silicate. The six minerals are listed below:

a) LREE-bearing fluocarbonates

  bastnaesite
  parisite
  roentgenite
  synchysite

b) monazite

c) britholite.

The fluocarbonates and monazite are enriched in LREEs (light rare earth elements) and contain major amounts of La, Ce and Nd. Britholite shows enrichment in the MREEs (middle rare earth elements) Nd, Sm, Gd and Dy, which are also present in minor amounts in the Y-bearing minerals xenotime and gadolinite. REEs also occur, in minor to trace amounts, in bipyramidal zircons.

Xenotime

Xenotime ($(Y,Gd,Dy,Er,Fe)PO_4$) cannot be seen in hand sample and is typically very fine grained with individual grains ranging from 2-50 μm in diameter. Locally it occurs as the euhedral, high relief, strongly birefringent grains shown in Plate 3.4b, which are easily identified in thin section using standard optical petrography. However, xenotime typically occurs as anhedral, brown or opaque grains and grain aggregates which are intergrown with other minerals on a micron scale. Such fine grained intergrowths can only be fully resolved using backscattered electron imagery. Plate 3.5a shows individual grains and aggregates of opaque xenotime in quartz. As shown in the backscattered electron image in Plate 3.5b, the xenotime actually contains minute Fe-oxide inclusions which may cause its opaque appearance. In Plates 3.6a, 3.6b, 3.7a and 3.7b xenotime is shown intimately intergrown with metamict thorite. There appears to be a strong association between xenotime and thorite in Y-enriched rocks of the T-zone. The two minerals are isomorphous (Vlasov, 1966) and are postulated to be contemporaneous here. In this typical association, xenotime may either enclose (Plate 3.7a), or be enclosed by (Plate 3.6b), thorite. Rarely, xenotime occurs as corroded ovoids which are overgrown by thin mantles of zircon as shown in Plates 3.8a and 3.8b. Xenotime is also isomorphous with zircon and is known to form epitaxial growths with it (Vlasov, 1966).

Xenotime, whether it is present as a single phase or intergrown with other phases as described above, is most commonly hosted by quartz. The anhedral or corroded grains may have been partially replaced by quartz. Locally, xenotime and thorite together occur in even more complex intergrowths associated with synchysite and siderite (see Plate 3.7a) or partially replaced by gadolinite and apatite (see Plate 3.7b). Dark purple fluorite is often associated with these complex intergrowths and may contain individual inclusions of xenotime. These xenotime inclusions form colourless haloes in the fluorite which elsewhere appears purple in plane polarized light.

Xenotime is probably one of the earliest formed minerals of economic interest. It appears to be earlier than the Be mineralization and is locally partially replaced by the Be,Y-bearing mineral gadolinite as shown in Plate 3.7b. Xenotime also appears to predate the LREE mineralization as it is locally enclosed in synchysite (see Plate 3.7a) or cross-cut by monazite as shown in Plates 3.7b and 3.8b.

Qualitative electron microprobe analyses indicate that xenotime of the T-zone contains major Y and P with minor amounts of Gd, Dy, Er and Fe which are probably substituting for Y. There are slight variations in REE content, with concomittant changes in Y content, from grain to grain but in general individual grains appear to be compositionally homogeneous. Figure 3.2 shows a characteristic energy dispersive spectrum of xenotime.

Based on the samples used in this study, xenotime is most abundant in the *quartz-thorite* unit of the Upper Intermediate zone. It also occurs in the *quartz-biotite(±chlorite)-oxides* unit of the Lower Intermediate zone and the Quartz zone but is probably of limited economic interest in these rocks.

In terms of Y and MREE content, xenotime is a desireable ore mineral. However, its fine grained nature and intimate association with thorite may pose metallurgical problems. The zircon-xenotime intergrowths appear to be rare but may also affect Y recoveries if the presence of zircon impedes the liberation of xenotime.

Gadolinite

A silicate tentatively identified as gadolinite ($((Y,Ce,Nd,Gd,Dy,Ca)_2FeBe_2(SiO_4)_2O_2)$, is the second most important Y-bearing mineral in the north T-zone in terms of Y and MREE content. It typically occurs as irregular masses partially replacing xenotime and thorite as shown in Plates 3.7b and 3.9a. It is not visible in hand sample, but once identified in thin section is easily recognized by its characteristic greenish brown colour in plane polarized light as shown in Plate 3.9a. Gadolinite also occurs locally as discrete subhedral, prismatic grains (see Plate 3.9b). Individual grains of gadolinite range from 100-500 μm in diameter and irregular masses may be several times larger.

As shown in plates 3.7b and 3.9b, apatite is commonly associated with gadolinite. Its presence in the T-zone appears to be restricted to those rocks which contain gadolinite. The development of apatite appears to be contemporaneous with the replacement of xenotime by gadolinite. This suggests that the replacement of an Y-phosphate by an Y-silicate allowed the development of a second phosphate. The abundance of purple fluorite (CaF_2), which occurs interstitial to all phases, may explain the development of a Ca-bearing phosphate in particular. The apatite appears to be essentially free of REEs.

Temporal relationships between gadolinite and other Be-bearing minerals are unclear as no direct cross-cutting relationships were observed. In terms of Y mineralization, gadolinite is the latest formed phase as it partially replaces preexisting xenotime and thorite. LREE-bearing minerals such as monazite appear interstitial to, and cross-cut, earlier formed gadolinite (see Plates 3.7b and 3.9a).

Qualitative electron microprobe analyses indicate that gadolinite of the T-zone contains major amounts of Y, total REEs, Si and Fe with minor Ca and trace amounts of Cl. It appears to be a REE-rich gadolinite where Ce, Nd, Gd and Dy substitute for Y and result in a relatively low Y content. Nd is the most abundant REE in gadolinite which contains lesser amounts of Gd, Dy and Ce respectively. Chemical analyses in the literature (Beus, 1966; Valsov, 1966) indicate that gadolinite may vary considerably in composition which results in varietal names such as Ce-gadolinite, a LREE-enriched variety, and calcio-gadolinite, a Ca-rich variety. Thor Lake gadolinite appears to be MREE-enriched with an abundance of Nd and to a lesser extent Gd, Dy and Ce. A Nd-selective variety of gadolinite has not yet been described in the literature.

As in xenotime, there is some compositional variation between grains in terms of REE content relative to Y content. Damage to gadolinite by the electron microprobe suggest that the mineral may be hydrated. In some gadolinite, where Y and REEs are partially replaced by Ca, a parallel substitution of OH^- for the corresponding O is known to occur (Beus, 1966). This substitution of OH^- for O may have occurred in the Ca-bearing gadolinite of the T-zone and would explain the dehydration effect mentioned above. Although Be is not detectable by energy dispersive analysis, based on the relative proportions of the elements detected and accompanying low element totals, in conjunction with its optical properties, this mineral has been tentatively identified as gadolinite. A characteristic energy dispersive spectrum of gadolinite is shown in Figure 3.3.

Gadolinite is most abundant in the *quartz-thorite* unit of the Upper Intermediate zone but was also identified in one sample of mineralized granite associated with chlorite and parisite. Based on the samples studied here, it appears to be quite rare and is probably of limited economic significance, locally contributing to Y enrichment in the Upper Intermediate zone.

Thorite

The third Y-bearing mineral is a Th-silicate tentatively identified as a member of the thorite group ($(Th,Fe,Y,P,Ca)SiO_4$). Megascopically, it is easily identified by its characteristic rusty brown colour and radioactivity. Thorite of the T-zone is metamict and in thin section appears dark brown or opaque as shown in Plates 3.9a and 3.10a. Typically it occurs as subhedral to anhedral grains and grain aggregates intergrown with xenotime and enclosed in quartz, fluorite, synchysite or gadolinite (see Plates 3.7a, 3.7b and 3.9a).

Individual grains average 5-20 μm in diameter and aggregates may be several times larger. In xenotime-poor rocks, aggregates of thorite are often present in biotite or chlorite. Plate 3.10b shows a framboidal aggregate of thorite in biotite. Less commonly, thorite is intergrown with ilmenite, K-feldspar and biotite which together form rounded inclusions in albite as described in Chapter 2 (see Plate 2.5b).

Thorite appears to be contemporaneous with xenotime and is probably earlier than Be and LREE mineralization. Its temporal relationship with Ga-bearing feldspar is unclear although its common association with biotite (±chlorite) suggests that it may be a later phase. Most Th appears to have been consumed during the development of thorite and is generally absent in phases such as monazite and zircon for which minor amounts of Th are often reported.

Qualitative electron microprobe analyses indicate that the thorite group mineral contains major concentrations of Th, Si, Y, P and Fe with minor to trace amounts of Ca. Thorite of the T-zone is compositionally inhomogeneous as illustrated in the backscattered electron image shown in Plate 3.10b. Qualitative electron microprobe analyses indicate that there is a negative correlation between Th, and Y, P and Fe, which substitute for Th. The darker areas in Plate 3.10b are more Fe-, Y- and P-rich than the brighter areas which are Th-rich. Although Y is not typically present in minerals of the thorite group, it has been noted in thorite from the Harding pegamatite (Lumpkin and Chakoumakos, 1986). The presence of Y in thorite of the T-zone is probably due to the contemporaneous growth of thorite with xenotime. Beam damage to thorite during electron microprobe analysis and low element totals suggest that the thorite may be hydrous. Other Y-bearing thorites are reported to contain up to approximately 9 weight % H_2O (Lumpkin and Chakoumakos, 1986). In minerals which contain abnormal amounts of nonessential water that is lost upon heating, the water is considered to have been introduced during metamictization (Mitchell, 1973). Hydration of thorite is probably a result of metamictization. A characteristic energy dispersive spectrum of the thorite group mineral is shown in Figure 3.4.

Thorite is obviously most abundant in the ***quartz-thorite*** unit of the Upper Intermediate zone. It also occurs as an accessory in mineralized granite, all units of the Lower Intermediate zone and the Quartz zone. In terms of Y content, thorite is probably a minor contributor to Y enrichment in the T-zone. However, its intimate association with xenotime may affect Y recoveries and is important in this respect.

LREE-bearing fluocarbonates

The most abundant REE-bearing minerals in the T-zone are the LREE-bearing fluocarbonates of the bastnaesite group listed, with mineral formulae, below:

a) bastnaesite	$(La,Ce,Nd)CO_3F$
b) parisite	$(La,Ce,Nd)_2Ca(CO_3)_3F_2$
c) roentgenite	$(La,Ce,Nd,Fe)_3Ca_2(CO_3)_5F_3$
d) synchysite	$(La,Ce,Nd,Fe)Ca(CO_3)_2F$.

The minerals are listed in order of decreasing REE content. Approximately 95% of LREE enrichment in the T-zone may be attributed to the presence of this mineral group. As a group, these minerals are easily identified in hand sample by their characteristic brick-red colour as shown in the hand sample photographs in Plates 2.16b and 2.23a. In thin section, these minerals are again easily recognized, as a group, by their reddish brown colour and local high birefringence as shown in Plates 2.17a, 2.17b and 2.18a. However, backscattered electron imagery and compositional information are neccessary to differentiate the four minerals accurately.

In the north T-zone, the REE-fluocarbonates typically occur as syntaxic intergrowths of two or three of the minerals which are present together within a single grain. Such syntaxic intergrowths, which simulate a single crystal, are termed polycrystals (Donnay and Donnay, 1953). According to these authors, the occurrence of these polycrystals is common in the bastnaesite group minerals and is the result of the inability of the system $CeFCO_3$-$CaCO_3$ to form solid solutions. Different minerals precipitate under different conditions and, where the species alternate and develop within a polycrystal, periodic changes in the system (possibly variable pH) are postulated (Donnay and Donnay, 1953).

Bastnaesite-parisite is the most common polycrystal combination and the two minerals together probably comprise approximately 80-90% of the REE-fluocarbonate content of the rocks. A mineral tentatively identified as roentgenite is locally intergrown with bastnaesite and parisite and is probably the third most abundant fluocarbonate. Synchysite appears to be the least common of the four and is usually present as a single phase.

The REE-fluocarbonate polycrystals display several habits and may be acicular, tabular or subhedral to anhedral blocky grains. All three polycrystal types may occur together within a single rock and appear to be contemporaneous. In general, the subhedral type are most common and occur throughout the T-zone rocks. Acicular polycrystals are rarer and occur mainly in quartz-rich assemblages of the Upper Intermediate zone. The tabular variety appears to be restricted to the *quartz-bastnaesite group* unit of the Upper Intermediate zone.

Acicular polycrystals usually occur as massive aggregates which form plumose textures (see Plate 2.17a) or radial sprays as shown in Plate 3.11a. They are typically composed of syntaxic intergrowths of bastnaesite and parisite. Either bastnaesite or parisite may predominate. The backscattered electron image in Plate 3.11b shows the irregular nature of the bastnaesite-parisite intergrowth in a bastnaesite-dominated acicular polycrystal. Individual needles may be less than 20 μm wide and 200 μm long but aggregates may be upwards of 1 X 2 cm in size. Acicular polycrystals commonly have interstitial purple fluorite and are often enclosed in quartz.

Subhedral to anhedral blocky polycrystals appear in thin section as shown in Plates 3.12a, 3.13a and 3.14a. These polycrystals appear to be the only type in which more than two phases are intergrown. A polycrystal containing more than two of the REE-fluocarbonates has not yet been described in the literature although it is theoretically possible and in some cases would actually be expected (Donnay and Donnay, 1953). Plate 3.12b shows a backscattered electron image of a parisite-dominated syntaxic intergrowth of parisite, roentgenite and bastnaesite. The intergrowth appears quite irregular except for the parallel alignment of bastnaesite blebs. The backscattered electron image in Plate 3.13b shows a roentgenite-bastnaesite-parisite polycrystal. In this roentgenite-dominated polycrystal, the bastnaesite and parisite display a regular lamellae-like intergrowth with roentgenite unlike the irregular intergrowths described above. A simple anhedral bastnaesite-parisite polycrystal is shown in the backscattered electron image in Plate 3.14b. It is bastnaesite-dominated and the intergrowth is irregular in nature. Rarely, synchysite occurs as thin rims on parisite-bastnaesite polycrystals. Subhedral REE-fluocarbonate polycrystals may vary in size from approximately 50 μm to 2 mm in diameter but are usually between 100 μm and 500 μm. These polycrystals are hosted by a variety of minerals but are most commonly enclosed in, or partially replaced by, quartz, ankerite, fluorite and K-feldspar.

Tabular polycrystals are typically bastnaesite-parisite intergrowths and often occur as radiating aggregates (see Plate 2.17b). The backscattered electron image in Plate 3.15a shows bastnaesite intergrown with parisite in a tabular grain. Lamellae-like bastnaesite within the intergrowths appears to be oriented parallel to the long axis of the grain. Single tabular polycrystals may be up to 300 μm in diameter and 2 mm long but usually occur in much larger aggregates. Quartz, fluorite or ankerite usually occur interstitial to these polycrystals.

Rarely, the REE-fluocarbonates occur as single phases. Bastnaesite is present locally as very fine grained, anhedral inclusions in columbite of the Wall and Lower Intermediate zones. Irregular masses of synchysite enclose xenotime-thorite intergrowths in the *quartz-thorite* unit of the Upper Intermediate zone. Other single phases are probably anhedral portions of preexisting polycrystals.

Bastnaesite is probably the most abundant of the REE-fluocarbonates. In thin section it commonly displays strong birefringence with upper third or lower fourth order interference colours (see Plates 2.17b, 3.13a and 3.14a) and appears colourless in plane polarized light. However, locally its birefringence is masked by the strong red colour of associated parisite as shown in Plate 3.11a. Compositionally, bastnaesite is the most REE-rich fluocarbonate. Qualitative electron microprobe analyses indicate that bastnaesite of the T-zone contains major amounts of La, Ce and Nd with minor to trace amounts of Sm and Ca. Ce is the most abundant REE with lesser La and Nd respectively. The presence of F was verifyed using qualitative wavelength dispersive analysis. A characteristic energy dispersive spectrum of bastnaesite is shown in Figure 3.5. Bastnaesite has been positively identified, using X-ray diffraction techniques, by Jambor (1985) and Buchan (1985).

In thin section, parisite locally appears colourless in plane polarized light (see Plate 3.12a) but its optical properties are typically masked by its reddish brown colour. Buchan (1985) and Jambor (1985) suggest that the turbid or semi-opaque appearance of some parisite is due to the presence of minute Fe-oxide inclusions. Combined qualitative electron microprobe analyses and backscattered electron imagery used in this study indicate that there are no discrete Fe-oxide inclusions in the fluocarbonate minerals. Rather, the colour and opacity of some parisite (as well as roentgenite and synchysite) appears to be due to the actual Fe content of the mineral(s) where Fe is substituting for REEs. Qualitative electron microprobe analyses indicate that parisite of the T-zone contains major La, Ce, Nd and Ca with minor to trace amounts of Fe. The relative abundances of the REEs in parisite are essentially the same as those in bastnaesite with Ce as the principal REE. A characteristic energy dispersive spectrum of parisite is shown in Figure 3.6 for comparison with the other fluocarbonates. Parisite has been positively identified using X-ray diffraction techniques by Jambor (1985) and Buchan (1985). Locally, parisite appears to be compositionally inhomogeneous as shown in the backscattered electron image in Plate 3.16b. Qualitative electron microprobe analyses indicate that the darker area in the image has the same relative proportions of REEs and Ca as the brighter areas but the accompanying element totals are lower. This information, in conjunction with evidence of beam damage during analysis, suggests that the darker area contains more volatiles and is probably altered parisite.

Qualitative electron microprobe analyses of a third REE-fluocarbonate, tentatively identified as roentgenite, indicate that it contains major La, Ce, Nd and Ca with minor Fe. It is differentiated from parisite by slightly but consistently higher concentrations of Ca and Fe and a lower concentration of La. As shown in Plates 3.12a and 3.13a, it appears almost opaque in thin section, probably due to its Fe content. A characteristic energy dispersive spectrum of roentgenite is shown in Figure 3.7 to illustrate compositional differences between it and associated REE-fluocarbonates. Relative proportions of REEs are again similar to those in bastnaesite (and parisite) with Ce and La as the most abundant REEs although Ce/La and Nd/La ratios appear to be higher in roentgenite. Of the four fluocarbonates, parisite and roentgenite are the most similar in terms of composition (Donnay and Donnay, 1953). A comparison of the spectra shown in Figures 3.6 and 3.7 illustrates this compositional similarity.

The fourth and least common of the REE-fluocarbonates has been tentatively identified as synchysite. Qualitative electron microprobe analyses indicate that this mineral contains major La, Ce, Nd, Fe and Ca with trace amounts of Th which latter may be due to associated thorite. Relative proportions of REEs appear to be similar to those in the other fluocarbonates with Ce as the most abundant REE although the concentration of Nd typically exceeds that of La in synchysite unlike the other fluocarbonates where La is always greater than Nd. Ce/La and Nd/La ratios, which are even higher in synchysite than in roentgenite, appear to increase from bastnaesite through the group to synchysite. Total REE concentrations in synchysite are substantially reduced compared to the other fluocarbonates, presumably due to substitution by Fe. A characteristic energy dispersive spectrum of synchysite is shown in Figure 3.8.

By definition, the different species within a polycrystal have formed contemporaneously. Temporal relationships between the bastnaesite group minerals and other LREE-bearing minerals are not clear although they often occur in the same rocks and are probably similar in terms of positioning in the mineralization sequence. In Plate 3.14a, monazite and REE-fluocarbonates are shown together in ankerite and appear to be contemporaneous. In general, LREE mineralization appears to be earlier than Be mineralization and later than Y- and MREE-enriched phases. In the Wall zone, REE-fluocarbonates occur interstitial to Ga-bearing feldspar which suggests that LREE mineralization is later than Ga mineralization. Based on the samples studied here, the bastnaesite group minerals appear to have been present throughout much of the mineralization sequence of rocks in the T-zone. Because temporal relationships between the various alteration assemblages of the T-zone are presently uncertain, it is not possible to compare the fluocarbonates from one zone directly with those of another. However, certain generalizations can be made for each alteration assemblage. The fluocarbonates are most abundant in the Upper Intermediate zone where they appear as late phases enclosed in quartz or ankerite with interstitial fluorite (see Plates 2.17a, 2.17b and 2.18a). In the Lower Intermediate zone and granite, these minerals appear to be earlier phases where they are often enclosed in, or partially replaced by, K-feldspar (see Plate 2.3b). Conversely, in the Wall zone the REE-fluocarbonates occur interstitial to K-feldspar (see Plate 2.7a).

The REE-fluocarbonate minerals are most abundant in the *quartz-bastnaesite group* unit of the Upper Intermediate zone where they occur as massive intergrowths which comprise approximately 90% of the rock. This unit of LREE-enrichment is currently considered to be the principal source of LREEs in the T-zone. Members of the bastnaesite group also occur as accessories in all other alteration assemblages of the T-zone. REE-fluocarbonates appear to be the most common and widespread of all the minerals of economic interest in the T-zone. The presence of these brick-red minerals corresponds directly to areas enriched in Ce, La and Nd.

In terms of total REE recoveries, syntaxic intergrowths of the bastnaesite group minerals do not pose a problem. However, it should be noted that a REE concentrate from the *quartz-bastnaesite group* unit of the Upper Intermediate zone will actually contain the three REE-fluocarbonates: bastnaesite, parisite and roentgenite. Varying proportions of the three species present within the rock will affect relative abundances of REEs to some extent.

Monazite

Monazite ((La,Ce,Nd)PO_4), is the second most common LREE-bearing mineral of the T-zone after the REE-fluocarbonate group. Typically it occurs as euhedral to subhedral grains (see Plates 3.2b, 3.14a and 3.15b) which range in size from 50-500 μm in diameter. Monazite is easily identified in thin section by its characteristic high relief, strong birefringence (third and fourth order interference colours) and habit. It is usually hosted, and locally partially replaced by, ankerite, K-feldspar, quartz or fluorite and is often associated with REE-fluocarbonate polycrystals (see Plate 3.14a). Rarely, subhedral monazite is associated with, and partially replaced by, phenakite as shown in Plate 3.2b. Anhedral grains and aggregates of monazite are present less commonly than the subhedral type and are typically associated with xenotime, thorite and gadolinite (see Plates 3.7b and 3.9a) or xenotime-zircon intergrowths as shown in Plates 3.8a and 3.8b.

Monazite appears to be contemporaneous with other LREE-bearing minerals in the T-zone. Locally it appears to cross-cut gadolinite and xenotime and is probably later than the Y mineralization. Conversely, monazite is locally partially replaced by phenakite and is probably earlier than the Be mineralization.

Qualitative electron microprobe analyses indicate that monazite contains major amounts of P, La, Ce and Nd. Where associated with the Y-bearing minerals xenotime and thorite, it also contains trace amounts of Th but is typically Th-free. Like the REE-fluocarbonates, Ce is the most abundant REE in monazite with lesser amounts of La and Nd respectively. A characteristic energy dispersive spectrum of monazite is shown in Figure 3.9. It illustrates the similarity in the relative proportions of REEs in monazite and the REE-fluocarbonates.

Based on the samples used in this study, monazite occurs as an accessory mineral in the biotite-bearing units of the Lower Intermediate zone and in the *quartz-thorite* and *quartz-feldspar* units of the Upper Intermediate zone. Rarely, it is present in the *breccia* unit of the Wall zone.

Monazite is of limited economic interest. It may contribute locally to LREE enrichment in the T-zone but is probably of minor importance.

Britholite

The third REE-bearing mineral present in the north T-zone has been tentatively identified as britholite ($((\mathrm{Ce,Nd,Gd,Dy,Y})_3\mathrm{Ca}_2(\mathrm{SiO}_4)_3(\mathrm{OH}))$). Its presence was noted in only one sample where it occurs as an anhedral grain intergrown with parisite and monazite in quartz. As shown in Plate 3.16a, it is fine grained and appears opaque in thin section. The backscattered electron image shown in Plate 3.16b shows the nature of the intergrowth between the three REE-bearing phases. All three are probably closely related in age although monazite and parisite are typically present at britholite grain boundaries and may be slightly later. All three minerals are partially replaced by surrounding quartz.

Qualitative electron microprobe analyses indicate that this REE-silicate contains major amounts of Si, Ce, Nd, Gd, Dy and Ca with trace amounts of Y and Cl. It is easily damaged during electron microprobe analysis which suggest that the mineral may be hydrous. Nd is the most abundant REE in the mineral which contains lesser amounts of Gd, Dy and Ce respectively. A characteristic energy dispersive spectrum of the REE-silicate tentatively identified as britholite is shown in Figure 3.10.

A comparison of the energy dispersive spectra of gadolinite (Fig.3.3) and britholite (Fig.3.10) suggests that the two minerals are very similar. Both are Nd-rich silicates with the same relative proportions of REEs. The principal difference is that britholite is essentially Y-free whereas gadolinite contains major Y. It is possible that the REE-silicate is actually a variety of gadolinite in which there is a complete substitution of REEs and Ca for Y although such a gadolinite does not appear to have been described in the literature (Vlasov, 1966). Output from the MinIdent program (Smith and Leibovitz, 1986), based on qualitative electron microprobe analysis of the REE-silicate, indicates that britholite and gadolinite are both possibilities and are equally likely. The mineral is tentatively identified as britholite here based on its low Y content and the absence of xenotime or apatite which are usually associated with gadolinite. However, the possibility remains that the REE-silicate may actually be an essentially Y-free gadolinite. Ion probe analysis of the REE-silicate would be useful in identifying this mineral based on its Be content. Gadolinite contains major amounts of Be whereas britholite does not.

Based on the samples used in this study, the REE-silicate tentatively identified as britholite is restricted to the *quartz-biotite(±chlorite)-oxides* unit of the Lower Intermediate zone. It appears to be very rare and is not of economic significance.

D. POSSIBLE BY-PRODUCTS: NIOBIUM, ZIRCONIUM AND GALLIUM

The two Nb-bearing minerals which have been identified in the T-zone are columbite and ashanite. Columbite is the most abundant of the two oxides and is also the most important Nb-bearing mineral in terms of Nb content. Ashanite, a Nb,U-bearing oxide, occurs rarely and is not a major contributor to Nb enrichment in rocks of the T-zone. Nb also occurs, in minor to trace amounts in Ti-oxides throughout the deposit.

Zircon appears to be the only Zr-bearing mineral in the T-zone. Three types of zircon were identified in this study.

Ga occurs exclusively in albite and K-feldspar where it substitutes for Al^{3+}.

Columbite

Columbite ($(Fe,Mn,Ti)Nb_2O_6$) typically occurs either as fined grained subhedral inclusions in quartz, albite and K-feldspar (see Plates 2.8a and 2.9b) or as larger grain aggregates which overgrow and replace biotite as shown in Plate 2.14b. Plate 3.17a shows columbite aggregates included in quartz and replacing lath-like biotite. Individual grains are on average 20-75 μm in diameter but aggregates are generally greater than 100 μm in size. Locally, columbite contains minute inclusions of anhedral bastnaesite and ashanite as shown in Plate 3.17b.

Columbite appears to have been present throughout much of the mineralization sequence of the T-zone. Its presence in earlier formed feldspar, later quartz and its replacement of biotite suggests that Nb mineralization probably took place over a lengthy time period.

Quantitative electron microprobe analyses of columbite from the Lower Intermediate and Wall zones are presented in Table 3.1. Based on its high Fe content, columbite of the T-zone probably represents the variety ferrocolumbite, where FeO:MnO is greater than 3:1 (Vlasov, 1966). The analyses in Table 3.1 compare favourably with ferrocolumbite analyses in the literature (Vlasov, 1966; Foord, 1982) and with FeO:MnO well above 3:1, columbite of the T-zone should be correctly referred to as ferrocolumbite. Ta concentrations are extremely low and in most cases are only slightly greater than the statistical detection limit calculated for Ta in Appendix I. Columbite appears to be compositionally homogeneous within discrete grains and shows little compositional variation from grain to grain or rock to rock as shown in Table 3.1.

Based on the samples used in this study, columbite is most common in the *quartz-biotite(±chlorite)-oxides* unit of the Lower Intermediate zone and is probably of economic interest in this rock type due to its abundance and occurrence as large grain aggregates. It is also commonly present in all units of the Wall zone and may be of economic interest in these rocks. However, columbite is typically very fine grained in the Wall zone and could be more difficult to extract than in the Lower Intermediate zone. Columbite also occurs locally in mineralized granite, the *quartz-feldspar-magnetite* unit of the Upper Intermediate zone and rarely, in the Quartz zone.

Ashanite

A second Nb-bearing mineral, tentatively identified as ashanite ($(\mathrm{(Nb,Ta,U,Fe,Mn)_4O_8})$), appears to be rare in rocks of the T-zone. Its presence is restricted to the *quartz-biotite(±chlorite)-oxides* unit of the Lower Intermediate zone where it occurs exclusively as anhedral grains enclosed in columbite (see Plate 3.17b). It is very fine grained and ranges from 2-10 μm in diameter.

A semi-quantitative electron microprobe analysis of the Nb,U-bearing mineral tentatively identified as ashanite is presented in Table 3.1. The mineral contains major Nb and U with minor to trace amounts of Fe, Ti, Mn and Ta. Although element concentrations are not directly comparable to those in the literature (Fleischer *et al.*, 1981) relative proportions of major constituents are similar. The major difference between ashanite described in the literature and the Nb,U-bearing mineral from the T-zone is that latter appears to be hydrous. The bright spots seen in Plate 3.17b are burn marks from electron microprobe analysis and indicate that the mineral may be hydrous. In Table 3.1, H_2O content is calculated as the difference of all other elements and approaches 11 weight % in the Nb,U-oxide. It is possible that hydration of the mineral is the result of metamictization where weakly bonded H_2O is absorbed by the metamict mineral. The Nb,U-oxide may simply be a metamict ashanite or conversely, it may be a different mineral species. Output from MinIdent (Smith and Leibovitz, 1986), based on semi-quantitative analysis of the the Nb,U-oxide indicate samiresite as another possibility. Samiresite, a recently discredited mineral name, is correctly termed plumbian uranpyrochlore (Hogarth, 1977). Analyses of the Pb-rich uranpyrochlore (Vlasov, 1966) indicate that it is hydrous and contains concentrations of major elements similar to those of the Nb,U-oxide. However, because it is defined as a Pb-rich mineral, the pyrochlore is probably not a viable alternate identity for the Nb,U-oxide which latter does not contain detectable levels of Pb. Based on the limited information available, the mineral has been tentatively identified as ashanite. Additional material and analytical data will be required before a positive identification can be made.

The Nb,U-oxide tentatively identified as ashanite is rare in rocks of the T-zone and is not of economic importance. It is included here for completeness.

Zircon

Three different types of zircon ($(Zr,Ca,Ti,Fe,Y,REEs,Th,U)SiO_4$) have been identified in the north T-zone. These are listed below:

a) bipyramidal

b) zonally metamictized

c) overgrowths on xenotime.

Bipyramidal zircon

The most common zircons in the north T-zone are colourless, euhedral to subhedral bipyramidal zircons which are, on average, 20-50 μm in diameter. They occur as individual grains, clusters and locally in strings which form skeletal outlines of an unidentified preexisting mineral as shown in Plate 3.18a. Such zircons are always hosted by quartz and are probably late stage minerals.

Qualitative electron microprobe analyses indicate that the bipyramidal zircons are composed mainly of Zr and Si with minor concentrations of Ca, Ti and Fe and trace amounts of Al, Ce, Nd, Sm, Gd and Hf. They are compositionally variable from grain to grain and some crystals are zoned as evidenced by variations in birefringence (see Plate 3.18a). Qualitative electron microprobe analyses indicate that zoning in these zircons is due to quite substantial variations in abundances and relative proportions of the minor and trace elements listed above. Some areas are easily damaged during electron microprobe analysis which suggests that they may be hydrous and that H_2O may also play a role in compositional zoning.

Based on the samples used in this study, bipyramidal zircons occur most commonly in Lower Intermediate zone units, the ***quartz-bastnaesite group*** unit of the Upper Intermediate zone and adjacent rocks of the Quartz zone. They also occur locally in granite and other units of the Upper Intermediate zone. Bipyramidal zircons typically comprise less than 2% of the rocks in which they occur and are therefore probably not of economic interest.

Zonally metamictized zircon

The second type of zircon is less common than the bipyramidal variety and occurs as euhedral to subhedral grains which range from 25-100 μm in diameter. They may occur as individual grains or aggregates with interstitial biotite (±chlorite) and columbite.

In thin section, these zircons display a pronounced zoning and anomalously low birefringence with interference colours ranging from first order grey to yellow. The zircons are strongly fractured and there is a marked difference in relief between the zones of a single grain (see Plate 3.18b).

The backscattered electron image shown in Plate 3.19a illustrates the complex nature of the zoning in such zircons. The core of each grain is occupied by a euhedral to subhedral grain varying in diameter from 10-50 μm. The cores themselves are zoned as shown in Plate 3.19b. The white and grey areas within the cores are compositionally similar as seen in Table 3.2. The difference in average atomic number between the two compositions is presumably due to minor variations in relative abundances of elements such as Hf and Y. The grey areas within the cores typically display the unusual, pitted texture shown in Plate 3.19b. The source or cause of this texture is uncertain but may be due to corrosion of preexisting zircon cores.

Zoning outside the core is oscillatory in nature changing regularly from dark grey to white from the core to the outer rim of each crystal. Each zone is 2-5 μm wide and follows the outline of the core. The oscillatory zoning always starts with a dark grey zone (darkest grey in backscattered electron image) immediately adjacent to the core and oscillates between dark grey and white towards the rim.

The dark grey zones, as indicated in Table 3.2, contain approximately 4 weight % Y and 3-4 weight % U which both substitute for Zr, and up to approximately 14 weight% H_2O. These analyses are comparable with certain zircon analyses in the literature (Deer *et al.*, 1982) although the H_2O content of the dark grey zones is considerably higher. It is possible that the dark grey zones are more H_2O-rich than zircons reported in the literature simply due to more intense alteration and subsequent hydration. However, it is also possible that the calculated H_2O content (calculated as the difference of all other analysed element concentrations) of the dark grey zones actually includes minor amounts of other elements such as REEs which were not analysed here but are known to occur in other U-bearing zircons (Deer *et al.*, 1982). These U-bearing zones are severely metamict, exhibiting extremely low birefringence (first order grey interference colour). The intensity of radioactivity in zircon is known to be inversely proportional to birefringence (Morgan and Auer, 1941). The dark grey zones display severe beam damage during electron microprobe analysis, as can be seen by the abundance of burn marks in the grey areas in Plates 3.19a and 3.19b. The severity of dehydration during analysis in these zones is due to high H_2O content and the high H_2O content itself may be due to the presence of very weakly bonded H_2O absorbed by the metamict zircon. The results of an experimental study involving the synthesis of zircon in a fluorinated environment indicate that in a F-rich environment there may be substantial substitution of $(OH,F)_4$ for the SiO_4 tetrahedron in zircon (Caruba *et al.*, 1985). This substitution could explain the high H_2O and accompanying low Si totals in the dark gray metamict zones (see Table 3.2).

The white zones are compositionally similar to the white areas of the zircon core. These areas contain approximately half the amount of H_2O present in the dark areas and do not appear altered like the U-bearing zones. Fracturing in the white zones (see Plates 3.19a and 3.19b) may be caused by radiation damage from adjacent U-bearing zones and their subsequent expansion during hydration. Trace amounts of Li, Be, B and F were detected by ion probe in both areas.

The origin of this unusual oscillatory metamictization is of considerable interest. It is clearly related to the oscillation in U content which in turn must reflect cyclic variations in the physio-chemical environment of formation. It is postulated here that the pronounced zonal metamictization is basically a result of the extreme variation in U content (from approximately 4% to virtually nothing). The radioactive decay of atoms in the U-rich zones will have been accompanied by recoil of the nucleii during α-particle emission which is known to produce severe lattice damage in regions extending out a few hundred angstroms from the nucleus (Pellas, 1954). The high concentrations of U in the dark grey zones will have resulted in intense metamictization within these zones but the process will have stopped abruptly (within a few hundred angstroms) at the edge of the zone. Superimposed on this process will have been the more pervasive but weaker metamictization effects produced by the passage of the α-particles. Such a model would explain why these zircons in general show lower than normal birefringence but contain certain zones (U-bearing) that have extremely low interference colours.

In other parts of the same rock which host the zonally metamictized zircons, another type of zircon occurs. These zircons are colourless, euhedral to subhedral and vary in diameter from 10-50 μm. In thin section, they typically display first order yellow interference colours and do not appear zoned as shown in Plate 3.20a. They occur as individual grains and aggregates enclosed in quartz or with interstitial biotite (±chlorite) and columbite.

In the backscattered electron image shown in Plate 3.20b, the zircons are actually weakly zoned. Such zircons are similar in composition (in addition to average size and general appearance) to the cores of the zonally metamictized zircons described above (see Table 3.2).

It is postulated that these zircons may actually be core-type grains which did not, or were not able to, develop additional zones. If such zircons are actually core-type grains, it remains unclear why they did not develop radioactive zones as described above. It is possible that they were isolated from the U,Y-bearing fluids by the quartz or mica which encloses them.

Based on the samples used in this study, these unusual zoned zircons occur only in the *quartz-biotite(±chlorite)-oxides* unit of the Lower Intermediate zone and may be restricted to rocks outside the hemispherical north body. Although their presence is rare in rocks of the northern part of the T-zone, zonally metamictized and associated core-type zircons together may comprise up to 20% of the rock and may be of potential economic interest.

Zircon overgrowths on xenotime

The third type of zircon appears to be the rarest in the northern part of the T-zone. It mantles corroded ovoids of xenotime and appears opaque in thin section as shown in Plates 3.8a and 3.8b. The zircon overgrowths reach a maximum width of 2 μm but are typically less than 1 μm in diameter. Because the spatial resolution of the electron microprobe is inadequate, quantitative analysis of this zircon type was not possible. Semi-quantitative data presented in Table 3.2 indicates that the zircon is homogeneous and contains minor Th, Fe, Ti and Ca with trace amounts of Hf and Al. The H_2O content, as calculated by the difference of all other elements, is approximately 11 weight %. The hydrous and opaque nature of the zircon is probably due to metamictization resulting from the presence of radioactive Th.

This type of zircon has only been identified in one sample which is from a lense of Lower Intermediate zone alteration in granite immediately below the hemispherical north body of the T-zone. The zircon is not of economic significance itself but if it impedes the liberation process for xenotime it may effect Y recovery grades. If this zircon-xenotime association is more widespread than indicated by the selection of samples studied here, then the zircon overgrowths could potentially pose a metallurgical problem.

Ga-bearing feldspar

Assay results indicate that in the north T-zone, economically significant concentrations of Ga are restricted to the Wall zone. All three feldspathic units contain Ga with the entire zone averaging 500 ppm Ga. Results of this study show that Ga enrichment in the Wall zone may be attributed to the presence of Ga-bearing albite and K-feldspar in which Ga substitutes for Al^{3+}. Ga content is highest in albite.

Albite

Albite is present in all three units of the Wall zone. It is most abundant in the albite *aplite* unit where it occurs as randomly oriented subhedral laths with interstitial chlorite (± biotite) and carbonate (see Plate 2.7b). These laths typically have irregular boundaries and are fine grained, ranging in length from 250-750 μm and from 50-200 μm in diameter. In the *core* and *breccia* units, aggregates of platy albite (cleavelandite) overgrow and partially replace K-feldspar. In thin section, albite typically occurs as aggregates of randomly oriented, subhedral laths with interstitial chlorite and fluorite (see Plate 2.10a). Locally the laths form radiating aggregates as shown in Plate 2.10b. Albite in these units also has irregular boundaries as in the *aplite* unit, but is usually coarser grained ranging in size from 0.5-3.5 mm in length and from 50-500 μm in diameter.

Initial exploratory electron microprobe work resulted in the discovery of variable cathodoluminescence in albite with colours ranging from brilliant blue to bright red. Cathodoluminescence occurs in certain minerals when, under electron bombardment, they emit nonthermal radiation in the visible spectrum (Hagni, 1984). It may be caused by structural defects (self-activated cathodoluminescence) but is usually due to the presence of minor amounts of certain elements, generally from the lanthanide or transition element series (Hagni, 1984). These minor elements are known as activators and may act either by producing the characteristic visible luminescence for a particular mineral, or by altering its colour or intensity (Plant, 1976). Variations in the cathodoluminescence of minerals depends not only on the presence of an activator element, but also on the amount of activator present, the physical environment in which the mineral formed and its content of quencher elements (Hagni, 1984).

Initial electron microprobe analyses of Wall zone albite, on randomly selected areas of red and blue cathodoluminescence, indicate that the two colours may be differentiated compostionally on the basis of Ga content. In general, the blue areas show Ga enrichment ranging from approximately 0.1 up to 0.5 weight % Ga whereas the red areas typically contain less that 0.05 weight % Ga. Although such analyses from randomly selected areas provided general compositional information, they did not explain the reason for the variations in Ga content within the confines of one colour. In order to understand the nature of variations in the cathodoluminescence of albite better, several photomicrographs were obtained with the cathodoluminescence microscope in the Department of Earth Science at Cambridge University. That particular instrument is a fore-runner of the Technosyn Cathodoluminescence microscope model number 8200 which is now available commercially (D.G.W. Smith, pers. comm.). The photomicrograph in Plate 3.21 illustrates the nature of cathodoluminescence of albite in the *aplite* unit of the Wall zone.

Photomicrographs, such as that shown in Plate 3.21 brought out several interesting features of the cathodoluminescent albite. It can be seen that individual laths may be composed of areas of red and blue cathodoluminescence or they may exhibit a simple blue cathodoluminescence with no associated red. The red areas typically appear as irregular relicts isolated in surrounding blue areas. They commonly occur towards the center of individual laths and are referred to here as cores. The blue areas envelop the relict red areas and locally comprise entire laths. Outer rims of individual laths (usually blue) are typically ragged in appearance.

In addition to textural information, Plate 3.21 shows that there are actually different intensities of red and blue colour. In order to determine whether the variations in Ga content encountered during initial analytical work were related to these intensity differences, specific analytical points were selected (using the photomicrograph shown in Plate 3.21) to include the intensity variations of each colour. The results are presented in Table 3.3.

Quantitative electron microprobe analyses of selected points indicate two basic differences between areas of blue and red cathodoluminescence: Ga content and molecular proportions of Ab and Or. In terms of Ga content, red areas show a maximum of 0.06 weight % Ga whereas the blue areas show a maximum of 0.19 weight % Ga. In addition, although both areas are entirely lacking in the An molecule, the red areas contain slightly more K than the blue areas which are on average Ab_{99} in composition. Exceptionally pure albite, such as that in the T-zone, commonly occurs with the cleavelandite habit (Deer *et al.*, 1963).

As shown in Table 3.3, there is no perceptible compositional difference between the areas of bright and pale red cathodoluminescence. However, there is a marked difference between the areas of bright blue and blue-white cathodoluminescence in terms of Ga content. The bright blue areas contain 0.08-0.09 weight % Ga whereas the blue-white areas contain approximately twice that amount. Based on the results of this study, a minimum concentration of 0.08 weight % Ga appears to trigger a blue cathodoluminescence in albite of the T-zone. The intensity of colour appears to correlate with increasing Ga content. The activator element for the red cathodoluminescence is uncertain although Fe^{3+} is thought to function as an activator for brilliant red cathodoluminescence in feldspars from fenites (Mariano, 1979).

Although not of economic importance, a few randomly selected albite grains from the Lower Intermediate zone and felsite dyke were also analysed for comparative purposes. Albite from the Lower Intermediate zone has the same patchy red and blue cathodoluminescence. The analyses presented in Table 3.3 represent an average of several blue areas of varying intensities and compare favorably with the bright blue areas in Wall zone albite. Feldspar of the Lower Intermediate zone is similar to that in adjacent granite which suggests that both may be of potential economic interest although not as attractive as the feldspathic rocks of the Wall zone. Albite phenocrysts in the later formed, unmineralized felsite dyke have a dull grey cathodoluminescence and do not contain detectable levels of Ga. Albite of the felsite also lacks Fe which may correspond to the absence of red cathodoluminescence.

K-feldspar

K-feldspar is present in all three units of the Wall zone. It is most abundant in the K-feldspar *aplite* unit where it occurs as euhedral to subhedral blocky grains or laths with interstitial fluorite or quartz (see Plate 2.6b). They typically have sharp grain boundaries and are generally less than 500 μm in length and 200 μm in diameter. In the *core* and *breccia* units, K-feldspar typically occurs as subhedral to anhedral blocky grains overgrown by albite with interstitial quartz and fluorite (see Plates 2.9b and 2.10b). It is generally coarse grained with individual grains ranging from 2-10 mm in diameter.

K-feldspar from the *aplite* and *core* units of the Wall zone have a red cathodoluminescence which is darker (less intense colour) that the red cores of albite. Their cathodoluminescence appears to be homogeneous, in contrast to the albite, and again the colour may be due to the presence of Fe^{3+}. Quantitative electron microprobe analyses presented in Table 3.4 indicate that K-feldspar contains Ga concentrations similar to those of red areas in albite with a maximum of 0.06 weight % Ga but averages slightly less. K--feldspar from the later, unmineralized felsite dyke has a dull grey cathodoluminescence and does not contain detectable amounts of Ga or Fe. Rb and Cs concentrations in these feldspars were not determined.

Discussion

The distribution of Ga in albite and K-feldspar, as evidenced by their characteristic cathodoluminescence, suggests that there were two stages of Ga mineralization. It is postulated here that an initial Ga-bearing fluid precipitated K-feldspar with an average content of less that 0.06 weight % Ga. Subsequently, albite with an average content of 0.06 weight % Ga crystallized from the initial Ga-bearing fluid. According to this proposed model, the areas of red cathodoluminescence represent albite precipitated from the initial fluid. After the initial albite formed, a second more Ga-rich fluid, in disequilibrium with the preexisting albite, partially replaced the original plagioclase feldspar. The replacement process would have been one of exchange where Ga in the fluid replaced Al^{3+} in the original feldspar. The isomorphism of Ga with Al is known to be favoured by an alkaline medium (Severov and Vershkovskaya, 1960). Excess Al may have been consumed in the subsequent growth of micaceous minerals which occur interstitial to feldspar.

Such a model would explain the textural relationships seen in Plate 3.21 where the Ga-rich blue areas envelop isolated relicts of the Ga-poor red areas. The areas of blue cathodoluminescence would in fact represent areas of the original feldspar in which the second fluid had exchanged Ga for Al. Albite laths with red and blue cathodoluminescence would have only been partially replaced whereas in laths that are entirely blue, the exchange would have been complete. Variations in the intensity of cathodoluminescence in albite and the corresponding changes in Ga content would also reflect the amount of exhange which occurred between the original feldspar and the Ga-rich fluid.

The origin of the Ga-rich fluids is also uncertain. Ga is known to accumulate in late magmatic solutions (Ganeev *et al.*, 1961) and in particular concentrates during albitization or Na metasomatism (Severov and Vershkovskaya, 1960). It is possible that after the initial albite formed, and as the process of albitization progressed, the fluid evolved to become more Ga-rich.

Economically significant concentrations of Ga are essentially restricted to the feldspathic assemblages of the Wall zone and the albite-rich units in particular. Lesser amounts are known to be present in the Lower Intermediate zone and may also appear in similar rocks of adjacent granite. As an ore mineral, feldspar is undesireable because Ga is tied up in the silicate structure where it substitutes for Al. In order to liberate the Ga, the feldspar must be broken down, the difficulties of which may exceed the value of the metal.

IV. DISCUSSION

The following chapter, divided into three parts, concludes the examination of the economic mineralogy of the north T-zone deposit. In the first part (A), certain general remarks are made concerning the results of this mineralogical study. In the second part (B), the possible origin and genesis of the deposit is discussed. Proposals for future research related to the north T-zone deposit are presented in the third part (C).

A. GENERAL REMARKS

One of the most important results of this study, aside from the identification of rare-metal-bearing minerals, has been the recognition of the complex mineral intergrowths in which they occur. In terms of beneficiation processes, the mode of occurrence of ore minerals is equally as important as the identification of the minerals themselves. Microbeam techniques have proven to be invaluable in this study by providing both compositional and textural information for the minerals of economic interest. Applications of electron microprobe and ion probe analysis, scanning electron imagery and cathodoluminescence microscopy to rocks of the north T-zone are documented throughout this study. Conversely, conventional X-ray diffraction techniques and optical petrography were of limited use in the study of such fine grained, mineralogically complex rocks. In particular, the use of microbeam techniques was essential in resolving Y and REE mineralogy in the T-zone, which is the most complex and economically crucial, where Y and REEs are currently being considered as probable by-products of Be mining.

Another general observation that is worthwhile noting is the ubiquitous presence of fluorite and carbonate minerals in rocks of the north T-zone. They occur as early and late stage minerals which suggests that both were present throughout much of the mineralization sequence and that the mineralizing fluids were undoubtedly rich in F^- and CO_3^{2-}. Be, Y and REEs are most commonly transported in solution as fluoride and carbonate complexes and less commonly as chloride or phosphate complexes (Mineyev, 1963; Beus, 1966; Vlasov, 1966). F^- and CO_3^{2-} in the mineralizing fluids, as evidenced by the abundance of fluorite and carbonate in the T-zone, were probably instrumental in the complexing of ore metals and their subsequent transport in solution. The abundance of F^- and CO_3^{2-} in the mineralizing fluids may also explain the predominance of REE-fluocarbonate minerals over other REE-bearing species. In addition to being a complexing agent, F has also been implicated in studies of the genesis of granophile mineral deposits as a fluxing agent for lowering of melting and crystallization temperatures (Collins and Strong, 1985). The abundance of fluorite and carbonate minerals in the T-zone is mentioned here because the presence of F^- and CO_3^{2-} in the mineralizing fluids may have been instrumental in the transport and deposition of economic Be-, Y- and REE-bearing minerals.

A final observation worth noting is the scarcity of Al in all minerals of economic interest with the exception of Ga-bearing feldspar. The most obvious examples are phenakite and bertrandite which form preferentially over the more common Be-bearing mineral beryl under conditions of low Si (relative to Be) and low Al (Beus, 1966). Allanite, an Al-bearing REE-silicate of the epidote group, is absent in the T-zone where REE-fluocarbonates predominate. This again may suggest conditions of formation in which Al and Si were scarce or being consumed by another mineral. Interestingly, allanite is locally abundant in the Lake-zone deposit which suggests that the economic mineralogy of the Lake-zone may vary substantially from that in the T-zone. The scarcity of Al in economic minerals of the T-zone may be due to the fact that most of the available Al was consumed during the early stages of feldspar and subsequent mica mineralization. In the case of phenakite, the Al-free species is actually more desireable than the common beryl because it contains a greater concentration of Be.

B. CONSIDERATION OF THE ORIGIN AND GENESIS OF THE NORTH T-ZONE

Although the origin and genesis of the T-zone is presently unclear, certain general observations and comparisons can be made. As suggested by Davidson (1982), the alteration and mineralization at Thor Lake are probably the end-products of magmatic differentiation of the Blachford Lake alkaline intrusive complex. The Grace Lake granite and Thor Lake syenite are the youngest, peralkaline phases of the complex and are enriched in the elements of economic interest. Both granite and syenite are transected by the T-zone and are postulated (either phase or possibly both together) to be the source, through magmatic differentiation, of rare-metal-bearing mineralizing fluids.

Zonation of alteration assemblages, in conjunction with certain mineral paragenetic relationships discussed in this study, suggest that the T-zone is the result of a successive series of metasomatic events. In general terms, the process would have been one of an early alkaline stage involving K and Na metasomatism followed by a later stage of greisenization involving several, pulsational mineralizing events which partially replaced earlier assemblages. This general sequence corresponds loosely with that proposed by Shcherba (1970) for postmagmatic processes in granitoid greisens.

Granite in the T-zone shows evidence of initial K and Na metasomatism where original perthite is partially replaced by K-feldspar or completely replaced by albite. Feldspathic assemblages of the Wall zone are assumed to be related to this period of metasomatic replacement although the presence of primary banding in the aplitic units suggests that they may have formed as late magmatic rather than postmagmatic phases. Albitization appears to have occurred after the development of K-feldspar in Wall zone rocks.

Rocks of the Lower Intermediate zone are similar to albitized (Na metasomatized) granite. They locally retain granitic textures but are characterized by Fe-rich mineral assemblages and may be the products of Fe metasomatism superimposed on earlier K and Na metasomatic assemblages.

The quartz-rich assemblages of the Upper Intermediate zone (with quartz, polylithionite and feldspar in addition to the economic minerals) are the most typical of greisen deposits. Megascopic textural features observed in underground workings at Thor Lake suggest that rocks of the Upper and Lower Intermediate zone probably represent a series of pulsational metasomatic events during which earlier assemblages were locally brecciated and partially replaced by later fluids. However, temporal relationships between the various units of the Upper and Lower Intermediate zones, and between minerals such as quartz which they have in common, remain unclear.

The barren Quartz zone is assumed to represent the final stage of greisenization in the deposit and may or may not be related to the silicification evident in other alteration zones.

The presence of Be-, Y-, REE-, Nb- and Zr-bearing minerals in several different rock types precludes the direct comparison of a particular mineral from rock to rock due to the uncertainty which exists concerning temporal relationships between host rock types. However, the general tendency for Y- and MREE-bearing minerals to form earlier than LREE-bearing minerals and Be minerals to form last is probably a function of stability differences of their complexes with changing physio-chemical conditions (Mineyev, 1963; Beus, 1966).

Temperatures and pressures of formation in the T-zone have not been studied here although the presence of open space (vugs) in the Upper Intermediate and Quartz zones implies relatively low pressures. According to Shcherba (1970), typical temperatures corresponding to greisenization range from 360-470 °C and from 450-500 °C for albitization. However, as noted by Collins and Strong (1985), the abundance of F in mineralizing fluids may substantially effect such temperatures. Pupin (1985) has illustrated the use of zircon typology (morphology) as a guide to crystallization temperatures in certain granitoid rocks. Although results of Pupin's (1985) study in granites cannot be compared directly to the F-rich greisen deposit in the T-zone, they do indicate that bipyramidal zircons (such as have been identified in the T-zone) are typically the lowest temperature type, corresponding to temperatures between 500 and 550 °C (±50 °C).

C. PROPOSALS FOR FUTURE RESEARCH RELATED TO THE NORTH T-ZONE

1. Ion probe determinations of Be to confirm the identities of the sulfosilicate tentatively identified as a member of the helvite group and the Y-silicate tentatively identified as gadolinite. Also, ion probe determinations of Be in the mineral tentatively identified as britholite to differentiate it conclusively from gadolinite.

2. Quantitative analyses of all Y- and REE-bearing minerals, in particular those with unusual compositions such as Nd-rich gadolinite which may be new varieties.

3. Detailed fluid inclusion study of quartz and fluorite from the various units of each alteration zone in order to determine temperature constraints and characterize mineralizing fluid(s). This may also aid in establishing temporal relationships between rock types.

4. Zircon dating of unaltered Thor Lake syenite and Grace Lake granite to determine the age difference (if any) between the two. Also to compare the age of unaltered syenite with that of altered syenite (2094±10 Ma) determined by Bowring *et al.* (1984).

THE UNIVERSITY OF ALBERTA

ECONOMIC MINERALOGY OF THE NORTH T-ZONE DEPOSIT, THOR LAKE, NORTHWEST TERRITORIES

by

© Louise de St. Jorre

A THESIS

SUBMITTED TO THE FACULTY OF GRADUATE STUDIES AND RESEARCH

IN PARTIAL FULFILMENT OF THE REQUIREMENTS FOR THE DEGREE

OF Master of Science

Department of Geology

Edmonton, Alberta

Fall, 1986

Table of Contents

Chapter Page

V. TABLES 103

VI. FIGURES 109

VII. PLATES 139

REFERENCES CITED 228

APPENDIX I: Quantitative electron microprobe analysis 233

APPENDIX II: Proposed technique for quantitative electron microprobe analysis of REE-bearing minerals 240

List of Tables

Table 2.1-Biotite and chlorite analyses. 104

Table 3.1-Columbite and ashanite analyses from the Lower Intermediate zone (138,91) and Wall zone (129). 105

Table 3.2-Zircon analyses. 106

Table 3.3-Albite analyses from the Wall zone (129), Lower Intermediate zone (164) and felsite dyke (85-2). 107

Table 3.4-K-feldspar analyses from the *aplite* (85-2) and *core* (182Y) units of the Wall zone, and the felsite dyke (85-6). 108

List of Figures

Figure 1.1-Location map for the Thor Lake rare-metal deposits, Northwest Territories, Canada. 110

Figure 1.2-Generalized geological map of the Blachford Lake intrusive suite showing locations of the T- and Lake-zones (after Davidson, 1978, 1982). 111

Figure 1.3-Generalized geological map of the five mineralized zones in the Thor Lake area (after Černý and Trueman, 1985) 112

Figure 2.1-Generalized geological map of the T-zone showing locations of sections A-B and C-D (after Trueman *et al.*, 1985). 113

Figure 2.2-Cross-section A-B through the T-zone. 114

Figure 2.3-Longitudinal section C-D through the T-zone. 115

Figure 2.4-Generalized paragenetic sequence of mineralization for unmineralized granite. .. 116

Figure 2.5-Generalized paragenetic sequence of mineralization for mineralized granite. 117

Figure 2.6-Generalized paragenetic sequence of mineralization for the K-feldspar *aplite* unit of the Wall zone. 118

Figure 2.7-Generalized paragenetic sequence of mineralization for the albite *aplite* unit of the Wall zone. 119

Figure 2.8-Generalized paragenetic sequence of mineralization for the *core* unit of the Wall zone 120

Figure 2.9-Generalized paragenetic sequence of mineralization for the *quartz-magnetite* unit of the Lower Intermediate zone. 121

Figure 2.10-Generalized paragenetic sequence of mineralization for the Lower Intermediate zone, *quartz-biotite(±chlorite)-feldspar* unit. 122

Figure 2.11-Generalized paragenetic sequence of mineralization for the Lower Intermediate zone, *quartz-biotite(±chlorite)-oxides* unit. 123

Figure 2.12-Generalized paragenetic sequence of mineralization for the *quartz-thorite* unit of the Upper Intermediate zone. 124

Figure 2.13-Generalized paragenetic sequence of mineralization for the *quartz-bastnaesite group* unit of the Upper Intermediate zone 125

Figure 2.14-Generalized paragenetic sequence of mineralization for the Upper Intermediate zone, *quartz-feldspar-magnetite* unit. 126

Figure 2.15-Generalized paragenetic sequence of mineralization for the *quartz-feldspar* unit of the Upper Intermediate zone. 127

Figure 2.16-Generalized paragenetic sequence of mineralization for the *quartz-mica-feldspar* unit of the Upper Intermediate zone. 128

Figure 3.1-Characteristic energy dispersive spectrum of the helvite group mineral. Be does not appear in spectrum due to absorption by the detector. 129

Figure 3.2-Characteristic energy dispersive spectrum of xenotime. 130

Figure 3.3-Characteristic energy dispersive spectrum of gadolinite. Be does not appear in spectrum due to absorption by the detector. 131

Figure 3.4-Characteristic energy dispersive spectrum of the thorite group mineral............ 132

Figure 3.5-Characteristic energy dispersive spectrum of bastnaesite. C and F do not appear in spectrum due to absorption by the detector. 133

Figure 3.6-Characteristic energy dispersive spectrum of parisite. C and F do not appear in spectrum due to absorption by the detector. 134

Figure 3.7-Characteristic energy dispersive spectrum of roentgenite. C and F do not appear in spectrum due to absorption by the detector. 135

Figure 3.8-Characteristic energy dispersive spectrum of synchysite. C and F do not appear in spectrum due to absorption by the detector. 136

Figure 3.9-Characteristic energy dispersive spectrum of monazite. 137

Figure 3.10-Characteristic energy dispersive spectrum of mineral tentatively identified as britholite... 138

List of Plates

Plate 2.1a-Unmineralized, altered granite of the T-zone. 141

Plate 2.1b-Microcrystalline quartz replacing albite lamellae in perthitic feldspar and along grain boundaries. Associated sericite aggregate mantled by quartz. Unmineralized granite. Crossed polars. Magnification X92. 141

Plate 2.2a-Albite with patchy, irregular twinning partially replaced by quartz at grain boundary. Unidentified mineral of prismatic habit (possibly acmite) partially pseudomorphed by magnetite and enclosed in quartz. Rounded inclusions in albite are K-feldspar-columbite intergrowths. Unmineralized granite. Crossed polars. Magnification X92. 143

Plate 2.2b-Mineralized granite of the T-zone showing "microbrecciated" texture caused by pervasive replacement of feldspar along fractures and parallel to cleavage.. 143

Plate 2.3a-Perthitic feldspar overgrown by K-feldspar. Dark lamellae in perthite are K-feldspar, light lamellae are albite. Unidentified acicular mineral is pseudomorphed by magnetite and enclosed in quartz. Mineralized granite. Crossed polars. Magnification X60... 145

Plate 2.3b-K-feldspar partially replacing anhedral LREE-bearing fluocarbonate polycrystals. K-feldspar displays unusual mottled texture. Mineralized granite. Crossed polars. Magnification X240... 145

Plate 2.4a-K-feldspar partially replaced by quartz, biotite and ankerite along fractures and grain boundaries. Mineralized granite. Crossed polars. Magnification X92. 147

Plate 2.4b-Altered acmite in albite. Acmite is partially to entirely replaced by magnetite, ankerite and quartz. Note patchy, irregular twinning in albite. Mineralized granite. Crossed polars. Magnification X92.................................. 147

Plate 2.5a-Semi-opaque inclusions in albite are thorite-bearing intergrowths. White box encloses area shown in Plate 2.5b. Mineralized granite. Crossed polars. Magnification X92.. 149

Plate 2.5b-Backscattered electron image showing intergrowth of K-feldspar, biotite, ilmenite and thorite within rounded inclusion in albite. Mineralized granite. Scale bar represents 10 μm. 149

Plate 2.6a-Drill core sample of albite *aplite* unit of the Wall zone (left). Hand samples of K-feldspar *aplite* unit unstained (center) and stained for K-feldspar (right). 151

Plate 2.6b-K-feldspar with interstitial quartz. K-feldspar *aplite* unit, Wall zone. Crossed polars. Magnification X60... 151

Plate 2.7a-K-feldspar with interstitial LREE-bearing fluocarbonate polycrystals. K-feldspar *aplite* unit, Wall zone. Crossed polars. Magnification X92. 153

Plate 2.7b-Randomly oriented albite laths with interstitial chlorite and ankerite. Albite *aplite* unit, Wall zone. Crossed polars. Magnification X92. 153

Plate 2.8a-Albite enclosed in, and partially replaced by, quartz. Opaque mineral is columbite. Albite *aplite* unit, Wall zone. Crossed polars. Magnification X92. 155

Plate 2.8b-Altered K-feldspar partially replaced by quartz and biotite. Albite *aplite* unit, Wall zone. Crossed polars. Magnification X92.......... 155

Plate 2.9a-*Core* unit of the Wall zone, unstained (left) and stained for K-feldspar. 157

Plate 2.9b-Early altered alkali feldspar (right) partially replaced by later K-feldspar (left). Columbite present as inclusions in both feldspar types. Note irregular, patchy twinning of later K-feldspar (left). *Core* unit , Wall zone. Crossed polars. Magnification X240. 157

Plate 2.10a-Randomly oriented albite laths with interstitial chlorite and fluorite. *Core* unit, Wall zone. Crossed polars. Magnification X60. 159

Plate 2.10b-Radiating aggregates of albite overgrowing K-feldspar. Note patchy twinning in K-feldspar. *Core* unit, Wall zone. Crossed polars. Magnification X60. 159

Plate 2.11a-*Breccia* unit of the Wall zone. 161

Plate 2.11b-*Quartz-magnetite* unit of the Lower Intermediate zone. 161

Plate 2.12a-K-feldspar overgrown and partially replaced by magnetite aggregates. Interstitial quartz and biotite. *Quartz-magnetite* unit, Lower Intermediate zone. Crossed polars. Magnification X368.......... 163

Plate 2.12b- *Quartz-biotite(±chlorite)-feldspar* unit of the Lower Intermediate zone. Note relict granitic texture. 163

Plate 2.13a-K-feldspar overgrown by aggregates of fine grained biotite. Associated opaque mineral is columbite. *Quartz-biotite(±chlorite)-feldspar* unit, Lower Intermediate zone. Crossed polars. Magnification X60. 165

Plate 2.13b-Albite partially replaced by lath-like and shreddy biotite. *Quartz-biotite(±chlorite)-feldspar* unit, Lower Intermediate zone. Crossed polars. Magnification X60.......... 165

Plate 2.14a- *Quartz-biotite(±chlorite)-oxides* unit of the Lower Intermediate zone.......... 167

Plate 2.14b-Lath-like biotite partially replaced by columbite, fluorite and quartz. *Quartz-biotite(±chlorite)-oxides* unit, Lower Intermediate zone. Plane polarized light. Magnification X60. 167

Plate 2.15a-Fine grained biotite partially replaced by chlorite aggregates. Associated opaque mineral is columbite. *Quartz-biotite(±chlorite)-oxides* unit, Lower Intermediate zone. Plane polarized light. Magnification X240.......... 169

Plate 2.15b-*Quartz-thorite* unit of the Upper Intermediate zone. Drill core (right) displays vermiform features typical of quartz-rich samples. 169

Plate 2.16a-Opaque area is complex intergrowth of thorite, xenotime, synchysite, siderite and fluorite. Host mineral is quartz. Fractures in quartz are filled with ankerite (±siderite) and thorite. *Quartz-thorite* unit, Upper Intermediate zone. Plane polarized light. Magnification X92. 171

Plate 2.16b-*Quartz-bastnaesite group* unit of the Upper Intermediate zone...................... 171

Plate 2.17a-Massive aggregates of acicular LREE-bearing fluocarbonates polycrystals displaying plumose texture. *Quartz-bastnaesite group* unit, Upper Intermediate zone. Plane polarized light. Magnification X92. 173

Plate 2.17b-Radiating aggregates of tabular LREE-bearing fluocarbonate polcrystals enclosed in quartz with interstitial microcrystalline quartz. *Quartz-bastnaesite group* unit, Upper Intermediate zone. Crossed polars. Magnification X60. 173

Plate 2.18a-Subhedral to euhedral LREE-bearing fluocarbonate polycrystals with interstitial quartz and fluorite. Aggregate of acicular polycrystals in top right corner. *Quartz-bastnaesite group* unit, Upper Intermediate zone. Plane polarized light. Magnification X92. 175

Plate 2.18b-*Quartz-feldspar-magnetite* unit of the Upper Intermediate zone. 175

Plate 2.19a-Prismatic acmite grains partially pseudomorphed by hematite. Host mineral is quartz. *Quartz-feldspar-magnetite* unit, Upper Intermediate zone. Crossed polars. Magnification X60. 177

Plate 2.19b-Radial aggregate of acmite needles partially replaced by hematite. Associated mica is polylithionite. Host mineral is quartz. *Quartz-feldspar-magnetite* unit, Upper Intermediate zone. Crossed polars. Magnification X92. 177

Plate 2.20a-Drill core sample of the *quartz-feldspar* unit of the Upper Intermediate zone. 179

Plate 2.20b-Albite partially replacing K-feldspar . Both feldspars are enclosed in, and partially replaced by, quartz. *Quartz-feldspar* unit, Upper Intermediate zone. Crossed polars. Magnification X92.................................. 179

Plate 2.21a-Remnant patch of alteration composed of altered albite and K-feldspar with interstitial ankerite and fluorite. All phases partially replaced by host quartz. Note angular boundaries of alteration patch. *Quartz-feldspar* unit, Upper Intermediate zone. Plane polarized light. Magnification X60. 181

Plate 2.21b-*Quartz-mica-feldspar* unit of the Upper Intermediate zone. 181

Plate 2.22a-Polylithionite enclosing anhedral relicts of K-feldspar. Quartz surrounds polylithionite and partially replaces the mica at grain boundaries. *Quartz-mica-feldspar* unit, Upper Intermediate zone. Crossed polars. Magnification X60.. 183

Plate 2.22b-*Quartz-mica* unit of the Upper Intermediate zone. 183

Plate 2.23a-Quartz zone sample showing blocky REE fluocarbonate grains enclosed in massive quartz. 185

Plate 2.23b-Felsite dyke from the T-zone. 185

Plate 3.1a-Optically continuous phenakite grains interstitial to quartz. Crossed polars. Magnification X60 187

Plate 3.1b-Optically continuous phenakite partially replaced at grain boundaries by microcrystalline quartz aggregates. Crossed polars. Magnification X60. 187

Plate 3.2a-Phenakite (optically discontinuous) grains surrounded by biotite aggregates. Phenakite contains inclusions of quartz and biotite. Crossed polars. Magnification X92 189

Plate 3.2b-Subhedral phenakite and associated monazite in ankerite. Crossed polars. Magnification X92. 189

Plate 3.3a-Bertrandite inclusions in quartz. Crossed polars. Magnification X240. 191

Plate 3.3b-Backscattered electron image showing euhedral bertrandite inclusions in quartz. Scale bar represents 10 μm 191

Plate 3.4a-Backscattered electron image showing member of helvite group as inclusion in phenakite. Scale bar represents 10 μm. 193

Plate 3.4b-Xenotime inclusions in quartz with associated dark purple fluorite and thorite. Crossed polars. Magnification X240. 193

Plate 3.5a-Individual grains and aggregates of opaque xenotime. Host mineral is quartz. White box encloses area shown in Plate 3.5b. Plane polarized light. Magnification X92. 195

Plate 3.5b-Backscattered electron image showing minute Fe-oxide inclusions in xenotime. Oxide inclusions may cause xenotime to appear opaque as in Plate 3.5a. Scale bar represents 10 μm 195

Plate 3.6a-Xenotime-thorite intergrowths enclosed in quartz. Fractures in quartz are filled with thorite. White box encloses area shown in Plate 3.6b. Plane polarized light. Magnification X240. 197

Plate 3.6b-Backscattered electron image showing nature of xenotime-thorite intergrowth. White spots are burn marks in thorite caused by the electron microprobe. Fractures in quartz are filled with thorite. Scale bar represents 5 μm 197

Plate 3.7a-Backscattered electron image showing xenotime and associated thorite enclosed in synchysite. All three minerals are partially replaced by surrounding siderite. Scale bar represents 5 μm. 199

Plate 3.7b-Backscattered electron image showing partial replacement of xenotime (and thorite) by gadolinite and associated apatite. Monazite appears to cross cut gadolinite. Fluorite occurs as a late phase interstitial to other minerals. Scale bar represents 10 μm. 199

Plate 3.8a-Xenotime grains with zircon overgrowths and associated monazite. Host mineral is quartz. White box encloses area shown in Plate 3.8b. Crossed polars. Magnification X368. 201

Plate 3.8b-Backscattered electron image showing zircon overgrowths on corroded ovoids of xenotime. Associated monazite appears to cross-cut xenotime and zircon. Scale bar represents 2 μm. 201

Plate 3.9a-Gadolinite with interstitial fluorite. Associated monazite and thorite also shown. Plane polarized light. Magnification X368. 203

Plate 3.9b-Gadolinite and apatite with interstitial fluorite. Crossed polars. Magnification X200. 203

Plate 3.10a-Thorite aggregates in biotite. Biotite occurs interstitial to albite. White box enclosed area shown in Plate 3.10b. Plane polarized light. Magnification X92. 205

Plate 3.10b-Backscattered electron image showing thorite aggregates. White spots are burn marks caused by the electron microprobe. Note compositional inhomogeneity in thorite. Scale bar represents 5 μm. 205

Plate 3.11a-Radiating aggregates of acicular LREE-bearing fluocarbonate polycrystals in quartz. White box encloses area shown in Plate 3.11b. Crossed polars. Magnification X92. 207

Plate 3.11b-Backscattered electron images showing syntaxic intergrowth of bastnaesite and parisite in acicular polycrystals. Scale bar represents 20 μm. 207

Plate 3.12a-Subhedral LREE-bearing fluocarbonate polycrystals in ankerite. Black spots in ankerite are holes. White box encloses are shown in Plate 3.12b. Plane polarized light. Magnification X240. 209

Plate 3.12b-Backscattered electron image showing syntaxic intergrowth of parisite, roentgenite and bastnaesite in a subhedral polycrystal. Scale bar represents 10 μm. 209

Plate 3.13a-LREE-bearing fluocarbonate polycrystal showing lamellae-like intergrowth of different phases. White box encloses area shown in Plate 3.13b. Crossed polars. Magnification X240. 211

Plate 3.13b-Backscattered electron image showing lamellae-like syntaxic intergrowth of roentgenite, bastnaesite and parisite. Scale bar represents 20 μm. 211

Plate 3.14a-LREE-bearing fluocarbonate polycrystal partially replaced by K-feldspar and ankerite. Associated monazite enclosed in ankerite. White box encloses area shown in Plate 3.14b. Crossed polars. Magnification X240. 213

Plate 3.14b-Backscattered electron image showing syntaxic intergrowth of bastnaesite and parisite in partially replaced polycrystal. Scale bar represents 20 μm. 213

Plate 3.15a-Backscattered electron image showing syntaxic intergrowth of bastnaesite and parisite in tabular polycrystals. Note lamellae-like intergrowth appears to run parallel to long axis of tabular grains. Scale bar represents 20 μm. 215

Plate 3.15b-Subhedral monazite grains enclosed in ankerite. Quartz appear to partially replace monazite and ankerite. Opaque inclusions in ankerite are thorite intergrowths with chlorite. Crossed polars. Magnification X92. 215

Plate 3.16a-Britholite intergrown with parisite, monazite and chlorite. Host mineral is quartz with associated purple fluorite. White box encloses area shown in Plate 3.16b. Plane polarized light. Magnification X92. 217

Plate 3.16b-Backscattered electron image of britholite, parisite, monazite and chlorite intergrowth in quartz. Note altered, inhomogeneous appearance of parisite. Scale bar represents 20 μm. 217

Plate 3.17a-Columbite aggregates included in quartz and replacing lath-like biotite. Note difference in relief between associated quartz and phenakite. Plane polarized light. Magnification X92. 219

Plate 3.17b-Backscattered electron image showing columbite with anhedral inclusions of bastnaesite and ashanite. White spots in ashanite are burn marks caused by the electron microprobe. Host mineral is quartz. Scale bar represents 5 μm... 219

Plate 3.18a-Bipyramidal zircons forming skeletal outline of unidentified preexisting mineral. Host mineral is quartz with associated altered K-feldspar and fluorite. Crossed polars. Magnification X92. 221

Plate 3.18b-Zonally metamictized zircons with interstitial biotite and columbite. Crossed polars. Magnification X240. 221

Plate 3.19a-Backscattered electron image of zonally metamictized zircons. White spots are burn marks caused by the electron microprobe. Scale bar represents 10 μm. 223

Plate 3.19b-Backscattered electron image showing core of zonally metamictized zircon in greater detail. Scale bar represents 5 μm. 223

Plate 3.20a-Core-type zircons postulated to be comparable to cores of zonally metamictized zircons. Interstitial biotite and columbite. Plane polarized light. Magnification X368. 225

Plate 3.20b-Backscattered electron image showing core-type zircons. Bright areas are columbite. Scale bar represents 20 μm. 225

Plate 3.21-Photomicrograph illustrating red and blue cathodoluminescence of Ga-bearing albite. Interstitial chlorite is nonluminescent. Associated quartz has pale red cathodoluminescence around Fe- and Nb-oxide inclusions. Fluorite has dark blue cathodoluminescence. Magnification X120. 227

V. TABLES

Table 2.1-Biotite and chlorite analyses.

Sample	91-1 med.gr. biotite	15-5A med.gr. biotite	15-5B med.gr. biotite	15-6 fine gr. biotite	15-7 fine gr. biotite	80-2 fine gr. biotite	15-6 chlorite	80-1 chlorite	80-3 chlorite
Si	17.96	16.96	17.38	16.97	17.15	18.64	12.61	12.11	12.21
Ti	.65	.22	.26	.26	.24	.59	nd	nd	nd
Al	7.74	6.55	6.33	6.70	6.49	5.86	8.78	8.47	8.63
Fe^{2+}	20.21	23.62	22.24	24.13	23.69	17.53	29.07	27.20	27.81
Mn	.57	.02•	nd	.06	.04	.07	.02•	.01•	.04
Mg	2.80	3.84	5.03	3.56	4.08	6.43	4.43	5.74	5.93
Na	.10	nd	nd	nd	nd	nd	nd	nd	nd
K	7.90	7.68	6.72	7.68	7.73	7.82	.13	nd	nd
F	1.92	.83	1.43	.93	.72	2.57	.10	.14	.20
Cl	.24	.30	.07	.42	.31	.11	nd	nd	nd
H**	.40	.47	.51	.39	.38	.42	1.28	1.51	1.32
O*	39.53	39.62	40.06	38.91	39.17	39.96	43.59	44.82	43.85
Total	100.00	100.00	100.00	100.00	100.00	100.00	100.00	100.00	100.00

BIOTITE STRUCTURAL FORMULA ON THE BASIS OF 22 (O, F, Cl)
CHLORITE STRUCTURAL FORMULA ON THE BASIS OF 28 (O, F, Cl)

Sample	91-1 med.gr. biotite	15-5A med.gr. biotite	15-5B med.gr. biotite	15-6 fine gr. biotite	15-7 fine gr. biotite	80-2 fine gr. biotite	15-6 chlorite	80-1 chlorite	80-3 chlorite
Si	5.91	5.81	5.84	5.78	5.82	6.02	6.00	5.86	5.80
Ti	.13	.04	.05	.05	.05	.11	nd	nd	nd
Al	2.65	2.34	2.22	2.38	2.29	1.97	4.35	4.26	4.27
Fe^{2+}	3.34	4.07	3.76	4.13	4.04	2.85	6.96	6.62	6.65
Mn	.10	.00	nd	.01	.01	.01	.00	.00	.01
Mg	1.07	1.52	1.95	1.40	1.60	2.40	2.44	3.21	3.25
Na	.04	nd	nd	nd	nd	nd	nd	nd	nd
K	1.87	1.89	1.62	1.88	1.89	1.81	.05	nd	nd
Sum	15.11	15.67	15.44	15.63	15.70	15.17	19.80	19.95	19.98
O	21.01	21.50	21.27	21.42	21.56	20.75	27.93	27.90	27.86
F	.93	.42	.71	.47	.36	1.22	.07	.10	.14
Cl	.06	.08	.02	.11	.08	.03	nd	nd	nd

* calculated from the equivalent weight of the other elements
** calculated as the difference of all other element concentrations (including O) and 100 %
nd - not detected
• - below statistical detection limit

Note: All analyses reported in weight % of the element.
For information on operating conditions, analytical procedure and data processing see Appendix I.

Table 3.1-Columbite and ashanite analyses from the Lower Intermediate zone (138,91) and Wall zone (129).

Sample	138-1A columbite	138-1B columbite	138-2A columbite	138-3A columbite	91-1B columbite	91-4C columbite	129-13A columbite	129-14A columbite	91-4D ashanite
Mg	1.13	1.18	1.11	1.05	1.13	1.06	1.12	1.04	1
Al	.99	1.00	.96	.98	1.02	.99	1.07	.96	0
Si	.38	.40	.34	.43	.47	.55	.52	.39	<1
Ca	.05	.07	nd	.08	.13	.18	.07	.18	<1
Ti	1.31	1.32	1.36	1.49	.99	.97	1.73	1.01	<1
Mn	1.50	2.19	1.78	3.02	2.23	2.28	1.85	2.20	<1
Fe^{2+}	15.41	14.53	14.68	13.55	15.29	15.26	15.30	14.19	3
Nb^{5+}	49.51	49.96	50.21	49.56	50.06	49.62	49.33	50.29	32
Ta^{5+}	.15+	.20	.23	.10+	.26	.35	.34	.25	<1
U	na	na	na	na	na	na	na	na	29
H**	-	-	-	-	-	-	-	-	1
O*	29.16	29.38	29.27	29.20	29.52	29.41	29.70	29.13	31
Total	99.59	100.22	99.94	99.45	101.08	100.68	101.02	99.62	~100.00

* calculated from the equivalent weight of the other elements
** calculated as the difference of all other element concentrations (including O) and 100%

nd - not detected na - not analysed
+ - below statistical detection limits

Note: All analyses reported in weight % of the element.
For information on operating conditions, analytical procedure and data processing see Appendix I.

Table 3.2-Zircon analyses.

Type	Zonally metamictized						Core-type	Overgrowths on xenotime
Sample	20-1 white core	20-3 white core	20-1 gray core	20-3 gray core	20-1 dk.gray zone	20-3 dk.grey zone	20-4 white area	121-4A
Si	14.12	14.25	14.12	14.25	11.83	11.21	14.19	11
Zr	45.00	44.72	45.00	44.72	33.94	32.78	43.86	35
Hf	.02	.02	nd	.09	.09	nd	.10	1
Y	.51	.41	.48	.29	4.46	4.07	.24	na
Al	.44	.26	.37	.36	.65	.84	.27	<1
Fe^{2+}	.47	.81	.47	.81	2.09	1.62	.95	3
Ti	.34	.48	.29	.39	.19	.16	.34	4
Ca	.20	.21	.33	.39	1.18	1.18	.18	2
Th	na	na	na	na	na	na	na	3
U^{6+}	nd	.19	nd	.45	3.16	4.58	.29	na
Ba	nd	nd	.10	.20	.76	.58	nd	na
F	.46	.46	.38	.38	.42	.39	.42	na
H**	.62	.55	.63	.50	1.35	1.63	.73	1
O*	37.83	37.41	37.85	37.18	39.88	40.96	38.43	39
Total	100.00	100.00	100.00	100.00	100.00	100.00	100.00	~100

* calculated from equivalent weight of the other elements

** calculated as the difference of all other element concentrations (including O) and 100%

nd - not detected   na - not analysed

Note: All analyses reported in weight % of the element.
For additional information see Appendix 1.

Table 3.3-Albite analyses from the Wall zone (129), Lower Intermediate zone (164) and felsite dyke (85-2).

Sample	129-12D bright red core	129-12B pale red core	129-12A bright blue rim	129-12C bright blue grain (no core)	129-12G blue-white rim	164-1 blue grain	164-3D blue grain	85-61 gray
Na	7.57	7.82	8.02	7.82	8.05	8.23	7.83	7.95
Al	10.32	10.42	10.34	10.34	10.27	10.29	10.15	10.39
Si	32.61	32.49	32.51	32.55	32.30	32.16	32.14	31.89
K	.26	.24	.09	.13	.18	.18	.15	.28
Ca	nd	nd	nd	nd	nd	nd	nd	.12
Fe^{2+}	.16	.22	.14	.16	.20	.12	.18	nd
Ba	nd	nd	nd	nd	nd	nd	nd	nd
Ga	.06±.04	.06±.02	.09±.06	.08±.05	.19±.05	.08±.06	.09±.03	nd
O*	49.09	49.15	49.11	49.10	48.89	48.76	48.49	48.44
Total	100.07	100.40	100.29	100.17	100.08	99.61	99.03	99.06
				STRUCTURAL FORMULA ON THE BASIS OF 8 OXYGENS				
Na	.86	.89	.91	.89	.92	.94	.90	.91
Al	1.00	1.00	1.00	1.00	1.00	1.00	.99	1.02
Si	3.03	3.01	3.02	3.02	3.01	3.00	3.02	3.00
K	.02	.02	.01	.01	.01	.01	.01	.02
Ca	-	-	-	-	-	-	-	.01
Fe	.01	.01	.01	.01	.01	.01	.01	-
Ba	-	-	-	-	-	-	-	-
Ga	-	-	-	-	.01	-	-	-
Sum	4.92	4.93	4.95	4.93	4.96	4.96	4.93	4.96
				MOLECULAR PROPORTIONS				
Ab	98.01	98.23	99.36	99.04	98.73	98.74	98.92	97.15
An	-	-	-	-	-	-	-	.85
Or	1.99	1.77	.64	.96	1.27	1.26	1.08	2.00

* calculated from the equivalent weight of the other elements
nd - not detected
Note: Colours refer to cathodoluminescence.
For additional information see Appendix I.

Table 3.4-Alkali feldspar analyses from the *aplite* (85-2) and *core* (182Y) units of the Wall zone, and the felsite dyke (85-6).

	85-2 1	85-2 2	182Y-6	182Y-5	85-6
SAMPLE	Dk. red	Dk.red	red	red	grey
Na	.22	.29	.29	nd	nd
Al	9.79	9.71	9.73	9.76	9.73
Si	30.76	30.67	30.72	30.49	30.38
K	13.46	13.35	13.17	13.67	13.05
Ca	nd	nd	nd	nd	nd
Fe^{2+}	.11	.14	.08	.15	nd
Ba	na	na	na	na	.24
Ga	.06±.01	.06±.04	.04±.03	.02±.02	nd
O*	46.63	46.47	46.49	46.26	45.96
Total	101.02	100.68	100.51	100.35	99.36

STRUCTURAL FORMULA BASED ON 8 OXYGENS

Na	.03	.03	.03	-	-
Al	1.00	.99	.99	1.00	1.00
Si	3.01	3.01	3.01	3.00	3.01
K	.94	.94	.93	.97	.93
Ca	-	-	-	-	-
Fe	.01	.01	.01	.01	-
Ba	-	-	-	-	-
Ga	-	-	-	-	-
Sum	4.99	4.99	4.97	4.98	4.94

MOLECULAR PROPORTIONS

Ab	2.73	3.50	3.62	-	-
An	-	-	-	-	-
Or	97.27	96.50	96.38	100.00	100.00

* Calculated from the equivalent weight of other elements

nd - not detected   na - not analysed

Note: Colours refer to cathodoluminescence.
For additional information see Appendix I.

VI. FIGURES

For a list of the mineral name abbreviations used in the figures and plates of the chapters which follow, see pages xx and xxi.

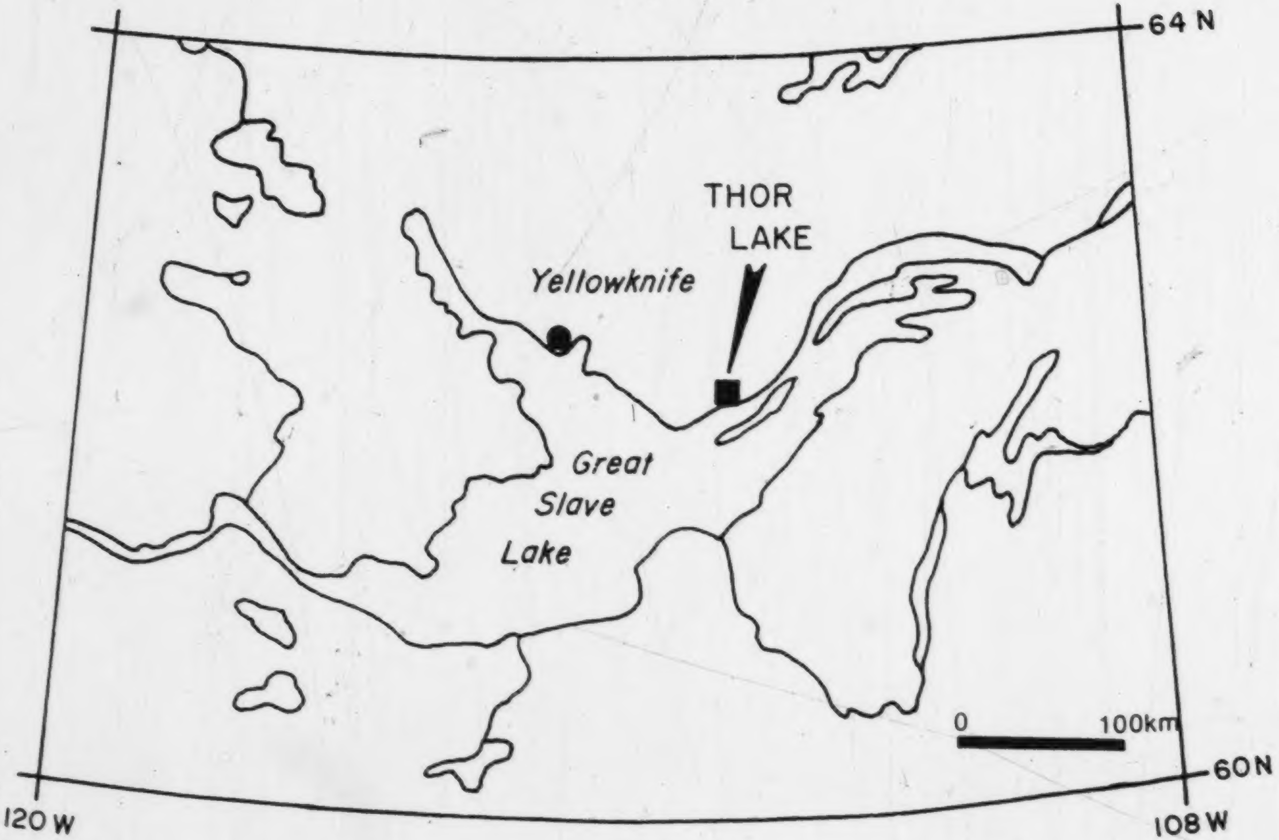
64 N
60N
120 W
108 W
THOR LAKE
Yellowknife
Great Slave Lake
0
100km

Figure 1.1-Location map for the Thor Lake rare-metal deposits, Northwest Territories, Canada.

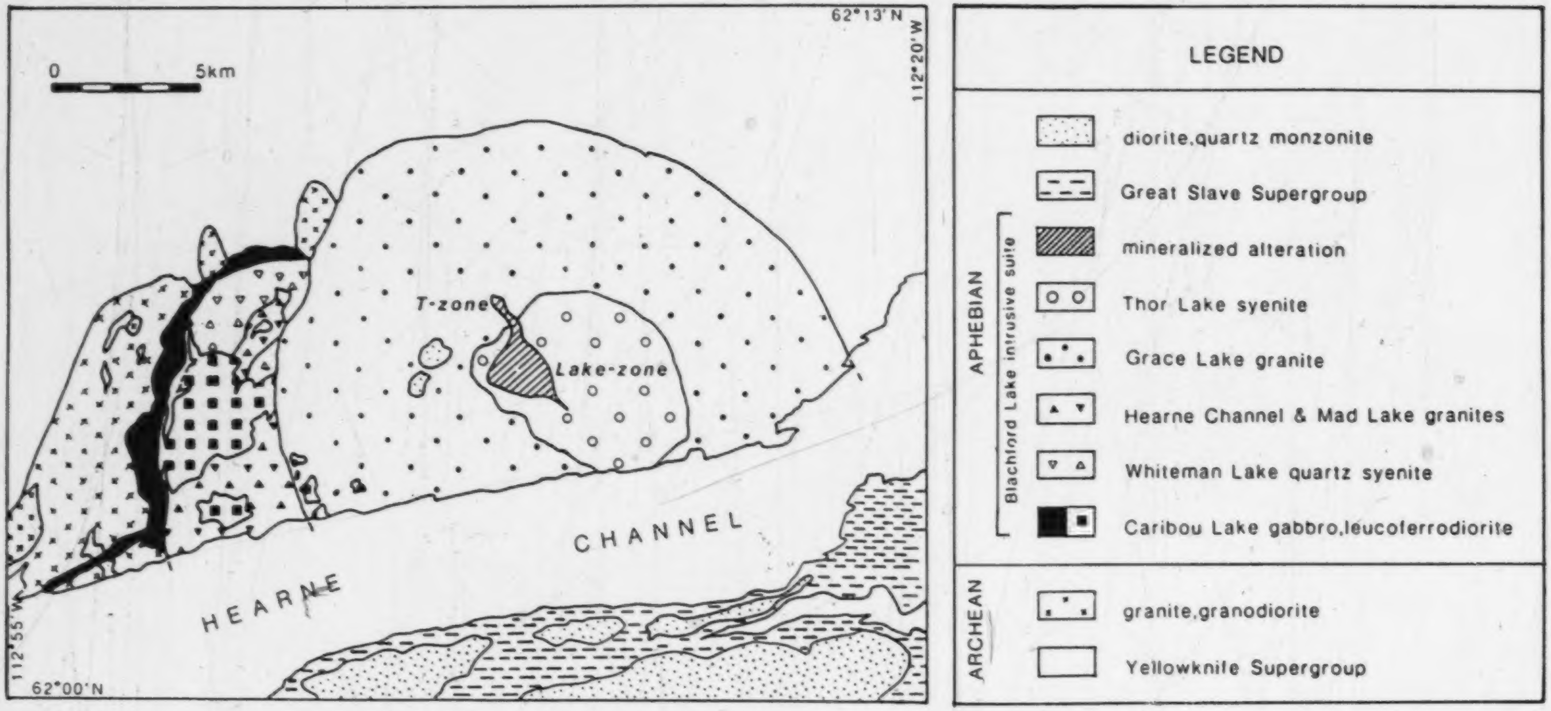
0
5km
62°13'N
112°20'W
112°55'W
62°00'N
T-zone
Lake-zone
CHANNEL
HEARNE
LEGEND
APHEBIAN
Blachford Lake intrusive suite
diorite,quartz monzonite
Great Slave Supergroup
mineralized alteration
Thor Lake syenite
Grace Lake granite
Hearne Channel & Mad Lake granites
Whiteman Lake quartz syenite
Caribou Lake gabbro,leucoferrodiorite
ARCHEAN
granite,granodiorite
Yellowknife Supergroup

Figure 1.2-Generalized geological map of the Blachford Lake intrusive suite showing locations of the T- and Lake-zones (after Davidson, 1978, 1982).

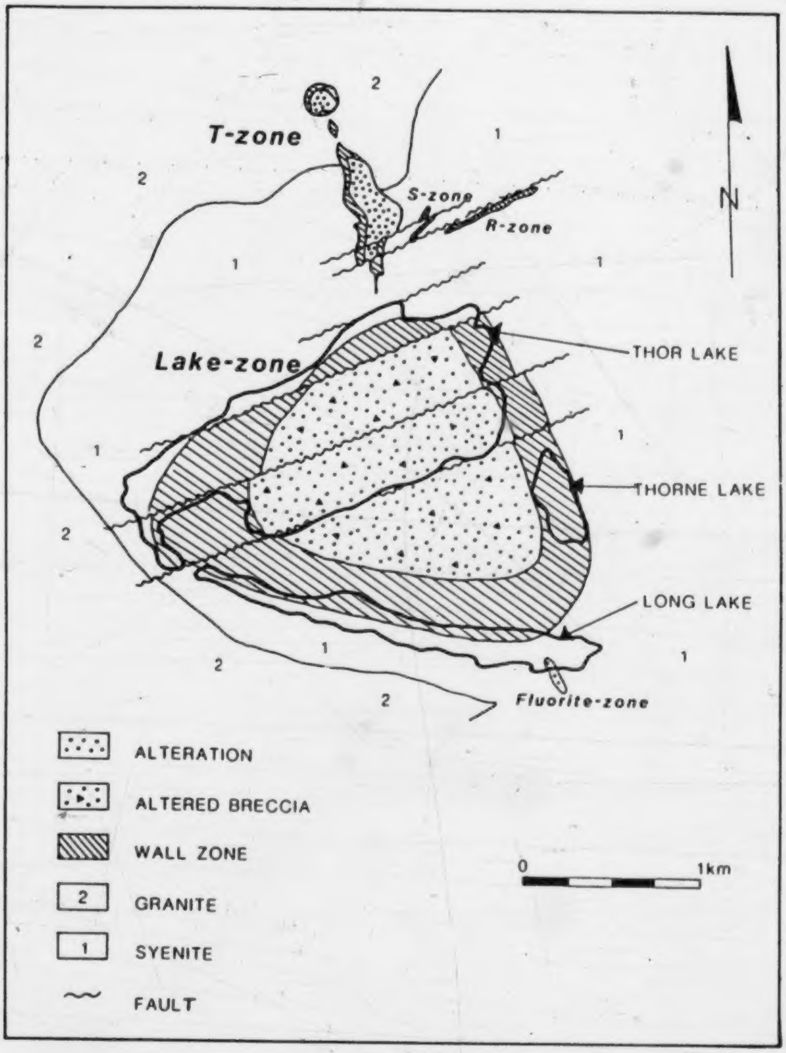
T-zone
S-zone
R-zone
Lake-zone
THOR LAKE
THORNE LAKE
LONG LAKE
Fluorite-zone
1
2
N
0
1km
ALTERATION
ALTERED BRECCIA
WALL ZONE
GRANITE
SYENITE
FAULT

Figure 1.3-Generalized geological map of the five mineralized zones in the Thor Lake area (after Černý and Trueman, 1985).

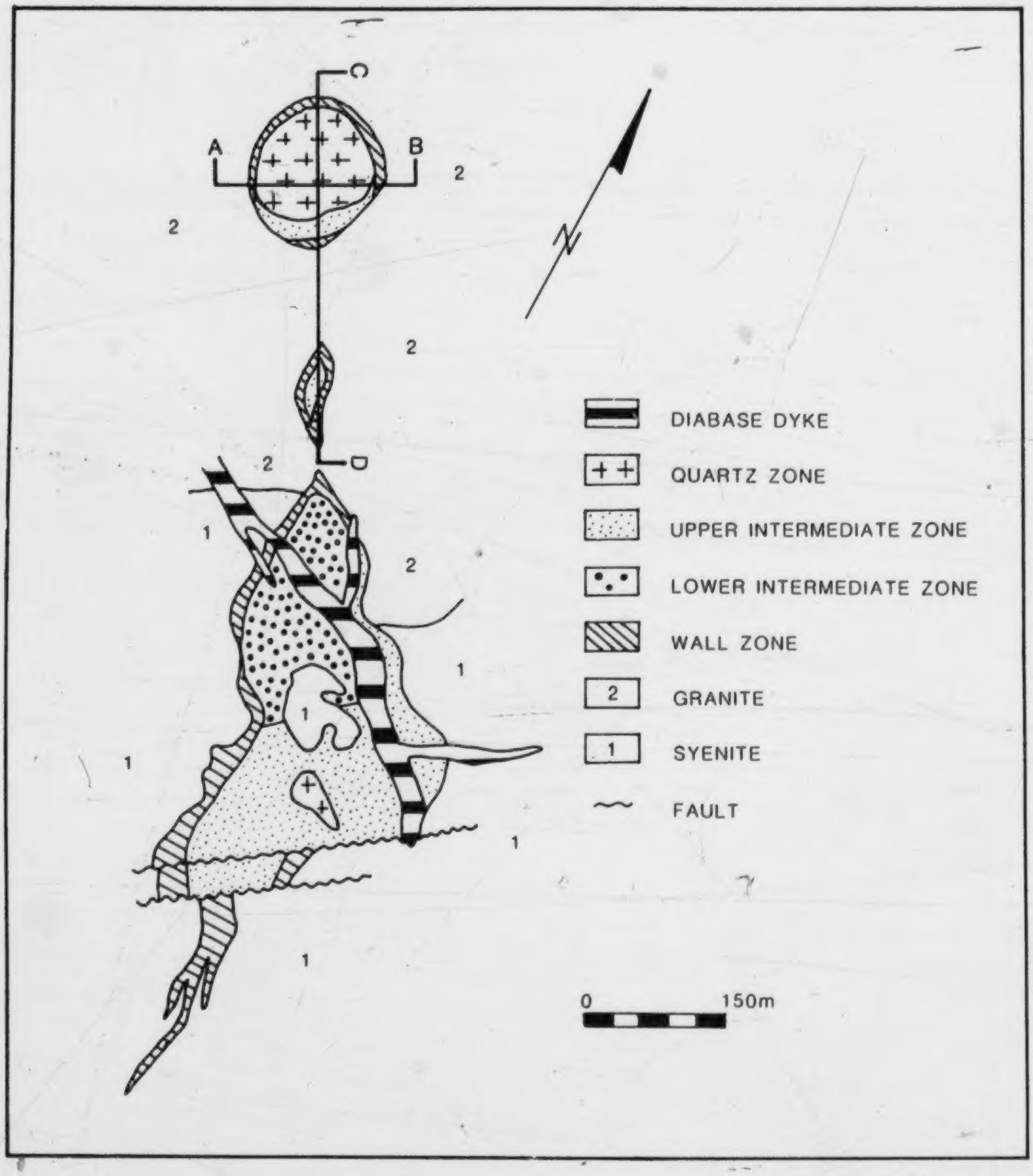
C
A
B
2
2
2
2
2
1
1
1
1
1
D
DIABASE DYKE
QUARTZ ZONE
UPPER INTERMEDIATE ZONE
LOWER INTERMEDIATE ZONE
WALL ZONE
2 GRANITE
1 SYENITE
FAULT
0
150m

Figure 2.1-Generalized geological map of the T-zone showing locations of sections A-B and C-D (after Trueman *et al.*, 1985).

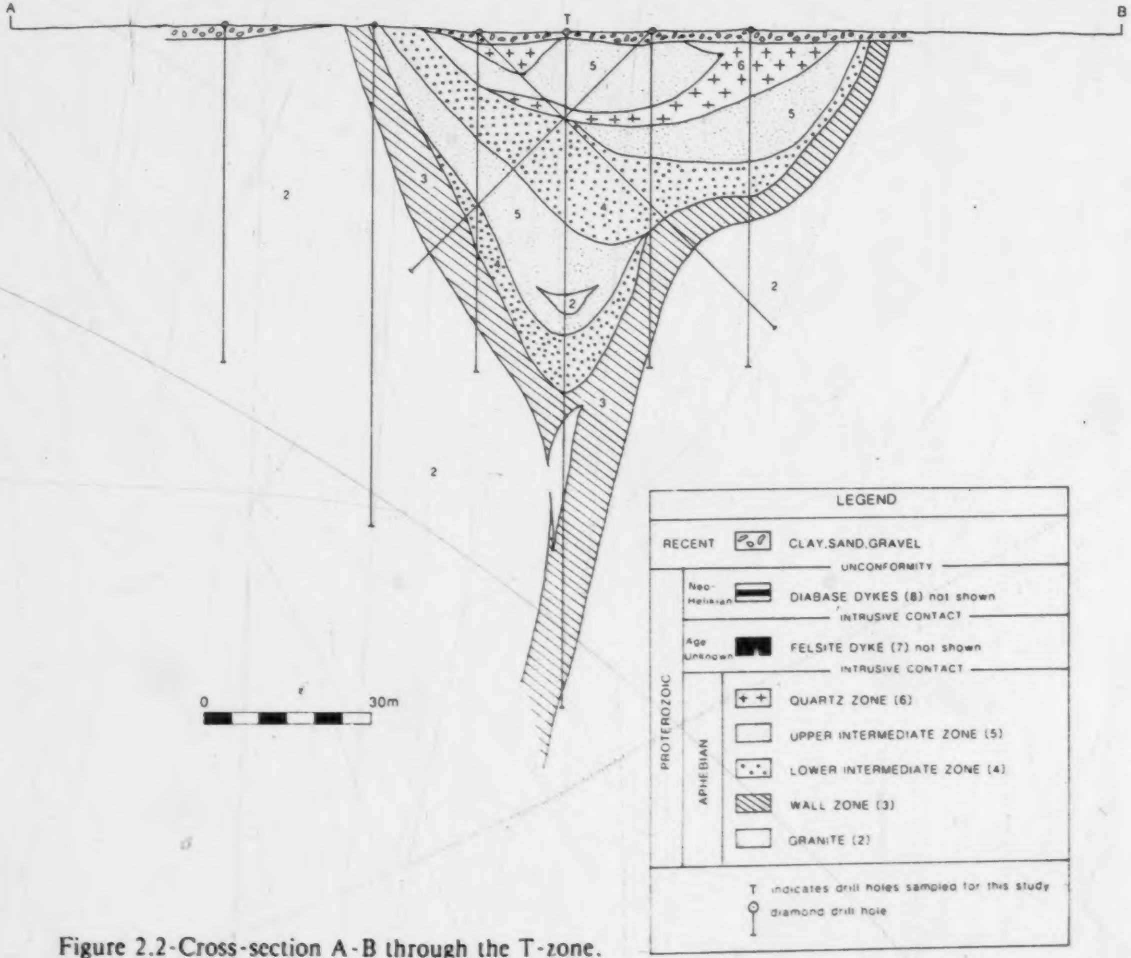
A
B
T
2
3
4
5
6
0
30m
LEGEND
RECENT
CLAY, SAND, GRAVEL
UNCONFORMITY
Neo-Helikian
DIABASE DYKES (8) not shown
INTRUSIVE CONTACT
Age Unknown
FELSITE DYKE (7) not shown
INTRUSIVE CONTACT
PROTEROZOIC
APHEBIAN
QUARTZ ZONE (6)
UPPER INTERMEDIATE ZONE (5)
LOWER INTERMEDIATE ZONE (4)
WALL ZONE (3)
GRANITE (2)
T indicates drill holes sampled for this study
diamond drill hole

Figure 2.2-Cross-section A-B through the T-zone.

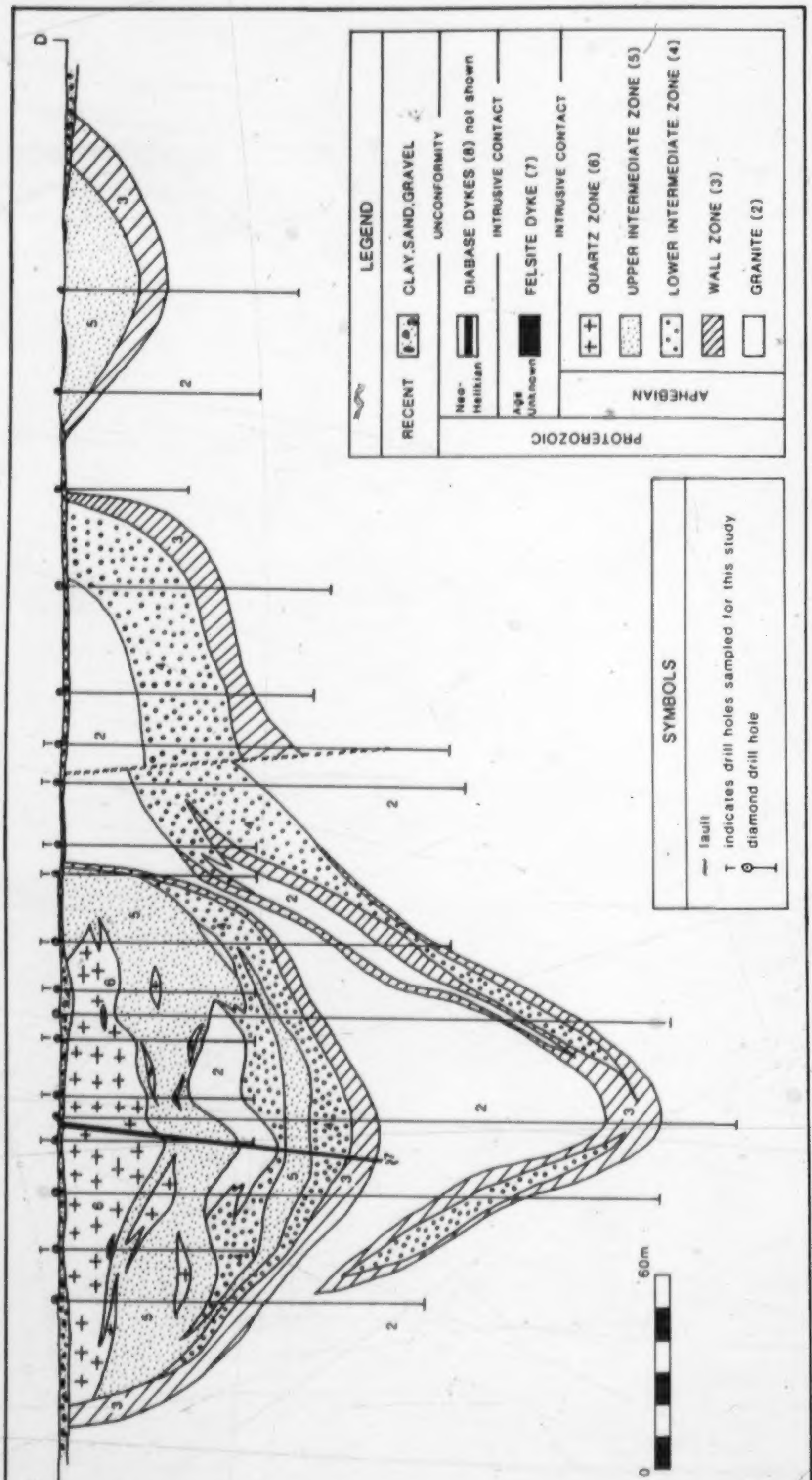
C
D
0
60m
2
3
4
5
6
LEGEND
RECENT
CLAY, SAND, GRAVEL
UNCONFORMITY
Neo-Helikian
DIABASE DYKES (8) not shown
INTRUSIVE CONTACT
Age Unknown
FELSITE DYKE (7)
INTRUSIVE CONTACT
QUARTZ ZONE (6)
UPPER INTERMEDIATE ZONE (5)
LOWER INTERMEDIATE ZONE (4)
WALL ZONE (3)
GRANITE (2)
PROTEROZOIC
APHEBIAN
SYMBOLS
fault
T indicates drill holes sampled for this study
diamond drill hole

Figure 2.3-Longitudinal section C-D through the T-zone.

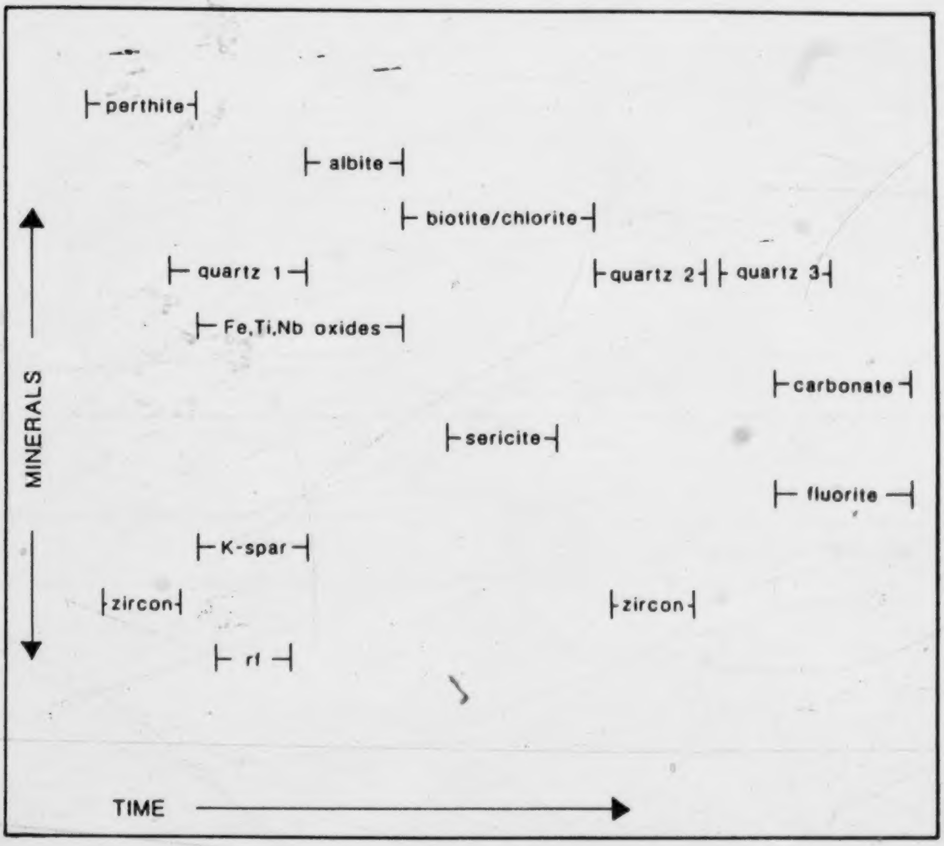
perthite
albite
biotite/chlorite
quartz 1
quartz 2
quartz 3
Fe,Ti,Nb oxides
carbonate
sericite
fluorite
K-spar
zircon
zircon
rt
MINERALS
TIME

Figure 2.4-Generalized paragenetic sequence of mineralization for unmineralized granite.

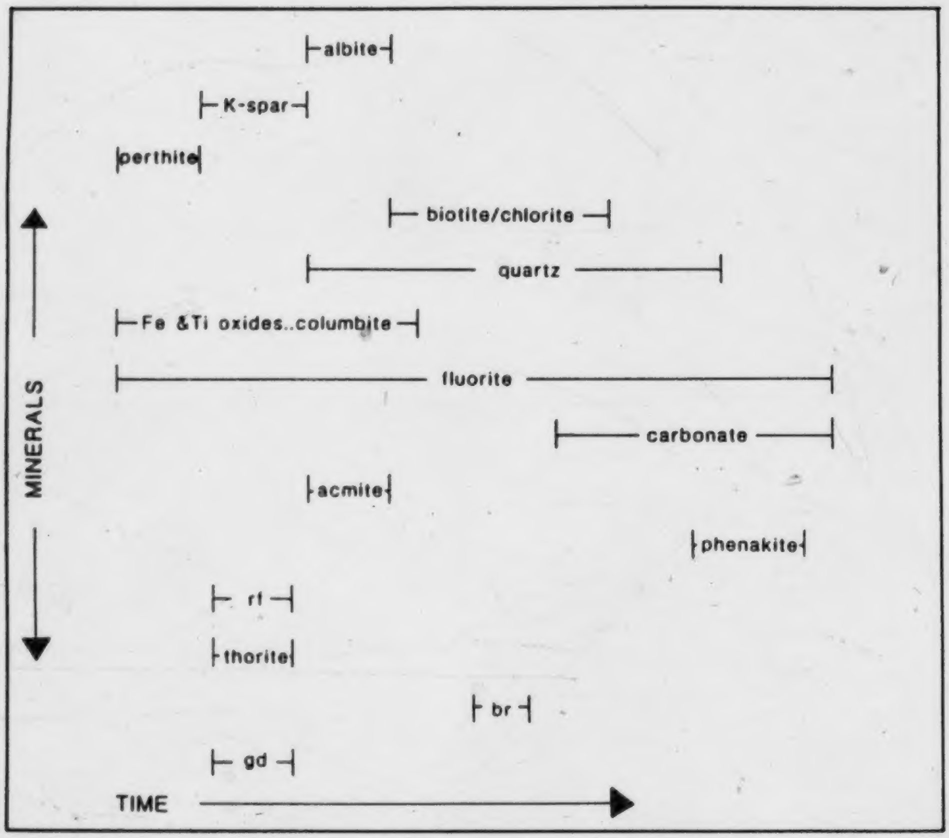

Figure 2.5-Generalized paragenetic sequence of mineralization for mineralized granite.

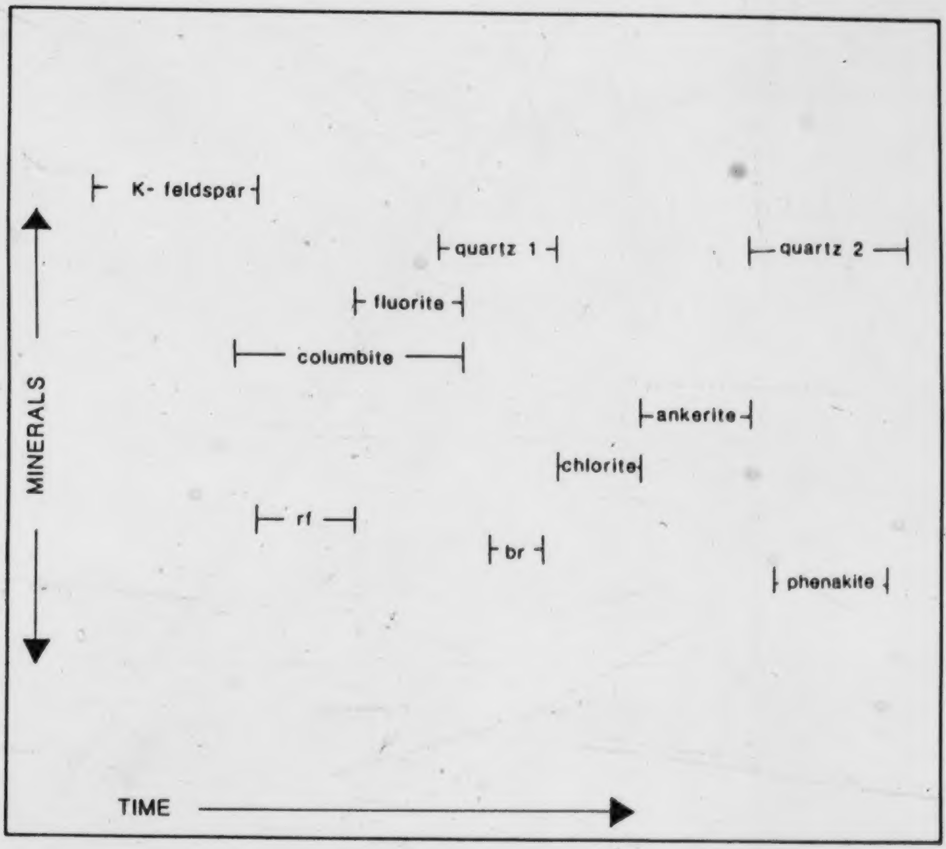

Figure 2.6-Generalized paragenetic sequence of mineralization for the alkali feldspar *aplite* unit of the Wall zone.

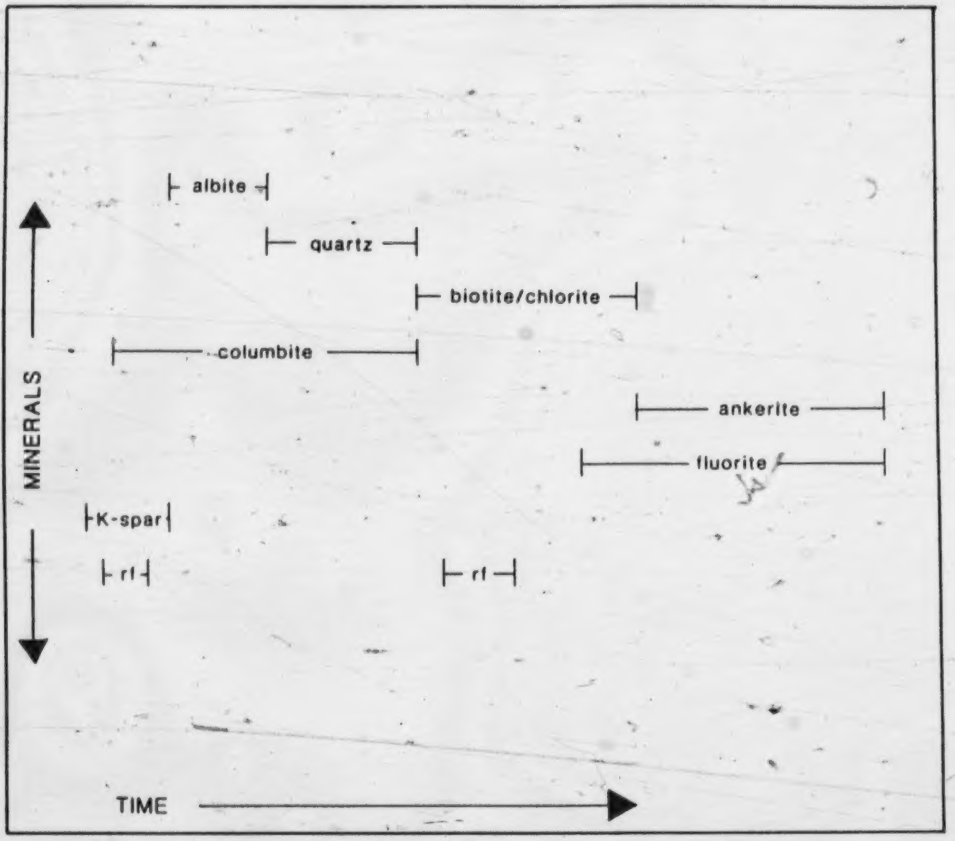

Figure 2.7-Generalized paragenetic sequence of mineralization for the albite *aplite* unit of the Wall zone.

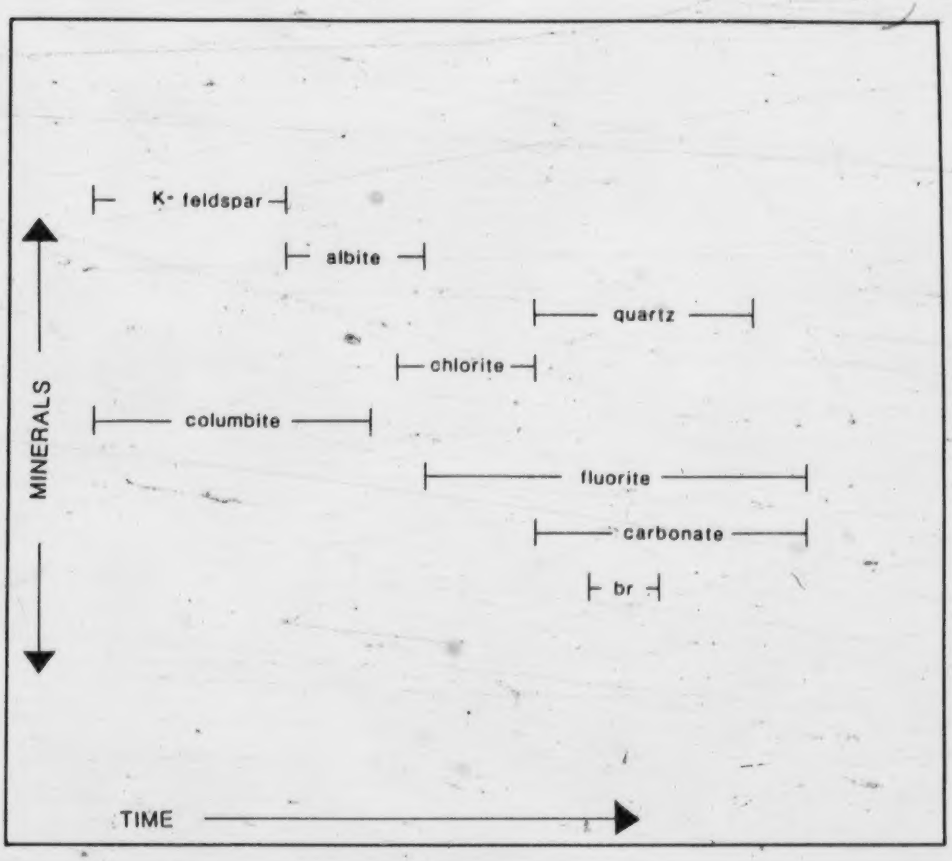

Figure 2.8-Generalized paragenetic sequence of mineralization for the *core* unit of the Wall zone.

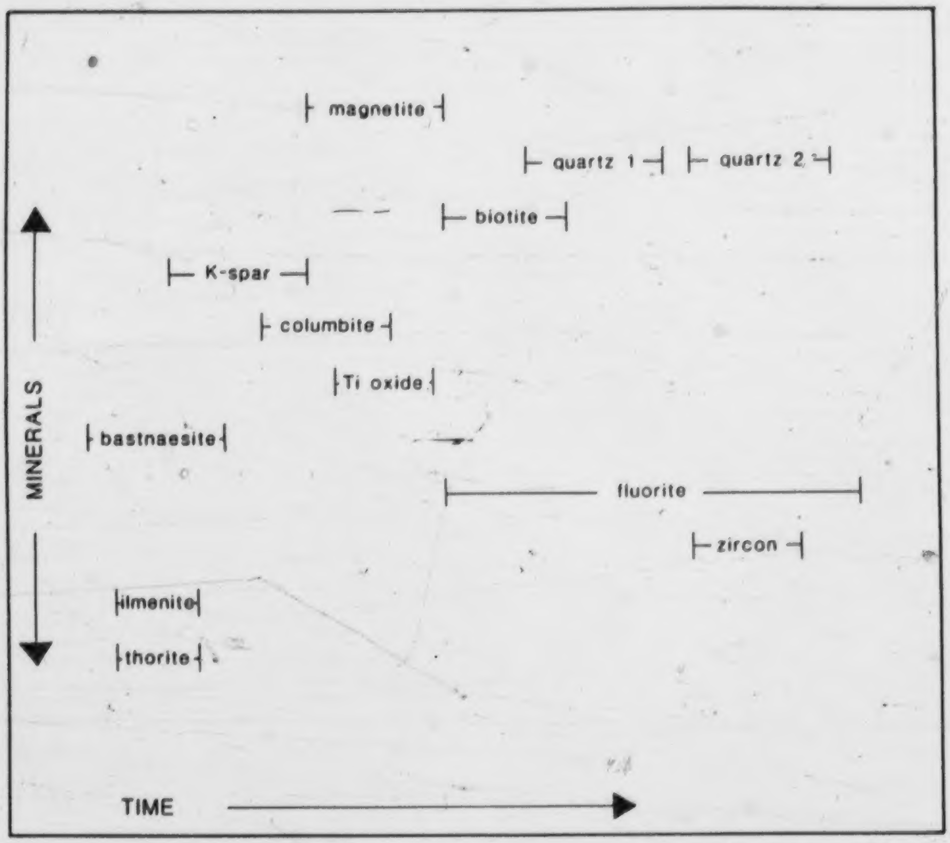
magnetite
quartz 1
quartz 2
biotite
K-spar
columbite
Ti oxide
bastnaesite
fluorite
zircon
ilmenite
thorite
MINERALS
TIME

Figure 2.9-Generalized paragenetic sequence of mineralization for the *quartz-magnetite* unit of the Lower Intermediate zone.

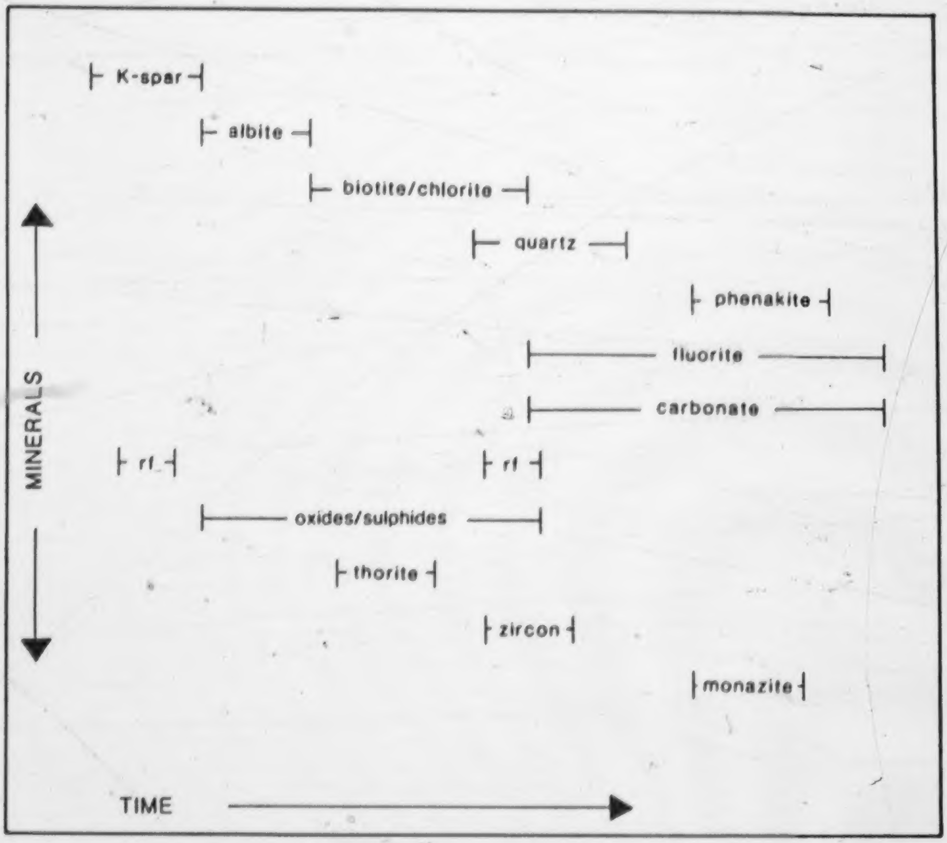
K-spar
albite
biotite/chlorite
quartz
phenakite
fluorite
carbonate
rf
rf
oxides/sulphides
thorite
zircon
monazite
MINERALS
TIME

Figure 2.10-Generalized paragenetic sequence of mineralization for the Lower Intermediate zone, *quartz-biotite(±chlorite)-feldspar* unit.

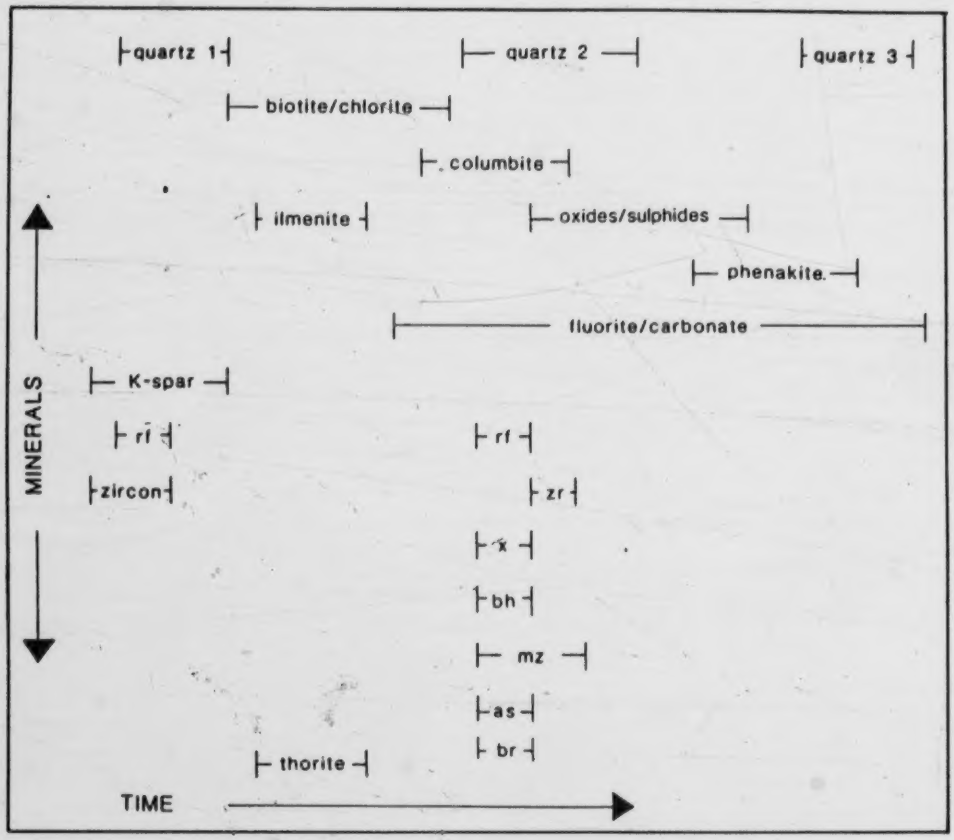
quartz 1
quartz 2
quartz 3
biotite/chlorite
columbite
ilmenite
oxides/sulphides
phenakite
fluorite/carbonate
K-spar
rf
rf
zircon
zr
x
bh
mz
as
br
thorite
MINERALS
TIME

Figure 2.11-Generalized paragenetic sequence of mineralization for the Lower Intermediate zone, ***quartz-biotite(±chlorite)-oxides*** unit.

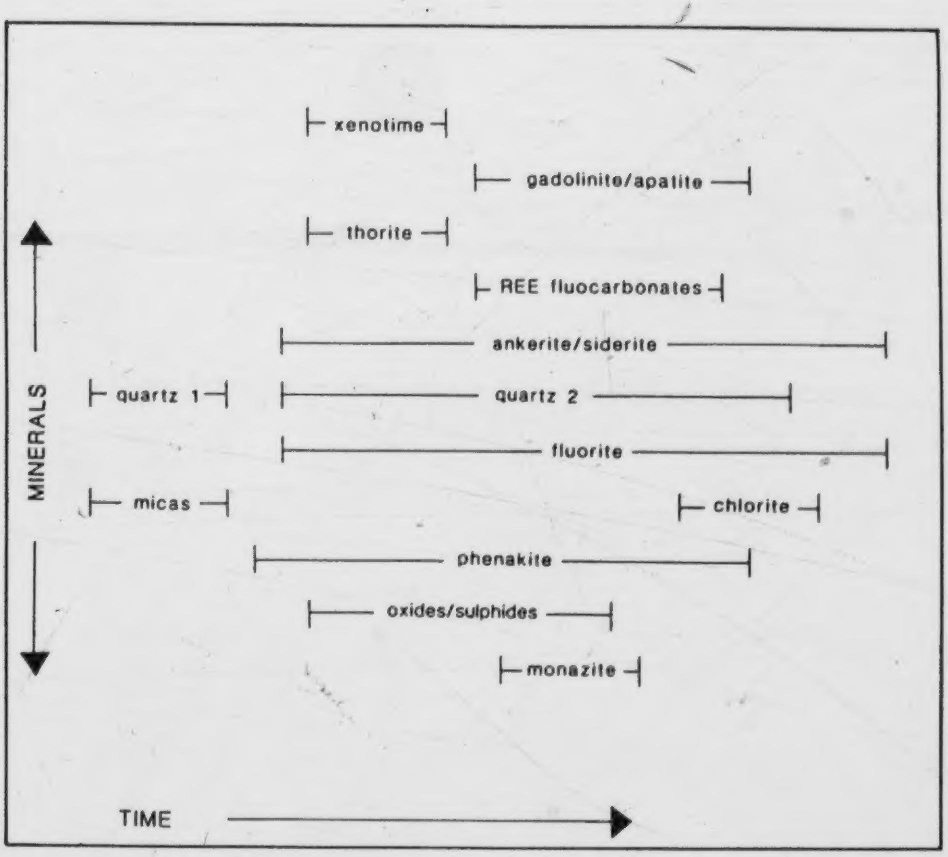

Figure 2.12-Generalized paragenetic sequence of mineralization for the *quartz-thorite* unit of the Upper Intermediate zone.

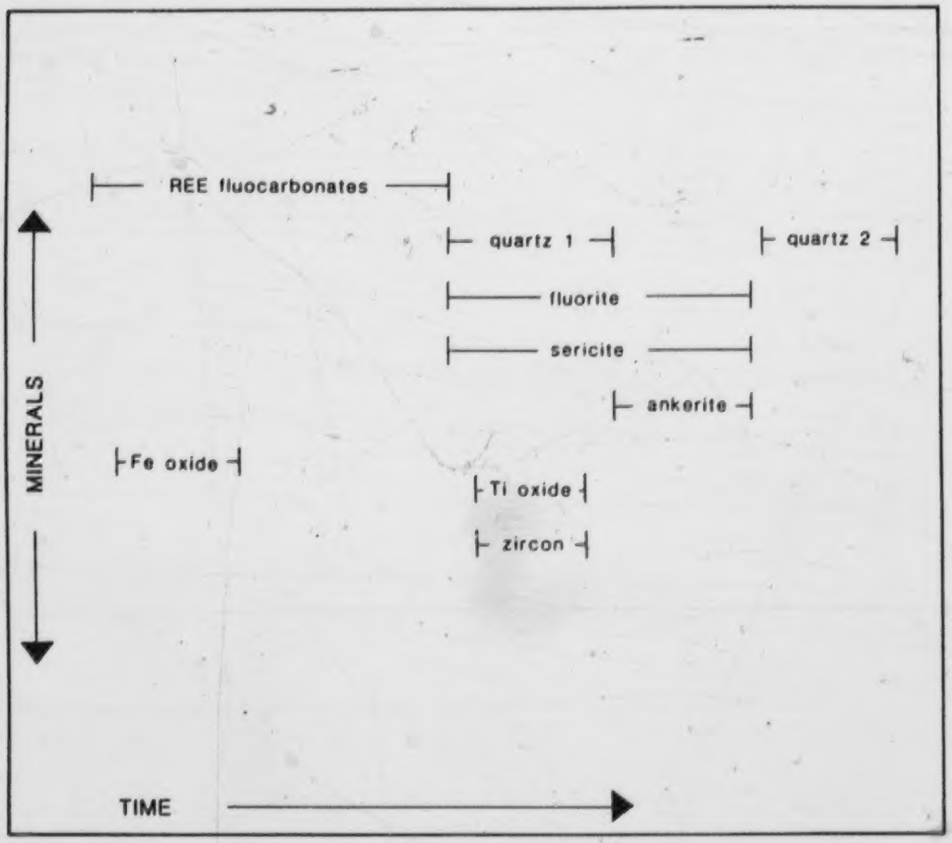
REE fluocarbonates
quartz 1
quartz 2
fluorite
sericite
ankerite
Fe oxide
Ti oxide
zircon
MINERALS
TIME

Figure 2.13-Generalized paragenetic sequence of mineralization for the *quartz-bastnaesite group* unit of the Upper Intermediate zone.

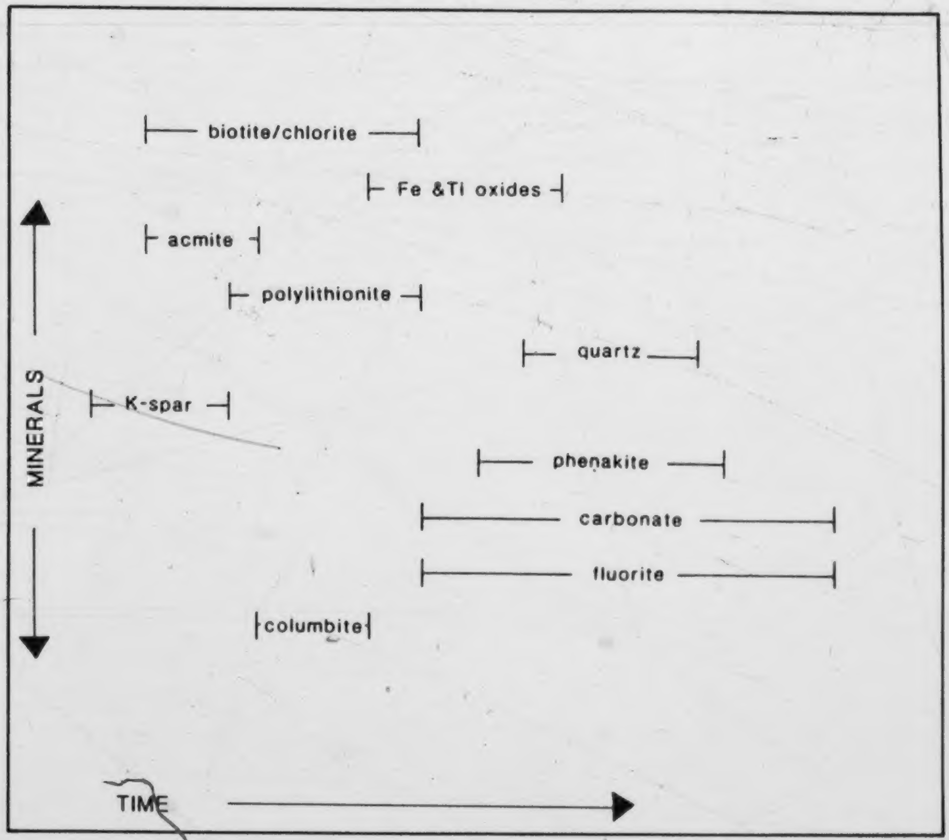
biotite/chlorite
Fe &Ti oxides
acmite
polylithionite
quartz
K-spar
phenakite
carbonate
fluorite
columbite
MINERALS
TIME

Figure 2.14-Generalized paragenetic sequence of mineralization for the Upper Intermediate zone, *quartz-feldspar-magnetite* unit.

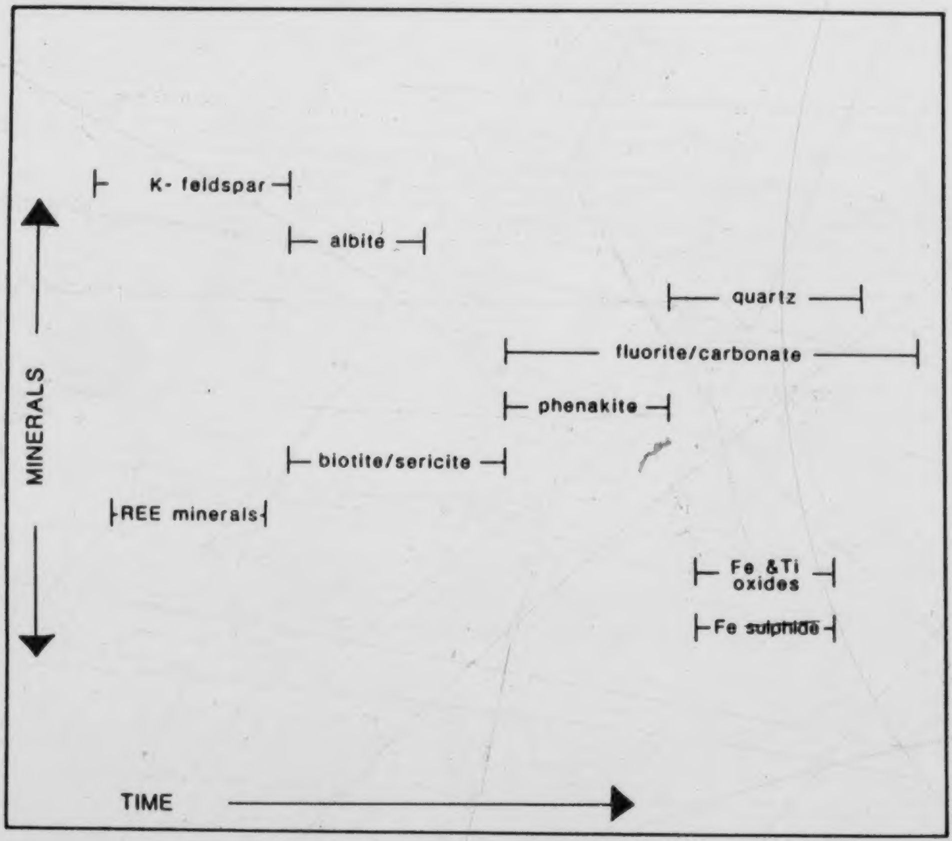
K- feldspar
albite
quartz
fluorite/carbonate
phenakite
biotite/sericite
REE minerals
Fe &Ti oxides
Fe sulphide
MINERALS
TIME

Figure 2.15-Generalized paragenetic sequence of mineralization for the *quartz-feldspar* unit of the Upper Intermediate zone.

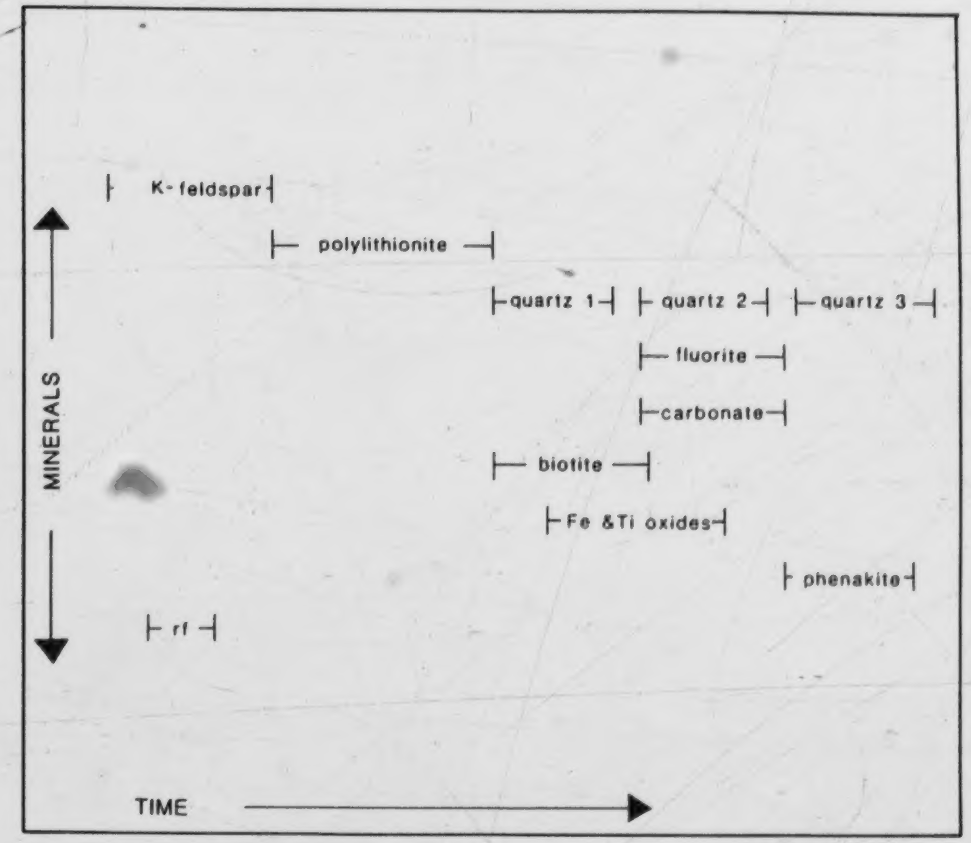
K-feldspar
polylithionite
quartz 1
quartz 2
quartz 3
fluorite
carbonate
biotite
Fe &Ti oxides
phenakite
rf
MINERALS
TIME

Figure 2.16-Generalized paragenetic sequence of mineralization for the *quartz-mica-feldspar* unit of the Upper Intermediate zone.

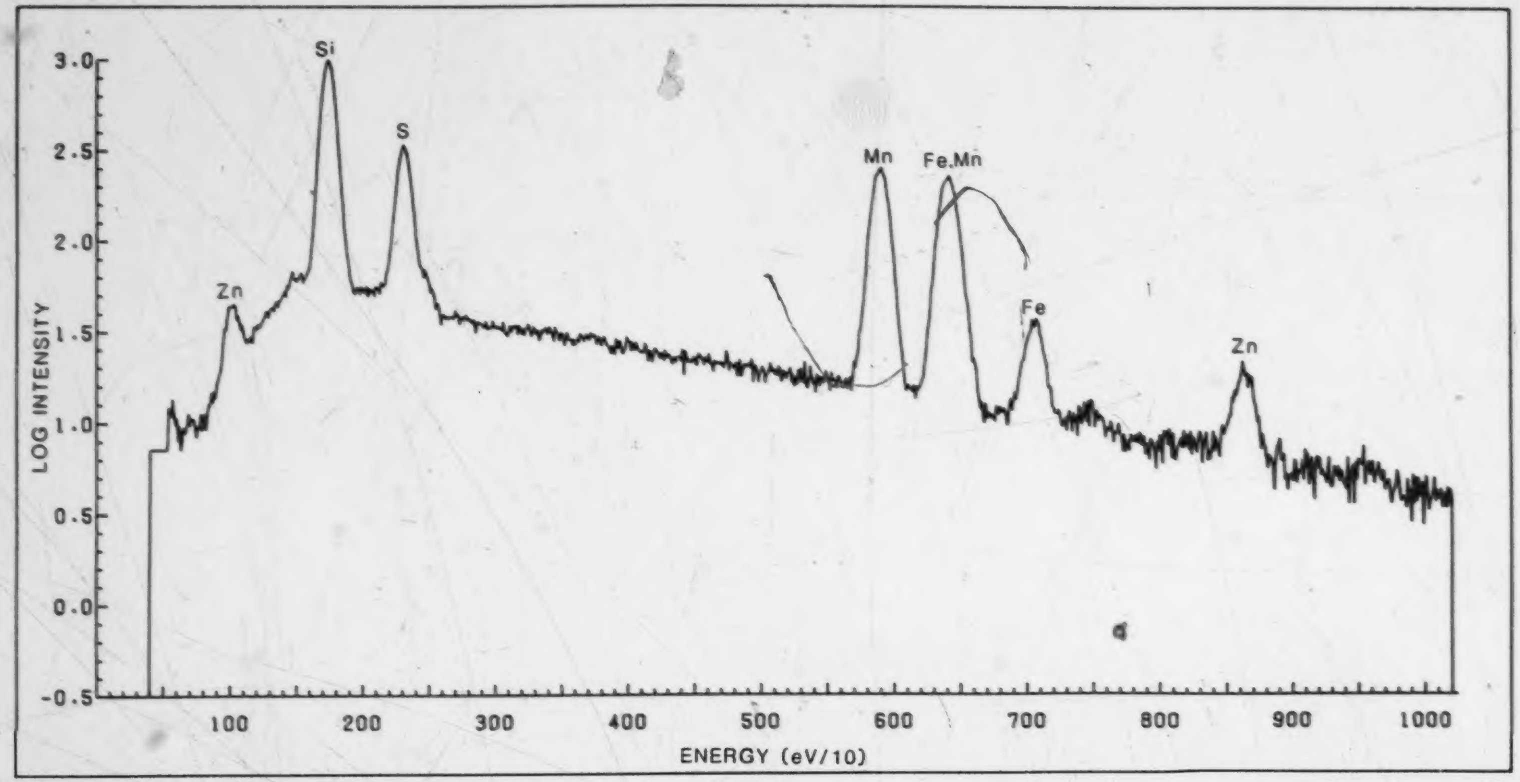

Figure 3.1-Characteristic energy dispersive spectrum of the helvite group mineral. Be does not appear in spectrum due to absorption by the detector.

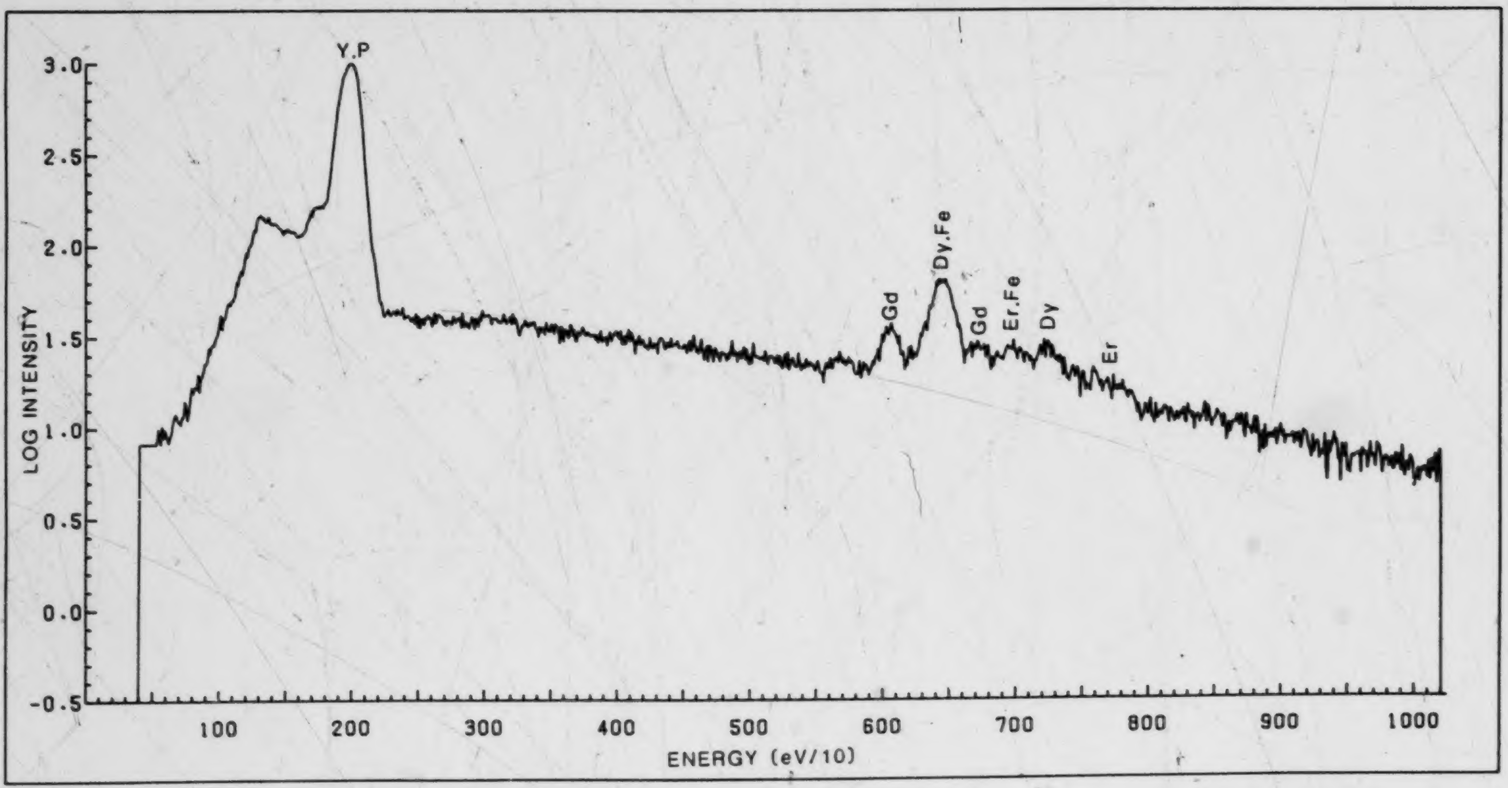

Figure 3.2-Characteristic energy dispersive spectrum of xenotime.

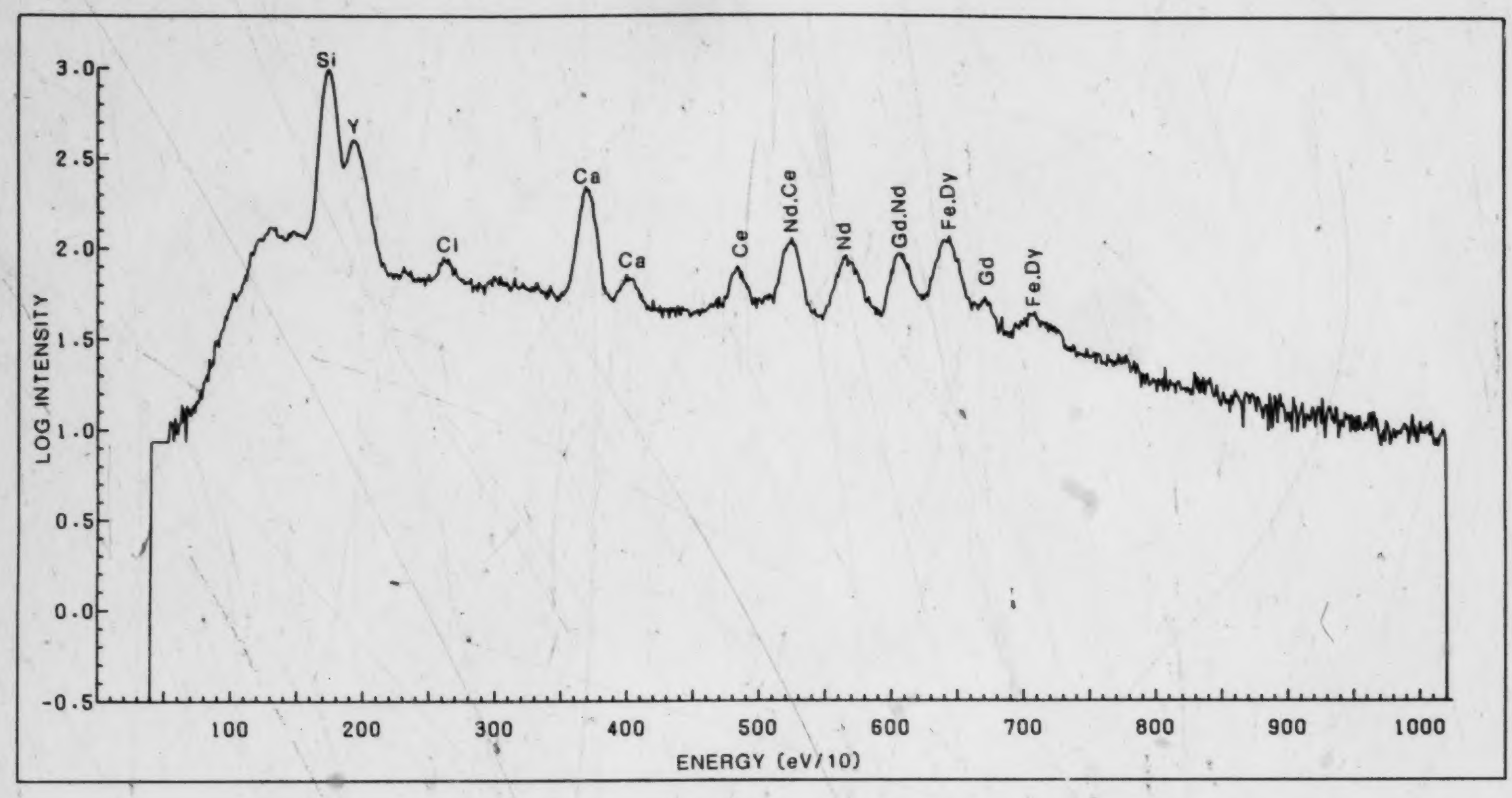

Figure 3.3-Characteristic energy dispersive spectrum of gadolinite. Be does not appear in spectrum due to absorption by the detector.

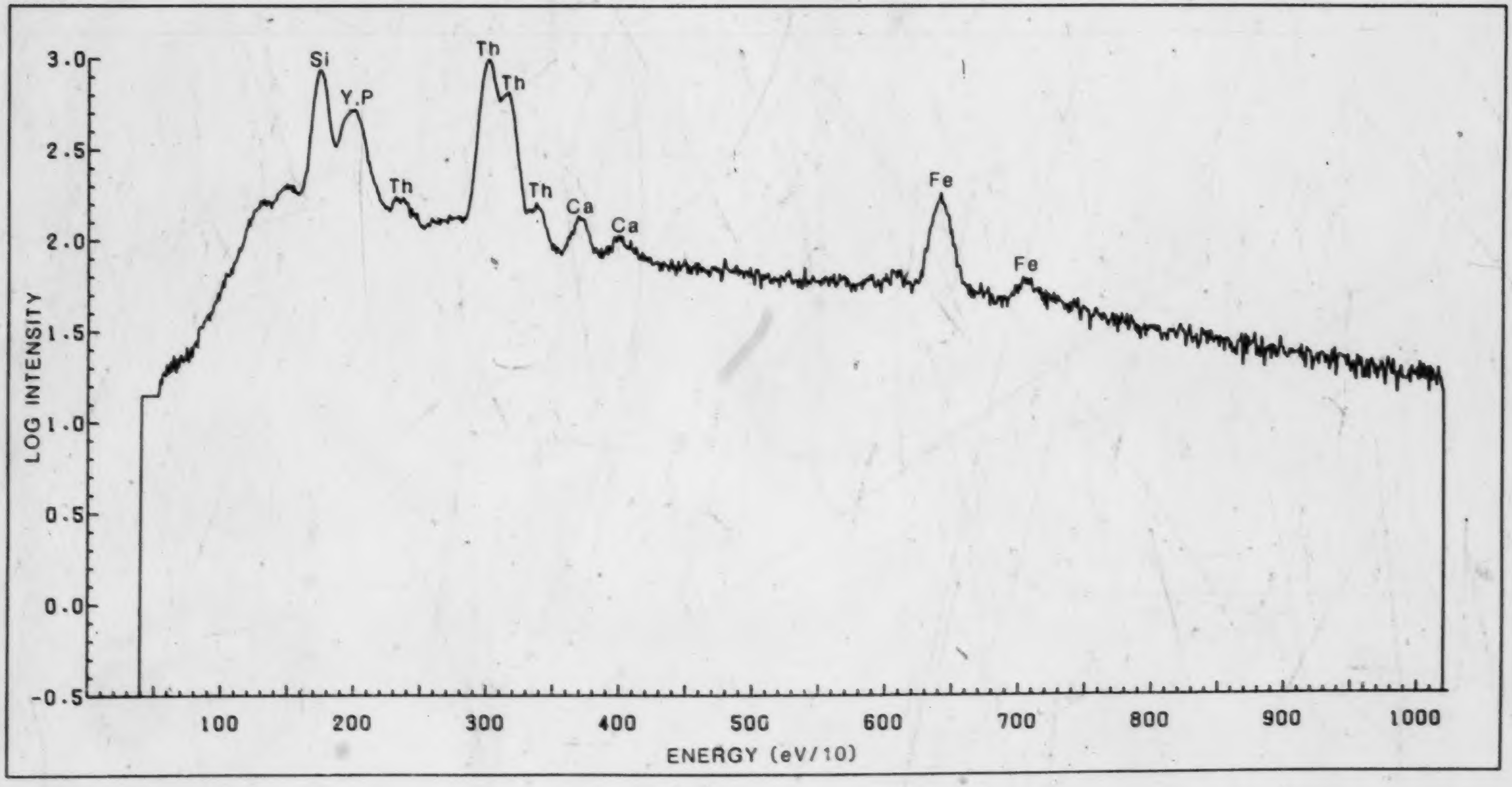

Figure 3.4-Characteristic energy dispersive spectrum of the thorite group mineral.

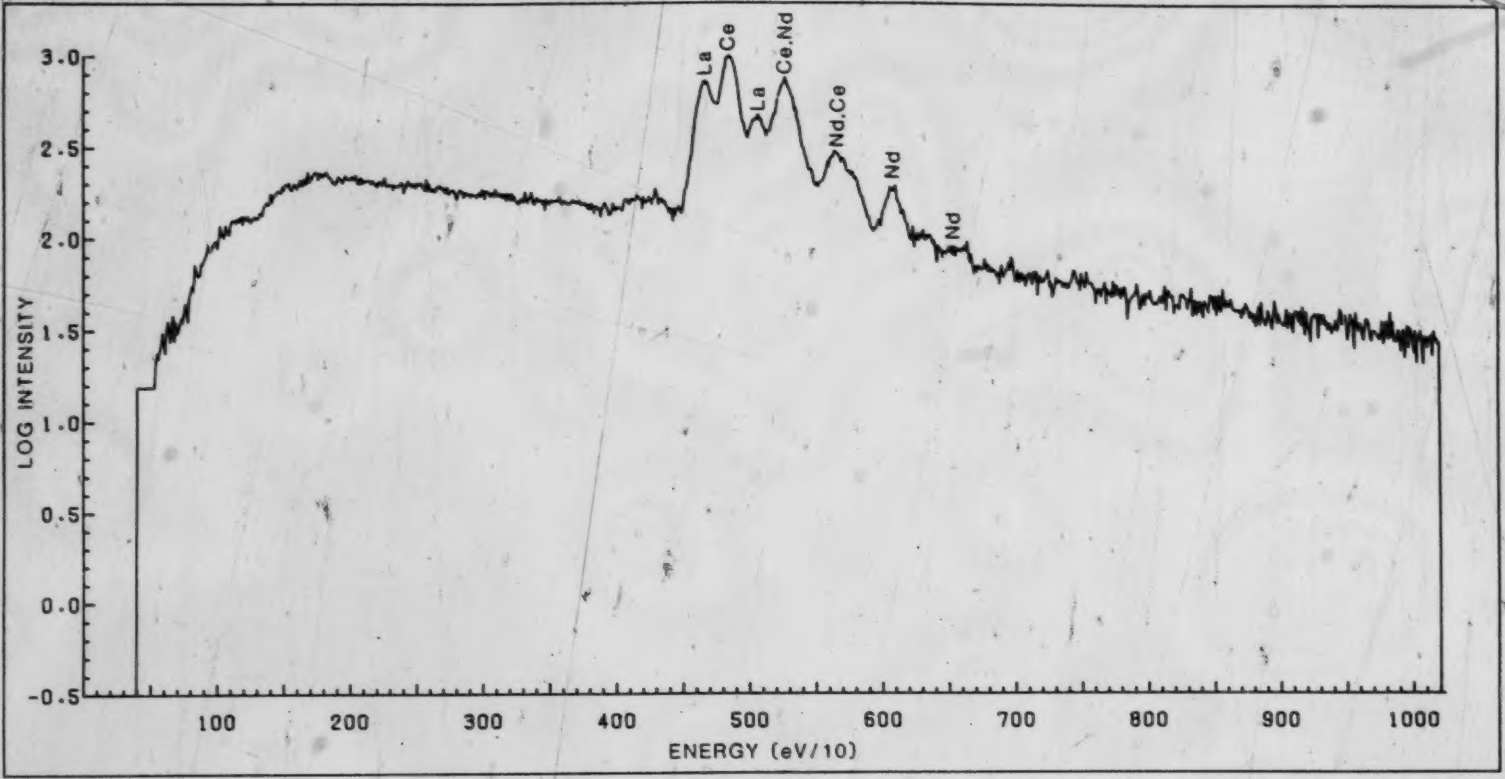

Figure 3.5-Characteristic energy dispersive spectrum of bastnaesite. C and F do not appear in spectrum due to absorption by the detector.

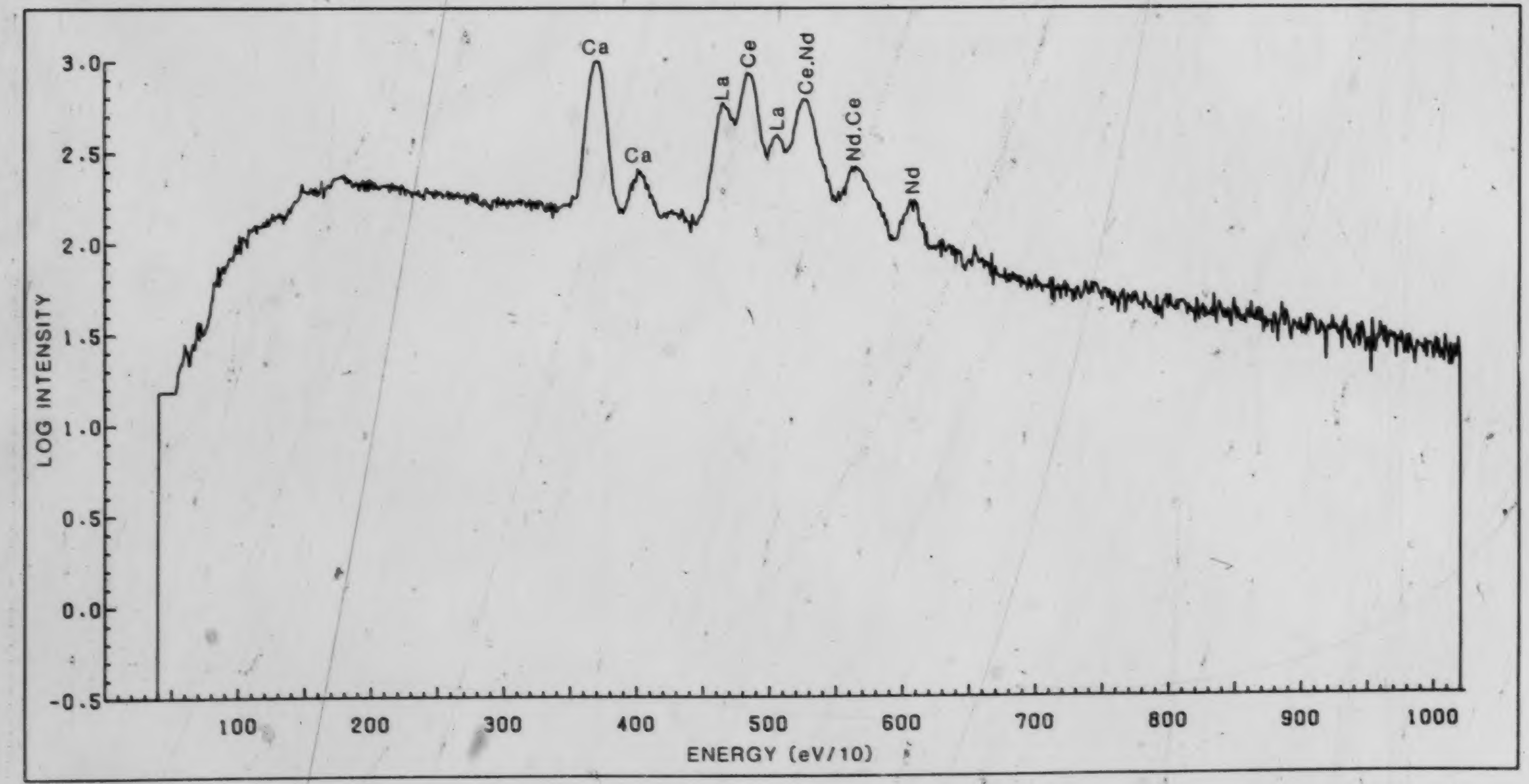

Figure 3.6-Characteristic energy dispersive spectrum of parisite. C and F do not appear in spectrum due to absorption by the detector.

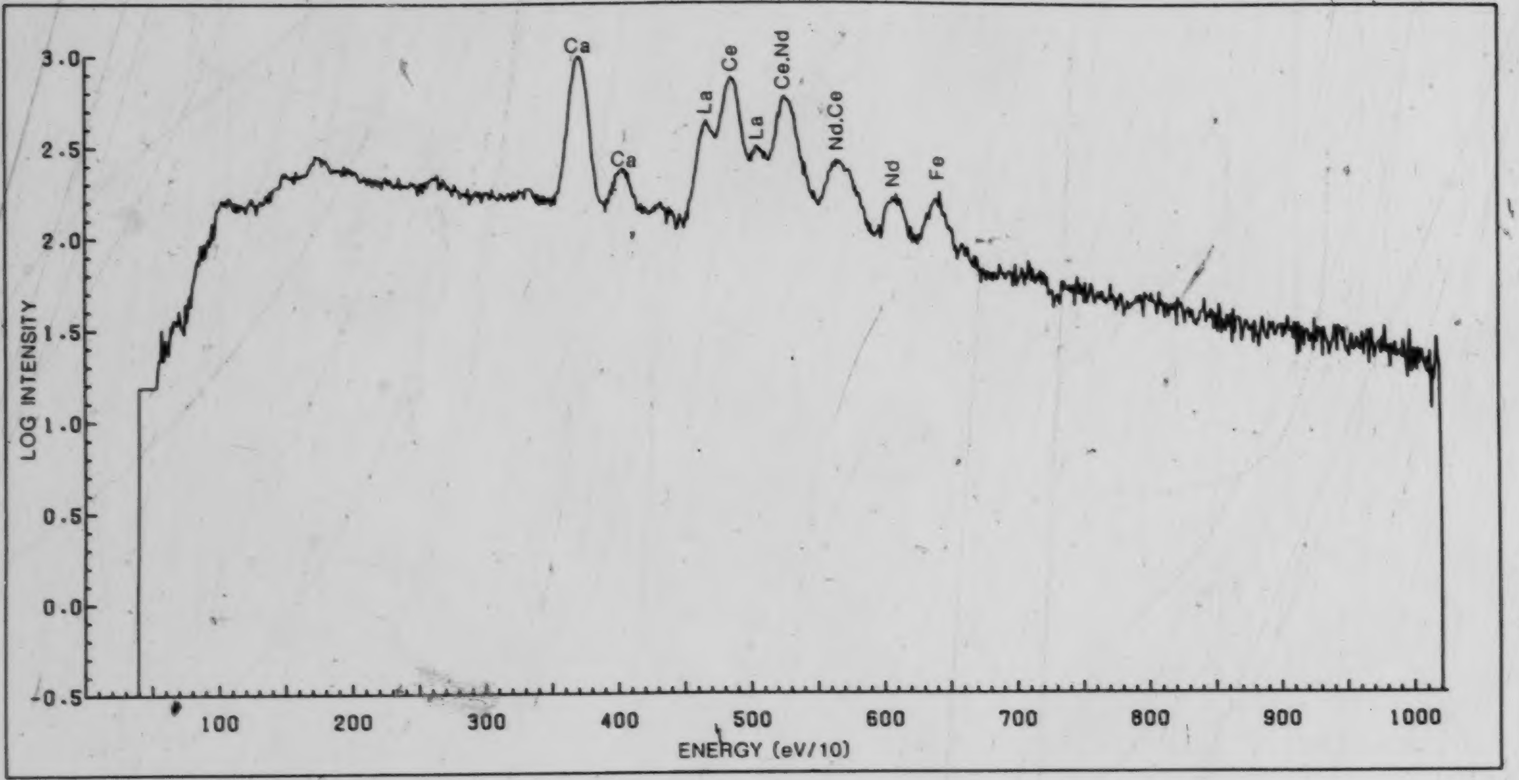

Figure 3.7-Characteristic energy dispersive spectrum of roentgenite. C and F do not appear in spectrum due to absorption by the detector.

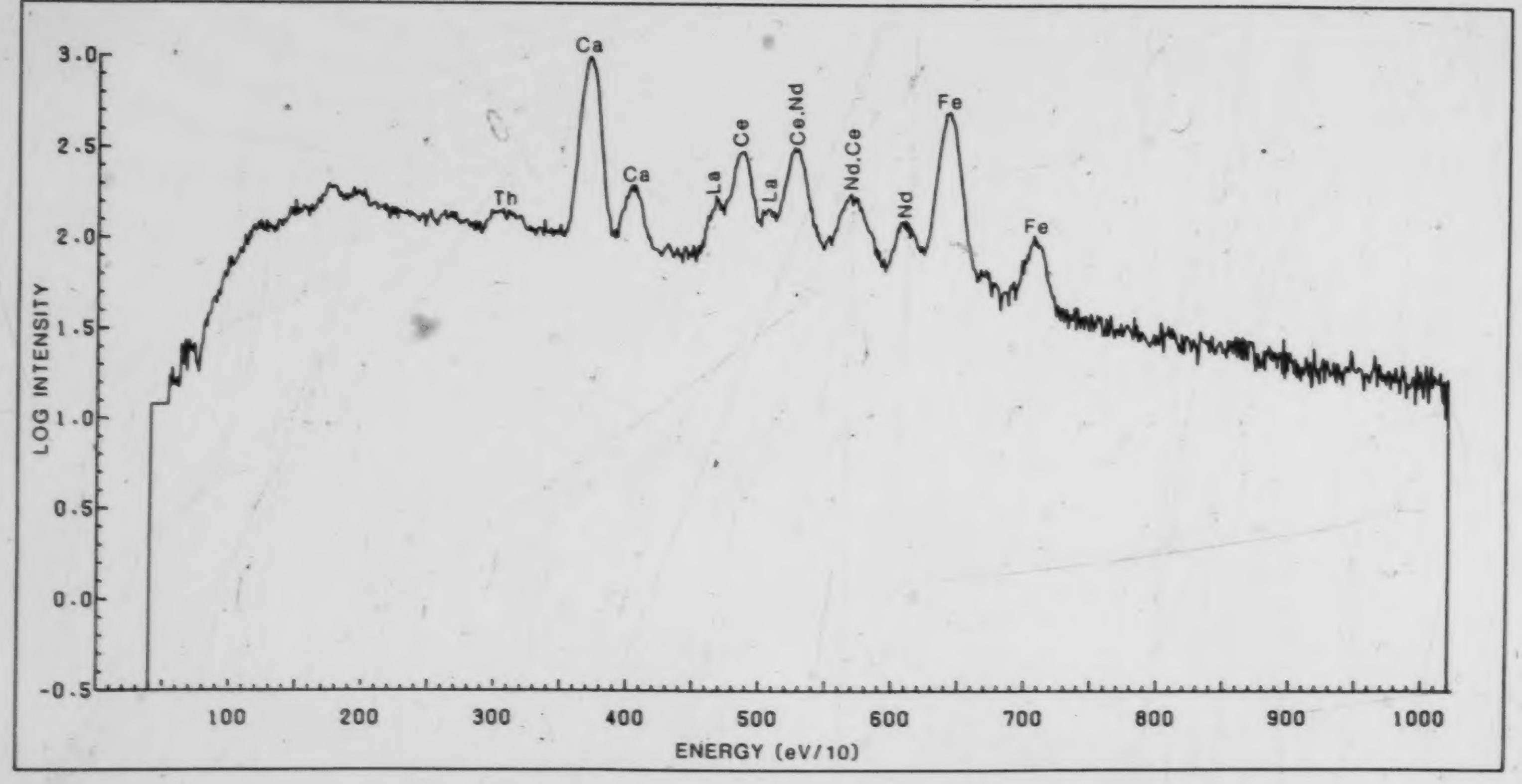

Figure 3.8-Characteristic energy dispersive spectrum of synchysite. C and F do not appear in spectrum due to absorption by the detector.

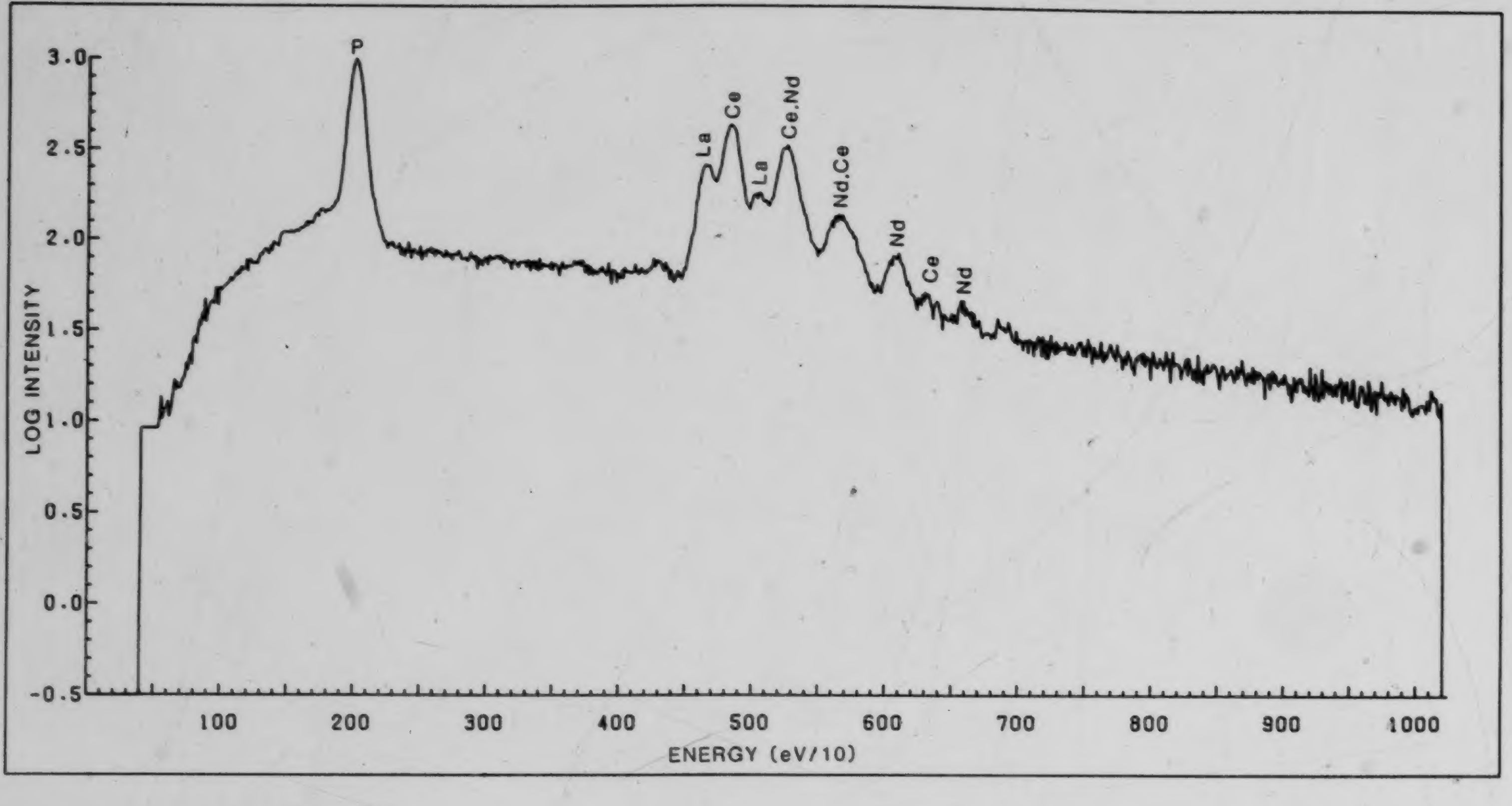

Figure 3.9-Characteristic energy dispersive spectrum of monazite.

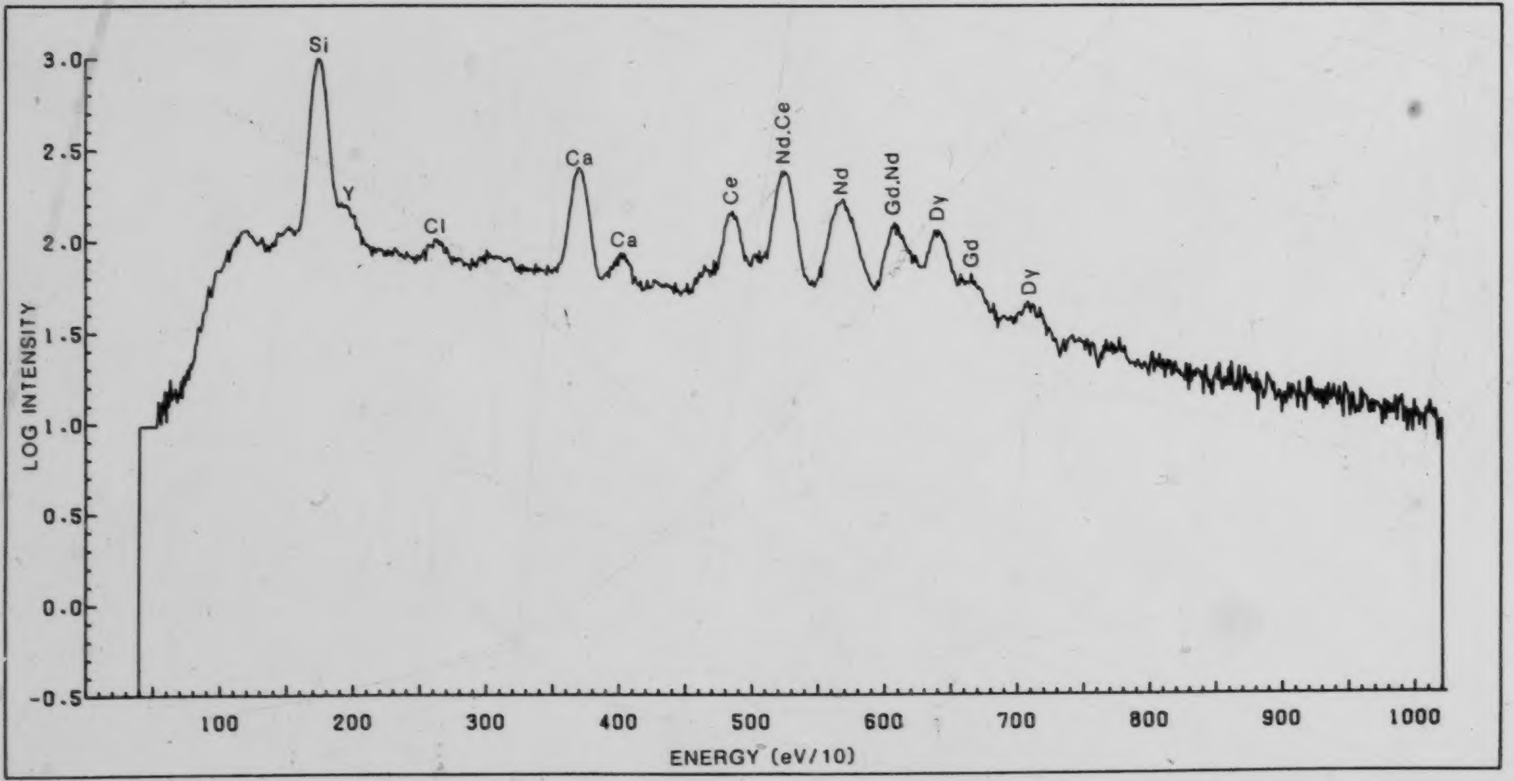

Figure 3.10-Characteristic energy dispersive spectrum of mineral tentatively identified as britholite.

VII. PLATES

Plate 2.1a-Unmineralized, altered granite of the T-zone.

Plate 2.1b-Microcrystalline quartz replacing albite lamellae in perthitic feldspar and along grain boundaries. Associated sericite aggregate mantled by quartz. Unmineralized granite. Crossed polars. Magnification X92.

CM

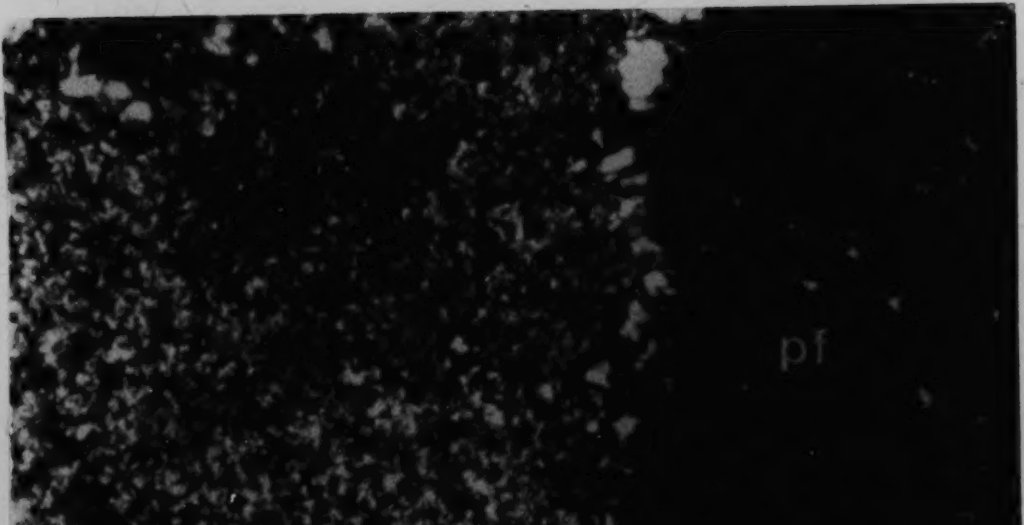
pf

Plate 2.2a-Albite with patchy, irregular twinning partially replaced by quartz at grain boundary. Unidentified mineral of prismatic habit (possibly acmite) partially pseudomorphed by magnetite and enclosed in quartz. Rounded inclusions in albite are K-feldspar-columbite intergrowths. Unmineralized granite. Crossed polars. Magnification X92.

Plate 2.2b-Mineralized granite of the T-zone showing "microbrecciated" texture caused by pervasive replacement of feldspar along fractures and parallel to cleavage.

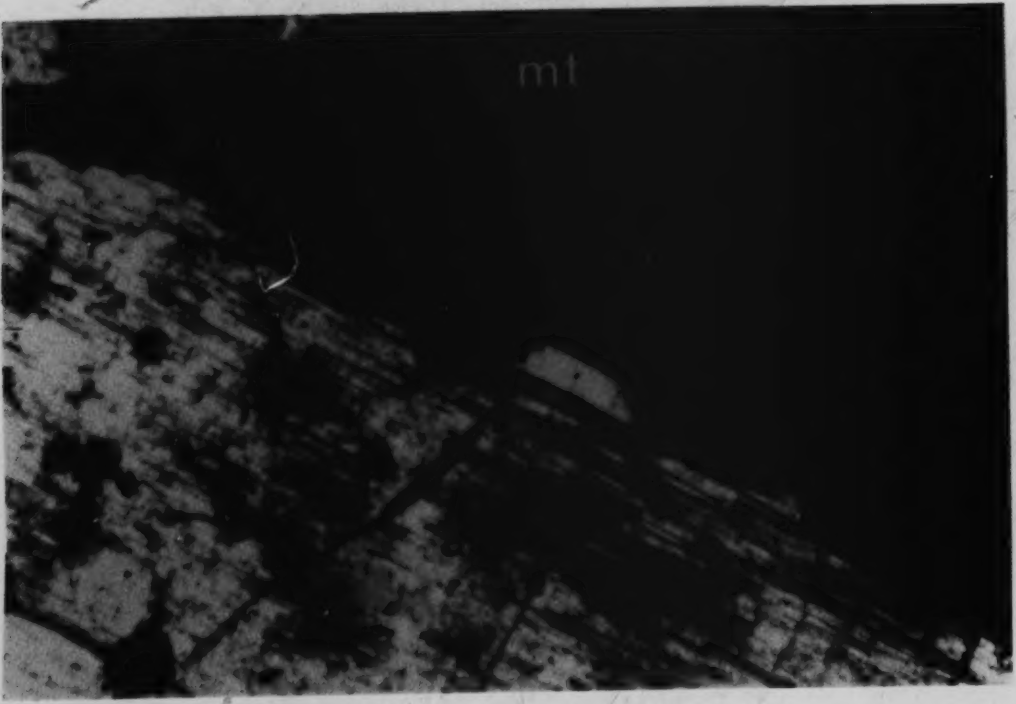
mt

cm

Plate 2.3a-Perthitic feldspar overgrown by K-feldspar. Dark lamellae in perthite are K-feldspar, light lamellae are albite. Unidentified acicular mineral is pseudomorphed by magnetite and enclosed in quartz. Mineralized granite. Crossed polars. Magnification X60.

Plate 2.3b-K-feldspar partially replacing anhedral LREE-bearing fluocarbonate polycrystals. K-feldspar displays unusual mottled texture. Mineralized granite. Crossed polars. Magnification X240.

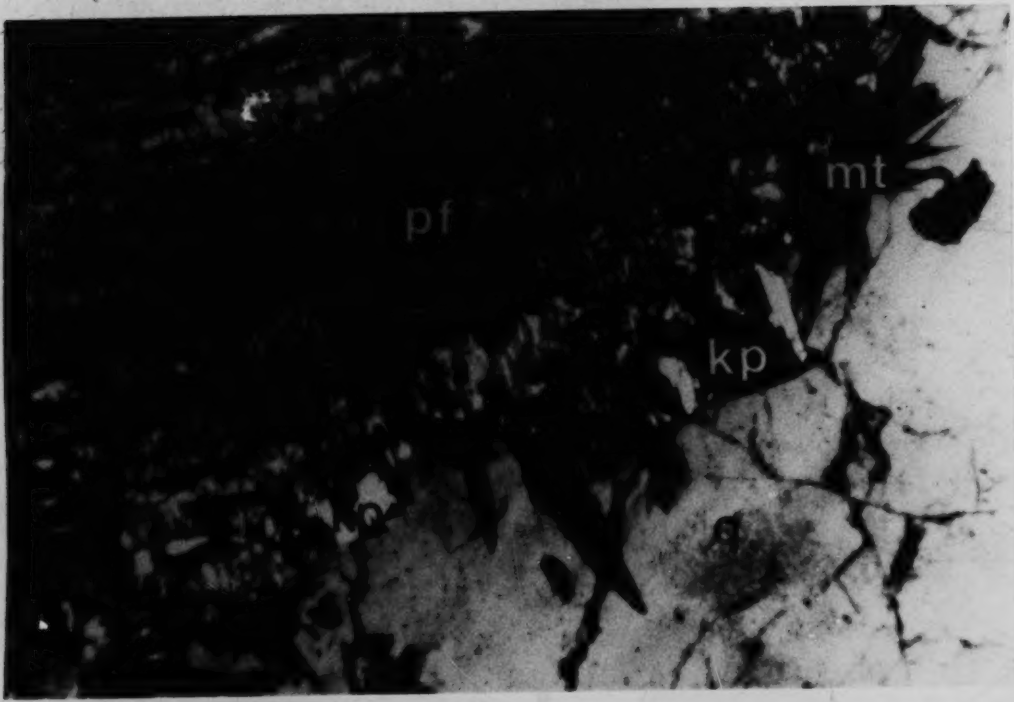
pf
mt
kp
g

Plate 2.4a-K-feldspar partially replaced by quartz, biotite and ankerite along fractures and grain boundaries. Mineralized granite. Crossed polars. Magnification X92.

Plate 2.4b-Altered acmite in albite. Acmite is partially to entirely replaced by magnetite, ankerite and quartz. Note patchy, irregular twinning in albite. Mineralized granite. Crossed polars. Magnification X92.

bt
q

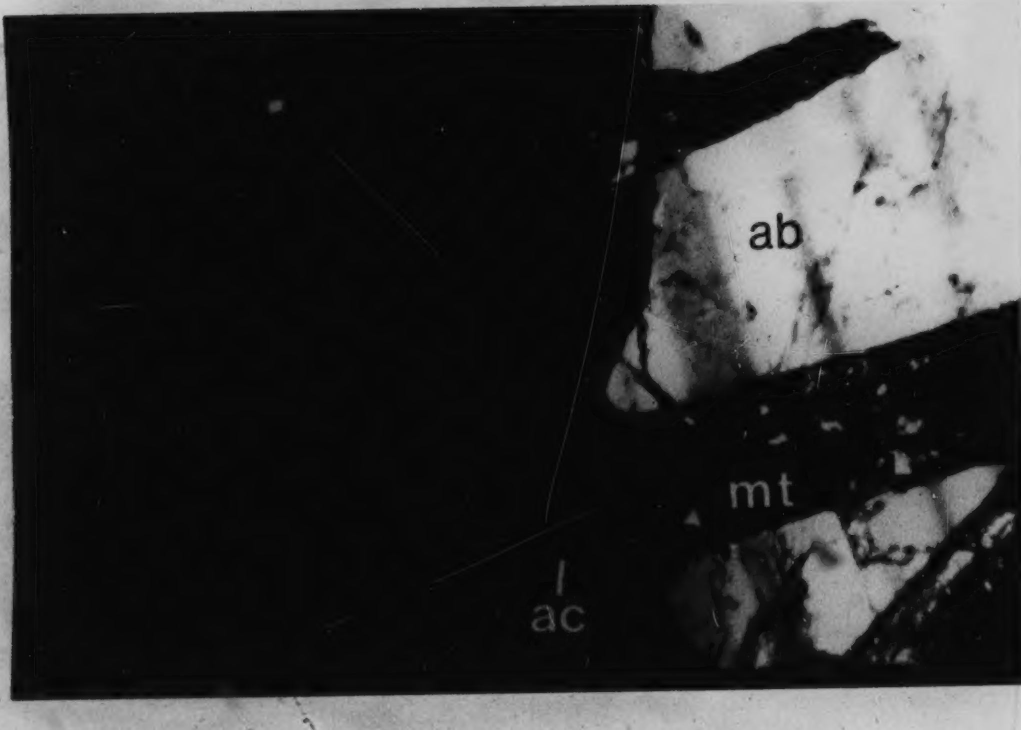
ab
mt
ac

Plate 2.5a-Semi-opaque inclusions in albite are thorite-bearing intergrowths. White box encloses area shown in Plate 2.5b. Mineralized granite. Crossed polars. Magnification X92.

Plate 2.5b-Backscattered electron image showing intergrowth of K-feldspar, biotite, ilmenite and thorite within rounded inclusion in albite. Mineralized granite. Scale bar represents 10 μm.

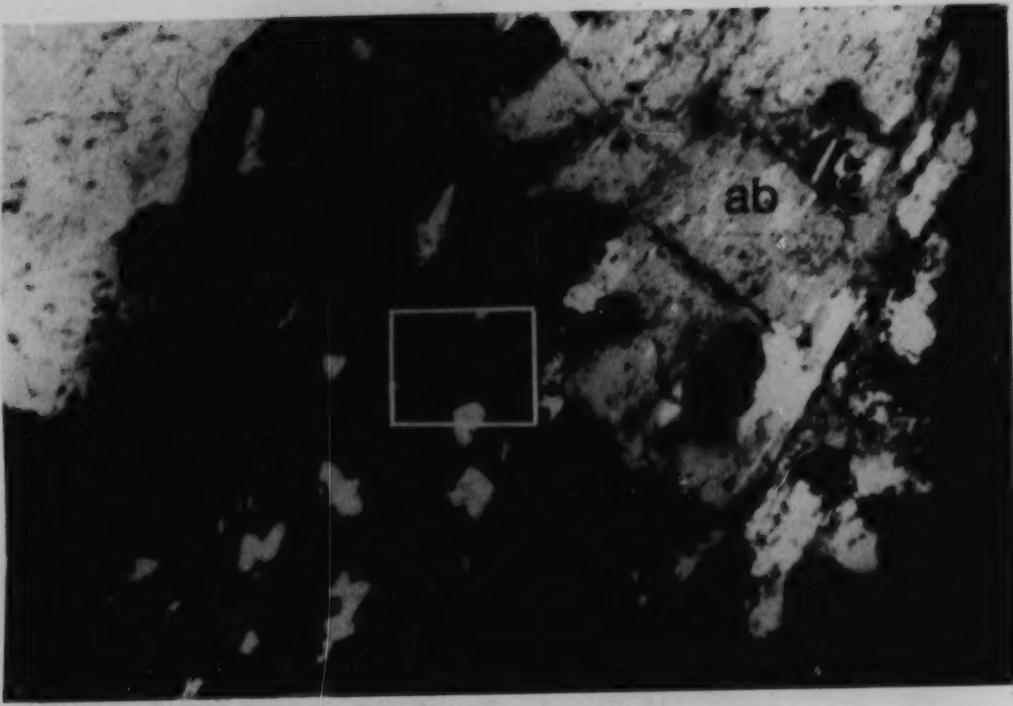
ab

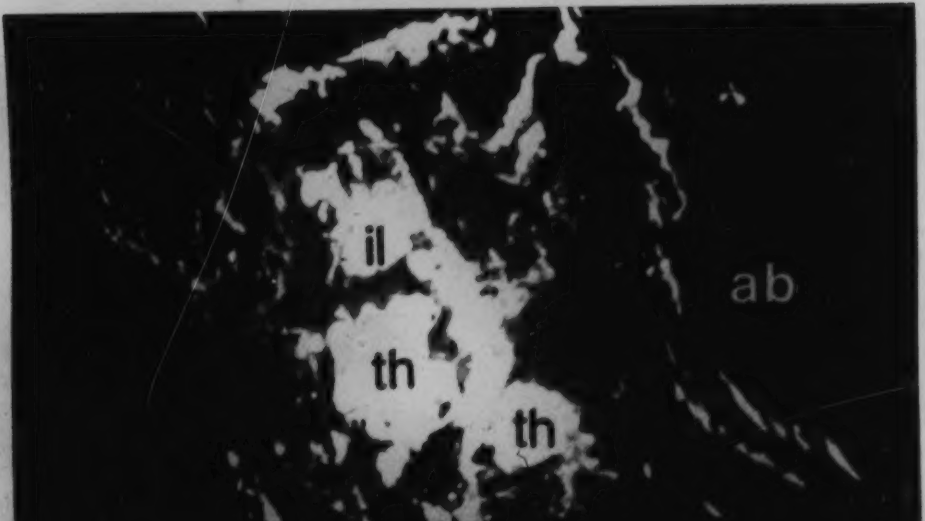
il
ab
th
th

Plate 2.6a-Drill core sample of albite *aplite* unit of the Wall zone (left). Hand samples of K-feldspar *aplite* unit unstained (center) and stained for K-feldspar (right).

Plate 2.6b-K-feldspar with interstitial quartz. K-feldspar *aplite* unit, Wall zone. Crossed polars. Magnification X60.

Plate 2.7a-K-feldspar with interstitial LREE-bearing fluocarbonate polycrystals. K-feldspar *aplite* unit, Wall zone. Crossed polars. Magnification X92.

Plate 2.7b-Randomly oriented albite laths with interstitial chlorite and ankerite. Albite *aplite* unit, Wall zone. Crossed polars. Magnification X92.

rf

ct
ab
ct
ab

Plate 2.8a-Albite enclosed in, and partially replaced by, quartz. Opaque mineral is columbite. Albite *aplite* unit, Wall zone. Crossed polars. Magnification X92.

Plate 2.8b-Altered K-feldspar partially replaced by quartz and biotite. Albite *aplite* unit, Wall zone. Crossed polars. Magnification X92.

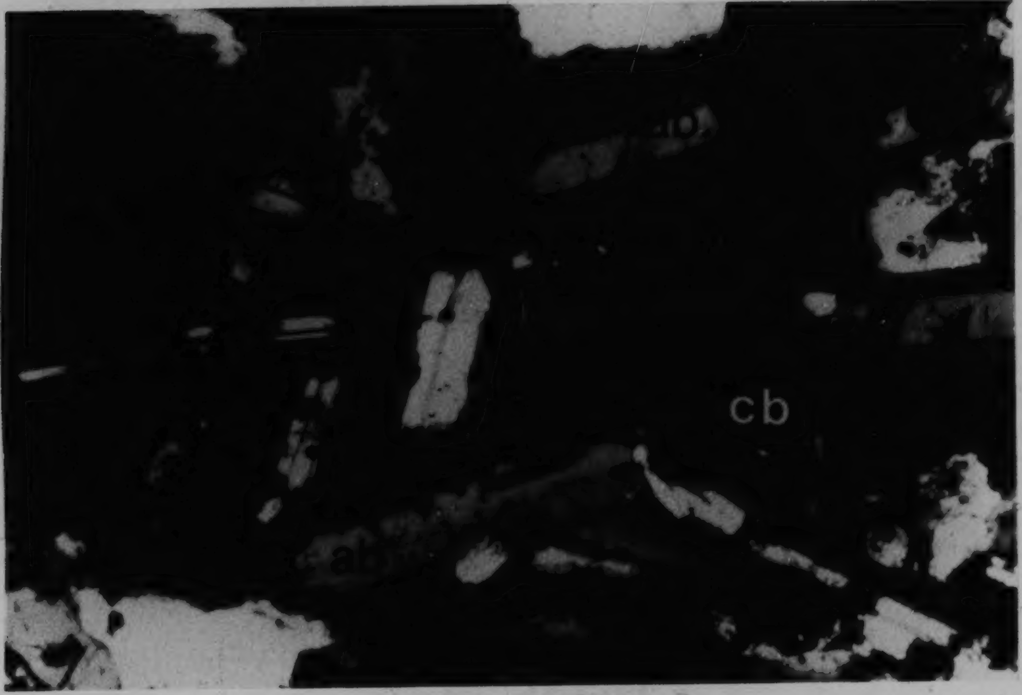
ab
cb
ab

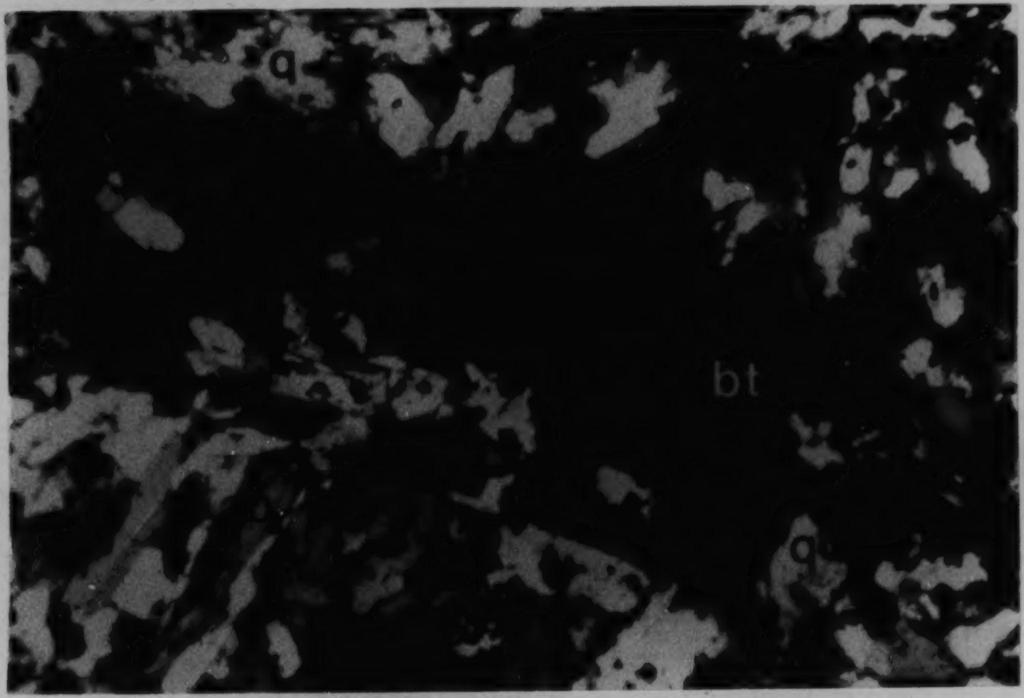
q
bt
q

Plate 2.9a-*Core* unit of the Wall zone, unstained (left) and stained for K-feldspar.

Plate 2.9b-Early altered K-feldspar (right) partially replaced by later K-feldspar (left). Columbite present as inclusions in both feldspar types. Note irregular, patchy twinning of later K-feldspar (left). *Core* unit , Wall zone. Crossed polars. Magnification X240.

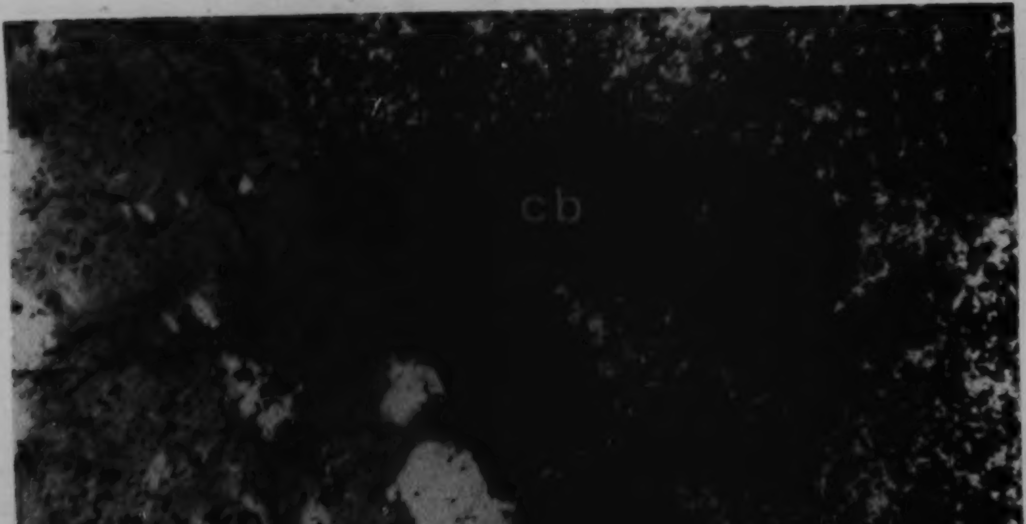
cb

Plate 2.10a-Randomly oriented albite laths with interstitial chlorite and fluorite. *Core* unit, Wall zone. Crossed polars. Magnification X60.

Plate 2.10b-Radiating aggregates of albite overgrowing K-feldspar. Note patchy twinning in K-feldspar. *Core* unit, Wall zone. Crossed polars. Magnification X60.

f

Plate 2.11a-*Breccia* unit of the Wall zone.

Plate 2.11b-*Quartz-magnetite* unit of the Lower Intermediate zone.

CM

CM

Plate 2.12a-K-feldspar overgrown and partially replaced by magnetite aggregates. Interstitial quartz and biotite. *Quartz-magnetite* unit, Lower Intermediate zone. Crossed polars. Magnification X368.

Plate 2.12b- *Quartz-biotite(±chlorite)-feldspar* unit of the Lower Intermediate zone. Note relict granitic texture.

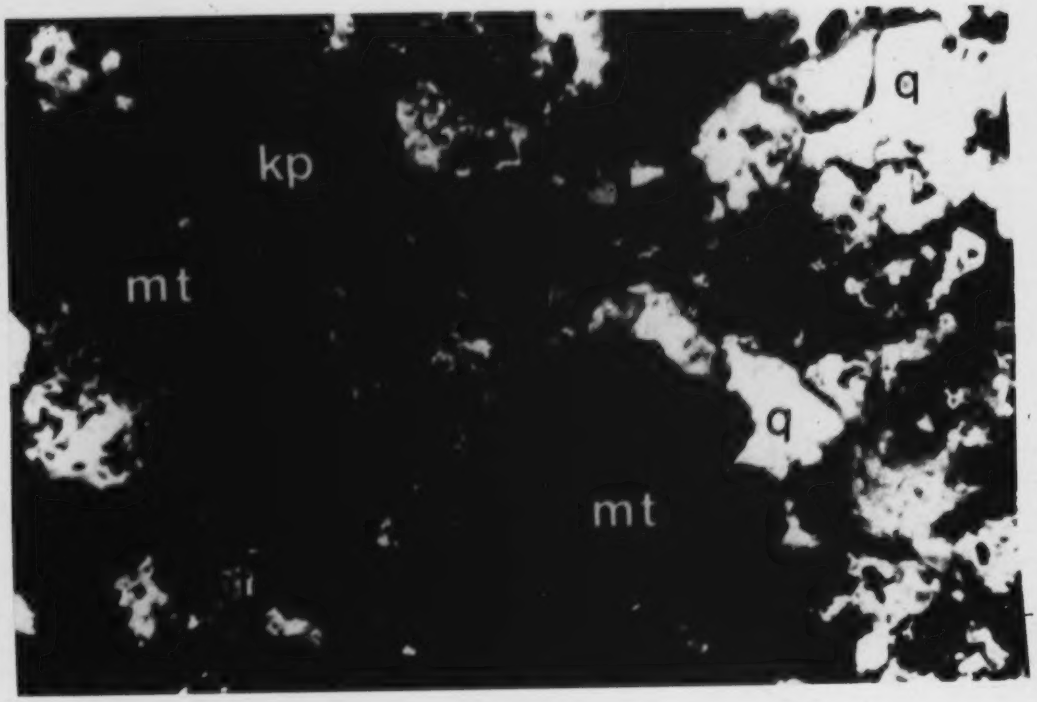
q
kp
mt
q
mt

CM

Plate 2.13a-K-feldspar overgrown by aggregates of fine grained biotite. Associated opaque mineral is columbite. *Quartz-biotite(±chlorite)-feldspar* unit, Lower Intermediate zone. Crossed polars. Magnification X60.

Plate 2.13b-Albite partially replaced by lath-like and shreddy biotite. *Quartz-biotite(±chlorite)-feldspar* unit, Lower Intermediate zone. Crossed polars. Magnification X60.

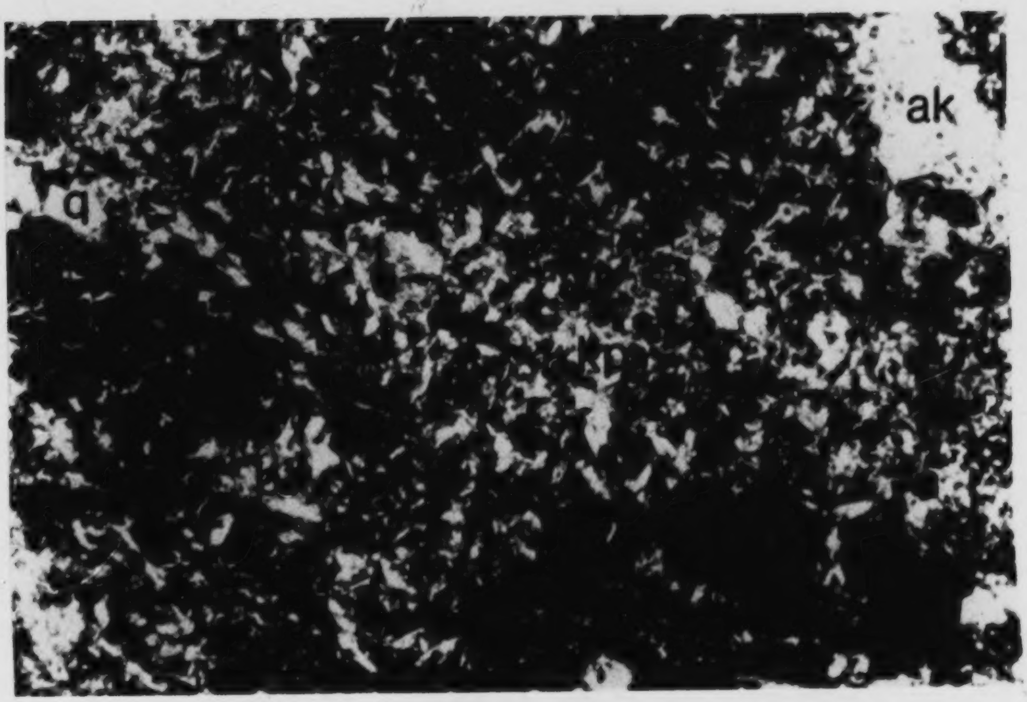
ak
q

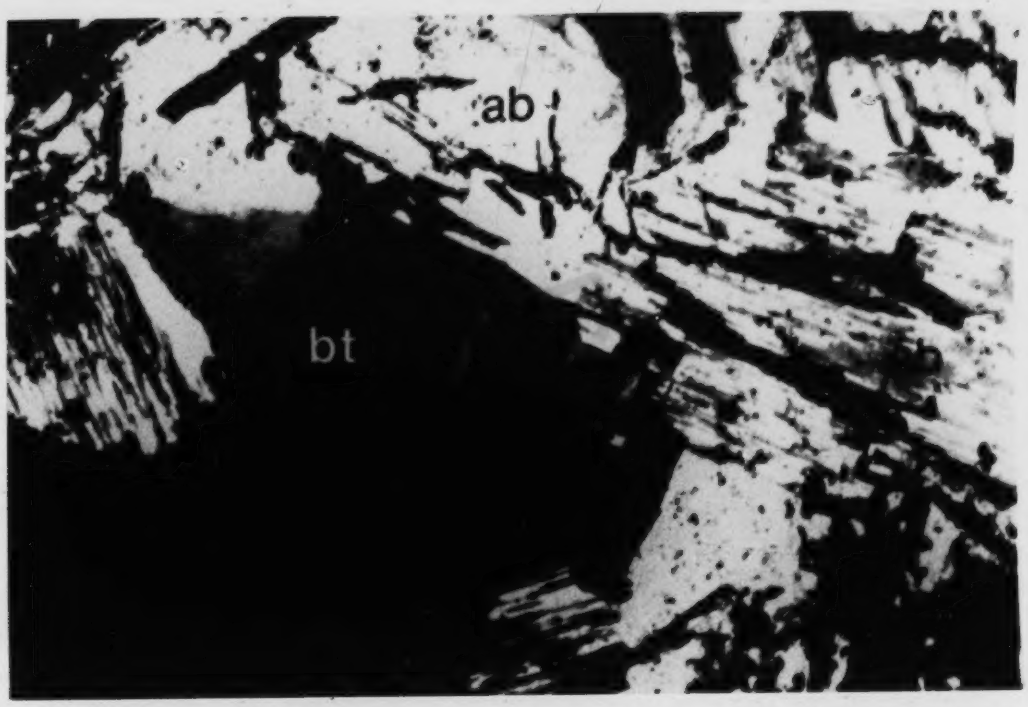
ab
bt

Plate 2.14a- *Quartz-biotite(±chlorite)-oxides* unit of the Lower Intermediate zone.

Plate 2.14b-Lath-like biotite partially replaced by columbite, fluorite and quartz. *Quartz-biotite(±chlorite)-oxides* unit, Lower Intermediate zone. Plane polarized light. Magnification X60.

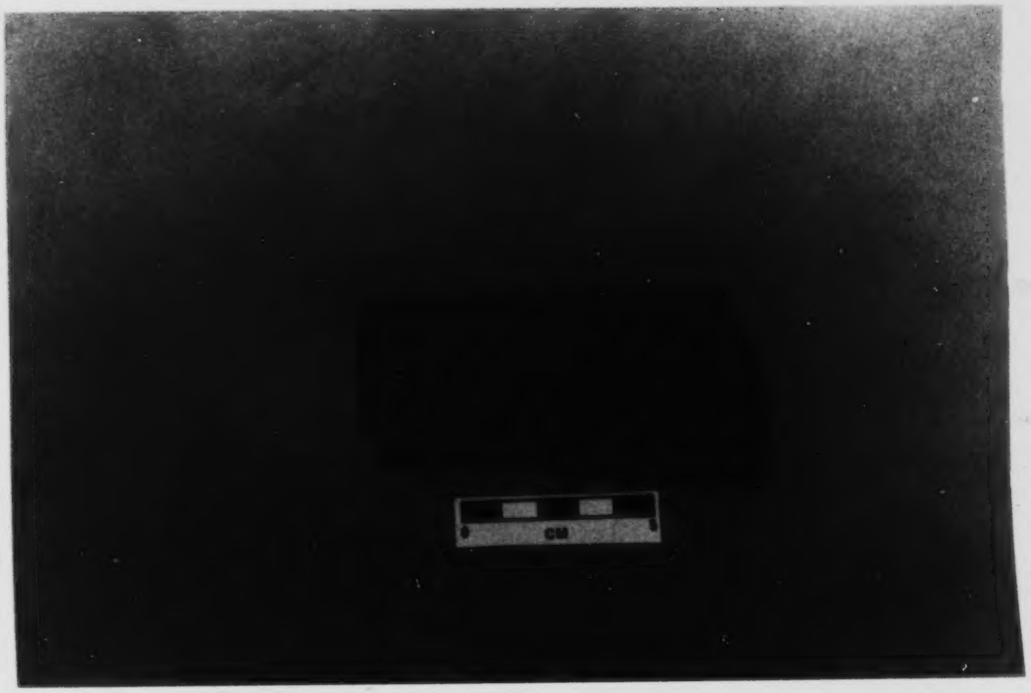
CM

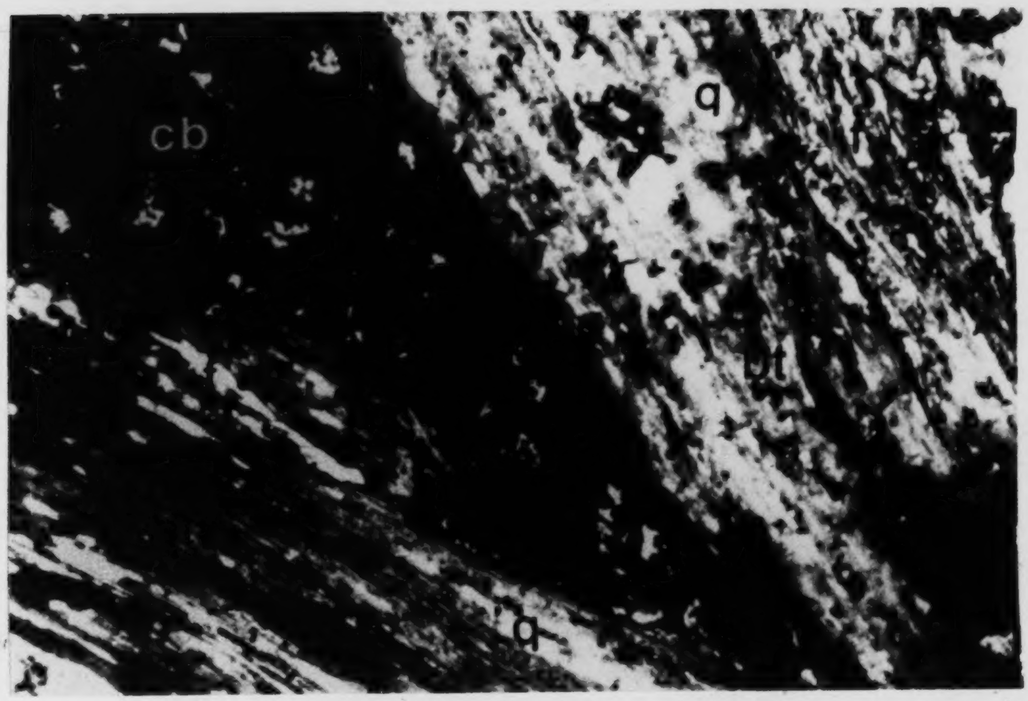
cb
q
bt
q

Plate 2.15a-Fine grained biotite partially replaced by chlorite aggregates. Associated opaque mineral is columbite. *Quartz-biotite(±chlorite)-oxides* unit, Lower Intermediate zone. Plane polarized light. Magnification X240.

Plate 2.15b-*Quartz-thorite* unit of the Upper Intermediate zone. Drill core (right) displays vermiform features typical of quartz-rich samples.

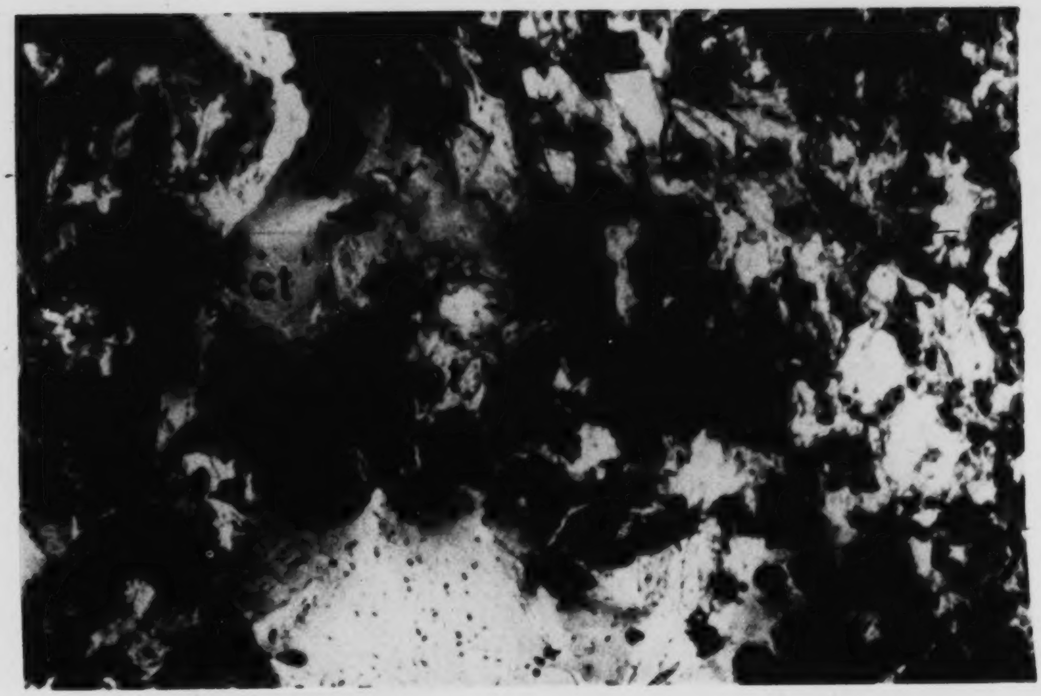
ct

CM

Plate 2.16a-Opaque area is complex intergrowth of thorite, xenotime, synchysite, siderite and fluorite. Host mineral is quartz. Fractures in quartz are filled with ankerite (±siderite) and thorite. *Quartz-thorite* unit, Upper Intermediate zone. Plane polarized light. Magnification X92.

Plate 2.16b-*Quartz-bastnaesite group* unit of the Upper Intermediate zone.

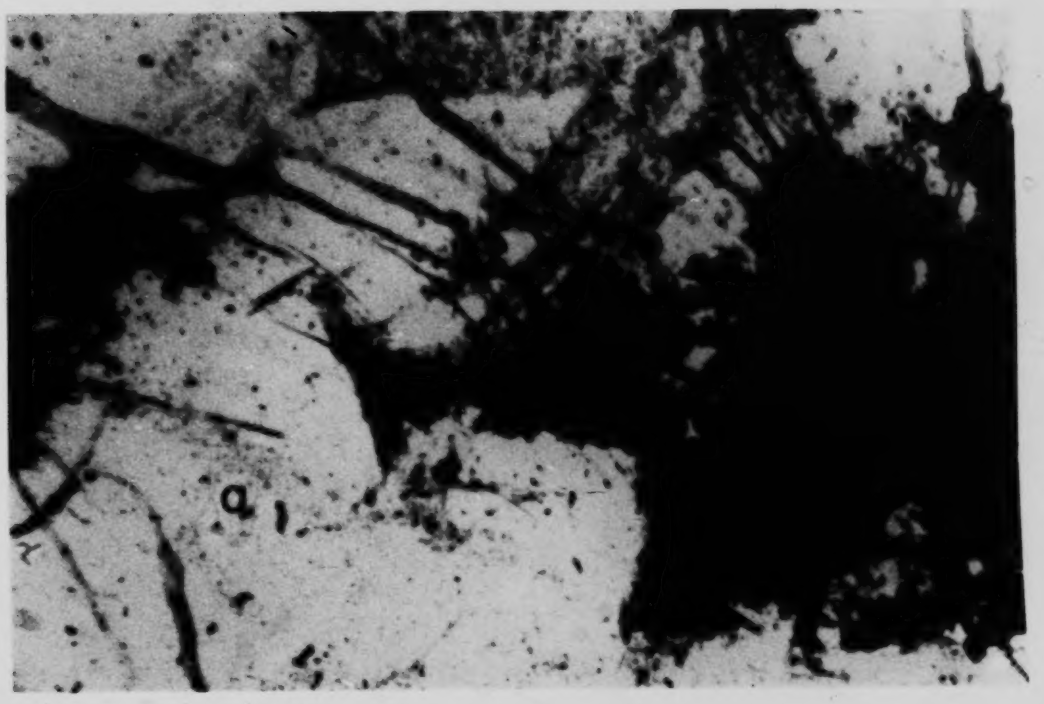
a

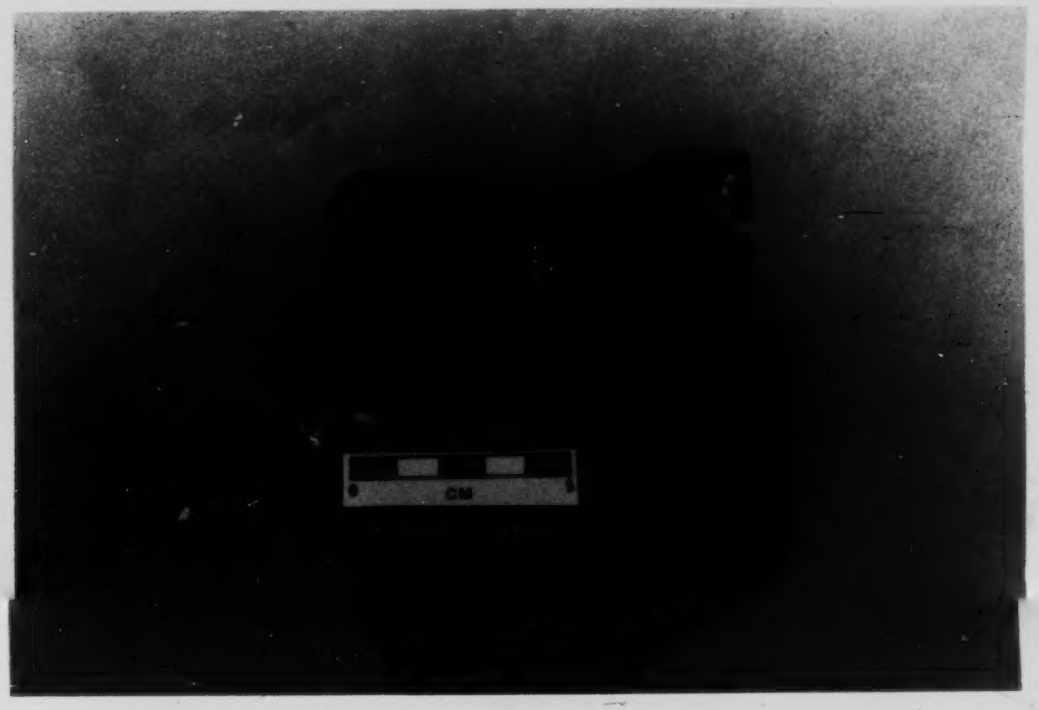
CM

Plate 2.17a-Massive aggregates of acicular LREE-bearing fluocarbonates polycrystals displaying plumose texture. *Quartz-bastnaesite group* unit, Upper Intermediate zone. Plane polarized light. Magnification X92.

Plate 2.17b-Radiating aggregates of tabular LREE-bearing fluocarbonate polcrystals enclosed in quartz with interstitial microcrystalline quartz. *Quartz-bastnaesite group* unit, Upper Intermediate zone. Crossed polars. Magnification X60.

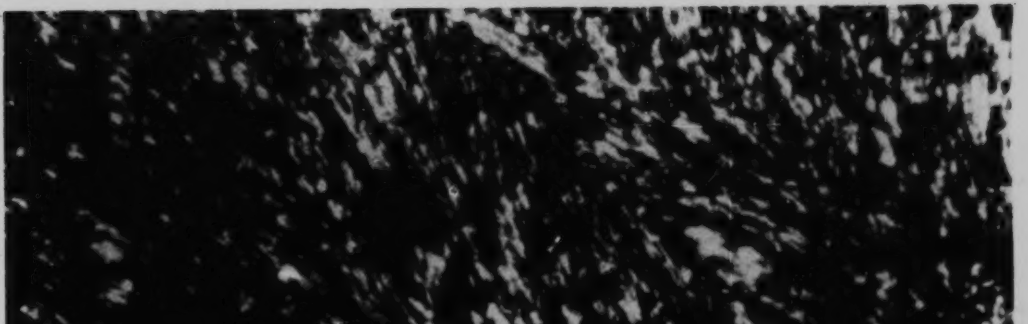

q

Plate 2.18a-Subhedral to euhedral LREE-bearing fluocarbonate polycrystals with interstitial quartz and fluorite. Aggregate of acicular polycrystals in top right corner. *Quartz-bastnaesite group* unit, Upper Intermediate zone. Plane polarized light. Magnification X92.

Plate 2.18b-*Quartz-feldspar-magnetite* unit of the Upper Intermediate zone.

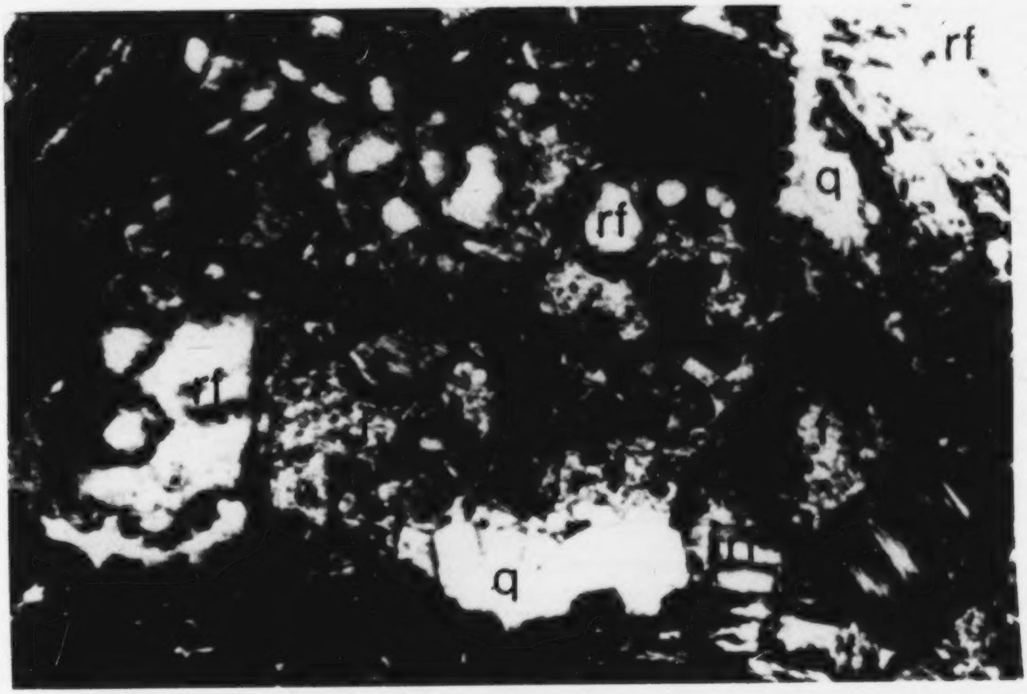
rf
q
rf
rf
q

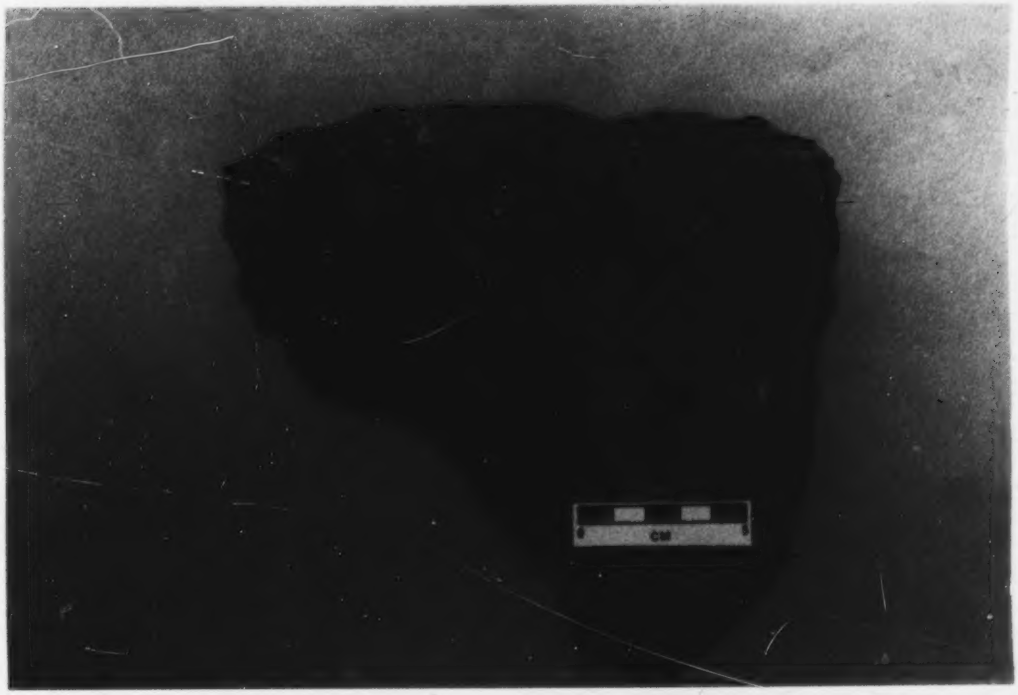
CM

Plate 2.19a-Prismatic acmite grains partially pseudomorphed by hematite. Host mineral is quartz. *Quartz-feldspar-magnetite* unit, Upper Intermediate zone. Crossed polars. Magnification X60.

Plate 2.19b-Radial aggregate of acmite needles partially replaced by hematite. Associated mica is polylithionite. Host mineral is quartz. *Quartz-feldspar-magnetite* unit, Upper Intermediate zone. Crossed polars. Magnification X92.

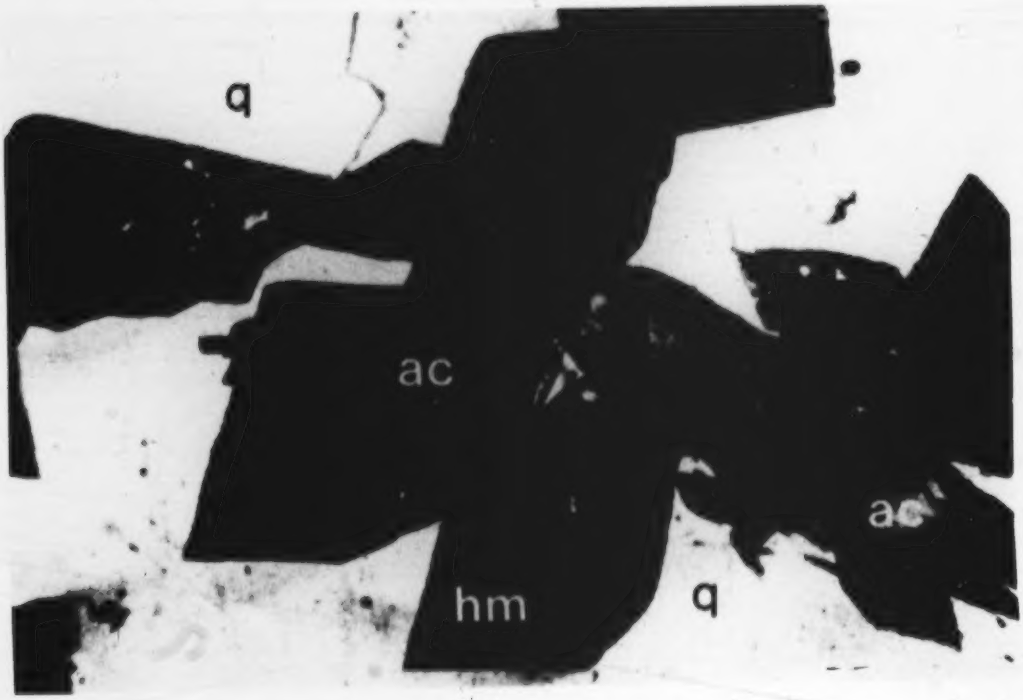
q
ac
ac
hm
q

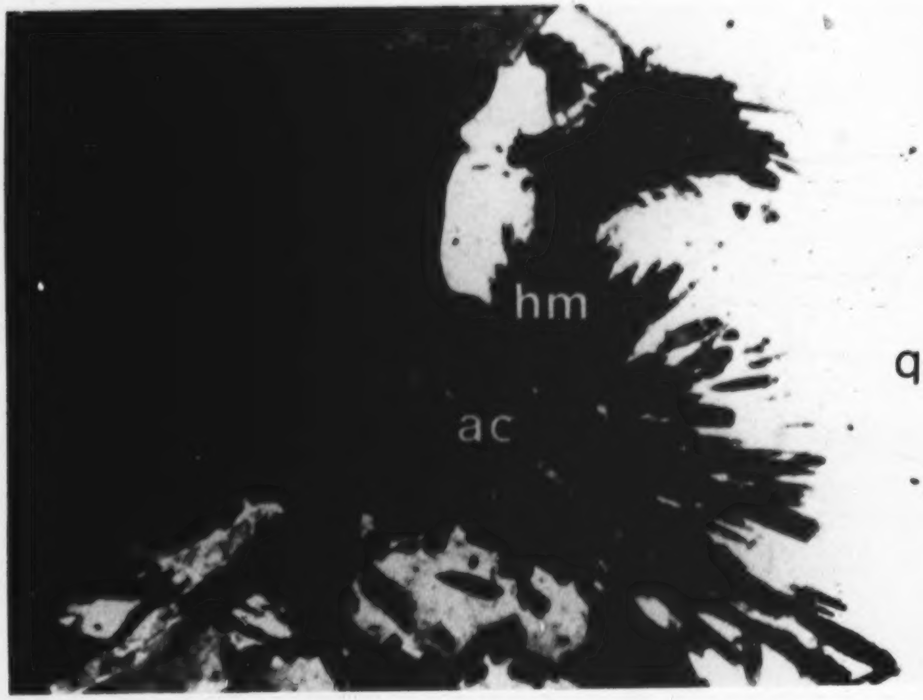
hm
q
ac

Plate 2.20a-Drill core sample of the *quartz-feldspar* unit of the Upper Intermediate zone.

Plate 2.20b-Albite partially replacing K-feldspar . Both feldspars are enclosed in, and partially replaced by, quartz. *Quartz-feldspar* unit, Upper Intermediate zone. Crossed polars. Magnification X92.

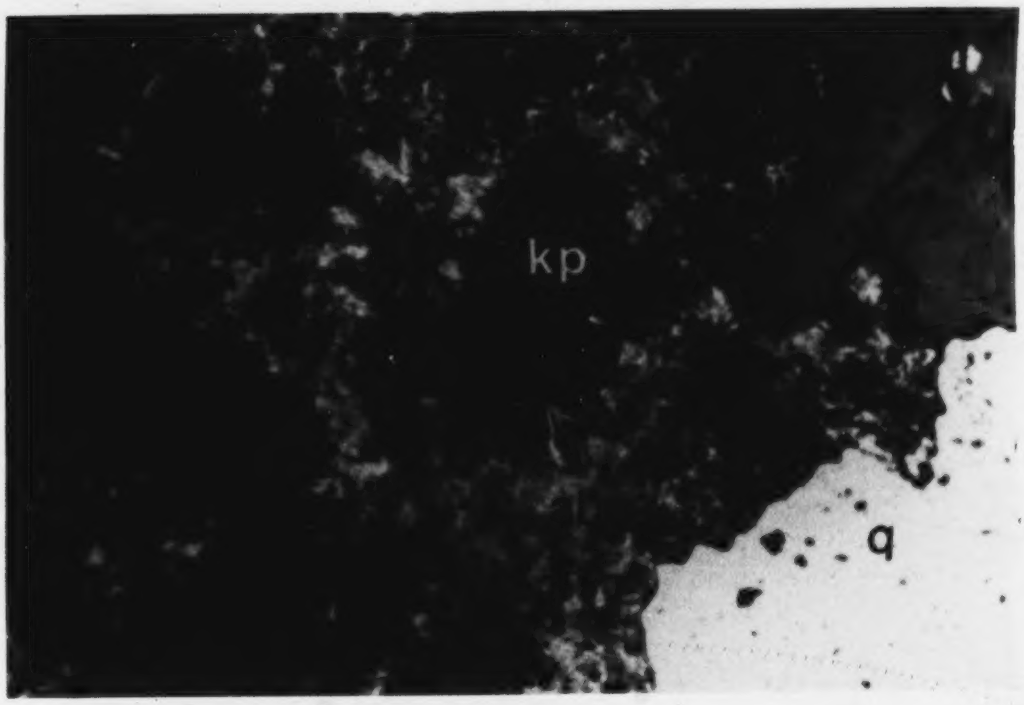
kp
q

Plate 2.21a-Remnant patch of alteration composed of altered albite and K-feldspar with interstitial ankerite and fluorite. All phases partially replaced by host quartz. Note angular boundaries of alteration patch. *Quartz-feldspar* unit, Upper Intermediate zone. Plane polarized light. Magnification X60.

Plate 2.21b-*Quartz-mica-feldspar* unit of the Upper Intermediate zone.

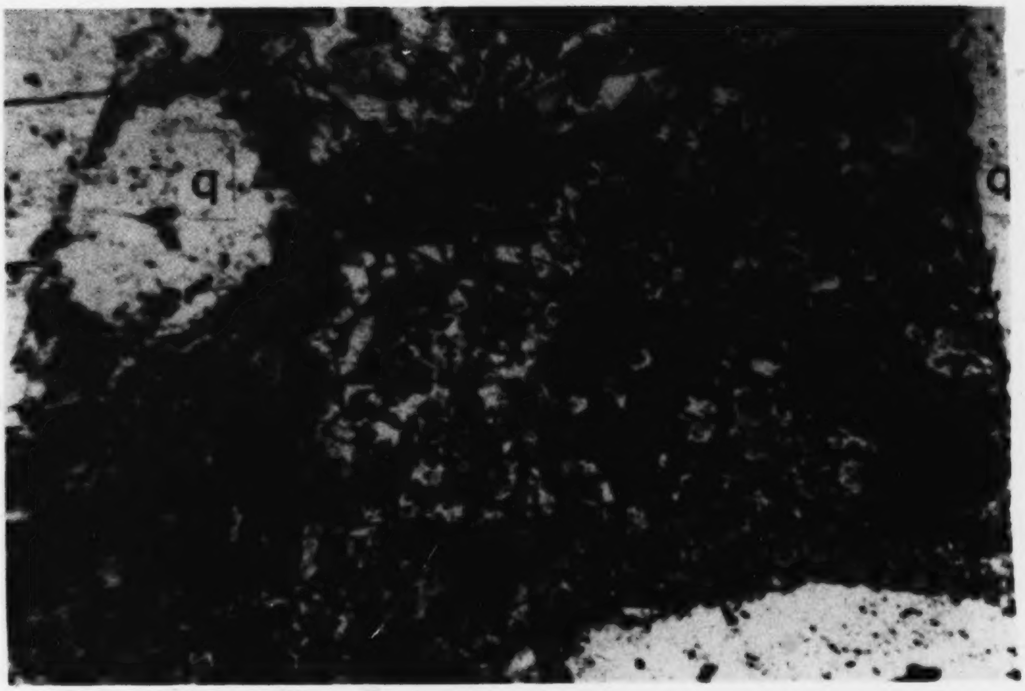
q
q

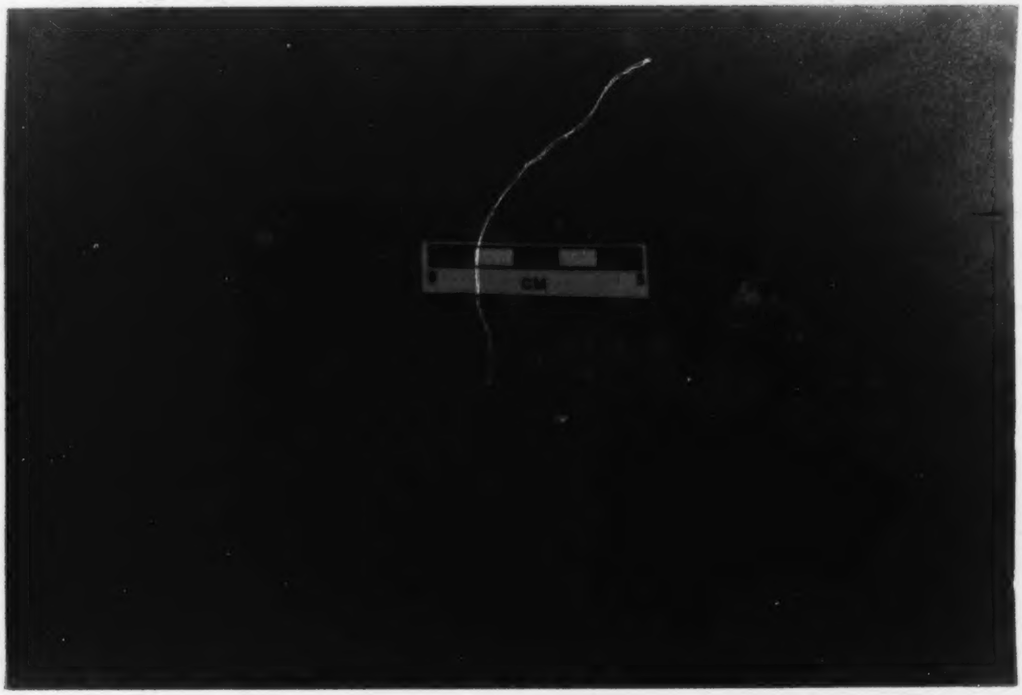
CM

Plate 2.22a-Polylithionite enclosing anhedral relicts of K-feldspar. Quartz surrounds polylithionite and partially replaces the mica at grain boundaries. *Quartz-mica-feldspar* unit, Upper Intermediate zone. Crossed polars. Magnification X60.

Plate 2.22b-*Quartz-mica* unit of the Upper Intermediate zone.

CM

Plate 2.23a-Quartz zone sample showing blocky REE fluocarbonate grains enclosed in massive quartz.

Plate 2.23b-Felsite dyke from the T-zone.

CM

CM

Plate 3.1a-Optically continuous phenakite grains interstitial to quartz. Crossed polars. Magnification X60.

Plate 3.1b-Optically continuous phenakite partially replaced at grain boundaries by microcrystalline quartz aggregates. Crossed polars. Magnification X60.

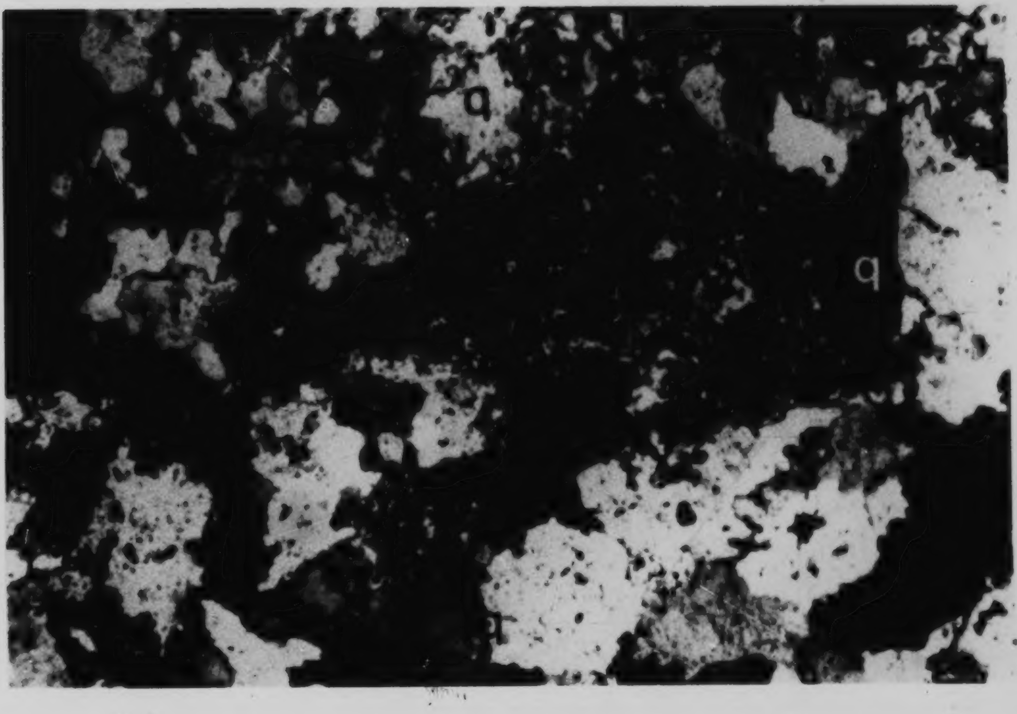
q
q
q

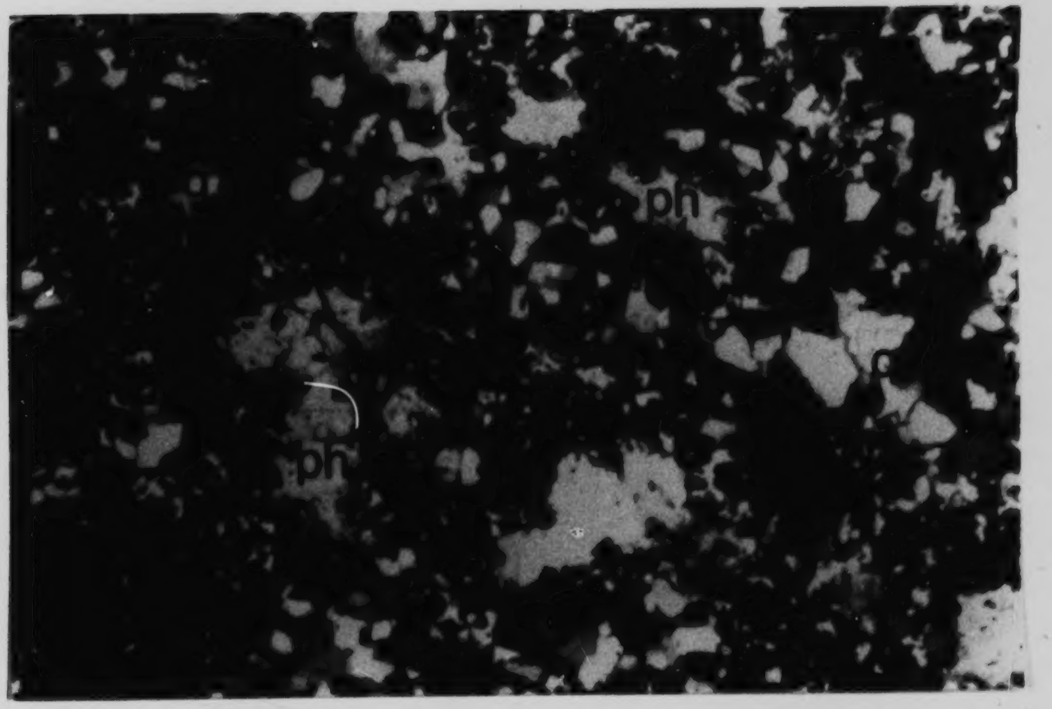
ph
ph

Plate 3.2a-Phenakite (optically discontinuous) grains surrounded by biotite aggregates. Phenakite contains inclusions of quartz and biotite. Crossed polars. Magnification X92.

Plate 3.2b-Subhedral phenakite and associated monazite in ankerite. Crossed polars. Magnification X92.

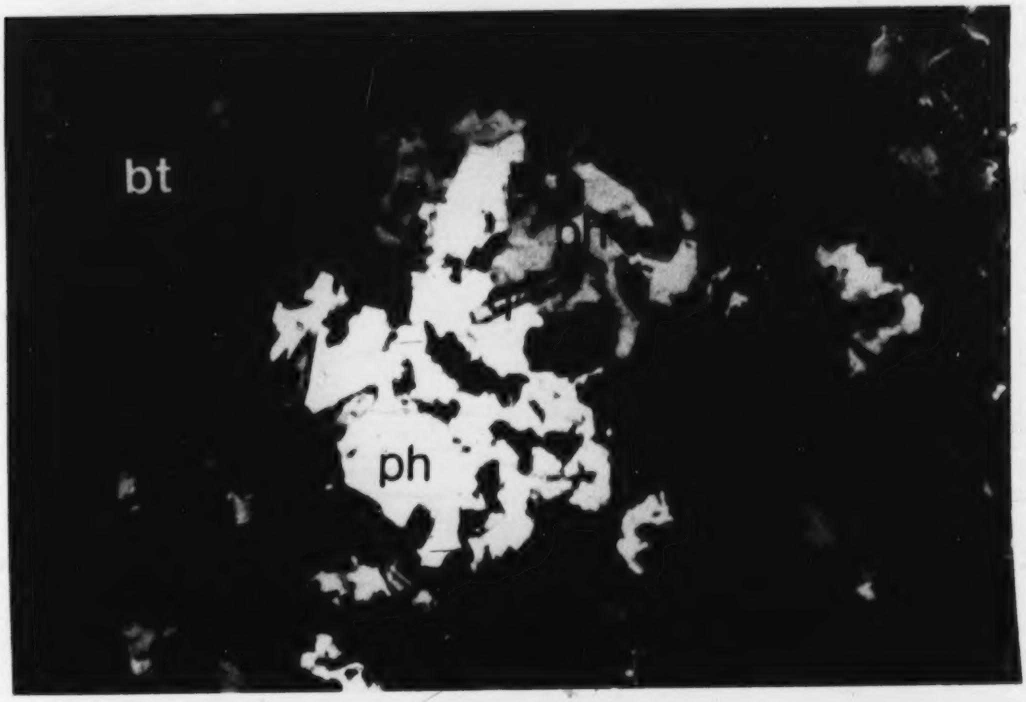
bt
ph
ph

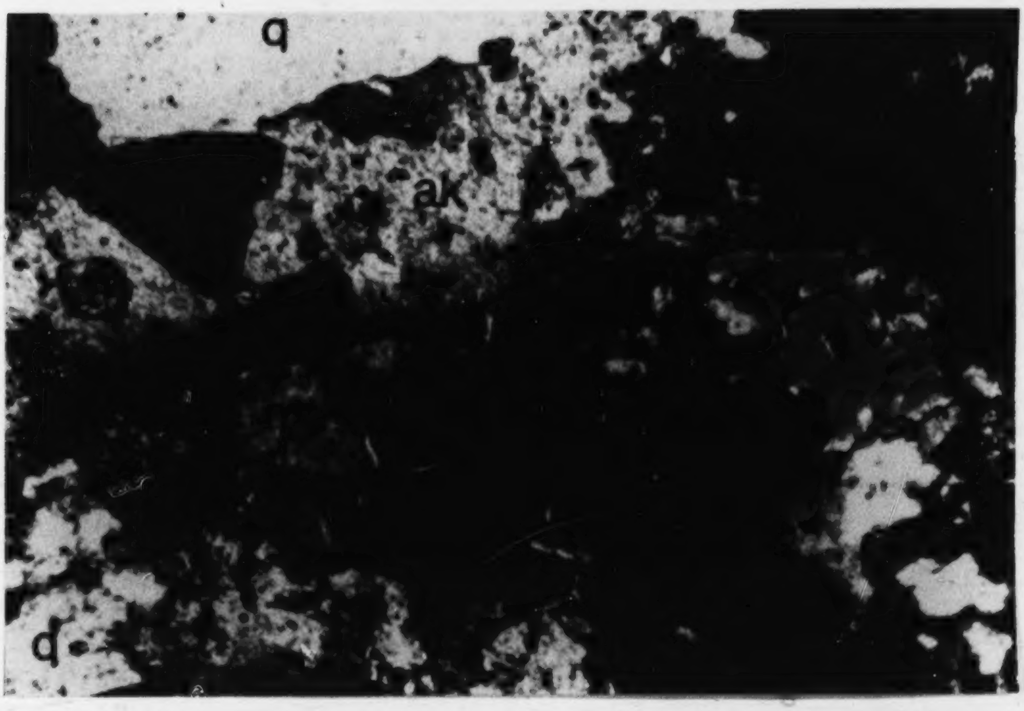
q
ak
q

Plate 3.3a-Bertrandite inclusions in quartz. Crossed polars. Magnification X240.

Plate 3.3b-Backscattered electron image showing euhedral bertrandite inclusions in quartz. Scale bar represents 10 μm.

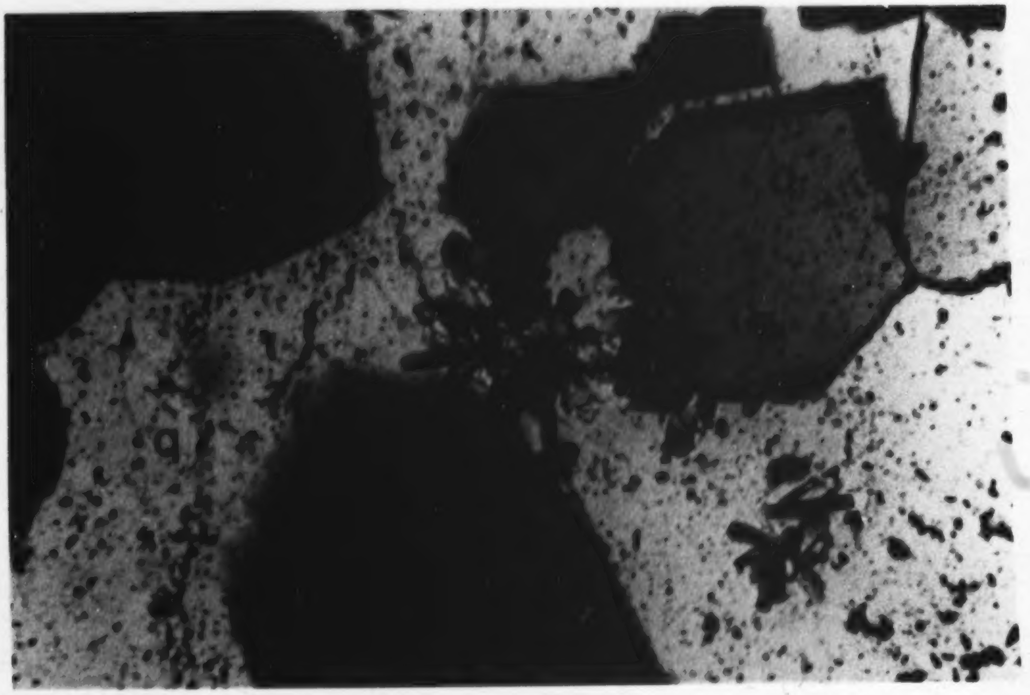
q

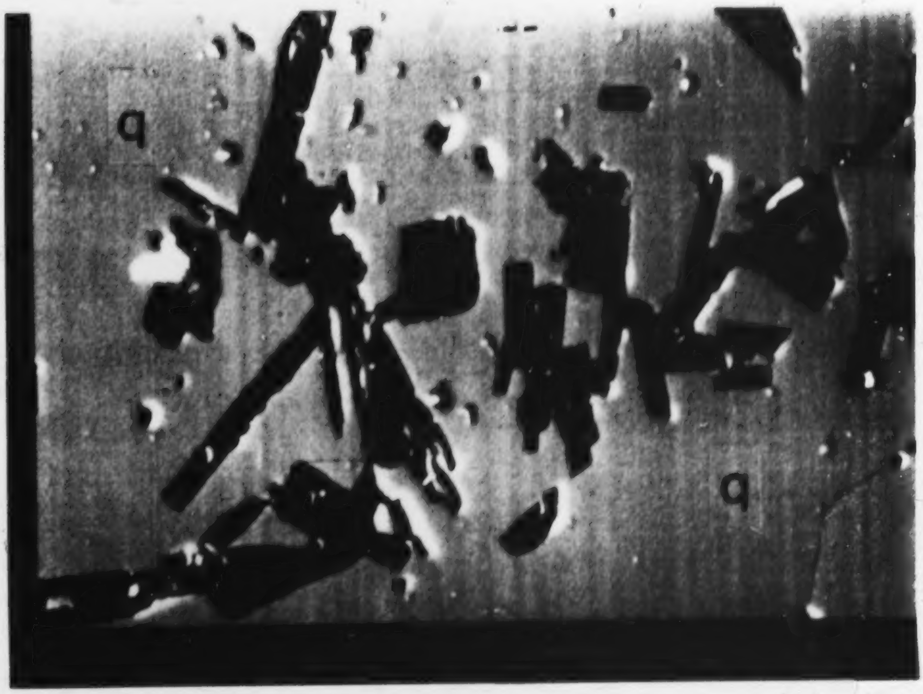
q
q

Plate 3.4a-Backscattered electron image showing member of helvite group as inclusion in phenakite. Scale bar represents 10 μm.

Plate 3.4b-Xenotime inclusions in quartz with associated dark purple fluorite and thorite. Crossed polars. Magnification X240.

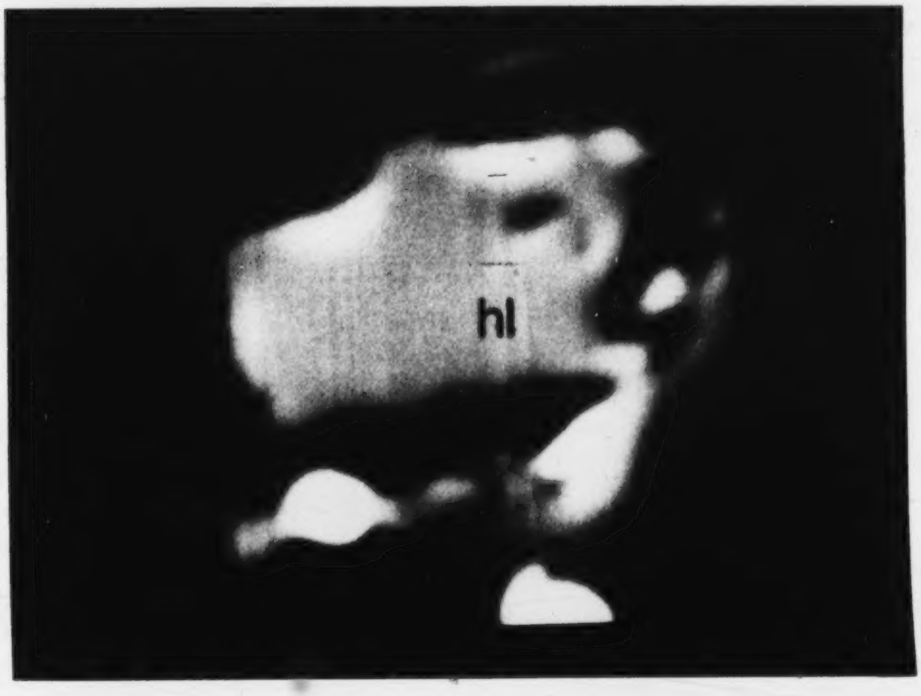
hl

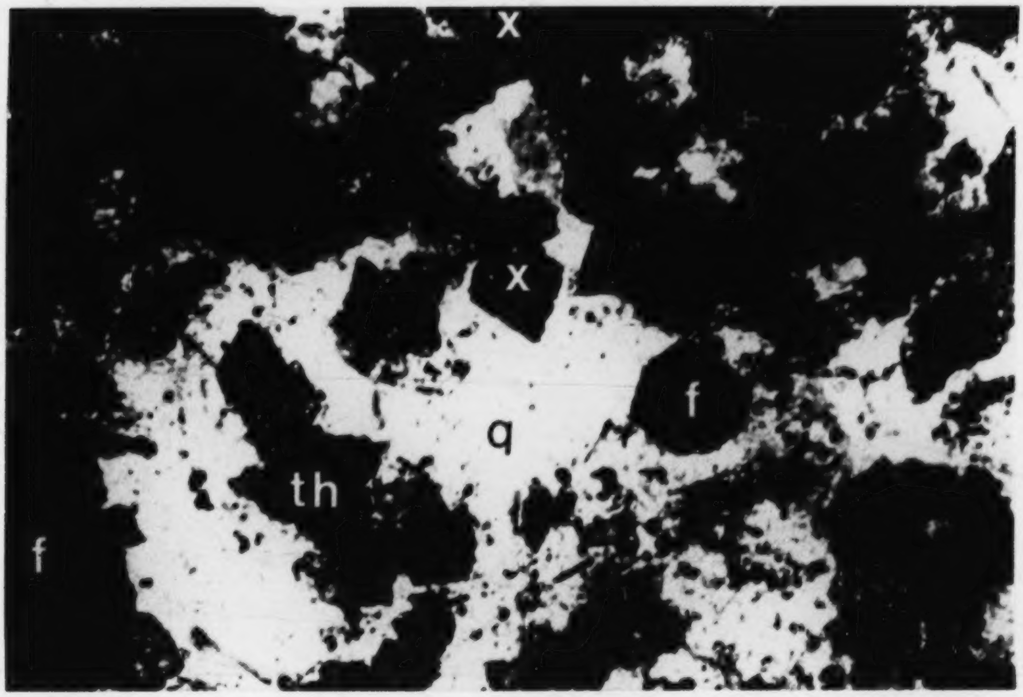
x
x
f
q
th
f

Plate 3.5a-Individual grains and aggregates of opaque xenotime. Host mineral is quartz. White box encloses area shown in Plate 3.5b. Plane polarized light. Magnification X92.

Plate 3.5b-Backscattered electron image showing minute Fe-oxide inclusions in xenotime. Oxide inclusions may cause xenotime to appear opaque as in Plate 3.5a. Scale bar represents 10 μm.

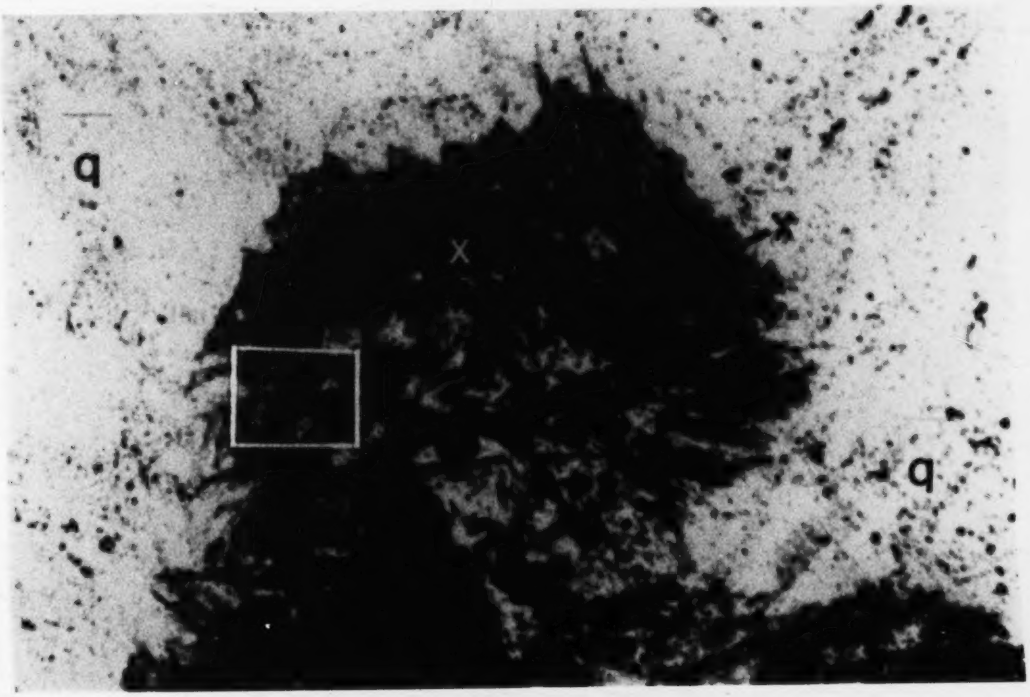
q
x
q

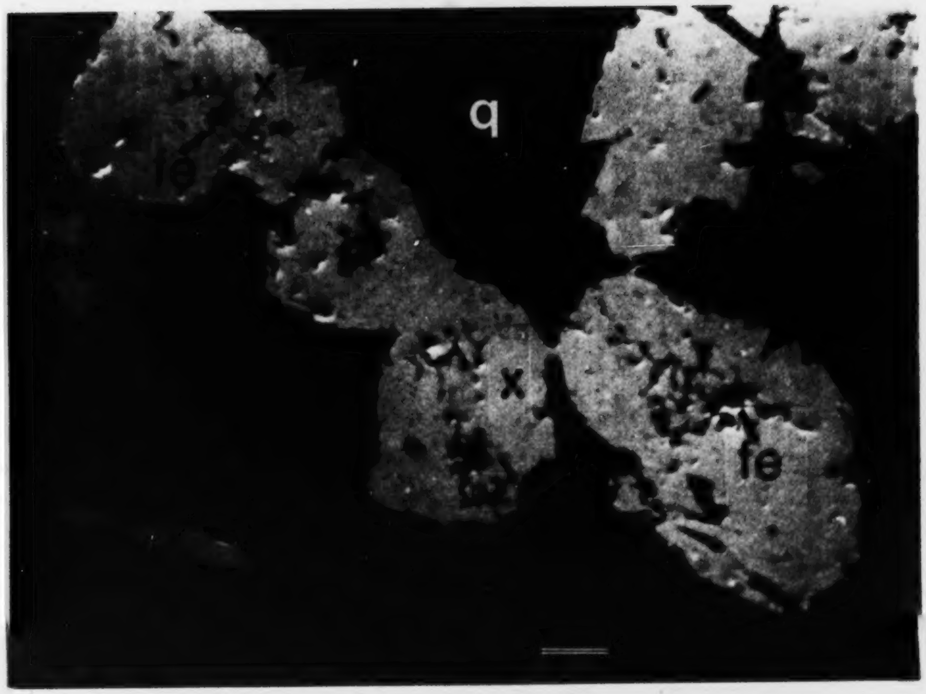
x
fe
q
x
fe

Plate 3.6a-Xenotime-thorite intergrowths enclosed in quartz. Fractures in quartz are filled with thorite. White box encloses area shown in Plate 3.6b. Plane polarized light. Magnification X240.

Plate 3.6b-Backscattered electron image showing nature of xenotime-thorite intergrowth. White spots are burn marks in thorite caused by the electron microprobe. Fractures in quartz are filled with thorite. Scale bar represents 5 μm.

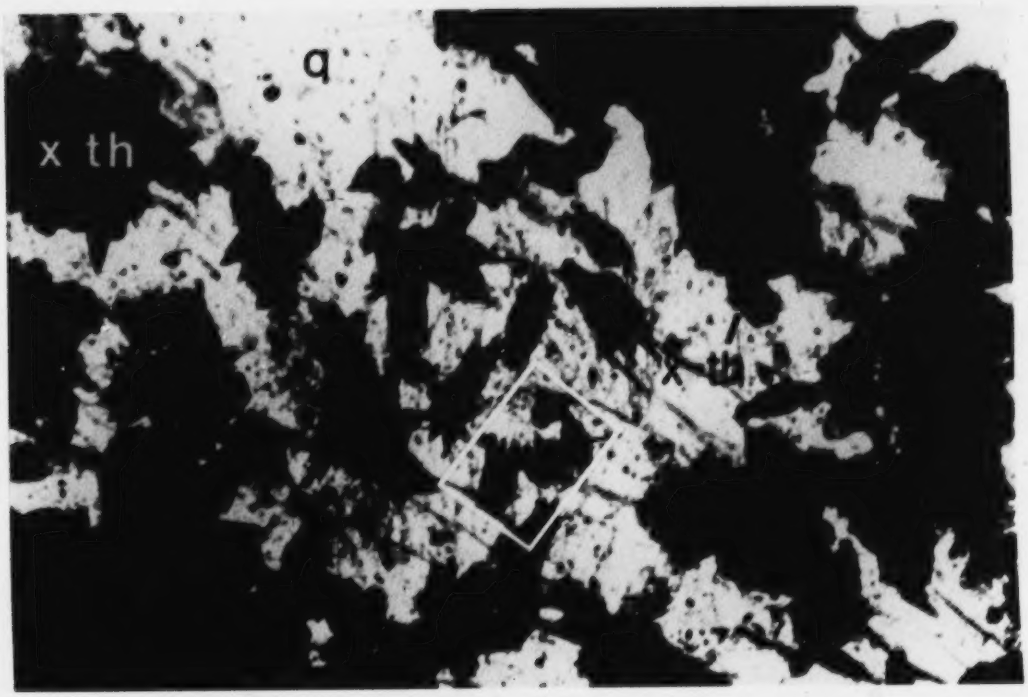
q
x th
x th

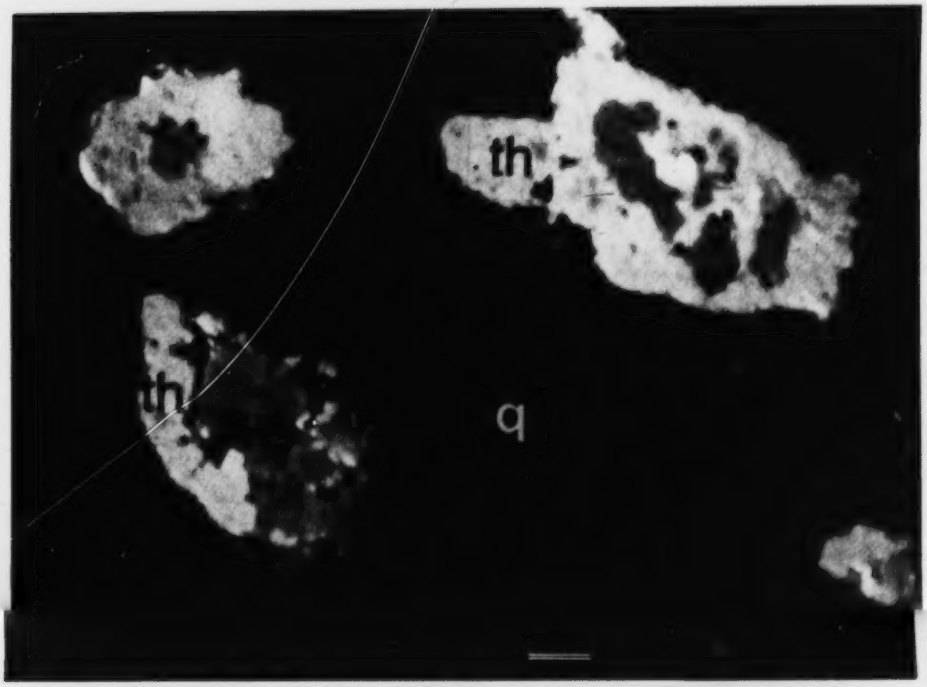
th
th
q

Plate 3.7a-Backscattered electron image showing xenotime and associated thorite enclosed in synchysite. All three minerals are partially replaced by surrounding siderite. Scale bar represents 5 μm.

Plate 3.7b-Backscattered electron image showing partial replacement of xenotime (and thorite) by gadolinite and associated apatite. Monazite appears to cross cut gadolinite. Fluorite occurs as a late phase interstitial to other minerals. Scale bar represents 10 μm.

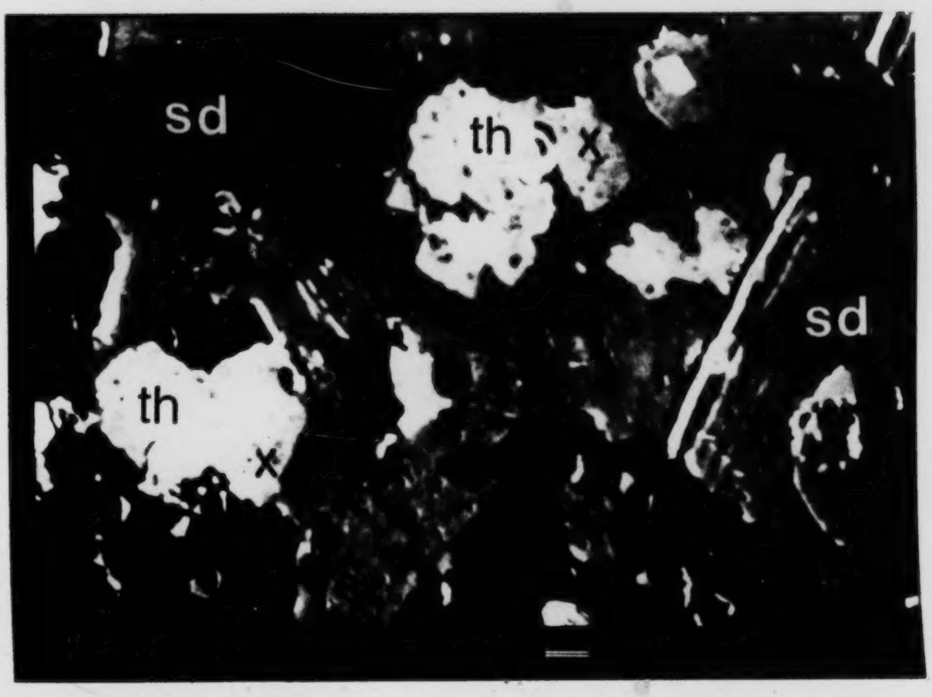
sd
th
x
sd
th
x

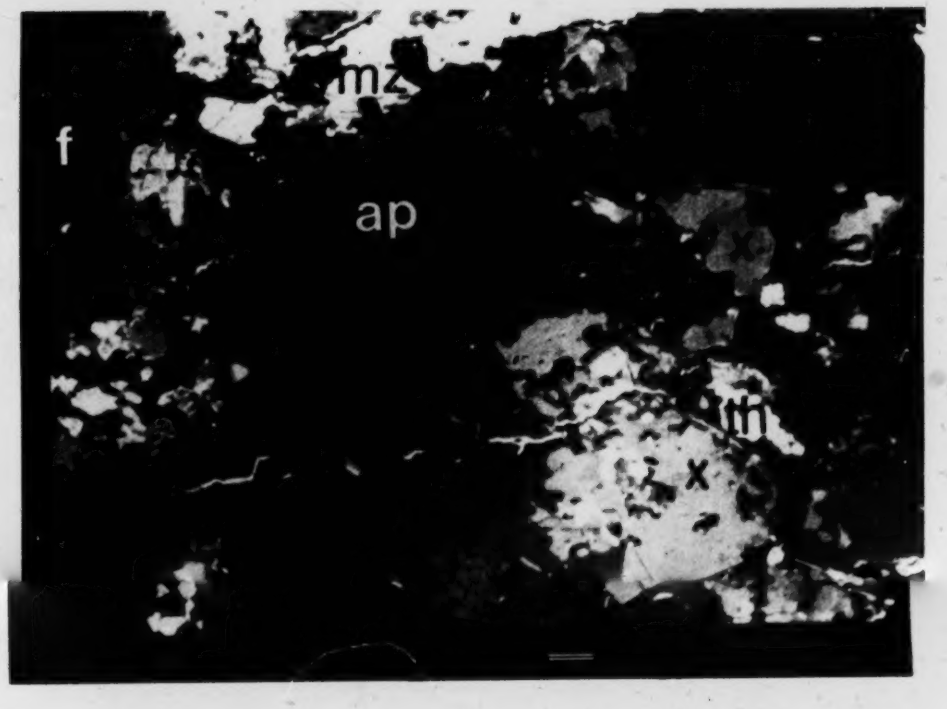
mz
f
ap
x
th
x

Plate 3.8a-Xenotime grains with zircon overgrowths and associated monazite. Host mineral is quartz. White box encloses area shown in Plate 3.8b. Crossed polars. Magnification X368.

Plate 3.8b-Backscattered electron image showing zircon overgrowths on corroded ovoids of xenotime. Associated monazite appears to cross-cut xenotime and zircon. Scale bar represents 2 μm.

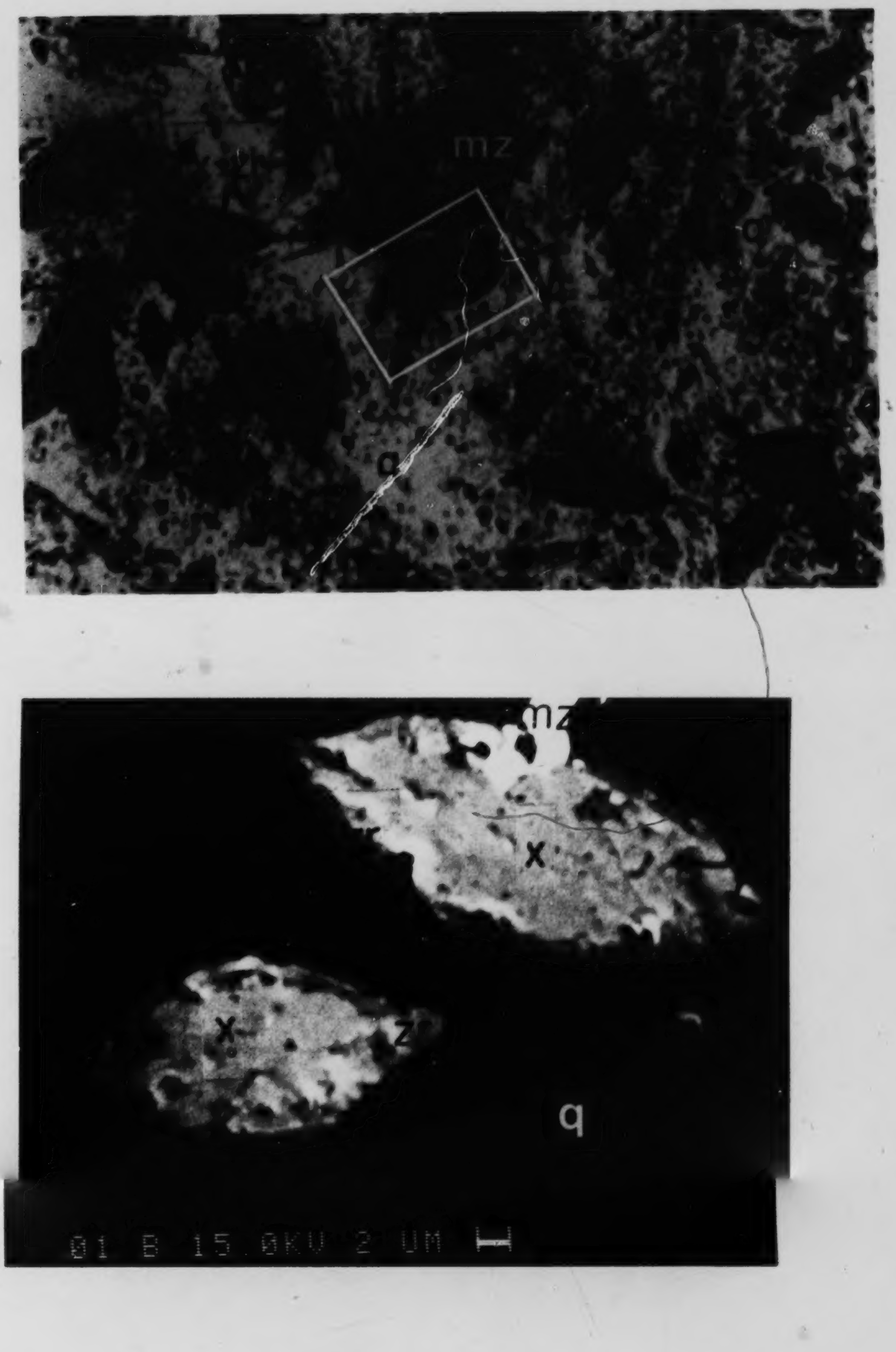
mz
q
mz
x
x
z
q
01 B 15.0KV 2 UM

Plate 3.9a-Gadolinite with interstitial fluorite. Associated monazite and thorite also shown. Plane polarized light. Magnification X368.

Plate 3.9b-Gadolinite and apatite with interstitial fluorite. Crossed polars. Magnification X200.

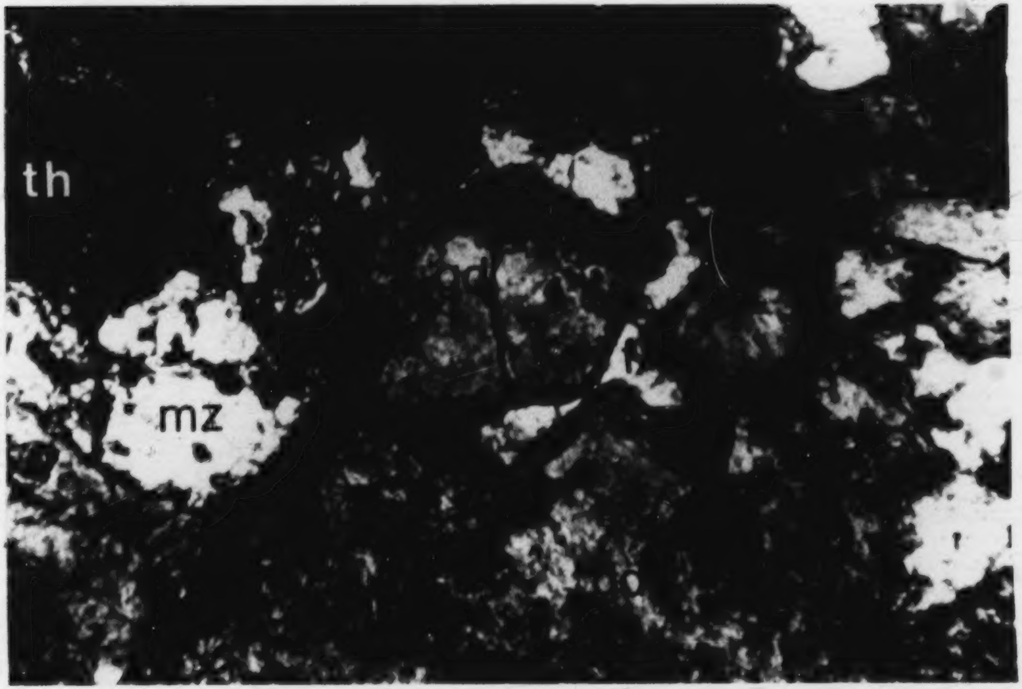
th
gd
mz

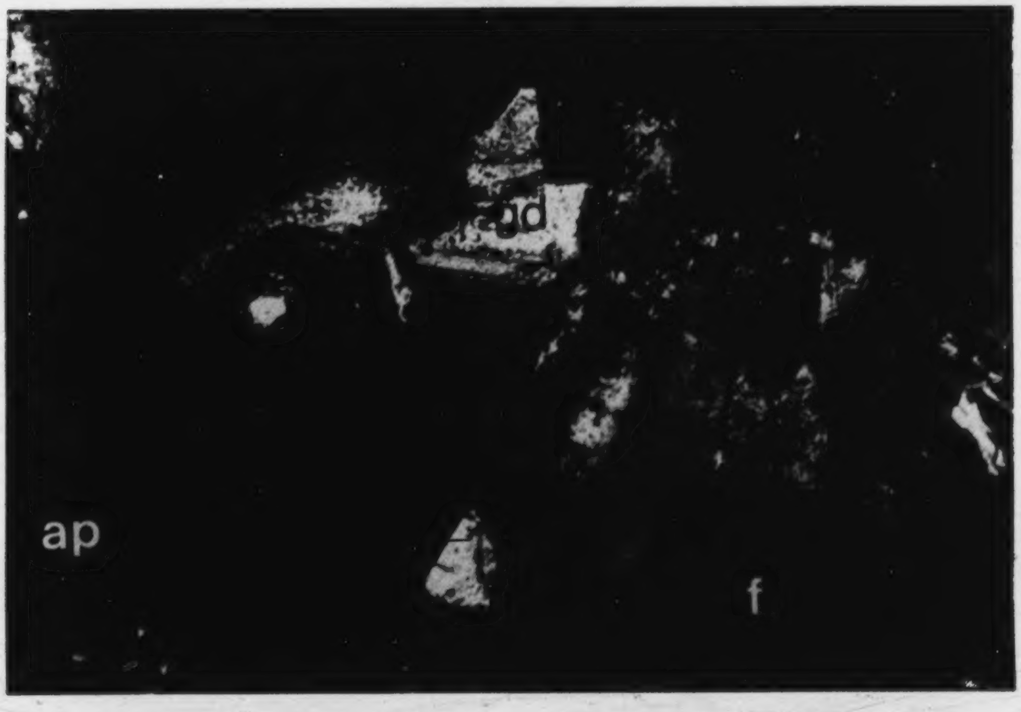
gd
ap
f

Plate 3.10a-Thorite aggregates in biotite. Biotite occurs interstitial to albite. White box enclosed area shown in Plate 3.10b. Plane polarized light. Magnification X92.

Plate 3.10b-Backscattered electron image showing thorite aggregates. White spots are burn marks caused by the electron microprobe. Note compositional inhomogeneity in thorite. Scale bar represents 5 μm.

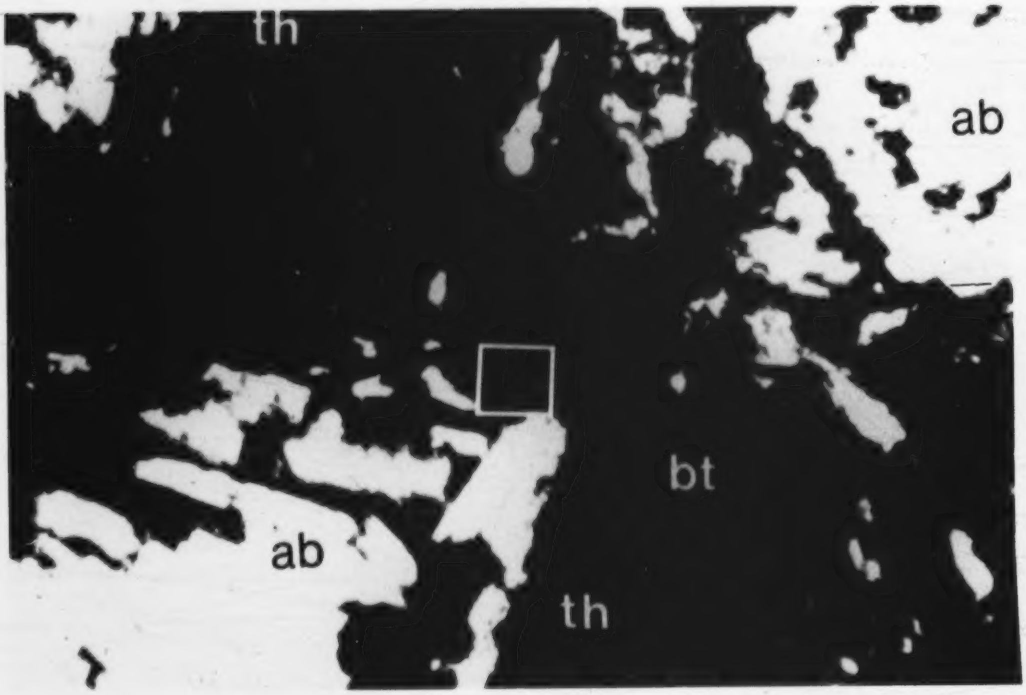
th
ab
bt
ab
th

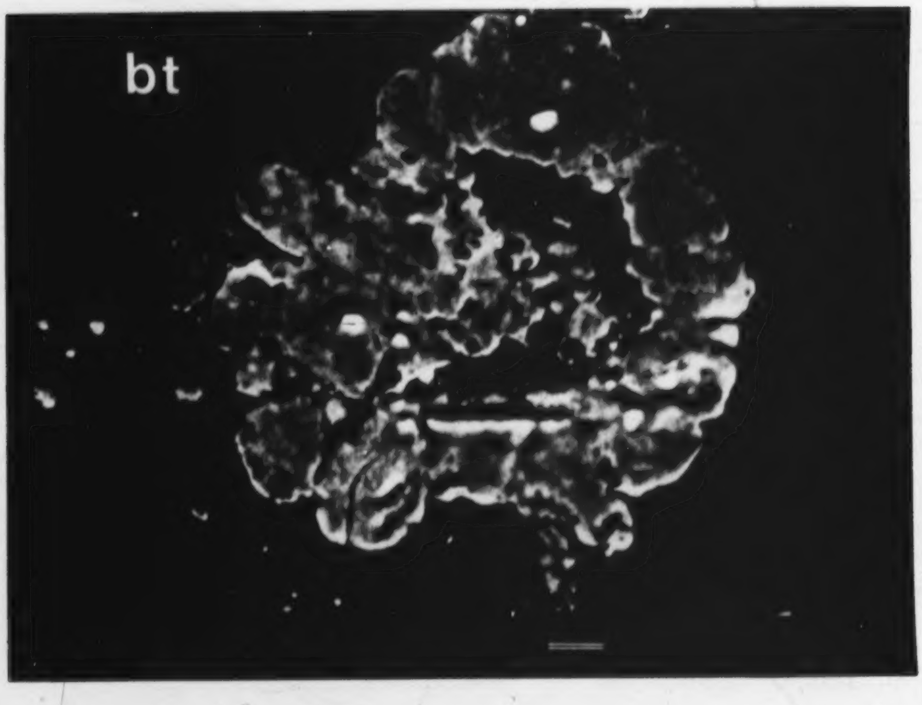
bt

Plate 3.11a-Radiating aggregates of acicular LREE-bearing fluocarbonate polycrystals in quartz. White box encloses area shown in Plate 3.11b. Crossed polars. Magnification X92.

Plate 3.11b-Backscattered electron images showing syntaxic intergrowth of bastnaesite and parisite in acicular polycrystals. Scale bar represents 20 μm.

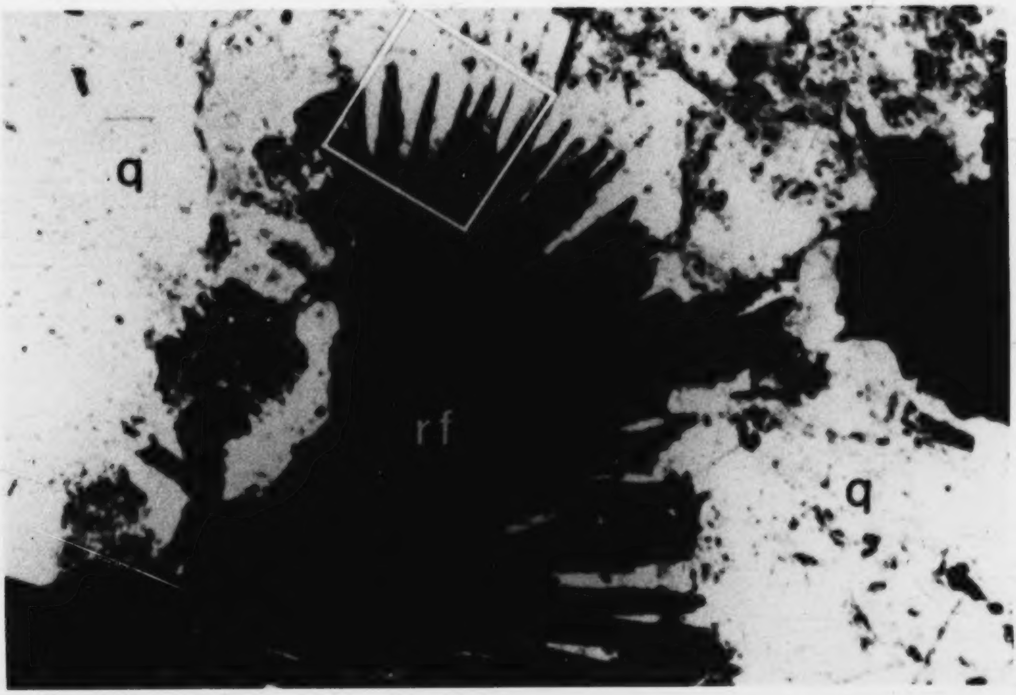
q
rf
q

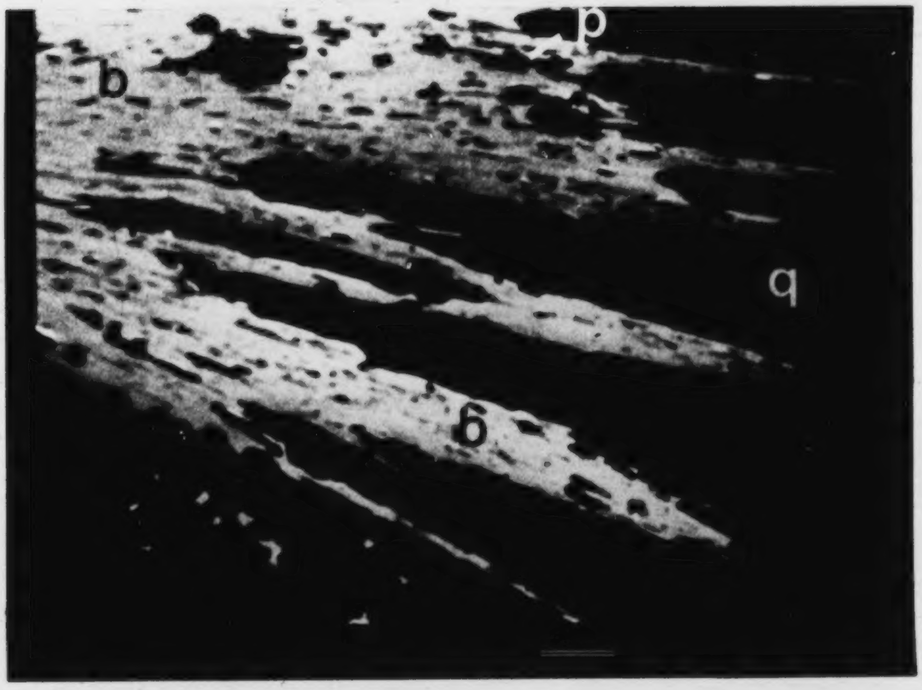
p
b
q
b

Plate 3.12a-Subhedral LREE-bearing fluocarbonate polycrystals in ankerite. Black spots in ankerite are holes. White box encloses are shown in Plate 3.12b. Plane polarized light. Magnification X240.

Plate 3.12b-Backscattered electron image showing syntaxic intergrowth of parisite, roentgenite and bastnaesite in a subhedral polycrystal. Scale bar represents 10 μm.

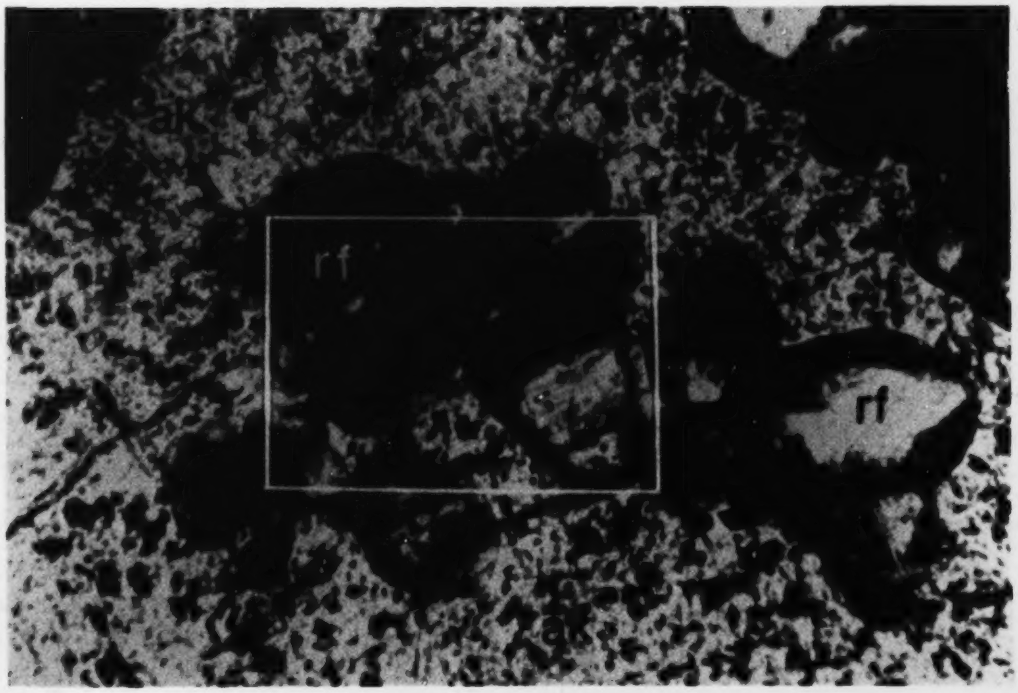
ak
rf
rf
ak

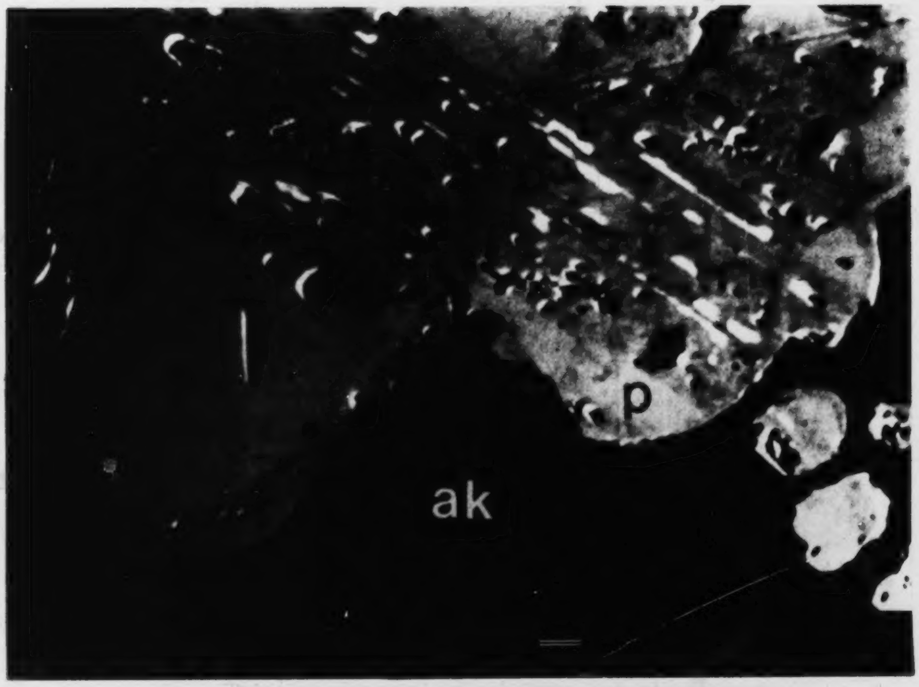
p
ak

Plate 3.13a-LREE-bearing fluocarbonate polycrystal showing lamellae-like intergrowth of different phases. White box encloses area shown in Plate 3.13b. Crossed polars. Magnification X240.

Plate 3.13b-Backscattered electron image showing lamellae-like syntaxic intergrowth of roentgenite, bastnaesite and parisite. Scale bar represents 20 μm.

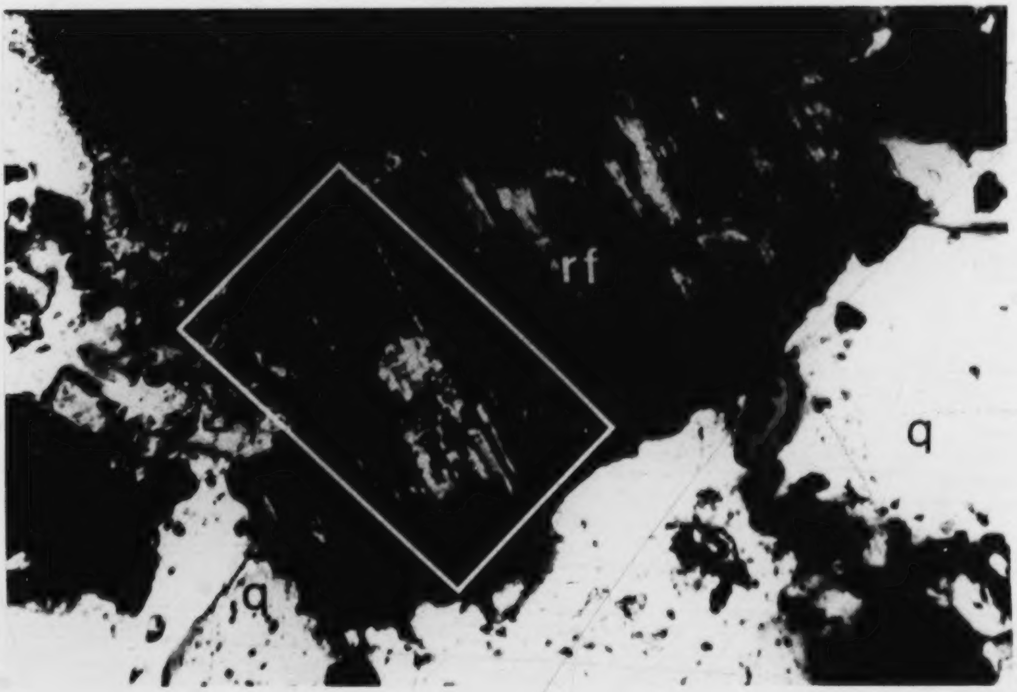
rf
q
q

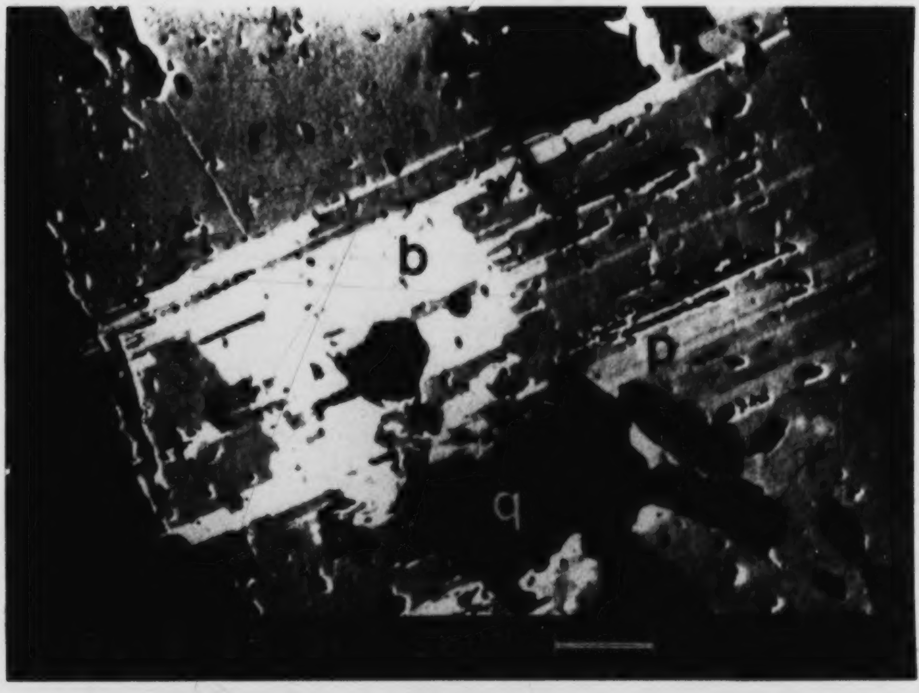
b
p
q

Plate 3.14a-LREE-bearing fluocarbonate polycrystal partially replaced by K-feldspar and ankerite. Associated monazite enclosed in ankerite. White box encloses area shown in Plate 3.14b. Crossed polars. Magnification X240.

Plate 3.14b-Backscattered electron image showing syntaxic intergrowth of bastnaesite and parisite in partially replaced polycrystal. Scale bar represents 20 μm.

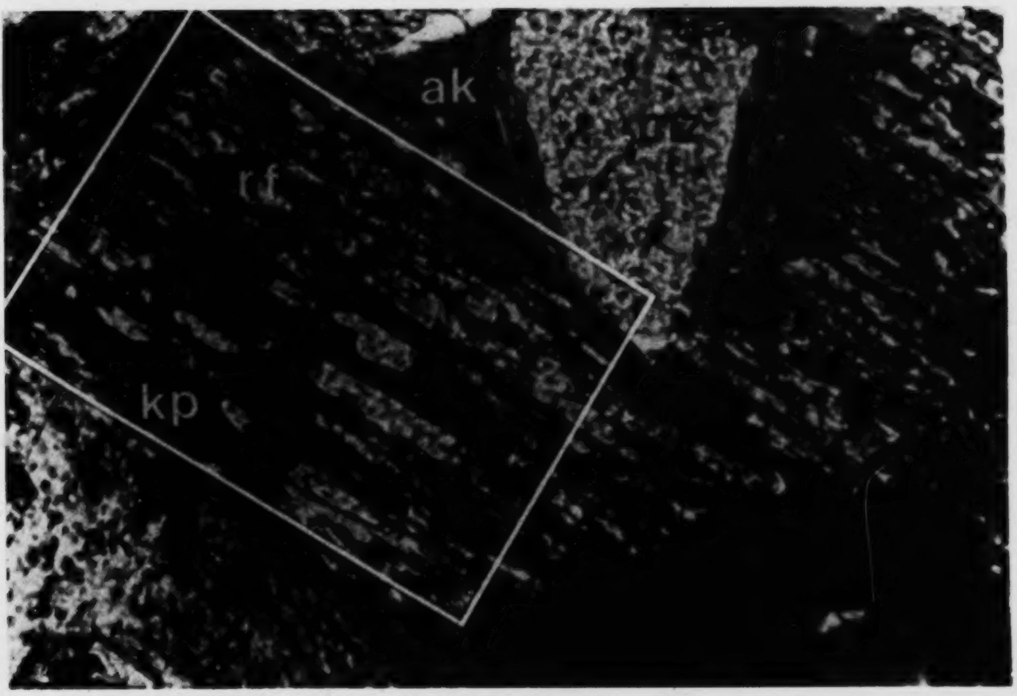
ak
rf
kp

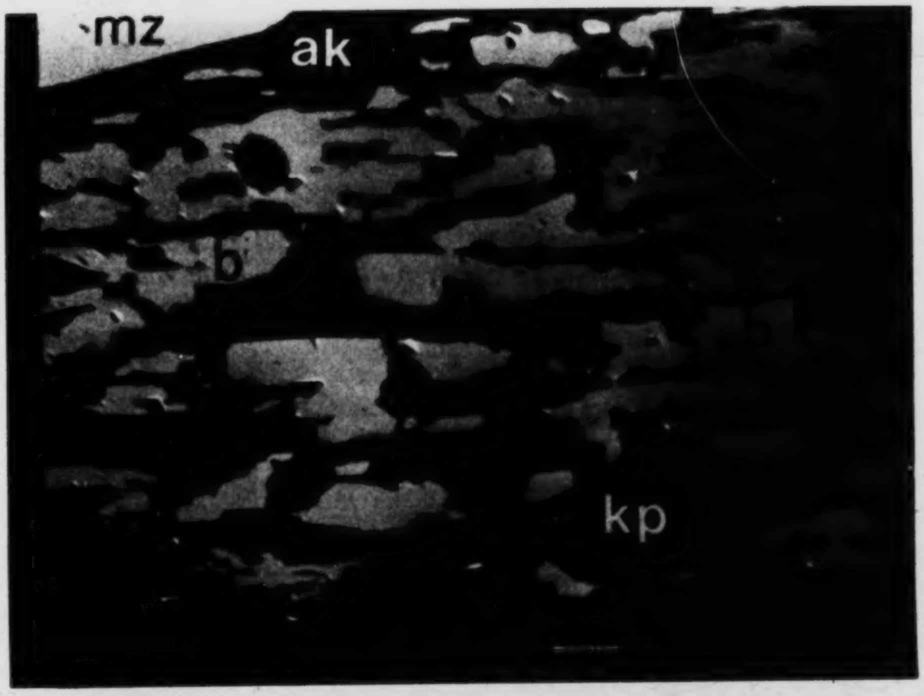
mz
ak
b
kp

Plate 3.15a-Backscattered electron image showing syntaxic intergrowth of bastnaesite and parisite in tabular polycrystals. Note lamellae-like intergrowth appears to run parallel to long axis of tabular grains. Scale bar represents 20 μm.

Plate 3.15b-Subhedral monazite grains enclosed in ankerite. Quartz appear to partially replace monazite and ankerite. Opaque inclusions in ankerite are thorite intergrowths with chlorite. Crossed polars. Magnification X92.

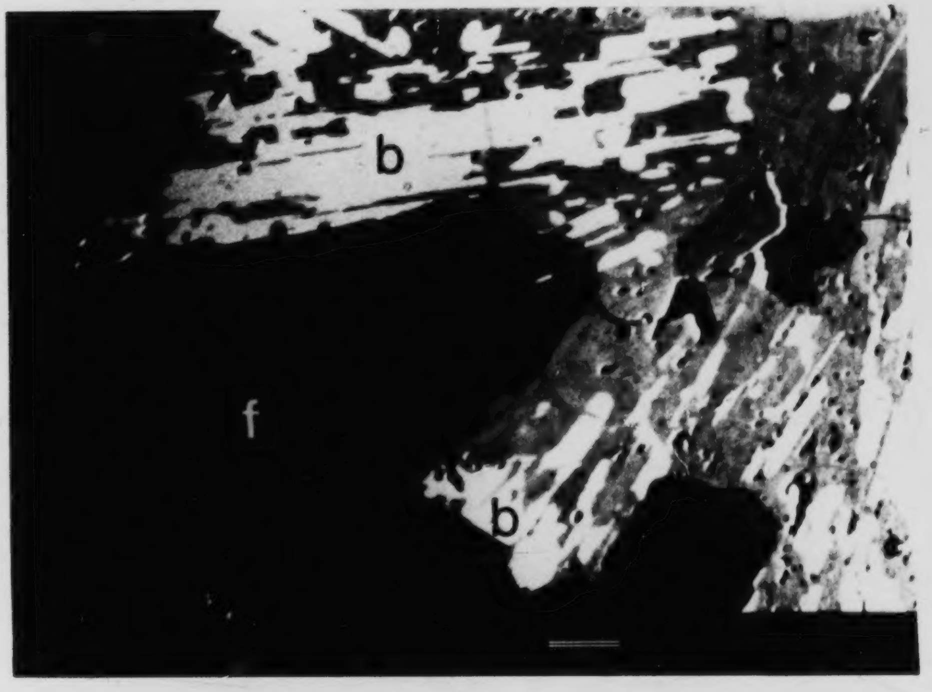
p
b
f
b

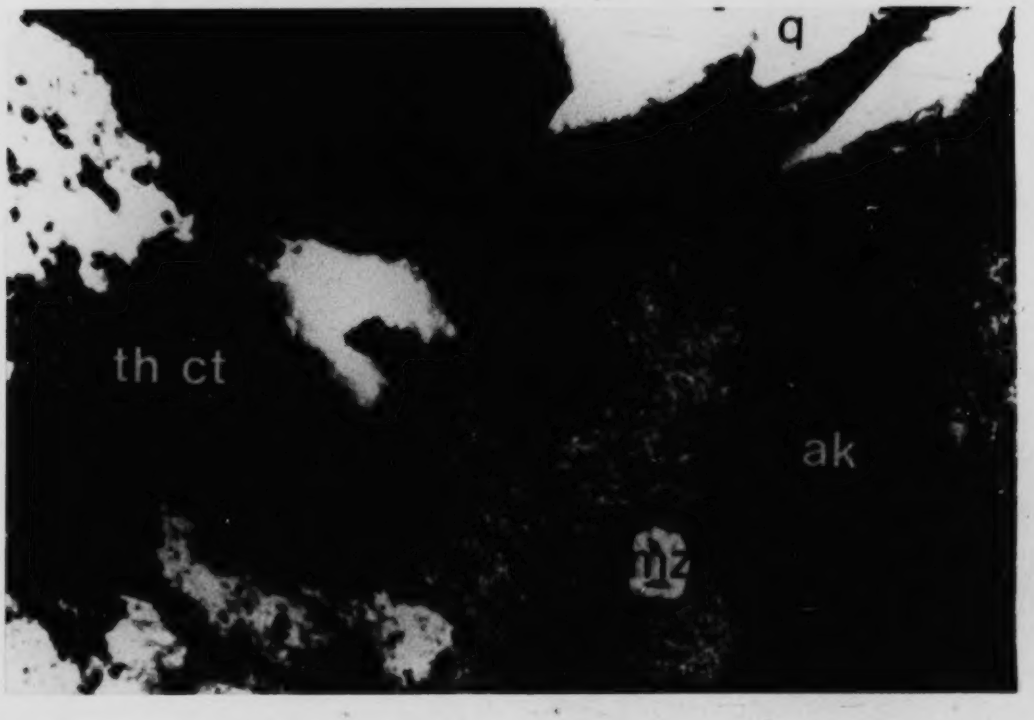
q
th ct
ak
mz

Plate 3.16a-Britholite intergrown with parisite, monazite and chlorite. Host mineral is quartz with associated purple fluorite. White box encloses area shown in Plate 3.16b. Plane polarized light. Magnification X92.

Plate 3.16b-Backscattered electron image of britholite, parisite, monazite and chlorite intergrowth in quartz. Note altered, inhomogeneous appearance of parisite. Scale bar represents 20 μm.

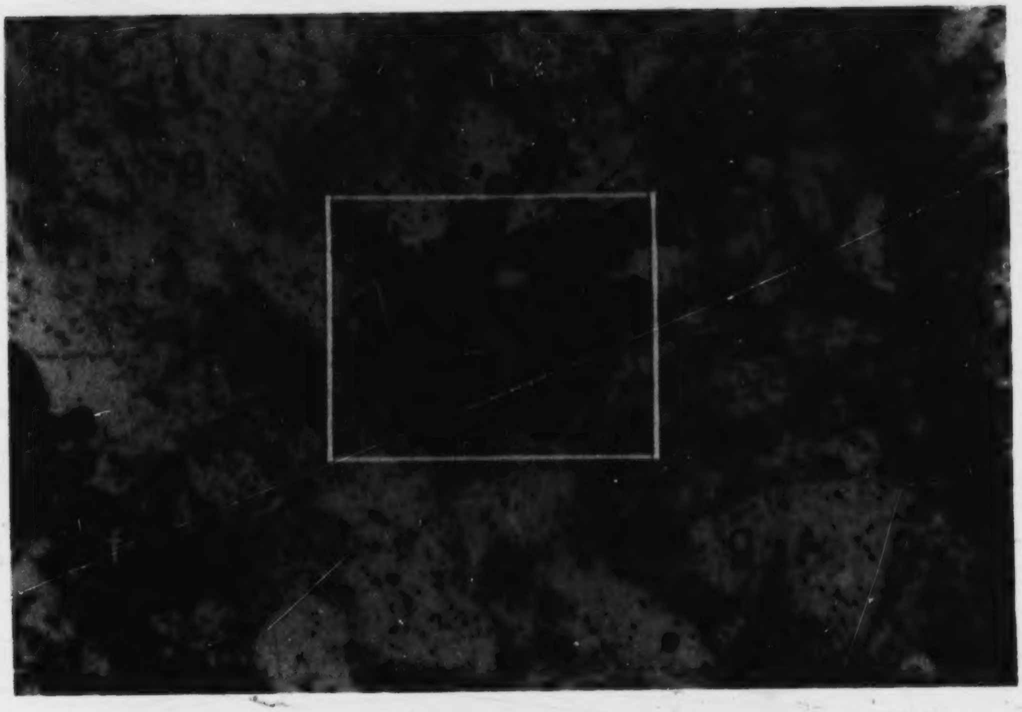
f
q

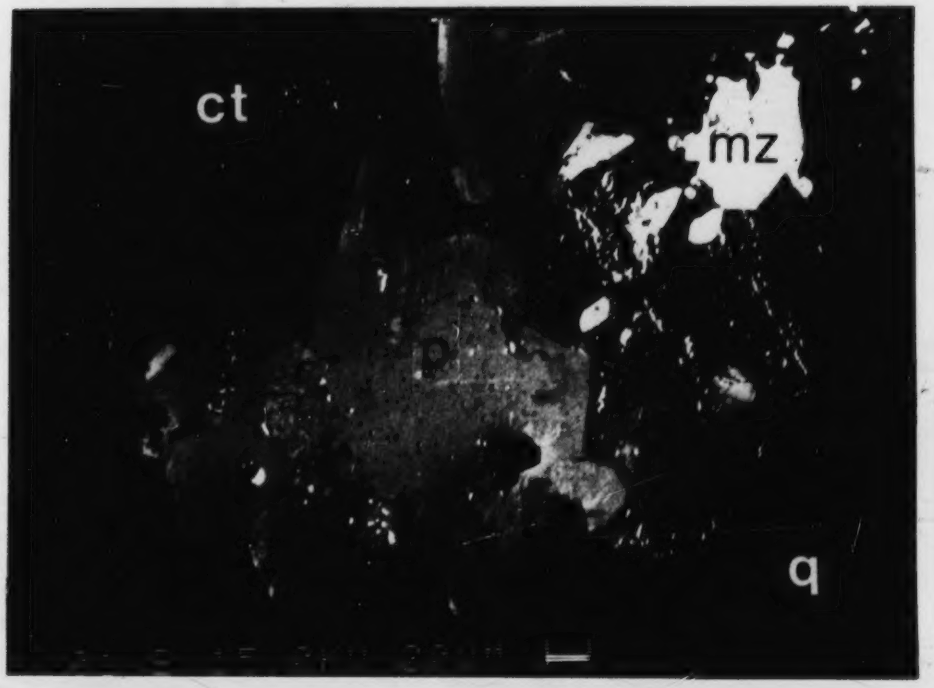
ct
mz
p
q

Plate 3.17a-Columbite aggregates included in quartz and replacing lath-like biotite. Note difference in relief between associated quartz and phenakite. Plane polarized light. Magnification X92.

Plate 3.17b-Backscattered electron image showing columbite with anhedral inclusions of bastnaesite and ashanite. White spots in ashanite are burn marks caused by the electron microprobe. Host mineral is quartz. Scale bar represents 5 μm.

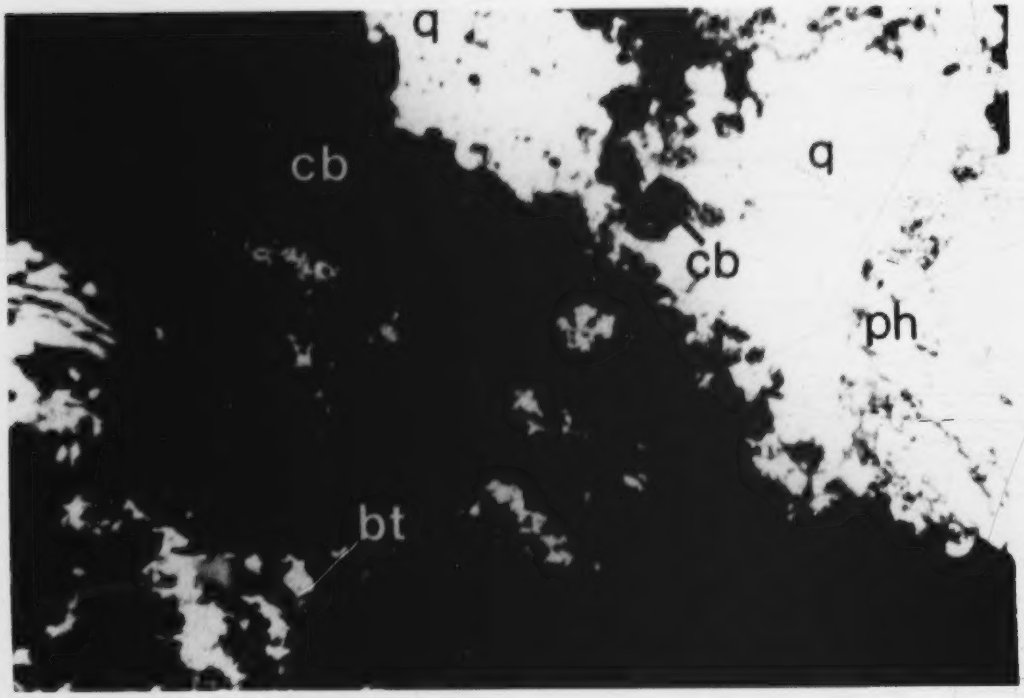
q
cb
q
cb
ph
bt

q
b
b

Plate 3.18a-Bipyramidal zircons forming skeletal outline of unidentified preexisting mineral. Host mineral is quartz with associated altered K-feldspar and fluorite. Crossed polars. Magnification X92.

Plate 3.18b-Zonally metamictized zircons with interstitial biotite and columbite. Crossed polars. Magnification X240.

zr
f

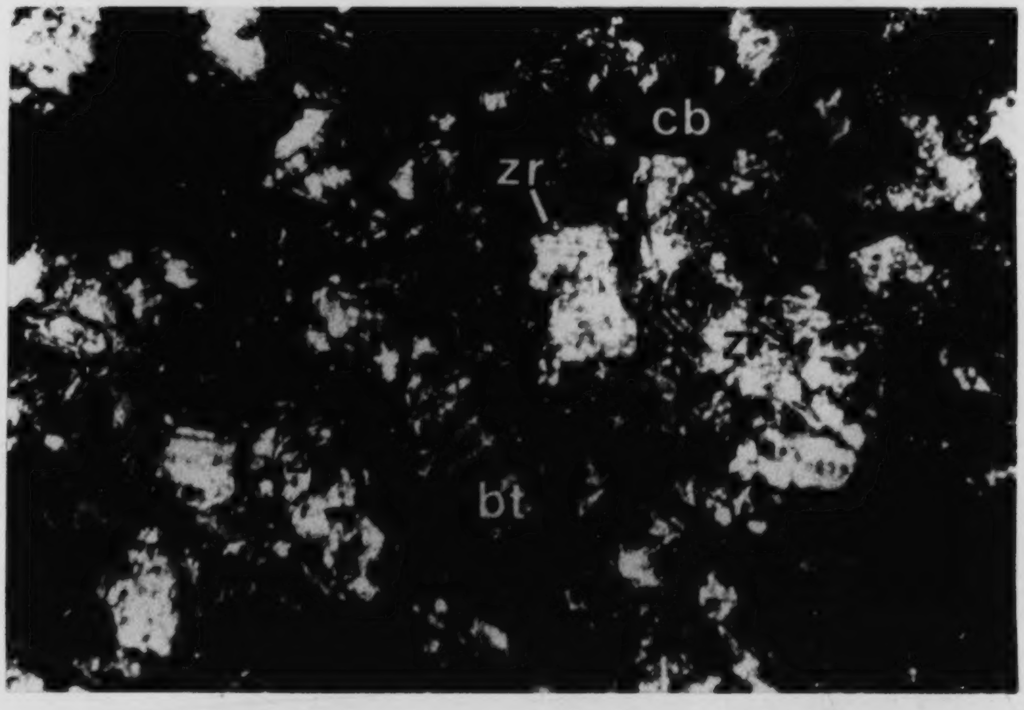
cb
zr
zr
bt

Plate 3.19a-Backscattered electron image of zonally metamictized zircons. White spots are burn marks caused by the electron microprobe. Scale bar represents 10 μm.

Plate 3.19b-Backscattered electron image showing core of zonally metamictized zircon in greater detail. Scale bar represents 5 μm.

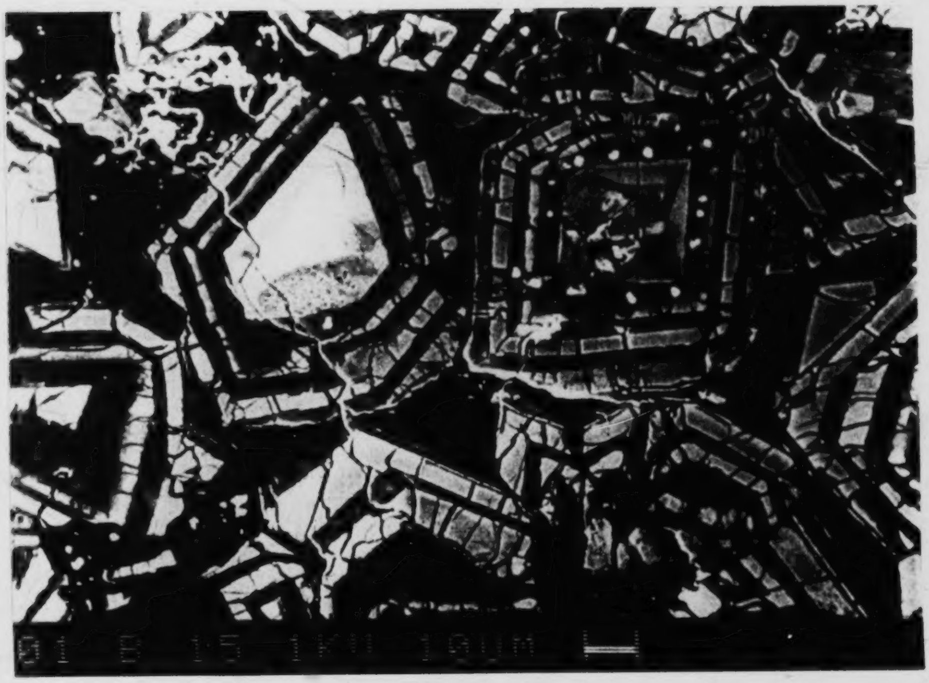
01 B 15 1KU 10UM

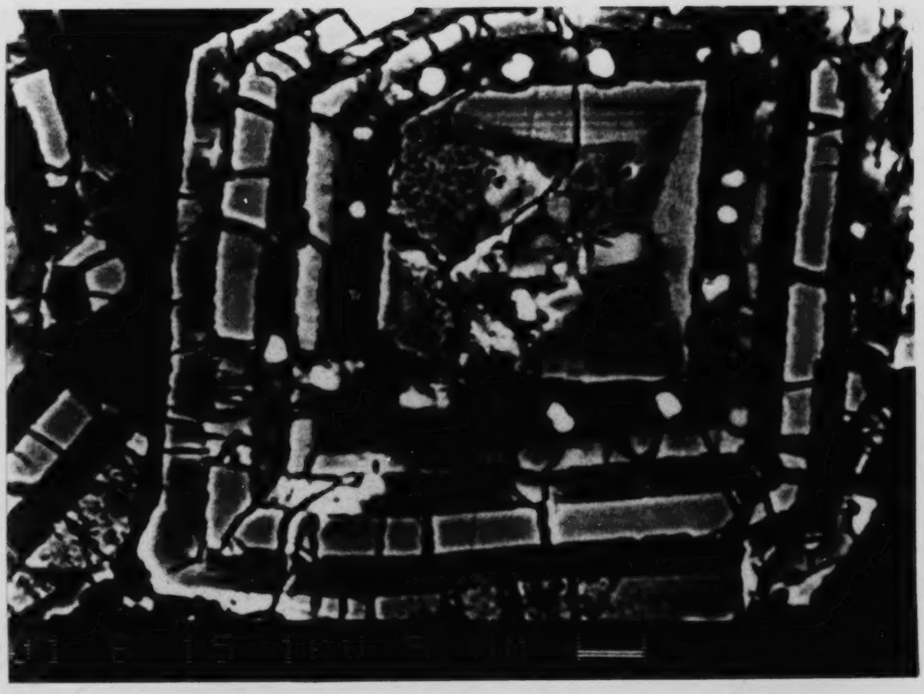

Plate 3.20a-Core-type zircons postulated to be comparable to cores of zonally metamictized zircons. Interstitial biotite and columbite. Plane polarized light. Magnification X368.

Plate 3.20b-Backscattered electron image showing core-type zircons. Bright areas are columbite. Scale bar represents 20 μm.

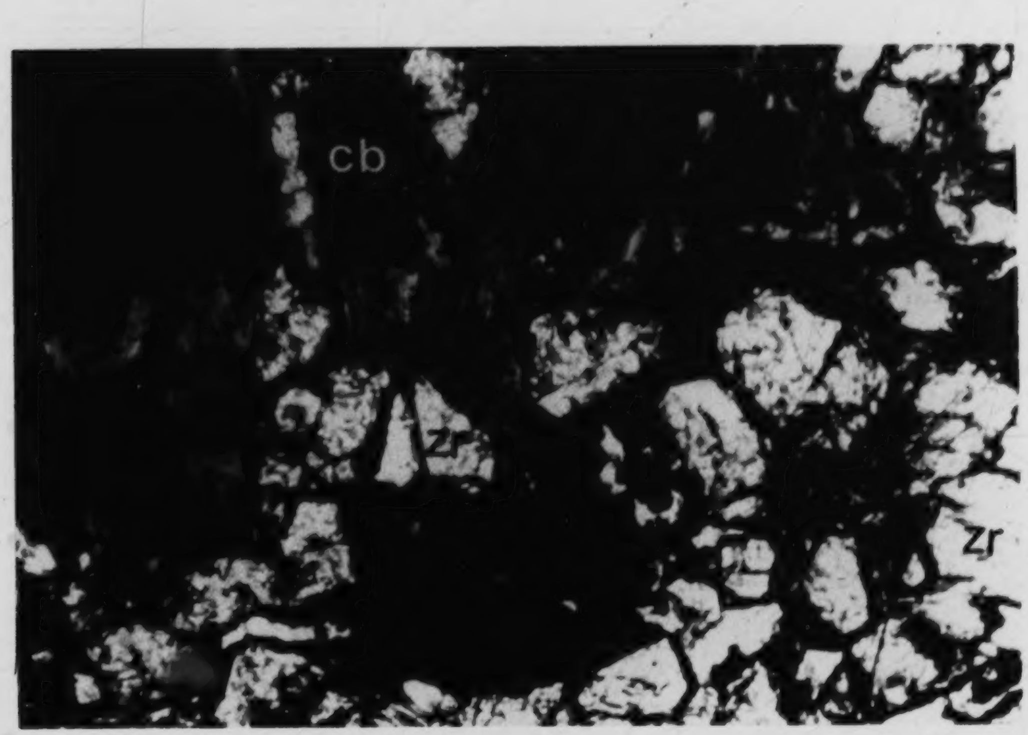
cb
zr
zr

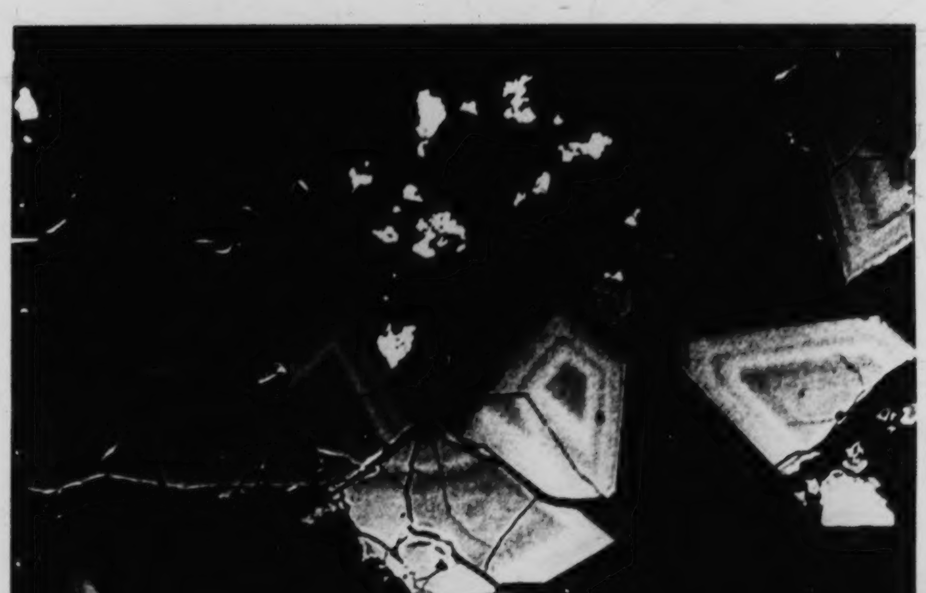
04 B 15.1KV 20UM

Plate 3.21-Photomicrograph illustrating red and blue cathodoluminescence of Ga-bearing albite. Interstitial chlorite is nonluminescent. Associated quartz has pale red cathodoluminescence around Fe- and Nb-oxide inclusions. Fluorite has dark blue cathodoluminescence. Magnification X120.

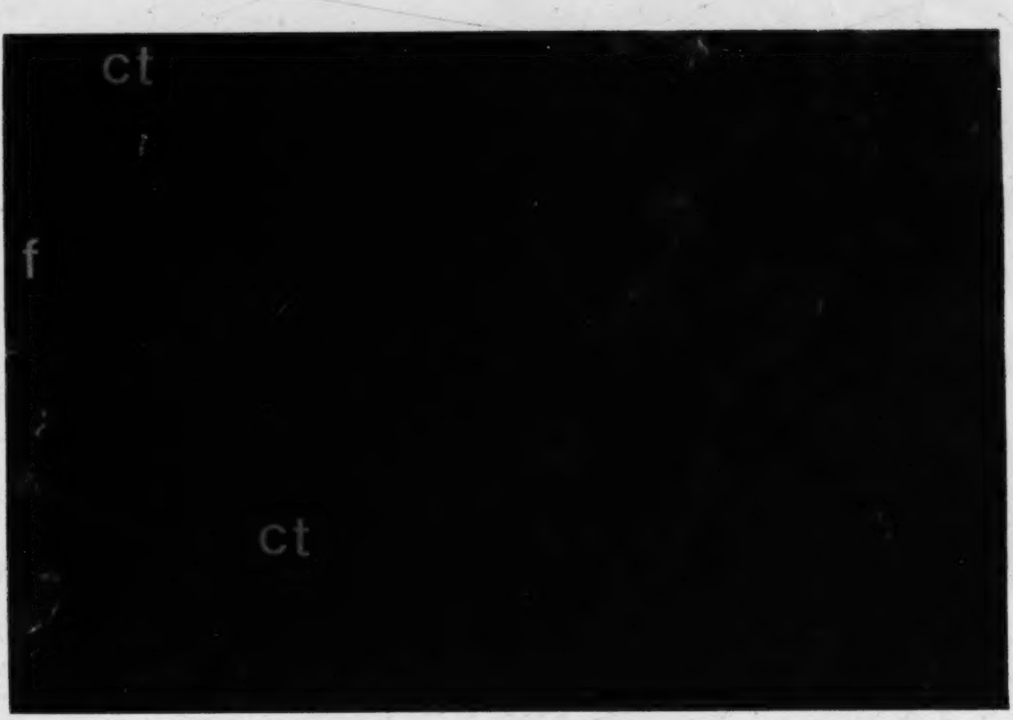
ct
f
ct

REFERENCES CITED

Amli, R. and Griffin, W.L. (1975) Microprobe analysis of REE minerals using empirical correction factors. American Mineralogist, 60, 599-606.

Banner, A.E. and Stimpson, B.P. (1974) A combined ion probe/spark source analysis system. Vacuum, 24, 511-517.

Bayliss, P. (1975) Nomenclature of the trioctahedral chlorites. Canadian Mineralogist, 13, 178-180.

Beus, A.A. (1966) Geochemistry of beryllium and genetic types of beryllium deposits. W.H. Freeman and Company, San Francisco.

Beus, A.A. and Zalashkova, N.Ye. (1964) Post-magmatic high temperature metasomatic processes in granitic rocks. International Geology Review, 6, 668-681.

Bowden, P. and Turner, D.C. (1974) Peralkaline and associated ring-complexes in the Nigeria-Niger Province, West Africa. In H. Sørensen, ed., The Alkaline Rocks, p.330-351. John Wiley and Sons, London.

Bowring, S.A., Van Schmus, W.R. and Hoffman, P.F. (1984) U-Pb zircon ages from Athapuscow aulacogen, East Arm of Great Slave Lake, N.W.T., Canada. Canadian Journal of Earth Sciences, 21, 1315-1324.

Brownell, G.M. (1959) A beryllium detector for field exploration. Economic Geology, 54, 1103-1114.

Buchan, R. (1985) Reconnaissance mineralogical examination of F-zone material (Lanthanide Zone). Unpublished internal report. Highwood Resources Limited.

Caruba, R., Baumer, A., Ganteaume, M. and Iacconi, P. (1985) An experimental study of hydroxyl groups and water in sythetic and natural zircons: a model for the metamict state. American Mineralogist, 70, 1224-1231.

Cavell, P.A. and Baadsgaard, H. (1986) Geochronology of the Big Spruce Lake alkaline intrusion. Canadian Journal of Earth Sciences, 23, 1-10.

Černý, P. and Trueman, D.L. (1985) Polylithionite from the rare-metal deposits of the Blachford Lake alkaline complex, N.W.T., Canada. American Mineralogist, 70, 1127-1134.

Collins, C.J. and Strong, D.F. (1985) The behaviour of fluorine in magmatic systems: A case study of Canada's largest fluorspar deposit. In R.P. Taylor and D.F. Strong, eds., Granite-related Mineral Deposits, Extended abstracts of papers presented at the CIM conference (Halifax, Canada), 66-71.

Currie, K.L. (1976) The alkaline rocks of Canada. Geological Survey of Canada, Bulletin 239.

Davidson, A. (1972) Granite studies in the Slave Province. Report of Field Activities, Part A, Geological Survey of Canada, Paper 72-1A, 109-115.

Davidson, A. (1978) The Blachford Lake Intrusive Suite: An Aphebian alkaline plutonic complex in the Slave Province, Northwest Territories. Current Research, Geological Survey of Canada, Paper 78-1A, 119-127.

Davidson, A. (1981) Petrochemistry of the Blachford Lake complex, District of Mackenzie. Geological Survey of Canada, Open File 764.

Davidson, A. (1982) Petrochemistry of the Blachford Lake complex near Yellowknife, Northwest Territories. In Y.T. Maurice, ed., Uranium in Granites, Geological Survey of Canada, Paper 81-23, 71-80.

Deer, W.A., Howie, R.A. and Zussman, J. (1962) Rock-forming Minerals, Volume 5, Non-silicates, p.347-356. Longmans, Green and Company, Limited, London.

Deer, W.A., Howie, R.A. and Zussman, J. (1963) Rock-forming Minerals, Volume 4, Framework Silicates, p.94-165. Longman Group Limited, London.

Deer, W.A., Howie, R.A. and Zussman, J. (1978) Rock-forming Minerals, Volume 2A, Single-chain Silicates, p.482-519. Longman Group Limited, London.

Deer, W.A., Howie, R.A. and Zussman, J. (1982) Rock-forming Minerals, Volume 1A, Orthosilicates, p.418-442. Longman Group Limited, London.

Donnay, G. and Donnay, J.D.H. (1953) The crystallography of bastnaesite, parisite, roentgenite, and synchisite. American Mineralogist, 38, 932-963.

Drysdall, A.R., Jackson, N.J., Ramsay, C.R., Douch, C.J. and Hackett, D. (1984) Rare element mineralization related to Precambrian alkali granites in the Arabian shield. Economic Geology, 79, 1366-1377.

Exley, R.A. (1980) Microprobe studies of REE-rich accessory minerals: Implications for Skye granite petrogenesis and REE mobility in hydrothermal systems. Earth and Planetary Science Letters, 48, 97-110.

Fleischer, M., Chao, G.Y., Francis, C.A. and Pabst, A. (1981) New mineral names. American Mineralogist, 66, 217-220.

Foord, E.E. (1982) Minerals of tin, titanium, niobium and tantalum in granitic pegmatites. In P. Černý, ed., Mineralogical Association of Canada Short Course Handbook, 8, 187-238.

Ganeev, I.G., Pachadzhanov, D.N. and Borisenok, L.A. (1961) Geochemistry of gallium, tin and some other elements in the process of greisenization. Geochemistry, Number 9, 830-839.

Geological Survey of Canada, Open File Report 124.

Hagni, R.D. (1984) Cathodolminescence microscopy applied to mineral exploration and beneficiation. In W.C. Park, D.M. Hansen and D.G. Hagni, eds., Applied Mineralogy, Proceedings of the Second International Congress of Applied Mineralogy in the Minerals Industry (Los Angeles, California), p.41-66. The Metallurgical Society of the AIME.

Hey, M.H. (1954) A new review of the chlorites. Mineralogical Magazine, 30, 277-292.

Hoffman, P.F. (1980) Wopmay Orogen: a Wilson cycle of early Proterozoic age in the northwest of the Canadian Shield. In D.W. Strangway, ed., The Continental Crust and its Mineral Deposits. Geological Association of Canada, Special Paper 20, 523-549.

Hogarth, D.D. (1977) Classification and nomenclature of the pyrochlore group. American Mineralogist, 62, 403-410.

Hylands, J.J. and Campbell, S.W. (1980) Progress report on Highwood Resources Thor Lake property. DIAND Cancelled Assessment File, 85 I/2.

Jackson, N.J., Drysdall, A.R. and Stoeser, D.B. (1985) Alkali granite and associated mineralization of the Arabian shield: a major peralkaline province. In R.P. Taylor and D.F. Strong, eds., Granite-related Mineral Deposits, Extended abstracts of papers presented at the CIM conference (Halifax, Canada), 142-148.

Jambor, J.L. (1985) Mineralogy of the beryllium-yttrium zones in the Thor Lake rare-metal deposit, Northwest Territories. Mineral Sciences Laboratories, CANMET, Report MRP/MSL 85-16(CR).

Jenkins, R. and DeVries, J.L. (1969) Practical X-ray Spectrometry, p.90-107. Philips, Eindhoven.

Leech, A.P. (1966) Potassium-argon dates of basic intrusive rocks of the District of Mackenzie, N.W.T. Canadian Journal of Earth Sciences, 3, 389-412.

Lumpkin, G.R. and Chakoumakos, B.C. (1986) Thorite group minerals from the Harding Mine, Taos County, New Mexico. Geological Association of Canada/Mineralogical Association of Canada Joint Annual Meeting, Program with Abstracts, 96-97.

Mariano, A.N. (1979) Enhancement and classification of fenitization by cathodoluminescence. Geological Association of Canada/Mineralogical Association of Canada Joint Annual Meeting, Program with Abstracts, p.65.

McGinn, G.J. (1976) A report to the president of Highwood Resources Ltd. on the Thor Claim Group, N.W.T. Unpublished internal report. Highwood Resources Limited.

Mineyev, D.A. (1963) Geochemical differentiation of the rare earths. Geochemistry, Number 11, 1129-1149.

Mitchell, R.S. (1973) Metamict minerals: A review. Mineralogical Record, 4, 177-182.

Morgan, J.H. and Auer, M.L. (1941) Optical, spectrographic and radioactivity studies of zircon. American Journal of Science, 239, 305-311.

Nockolds, S.R. (1954) Average chemical compositions of some igneous rocks. Bulletin of the Geological Society of America, 65, 1007-1032.

Northern Miner (1986) Tantalum find in Greenland. Northern Miner, vol.71, no.52, p.24.

Pellas, P. (1954) Sur la formation de l'état métamicte dans le zircon. Bulletin de la Societé francais de Minéralogie et Cristallographie, 127, 447-460.

Plant, A.G. (1976) Applications of microbeam techniques to mineralogy. In D.G.W. Smith, ed., Mineralogical Association of Canada Short Course Handbook, 1, 107-134.

Pupin, J.P. (1985) Magmatic zoning of Hercynian granitoids in France based on zircon typology. Schweizerishe Mineralogische und Petrographische Milleilungun, 65, 29-56.

Roeder, P.L. (1985) Electron-microprobe analysis of minerals for rare-earth elements: Use of calculated peak-overlap corrections. Canadian Mineralogist, 23, 263-271.

Severov, E.A. and Vershkovskaya, O.V. (1960) O povedenii galliya v protesse albitizatsii granitoidov. Doklady Akademii Nauk SSSR, 135, 1498-1500.

Shcherba, G.N. (1970) Greisens. International Geology Review, 12, 114-255.

Smirnov, V.I. (1977) Ore deposits of the USSR, Volume III. Pitman Publishing, London.

Smith, D.G.W. and Gold, C.M. (1979) EDATA2: A FORTRAN IV Computer program for processing wavelenth and/or energy-dispersive electron microprobe analyses. Proceedings of the 14th Annual Meeting, Microbeam Analysis Society (San Antonio, Texas, 1979) p.273-278. San Francisco Press.

Smith, D.G.W. and Leibovitz, D.P. (1986) MinIdent: A data base for minerals and a computer program for their identification. Canadian Mineralogist, 24 (in press).

Smith, D.G.W. and Reed, S.J.B. (1981a) The calculation of background in wavelength-dispersive elcetron microprobe analysis. X-ray Spectrometry, 10, 198-202.

Smith, D.G.W. and Reed, S.J.B. (1981b) Rare earth element determinations by energy-dispersive electron microprobe techniques. The Institute of Physics Conference Series, Number 61: Chapter 4, 159-162.

Stockwell, C.H. (1932) Great Slave Lake-Coppermine River area, Northwest Territories. Geological Survey of Canada, Summary Report, Part C, 37-64.

Thomas, D.G. (1977) Geology, geophysics and diamond drilling on the Thor and NB Claims, N.W.T. Unpublished internal report. Highwood Resources Limited.

Trueman, D.L., Pedersen, J.C., de St. Jorre, L. and Smith, D.G.W. (1985) The Thor Lake, N.W.T. Rare-metal deposits. In R.P. Taylor and D.F. Strong, eds., Granite-related mineral deposits, Extended abstracts of papers presented at the CIM conference (Halifax, Canada), 279-284.

Vlasov, K.A. (1966) Geochemistry and Mineralogy of Rare Elements and Genetic Types of their Deposits, Volumes I and II. Israel Program for Scientific Translation, Jerusalem.

Wanless, R.K., Stevens, R.D., Lachance, G.R. and Delabio, R.N. (1979) Age determinations and geologic studies; K-Ar isotopic ages, report 14. Geological Survey of Canada, Paper 79-2, 34-38.

APPENDIX I: Quantitative electron microprobe analysis

An ARL SEMQ microprobe fitted with an ORTEC EEDSII energy dispersive spectrometer and four wavelength dispersive (crystal) spectrometers was used to collect data presented in Table 2.1 and Tables 3.1 to 3.4. TAP and PET crystals (with P10 gas flow proportional counters) and LiF crystals (with Xe-filled sealed proportional counters) were used for wavelength dispersive analysis (WDA). For WDA, analytical lines for elements and the crystals on which they were recorded are listed below:

TAP	F Kα, Na Kα, Al Kα
PET	Si Kα, Cl Kα, Ca Kα, Y Lα, Zr Lα
LiF(200)	Ti Kα, Mn Kα, Fe Kα, Ga Kα, Ba Lα, Hf Lα, Ta Lα, U Mα

The stability of the instrument during an analytical run was monitored in two ways. First, a calibration standard (willemite) was run at the beginning and the end of each analytical session. This standard was run in order to monitor instrumental drift in the energy dispersive system and also to monitor possible large changes in probe current with time by noting variations in the total number of counts in the full spectrum. Secondly, a Faraday cage measurement (used to record the ratio of probe current to aperture current) was taken at the beginning of an analytical run before any standards had been analysed and at the end of a session before the final calibration standard was run.

All data were processed through EDATA2 (Smith and Gold, 1979) which is a FORTRAN IV program for processing energy and/or wavelength dispersive electron microprobe data. EDATA2 employs ZAF corrections and also corrects for probe current variations, instrumental drift, escape peak generation, electronic noise, background subtraction and the overlap of analytical lines. Dead time corrections are applied automatically and electronically by the instrument and related pulse-pile up counting losses are minimised electronically.

Errors in elemental concentrations obtained by electron microprobe analysis are difficult to estimate accurately because the uncertainty of several influential factors is unknown. First, there are uncertainties in the accuracy of peak:background ratios, particularly in EDA where backgrounds are calculated and not measured as in WDA. The level of uncertainty attached to peak:background ratios increases as the ratio decreases and the background intensity becomes as important as the peak intensity. The degree of uncertainty in the elemental concentrations in a standard is also unknown. In addition, the uncertainty associated with ZAF corrections is unknown and can only be estimated. There are many other factors (such as sample contamination, sample damage, coating variations between sample and standard) which may also cause errors in electron microprobe analysis and are difficult to assess.

Although the error in an electron microprobe analysis may be estimated on the basis of counting statistics such as described by Jenkins and DeVries (1969), it is only an approximation. Such error calculations were not attempted here. Because the uncertainty of the many factors which may effect an analysis are unknown, calculated errors based only on counting statistics may be misleading by implying too high a degree of accuracy.

Statistical detection limits were calculated for minor elements of interest such as Ga in feldspar where the detection limit is equal to:

$$\frac{\text{expected deviation of background on sample X ZAF sample X wt \% element in standard}}{\text{net peak counts on standard X ZAF standard}}$$

All compositional data are given in weight % of the element and have been arbitrarily rounded to two decimals which is not significant in terms of accuracy.

A list of the electron microprobe standards used in this study are listed below:

albite (Cleavelandite)	CCNM0029
barite	CCNM0035
biotite	CCNM0037
diopside (Wakefield)	CCNM0087
fluorapatite (Durango)	CCNM0102
grunerite	CCNM0127
Hf metal	CCNM0136
ilmenite (Odergaarden)	CCNM0152
kaersutite (Kakanui)	CCNM0163
$KTaO_3$	CCNM0361
labradorite	CCNM0494
Nb metal	CCNM0362
$Nd_3Ga_5O_{12}$	CCNM0090
sanidine (Hohenfels)	CCNM0279
ThO_2	CCNM0521
U metal	CCNM0320
U_3Si	CCNM0363
willemite	CCNM0332
zircon	CCNM0353
cubic zirconia	CCNM0504

Biotite and chlorite

All analyses were obtained using combined energy dispersive analysis (EDA) and wavelength dispersive analysis (WDA) techniques. F, Na, Cl and Mn were determined using WDA and the remaining elements were analysed simultaneously using EDA.

Data were collected using an operating voltage of 15 kV, an average probe current of 3.3 nA and a counting time of 240 seconds. A point beam, shifted every 30 seconds, was used for all analyses on both sample and standard materials.

Statistical detection limits were calculated for F, Na, Cl and Mn for a 99 % confidence level. The detection limits are:

F	0.08 weight %
Na	0.06 weight %
Cl	0.06 weight %
Mn	0.03 weight %

Microprobe standards, and the elements for which they were used, are listed below:

biotite	Mg, K
fluorapatite	F, Cl
grunerite	Fe
kaersutite	Na, Al, Si, Ti
willemite	Mn

Columbite and ashanite

Columbite analyses are quantitative and the ashanite analysis is semi-quantitative. All analyses were obtained using combined EDA and WDA techniques. Ta was determined using WDA and the remaining elements were analysed simultaneously by EDA.

Data were collected using an operating voltage of 15 kV, an average probe current of 3.8 nA and a counting time of 240 seconds. A point beam, shifted every 30 seconds, was used for all analyses on both sample and standard materials. For a 99 % confidence level, the statistical detection limit for Ta was calculated to be 0.17 weight %.

Microprobe standards, and the elements for which they were used, are listed below:

ilmenite	Ti, Fe
$KTaO_3$	Ta
Nb metal	Nb
willemite	Si, Mn
U_3Si	U
default	Mg, Al, Ca

Zircon

All analyses are quantitative except for the zircon overgrowths on xenotime which are semi-quantitative. All quantitative analyses were obtained by WDA. Data were collected using an operating voltage of 15 kV and a counting time of 240 sec. A point beam, shifted every 30 seconds, was used for all analyses on both sample and standard materials.

Microprobe standards, and the elements for which they were used, are listed below:

barite	Ba
diopside	Ca
fluorapatite	F
ilmenite	Ti, Fe
sanidine	Al
U metal	U
zircon	Si, Zr
cubic zirconia	Y, Hf

The semi-quantitative analysis was carried out by EDA. Data were collected using an operating voltage of 15 kV, an average probe current of 3.7 nA and a counting time of 240 seconds. Due to the fine grain size of the zircon, a point beam was used. The beam was shifted every 60 seconds as there were only four areas of adequate size for analysis.

Microprobe standards, and the elements for which they were used, are listed below:

Hf metal	Hf
kaersutite	Al, Ca, Ti, Fe
ThO_2	Th
willemite	Mn
zircon	Si, Zr

Albite

Ga was determined by WDA. Ga data were collected using an operating voltage of 20 kV and a higher than normal probe current of 7.2 nA because of the low concentration of Ga present in albite. Total peak counts were based on on average of ten 40 second counts. A point beam, shifted every 40 seconds, was used for all analyses on both sample and standard materials.

All other elements were determined using EDA on the same areas previously analysed for Ga by WDA. Data were collected using an operating voltage of 15 kV, an average probe current of 3.8 nA and a counting time of 240 seconds. A point beam, shifted every 30 seconds, was used for all analyses.

For a 99 % confidence level, the statistical detection limit for Ga was calculated to be 0.02 weight %. Ranges in Ga content shown in Table 3.3 were determined from lower limit calculations using raw counts where the lower limit is equal to:

$$\frac{\text{(lowest counts on sample - background) X ZAF sample X wt \% Ga in standard}}{\text{(highest counts on standard - background) X ZAF standard}}$$

Slightly low Na concentrations in all albite analyses are probably due to the migration of Na in the samples during point beam analysis.

Microprobe standards, and the elements for which they were used, are listed below:

albite	Na, Al, Si
labradorite	Ca
$Nd_3Ga_5O_{12}$	Ga
sanidine	K
default	Fe, Ba

Note: default standard values are those determined on some previous occasion under carefully controlled conditions and then stored for subsequent use when analytical standard values have not been obtained.

K-feldspar

K-feldspar analyses, like albite, were done as two separate runs. Ga was determined using WDA with an operating voltage of 20 kV and an average probe current of 7.2 nA. Total peak counts were based on a average of ten 40 second counts. A point beam, shifted continuously, was used for all analyses on both sample and standard materials to prevent the migration of light elements which had occurred previously in albite analysis.

All other elements were determined using EDA on the same areas previously analysed for Ga by WDA. Data were collected using an operating voltage of 15 kV, an average probe current of 3.8 nA and a counting time of 240 seconds. A point beam, shifted continuously, was used for all analyses.

For a 99 % confidence level, the statistical detection limit for Ga was calculated to be 0.01 weight %. Ranges in Ga content shown in Table 3.4 were determined from lower limit calculations.

Microprobe standards, and the elements for which they were used, are listed below:

labradorite	Na, Ca
$Nd_3Ga_5O_{12}$	Ga
sanidine	Al, Si, K
default	Fe, Ba

APPENDIX II: Proposed technique for quantitative electron microprobe analysis of REE-bearing minerals

As part of this study, an attempt was made to develop a technique for the quantitative wavelength dispersive analysis of REE-bearing minerals that was to be used to characterize the Y- and REE-bearing minerals of the T-zone. Owing to environmental instabilities which affected the performance of the instrument being used, the technique could not be developed. However, the proposed technique is presented here in the hope that it may be of interest and of use in future studies.

Introduction

In electron microprobe analysis of REEs, the complex L series of lines are used because the K series is too high in energy and the M series too low. The L spectrum for each REE has at least 10 lines and with several REEs present in a single mineral, the potential for spectral interferences (between REEs in addition to other elements present) is great. It is necessary then to determine the degree of this interference (peak overlap) between the elements of interest.

Although EDA is routine for elements in the atomic number range 11 to 35 where K lines are used, the interferences between L and M lines used for elements with atomic numbers greater than 35 are quite severe. Smith and Reed (1981b) demonstrated the potential of EDA for REEs using overlap coefficients for REE L lines. Their results were encouraging but suggest that wavelength dispersive techniques are more suitable for quantitative REE analysis because interferences are less severe and there are better peak:background ratios than in EDA owing to the superior resolution of the wavelength dispersive system.

Although WDA is preferable to EDA for REE analysis, WDA involves the time consuming process of measuring peak and background intensities for each element present in a certain mineral. In the case of REE-bearing minerals, which may contain upwards of 14 elements, the process can be very tedious. That is, a total of almost 100 measurements (including peak and background measurements on sample and standard materials) would have to be made for a single mineral. In addition to the lengthy data acquisition time, there is the difficulty of finding a suitable position for accurate measurement of background intensities owing to the complexity of overlapping lines. Accurate determinations of background intensities are essential to the calculation of peak overlap corrections and are of particular importance in cases where high intensity peaks (high element concentration) interfere with low intensity peaks (low element concentration).

Previous studies

Some success has been achieved with WDA of REEs in previous studies. Amli and Griffin (1975) used empirical correction factors (determined for the REEs using binary and ternary mixtures of REE-oxides) for analyses of several REE-bearing minerals. Although their results were encouraging, the empirical correction factors were dependent on the change in resolution and efficiency, over the wavelength region of the spectrometer used in their microprobe. Use of these correction factors is limited then to analysts with spectrometers that show the same resolution and effeciency change with spectrometer setting as that of Amli and Griffin.

Exley (1980) selected specific L α_1 and L β_1 peaks for the analysis of REEs, to avoid the need for interference corrections as describe by Amli and Griffin (1975). Although this technique minimized interferences between particular L α_1 and L β_1 peaks, interferences from less intense, but present, additional L β and L γ peaks are not accounted for.

Roeder (1985) calculated peak overlap corrections for the L α_1, L β_1, L β_2, L β_3 and L γ_1 lines measured on REE phosphate standards. Roeder's technique is preferable to that of Amli and Griffin (1975) because it can be used to calculate peak overlap for a spectrometer of any resolution or efficiency. However, as with all those described above, Roeder's technique still requires the time consuming process of selecting appropriate background positions (if available) for all the REEs and taking background measurements.

The analytical technique proposed here includes a procedure for calculating background intensities in addition to peak overlap corrections. Calculated background intensities would significantly reduce data acquisition time.

Background correction

The characteristic peaks used in microprobe analysis are superimposed on background. In WDA the background is attributed primarily to continuum radiation which is a complete spectrum of wavelengths resulting from the random deceleration of incident electrons in the target material. Other contributing factors to background in WDA are second (and higher) order reflections of characteristic or continuum radiation, scattered radiation, fluorescence from the diffracting crystal, high energy electrons penetrating the detector window and electronic noise. The accurate determination of background intensities is essential in quantitative electron microprobe analysis in order to correct the characteristic peak intensities for contributions from background radiation.

In WDA, background intensities are commonly determined by off-setting the spectrometer on either side of the analytical peak and interpolating the intensity below the peak. In the case of Y- and REE-bearing minerals, the complexity of overlapping L lines makes the selection of suitable positions for background measurement very difficult. In order to obtain accurate background intensities over the range of REE L lines and reduce data acquisition time, the technique for background corrections proposed here, based on previous work by Smith and Reed (1981a), would use normalized background intensities on a specific crystal spectrometer.

Background measurements in EDA are even more difficult than in WDA owing to the relatively poor resolution of the former. Because it is often impossible to measure background intensities experimentally in EDA, calculated background intensities are used. During an analytical run the calculated background is scaled by taking background measurements at several positions in the spectrum to account for any variation in operating conditions.

EDATA2 (Smith and Gold, 1979) contains a procedure for accurately calculating background in EDA given operating conditions and average atomic number of the sample. The procedure for background corrections used in EDATA2 for EDA would be modified for WDA of REEs and other elements commonly present in REE-minerals. Instead of storing a normalized background spectrum for calculation of background in a sample as is used in

EDA, the modified procedure would store a normalized background intensity for each element of interest on a specific spectrometer. Given compositional information for a sample, the background for each element in that sample could be calculated using the stored normalized background intensities of particular spectrometers. Where the compositions are well known (as in standard materials) the calculation is made only once. In samples of unknown average atomic number the calculation is iterative. As in EDA, during an analytical run the calculated background for each spectrometer is scaled by taking background measurements in a few positions in that portion of the spectrum covered by the spectrometer to account for any variations in operating conditions. This technique would reduce significantly the number of measurements required for the analysis of a single REE-bearing mineral from almost 100 measurements to a small fraction of that.

Determination of backgrounds

Initially, a list of elements would be compiled to include the REEs and other elements which commonly occur in REE-bearing minerals (such as Si, P, Y). Based on qualitative electron microprobe data from the minerals of interest in this study, a list of 26 elements was compiled (see Table II-1). Next, appropriate standards would be selected for all the elements of interest. In terms of REE standards, REE-Al alloys are considered to be superior to metals, silicate glasses and pure oxides beacuse the Al alloys are stable whereas the other materials tend to oxidize, degrade or hydrate more easily. The REE-Al alloys are also desirable standards because they contain only one REE; with such simple compostions, the alloys are not subject to the complex spectral interferences present in standards such as silicate glasses or natural minerals which contain several REEs. Minimal interferences in the standards are crucial to the accurate determination of backgrounds as outlined here. The standards selected for use in this study are listed in Table II-1. Where Al alloys were not available, other single REE-bearing standards were substituted such as LaB_6 (lanthanum hexaboride), $SmFeO_3$ (samarium ferrite) and thulium and ytterbium metals.

In order for this technique to work, the data for each element must be recorded with a particular spectrometer and this spectrometer would be used on all subsequent occasions for that element. For example, all La measurements including background, overlaps and analyses would be recorded with an LiF crystal on a specific spectrometer. An ARL SEMQ electron microprobe with four wavelength dispersive (crystal) spectrometers was used in this study. On Channels 1 and 2, LiF crystals were used with Xe-filled sealed proportional counters. TAP and PET crystals (with P10 gas flow proportional counters) were used on Channels 3 and 4 respectively. Table II-2 lists the spectrometer/diffracting crystal combinations used for each of the 26 elements of interest in this study. These combinations were selected specifically for efficeincy in this particular study, but may be a useful guide for future work.

After selecting the appropriate spectrometer/crystal combinations, individual pulse height analyser settings would be selected for each element in order to minimize the contributions to background by electronic noise and second order reflections without causing serious attenuation of the analytical peaks. Again, these particular settings would have to be used in all subsequent work for consistent, accurate results.

The background measurements would be taken at the peak position for each element of interest. These determinations would be made on standards which are known to lack the element of interest and have no other interfering lines in the region of interest. It is suggested here that five standards, of simple composition and variable average atomic numbers, would be suitable for background determinations. As an example: quartz, ilmenite, LaB_6, Nb-metal and ThO_2 are five standards with relatively simple compositions (1 or 2 element spectrum) and which represent a good variation in average atomic number ranging form 10.4 to 80.1. Background measurements would be made on at least three of the five standards (depending on peak interferences in the region of interest) in order to avoid errors due to unsuspected small concentrations of the element of interest and also to demonstrate the applicability of the procedures which would be used to calculate backgrounds for different atomic numbers.

Based on the background measurements taken for a series of elements recorded on a particular spectrometer, normalized background intensities could be calculated for that spectrometer over the range of elements covered by that spectrometer. The normalized background for each spectrometer would then be stored for use during processing of analytical data. Whereas in EDA a single normalized background spectrum is stored, in this case several partial spectra would be stored with one for each spectrometer to cover the range of elements recorded with that spectrometer. During subsequent overlap measurements and analyses, a few background measurements would be taken for each spectrometer and the calculated background would be scaled accordingly. Then, the background under each analytical peak of interest could be calculated and the characteristic peak intensities corrected for contributions from background radiation.

Overlap corrections and overlap measurements

In order to correct for spectral interferences which are quite severe in REE-bearing minerals, measurements of the degree of overlap between the analytical lines of interest would be made. Based on these measurements, overlap coefficients would then be calculated for all the elements of interest.

Peak overlap measurements would first involve measuring and recording the peak intensity of the analytical line on a standard known to contain that element. Then, with the spectrometer set at the peak position for the analytical line other standards which contain elements with possible overlapping lines in the region of interest would be analysed. This procedure would be used for all elements of interest.

Once the measurements had been taken, background corrections would be applied by the modified version of EDATA2 and overlap coefficients could be calculated based on the intensities of interferences (if any). The overlap coefficients generated by EDATA2 are corrected for matrix effects, including complete differential ZAF effects. The overlap coefficients are corrected for these effects, both at the time of their generation and their subsequent use in data processing of unknown mineral samples.

Gross fluctuations in environmental conditions related to building renovations, severely affected the electrical and mechanical performance of the instrument being used. During renovations, the 110 volt AC power supply to the building was varying up to 10% below the proper voltage which affected the electronic circuitry of the microprobe, causing problems with preamplifiers, amplifiers and pulse height analysers. In particular, this variation in power supply created problems with drift of the detector pulses in and out of the bottom and upper windows. That is, when the voltage supply was lower than normal, the detector pulses as a result were smaller and more likely to be lost out the bottom window. Conversely, when the voltage was higher than normal, the detector pulses as a result were larger and more likely to be lost out the upper window. In addition, arc welding during building renovations caused erratic bursts of high voltage electronic noise which propagated through the building wiring and entered the pulse processing and counting circuitry of the electron microprobe. This type of interference may cause serious errors in peak and background measurements.

The problems created by unsuitable environmental conditions, as described above, made it impossible to achieve consistent results which are essential to the technique for REE analysis proposed here. Therefore, the development of the technique was not completed during this study. However, this technique when fully developed, could prove to be very useful in the WDA of REE-bearing minerals by providing accurate background intensities in a fraction of the time required to determine background measurements by conventional techniques. In addition, overlap coefficients could be generated that would be corrected for matrix effects both at the time of their generation and their use. It should be noted that in order to use a stored normalized background for the calculation of background intensity in a particular analytical region, it is essential that data is acquired in the same manner as that of the normalized background. That is, the same crystal spectrometer and pulse height analyser settings must be used for this method to produce accurate, reliable results.

TABLE II-1: LIST OF ELEMENTS AND MICROPROBE STANDARDS

Element	Standard
F	CaF_2
Al	$CeAl_2$
Si	quartz
P	fluorapatite (Durango)
Cl	tugtupite
Ca	diopside (Wakefield)
Ti	ilmenite (Odergaarden)
Mn	willemite
Fe	hematite
Y	YAG ($Y_3Al_5O_{12}$)
Zr	Zr metal
Nb	Nb metal
La	LaB_6
Ce	$CeAl_2$
Pr	$PrAl_2$
Nd	$NdAl_2$
Sm	$SmFeO_3$
Gd	$GdAl_2$
Tb	$TbAl_2$
Dy	$DyAl_2$
Ho	$HoAl_2$
Er	$ErAl_2$
Tm	Tm metal
Yb	Yb metal
Th	ThO_2
U	U_3Si

TABLE II-2: SPECTROMETER/DIFFRACTING CRYSTAL COMBINATIONS USED FOR ELEMENT ANALYSIS

Spectrometer/Crystal	Elements
Channel 1/LiF	Ti, Fe, Ce, Nd, Gd, Dy, Er, Yb
Channel 2/LiF	Mn, La, Pr, Sm, Tb, Ho, Tm
Channel 3/TAP	F, Al
Channel 4/PET	Si, P, Cl, Ca, Y, Zr, Nb, Th, U